THE
PHYSICAL REVIEW
A Journal of Experimental and Theoretical Physics Established by E. L. Nichols in 1893

VOL. 58, NO. 2 JULY 15, 1940 SECOND SERIES

Distribution in Angle of Protons from the Deuteron-Deuteron Reaction

R. D. HUNTOON,[a] A. ELLETT, D. S. BAYLEY,[b] AND J. A. VAN ALLEN[c]
State University of Iowa, Iowa City, Iowa

(Received April 9, 1940)

The distribution in angle of the protons from the deuteron-deuteron reaction has been measured with a gas target over a range of bombarding energy from 60 to 390 Kev. The results are representable by

$$N(\theta)=1+A\cos^2\theta$$

in which θ is the angle which the proton's velocity makes with the direction of the deuteron beam as measured in the center-of-mass coordinate system and $N(\theta)$ is the number observed per unit solid angle at θ. The value of A is found to be markedly dependent on bombarding energy.

INTRODUCTION

MEASUREMENTS of the angular distribution of the protons emitted in the reaction

$$H^2+H^2\rightarrow H^3+H^1$$

have shown that the distribution is markedly anisotropic and that it is probably of the form $1+A\cos^2\theta$ in the center-of-mass coordinate system.[1-5]

Different investigators have not obtained concordant results on the value of A nor on the question of its energy dependence. Satisfactory interpretation of their measurements is made difficult, however, by two practical factors inherent in the use of thick deuterium targets: (1) an uncertainty in the actual collision energy of an incident deuteron caused by surface contamination, and (2) an uncertainty in the character of the target—that is, in the distribution of deuterium and in the stopping power during prolonged bombardment.

The seriousness of these uncertainties is even greater since *both* yield and angular distribution data on the same or an equivalent thick target must be known as a function of bombarding energy in order to deduce thin-target (i.e., theoretically interesting) angular-distribution data.

A suitably arranged gaseous target is free of these uncertainties and is very attractive as an experimental possibility. It has been found feasible to use such a target of deuterium gas in a careful study of the angular distribution of the protons at several bombarding energies.

The simplicity and importance of the deuteron-deuteron reaction recommend such a study.

HIGH VOLTAGE EQUIPMENT

The magnetically analyzed deuteron beam of 10 to 20 microamperes used in this work was

[a] Now at New York University.
[b] Now at University of Pennsylvania.
[c] Now at Department of Terrestrial Magnetism, Carnegie Institution of Washington.
[1] Kempton, Browne and Maasdorp, Proc. Roy. Soc. **A157**, 386 (1936).
[2] H. Neuert, Physik. Zeits. **38**, 122 (1937).
[3] Haxby, Allen and Williams, Phys. Rev. **55**, 140 (1939).
[4] H. Neuert, Physik. Zeits. **39**, 890 (1938).
[5] H. Neuert, Ann. d. Physik **36**, 437 (1939).

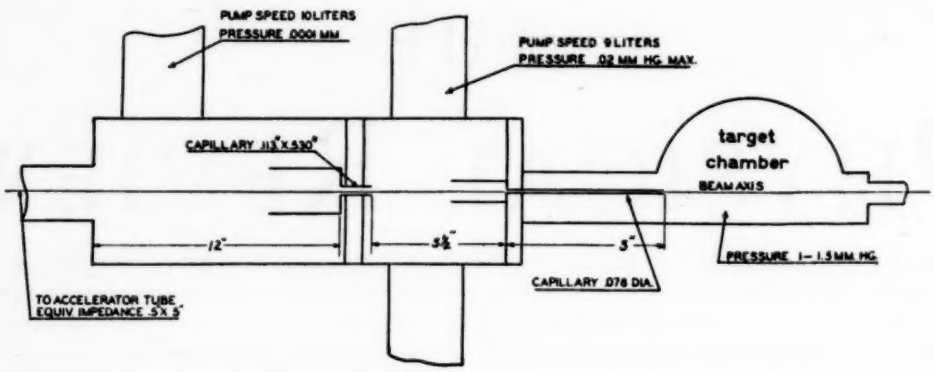

FIG. 1. Schematic diagram of pumping system used to maintain the necessary pressure differential between the target chamber and the accelerating tube.

obtained in a five-foot accelerating tube provided with a low voltage ion source. Rectified potentials up to 400 kilovolts were available from a transformer-rectifier-quadrupler of Cockcroft-Walton type.

The average energy of the deuteron beam was determined with an accuracy of about 5 percent with a high resistance voltmeter of standard type.[6] The voltmeter consisted of 455 ten-megohm IRC metalized resistors, which had been carefully calibrated for resistance as a function of current. The voltmeter was checked for linearity by setting the deflecting magnet, then raising the voltage to bring successive m/e components of the beam into the narrow entrance canal of the target chamber.

GAS TARGETS

A gas target can be a close approximation to an ideally thin target. The stopping power of deuterium gas at a pressure of 1 mm of Hg for 100-kev deuterons is about 0.2 kev per cm and the number of disintegrations produced by a beam of one microampere in 3 or 4 mm of path is sufficient to give a workable counting rate in a reasonably small solid angle. Thus, the energy loss of the beam in traversing the target is quite negligible for the energies used in these experiments.

At *low* bombarding energies the advantages of such a target are lost if the deuteron beam is admitted to the target chamber through a foil. Foils sufficiently thick to stand up under the intense beams necessary introduce a large energy loss difficult to measure accurately, a straggling large compared to the residual energy, and a spread in energy due to variations in foil thickness.

These difficulties are avoided by admitting the beam through a tube of sufficiently small bore to permit the maintenance of the necessary pressure difference between the target chamber and the accelerating tube. While the beam must, of course, traverse a certain minimum distance through a gas of increasing density in order to reach the effective target volume the apparatus can easily be arranged so that this path does not exceed 15 cm. The resulting total energy loss is about 2 kev per mm of gas pressure in the target chamber. The straggling produced is obviously negligible. The effective collision energies of the deuterons in the beam can thus be known with an error of less than one percent for bombarding energies greater than 50 kev.

The gas flow from such a chamber is easily handled by a two-stage differential pumping system as shown schematically in Fig. 1. With the geometrical arrangement indicated it is possible to get a beam of approximately a microampere through the target volume. With a gas pressure of 1.5 mm of Hg the yield from 5 mm of beam length is about 500 protons per minute into a solid angle of 0.007 steradian at 90°. Under these conditions one-half liter of deuterium at NTP is required per hour of operation. No provision was made for recovering the gas.

Although the use of a smooth wall capillary

[6] Hafstad, Heydenburg and Tuve, Phys. Rev. **50**, 504 (1936).

to admit the beam to the target volume is desirable because of its greater impedance to gas flow from the target chamber experience has shown that the use of such a tubular capillary introduces what appears to be a serious loss of energy in the incident beam. The result is an apparent equatorial asymmetry in the observed angular distribution.

The substitution of a series of thin diaphragms to reduce small angle scattering as shown in Fig. 2 removes this effect and gives an angular distribution with the proper equatorial symmetry.

Target Chamber

The apparatus used is shown in Fig. 2 (a, b, c). Essentially it consists of a regular twelve-sided right cylinder *A* whose thick walls are pierced by 12 holes with coplanar axes bored in the centers of its 12 faces. Into one of these holes is set a tube *B* which carries the system of 5 diaphragms through which the beam enters the target chamber.[7] The sizes of these diaphragms and the inside diameter of the intervening spacers are so chosen that no part of the spacers can be seen by ***both*** the incident beam and the target volume. Only the edges of the diaphragms can scatter directly into the target volume, and this scattering is minimized by making these diaphragms thin in comparison to their spacing. The beam

[7] Note that 2(a) and 2(b) are drawn with the beam entering from the bottom. In use the entrance canal was uppermost.

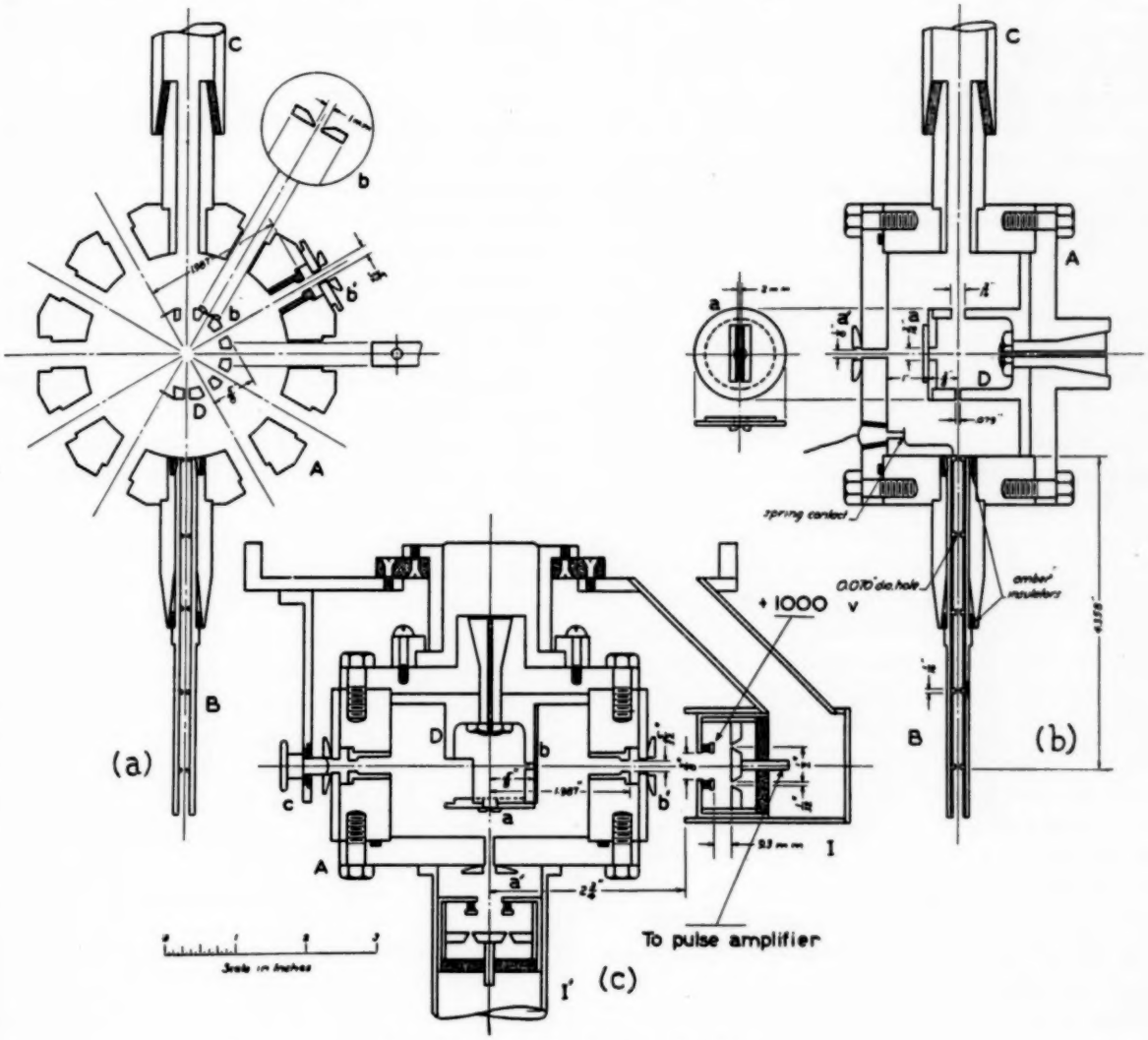

Fig. 2 (a, b, c). Final target chamber.

is allowed to escape from the target chamber before its main portion strikes a metal surface, in this case the bottom of an insulated cup C. This reduces the intensity in the vicinity of the ionization chambers of the neutrons produced where the beam is stopped, and thus aids in keeping down the background count.

The method of making observations is evident from the figures. The stationary ion chamber I' views the beam from a fixed azimuth (90°) and receives particles from a length of beam and within a solid angle determined by the diaphragms a, a'. The number of protons entering this chamber is simply a measure of the number of disintegrations produced by the bombarding beam.

The movable ion chamber I sees the beam through apertures b, b'. The aperture b' is a circular hole $\frac{5}{32}''$ in diameter in the center of a brass plug which fits tightly into one of the 12 regularly spaced holes mentioned above. Between the aperture b' and the ion chamber is a vacuum-tight aluminum window (0.0015 inch thick) supported as shown in the sketch. The hole in this window support is large enough so that it does not define the solid angle. The other defining aperture, b, is a slot perpendicular to the beam carried on another twelve-sided metal cylinder D which is mounted so as to be accurately coaxial with the cylinder A. The slots b are made amply long so that the ion chamber can see the full diameter of the beam.

The position of these slots on the cylinder D was determined as follows. Circular holes $\frac{1}{8}''$ in diameter were bored in the centers of the flat faces of the cylinder D. Into these could be fitted a cylindrical metal plug one end of which had been cut away from opposite sides so as to leave two parallel flat faces equidistant from the axis of the cylinder. This plug was inserted into the $\frac{1}{8}''$ holes mentioned above, the slit edges were set up against its flat faces, and the slits were then fastened in place. The plug could be withdrawn, rotated 180° about its axis, and reinserted with an equally good fit, showing that the center of the slit coincided with the axis of the hole. This procedure also arranged that the slits were all quite closely the same width, a fact which was subsequently checked by means of a micrometer microscope.

The placing of the cylinder D in correct azimuth relative to A was secured as follows. With the cylinder D removed it was first verified that the axes of the 12 holes in the cylinder A were coplanar and possessed a common point of intersection. This was done by passing a close fitting piece of ground rod through a pair of diametrically opposite windows and measuring the distances from this rod to the faces of the cylinder A which were parallel to it, and measuring the distances to the ends of the cylinder. By this means it was verified that the constructed chamber did not deviate from the desired geometry by more than 0.001″ in the dimensions referred to. The cylinder D was then placed in correct azimuth by inserting into the holes b rods which had on their inner ends concentric cylindrical portions of such size that they fitted closely into the holes in D.

Apertures in only one-half of the target chamber were used in the actual observations. The diametrically opposite ones were provided for convenience in checking accuracy of machining, in aligning D, and in assuring the correct location of the movable ion chamber.

Shields (not shown) were so placed that the exit windows b' could see no part of the beam save that in the effective target volume.

The entrance canal B is insulated from the target chamber and is connected to an external lead. Cup C is insulated also. These features are useful in aligning the canal with the beam and in maintaining as large a current as possible through the target chamber. None of the measurements depends on a knowledge of this current, however.

The pumping system was essentially that shown in Fig. 1. Since the impedance of the system of diaphragms (Fig. 2) was only about one-fifth that of the capillary of Fig. 1, it was necessary to operate with a deuterium pressure of 0.3 mm of Hg in the target chamber instead of the 1.5 mm referred to previously.

Counting Equipment

As described above there is a fixed ionization chamber located at $\alpha=90°$, where α is the angle with respect to the forward direction of the beam as measured in the laboratory. A

second ionization chamber is mounted on a heavy spindle whose axis coincides with the transverse axis of the scattering chamber. This second chamber counts in turn the protons ejected through each of the five windows (b' of Fig. 2c) at the angles $\alpha=30°$, 60°, 90°, 120°, 150°. Its position with respect to a window is accurately determined by a diametrically opposite aligning pin (c of Fig. 2c).

Each chamber has a depth of 9.3 mm. The pulses were amplified by independent linear amplifiers, passed through thyratron pulse sharpeners and high vacuum-tube scale-of-two circuits.[8] The outputs of the scalers actuated multivibrator type driving circuits which delivered a power pulse to mechanical recorders.

Since the highest counting rate used was about three protons per second the counting losses due to resolving time of the mechanical recorders were negligible.

Visual checking of the amplifier output with an oscilloscope guarded against spurious counts due to sparks or acoustic disturbances.

TABLE I. *Distribution in angle of protons from deuteron-deuteron reaction.*

E (KEV)	α	$I(\alpha)$	$N(\alpha)$	θ	$N(\theta)$	STATISTICAL PROBABLE ERROR ±%
390	150°	3.25	1.62	153.7°	2.02	2.3
	120	1.43	1.24	126.3	1.41	4.3
	90	1.00	1.00	97.3	1.00	5.2
	60	1.50	1.30	66.3	1.14	4.2
	30	4.75	2.38	33.7	1.92	1.5
320	150	3.38	1.69	153.3	2.07	2.0
	120	1.42	1.23	125.8	1.38	3.3
	90	1.00	1.00	96.7	1.00	2.4
	60	1.49	1.29	65.8	1.15	3.2
	30	4.45	2.22	33.3	1.83	1.7
260	150	3.06	1.53	152.8	1.82	1.5
	120	1.32	1.14	125.1	1.27	6.3
	90	1.00	1.00	95.9	1.00	2.4
	60	1.46	1.26	65.1	1.14	4.7
	30	4.14	2.07	32.8	1.74	1.3
210	150	3.02	1.51	152.7	1.78	3.7
	120	1.37	1.19	124.6	1.30	4.8
	90	1.00	1.00	95.3	1.00	2.4
	60	1.60	1.38	64.6	1.27	3.4
	30	4.08	2.04	32.7	1.75	1.5
140	150	3.02	1.51	152.2	1.72	2.9
	120	1.38	1.19	123.7	1.29	4.7
	90	1.00	1.00	94.3	1.00	2.4
	60	1.48	1.28	63.7	1.20	4.2
	30	3.69	1.84	32.2	1.62	2.5
60	150	2.46	1.23	151.4	1.34	2.6
	120	1.33	1.15	122.4	1.20	5.2
	90	1.00	1.00	92.7	1.00	2.4
	60	1.40	1.21	62.4	1.15	4.5
	30	2.91	1.46	31.4	1.34	2.6

[8] Lifschutz and Lawson, Rev. Sci. Inst. 9, 83 (1937).

COUNTING PROCEDURE

The measurement of the angular distribution was made as follows. During a counting interval the fixed (monitor) chamber counts a number of protons F proportional to the total number of disintegrations produced in the effective target volume. In the same interval the movable chamber records a count M consisting of the protons emerging through one of the five windows[9] plus a background count apparently due to neutron recoils in the ionization chamber. The background in the fixed chamber was negligible since it counted a number of protons of the order of ten times that counted in a given interval by the movable chamber and since further the fluctuations in background count were never observed to exceed reasonable statistical expectations.

To correct for the background of the movable ionization chamber a measure of its magnitude was made at frequent intervals during a run at any one window by excluding the protons from the ionization chamber with a heavy aluminum foil and recording the background count. This was done without moving the chamber.

During a counting interval under these conditions the movable chamber records a background count B while the monitor chamber records a count F_b still proportional to the number of disintegrations in the target volume. A run at any one window then consists of several counting intervals interspersed with background counting intervals. Calling $\bar{F}$, $\bar{M}$, $\bar{B}$, $\bar{F}_b$ the total numbers of the respective counts obtained during a run, the quantity

$$\frac{1}{\bar{F}}\left(\bar{M}-\frac{\bar{F}}{\bar{F}_b}\bar{B}\right)=\frac{\bar{M}}{\bar{F}}-\frac{\bar{B}}{\bar{F}_b}$$

[9] In order to make the signal to noise ratio in the amplifier output as large as possible, the protons were slowed to within two or three centimeters of the end of their range by aluminum foils of stopping power appropriate to the value of proton energy for the window under consideration and to the bombarding energy.

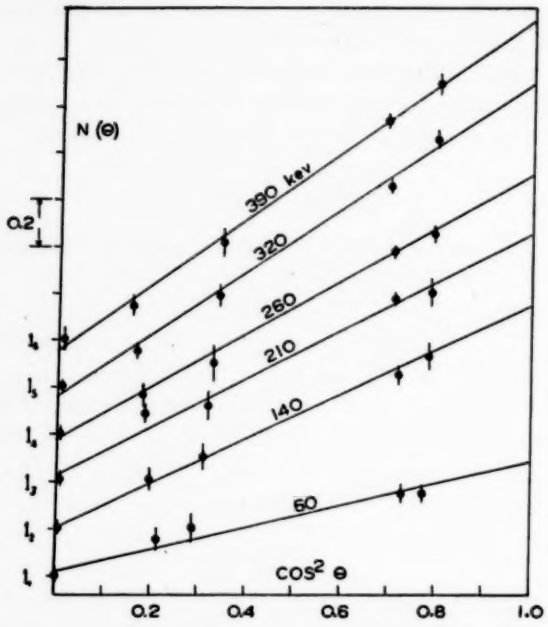

FIG. 3. Angular distribution of the ejected protons plotted against $\cos^2\theta$. Note that the scale for successive curves is shifted 0.2 unit of ordinate. The length of the vertical bar through each point is equal to twice the statistical probable error of that point.

was calculated. The experimental values of this quantity, normalized to unity at $\alpha=90°$, are tabulated as $I(\alpha)$ in Table I. No geometric or other corrections have been applied in calculating $I(\alpha)$, other than the background correction just described.

Several thousand protons were observed at each window at each voltage. The statistical probable errors given in the last column of Table I were calculated in the usual way, remembering that $I(\alpha)$ is the function of experimental data written in the paragraph above.

RESULTS

Examination of the geometry of the target chamber shows that the effective target volume

TABLE II. *Values of $A(E)$ as obtained from Fig. 3.*

E(kev)	60	140	210	260	320	390
A	0.46	0.95	1.02	1.17	1.38	1.49

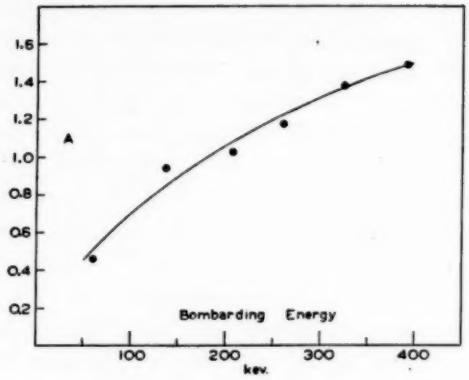

FIG. 4. Values of A as a function of the energy of the incident deuterons.

is with negligible error proportional to $1/\sin\alpha$. Thus, the laboratory angular distribution

$$N(\alpha)=I(\alpha)\sin\alpha.$$

This distribution $N(\alpha)$ has been transformed to the corresponding distribution $N(\theta)$ in the center of mass system.[3]

The results are tabulated in Table I and are exhibited graphically as a function of $\cos^2\theta$ in Fig. 3.

It is evident that the distribution can be reasonably well represented by an equation of the form

$$N(\theta)=1+A(E)\cos^2\theta$$

in which A is a function of the bombarding energy E.

Table II shows the values of $A(E)$ as obtained from the slopes and intercepts of the curves of Fig. 3. These values are quite well represented by the expression $A=A_0E^1$. In Fig. 4 the data of Table II are plotted. Note that E is the bombarding energy as measured in the laboratory.

ACKNOWLEDGMENT

It is a pleasure to acknowledge the skilful assistance of our instrument maker, Mr. J. G. Sentinella, who constructed the target chamber and gave valuable help at all stages of the work.

Magnetic Moments of Odd Nuclei

H. MARGENAU,* *Yale University, New Haven, Connecticut*

AND

E. WIGNER, *Princeton University, Princeton, New Jersey*

(Received May 15, 1940)

To understand the grouping of the nuclear magnetic moments a generalization of Schmidt's single-particle model is considered. In the first approximation, the ground state of an odd nucleus is taken to be a doublet state with definite partition quantum numbers, but involving both possible values of the azimuthal quantum number L. Only very general assumptions are made concerning the detailed composition of the wave function. On this basis the *orbital* part of the magnetic moment turns out to be essentially that following from the liquid drop model; the *spin* part is identical with that of Schmidt. The limits of the magnetic moments, when plotted against J, are given by the solid lines on Fig. 1. Next, we have calculated the deviations from the magnetic moments thus obtained which arise from the admixture of states with higher partition quantum numbers to the original wave function. The result is that the magnetic moment is not greatly changed even when the partition quantum numbers are no longer sharp. (Cf. Fig. 2.) The present model fails to explain the near equality of the moments of isotopes which has been found experimentally.

MAGNETIC MOMENTS OF ODD NUCLEI

1. The rapid accumulation of experimental data on the magnetic moments of nuclei throughout the periodic table on the one hand and the great accuracy which can now be achieved in their measurement on the other, encourage theoretical consideration in this field. Previous calculations of magnetic moments may be divided into two groups: those proceeding with detailed assumptions about nuclear forces and the structure of the nucleus,[1] and others in which more general and qualitative ideas are used. The former calculations are restricted to light nuclei. They involve rather detailed assumptions concerning the nuclear wave functions such as the independent particle model or the α-particle model. Furthermore, Russell-Saunders coupling was assumed throughout until recently when Rose and especially Phillips emphasized the significance of the spin-spin interaction, particularly for the magnetic moments of even nuclei with odd number of protons and neutrons. These calculations were extended and critically reviewed recently by Inglis.[2]

The more schematic considerations of Schüler, Schmidt and Hund[3] as well as those of the present paper are based on the fact that the magnetic moments μ, plotted as function of the total angular momentum J, lie between two rather close curves. This regularity holds for odd nuclei, and the two curves for nuclei with an odd number of protons and those for nuclei with an odd number of neutrons are different. The experimental material at present available is illustrated in Fig. 1.

In order to explain this regularity, the above authors assumed tentatively that the whole magnetic moment is due to a single particle, which is a proton in the former and a neutron in the latter case. Its state can be described by a total and an orbital angular momentum. The former is the total J of the nucleus, the latter, l, is either $J+\frac{1}{2}$ or $J-\frac{1}{2}$. The magnetic moment is calculated by the customary Landé-Goudsmit formula and should lie either on the upper or on the lower broken line of Fig. 1, corresponding to the two possibilities $l=J\pm\frac{1}{2}$.

One would be tempted to interpret the fact that the observed magnetic moments lie *between* rather than *on* these curves by assuming a deviation from the L–S scheme. However, no

* Member of Institute for Advanced Study, Princeton, Autumn, 1939.

[1] M. E. Rose and H. Bethe, Phys. Rev. **51**, 205 (1937); H. Bethe, Phys. Rev. **53**, 842 (1938); L. R. Hafstad and E. Teller, Phys. Rev. **54**, 681 (1938); M. E. Rose, Phys. Rev. **56**, 1064 (1939); M. Phillips, Phys. Rev. **57**, 160 (1940); D. Inglis, Phys. Rev. **51**, 531 (1937); **53**, 882 (1938); **55**, 329 (1939); R. G. Sachs, Phys. Rev. **55**, 825 (1939).

[2] D. R. Inglis, Phys. Rev. **56**, 1175 (1939).

[3] Th. Schmidt, Zeits. f. Physik **106**, 358 (1937); H. Schüler, Zeits. f. Physik **107**, 12 (1937); F. Hund, Physik Zeits. **38**, 929 (1937).

such deviation exists in the nonrelativistic[4] one-body problem, on account of the parity rule. The nearest one could come to the above picture would be to assume for the correct wave function a linear combination of two wave functions of the above kind. These would correspond, respectively, to an even and an odd state of the core, both with angular momentum zero. The orbital angular momentum of the outside particle would be $J-\frac{1}{2}$ in one and $J+\frac{1}{2}$ in the other wave function. Such a model would naturally and directly lead to magnetic moments between the two Schmidt curves. The assumption concerning the angular momentum of the core finds support in the fact that all nuclei with an even number of both protons and neutrons have no angular momentum. The assumption that the whole orbital angular momentum is carried by one particle is to some extent supported by the remark of Hund that the total angular momentum is never greater than $\frac{1}{2}$ plus what the angular momentum of a single particle would be, assuming a reasonable shell structure.[5]

In spite of this, and in spite of the apparent success of the above model for the explanation of nuclear magnetic moments, it seems to us to be somewhat too specialized. In the first place, it is hard to understand that the core wave function should contain only states with zero angular momenta, considering that states with higher angular momenta of the core alone (an even-even nucleus) are known in many cases to be very close to the normal state. It appears indeed highly doubtful that the first excited state of even-even nuclei is a state with zero angular momentum in the majority of all cases. In addition to this, no simple two-particle operator has matrix elements between two wave functions of the above described character. The fact that both occur in an actual wave function would be, therefore, most probably due to the coupling of both to a third part in the wave function which corresponds to a core with a finite angular momentum. Although this third part could be very small, it appears improbable that it should couple only such states in which the core has no angular momentum. It may be mentioned, furthermore, that, as Bethe[6] has pointed out, there should be a marked difference between the Couloumb energies of nuclei with even and odd Z if a single particle model were valid for the last particle. Recent measurements indicate that such an effect, if it exists, is very small.[7] We have decided, therefore, to look for a more general model which is capable of explaining the grouping of the magnetic moments between the two Schmidt curves.

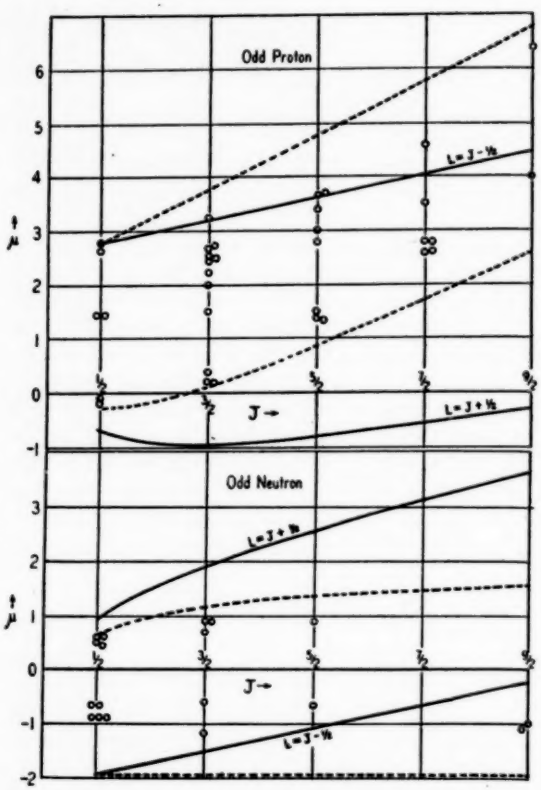

FIG. 1. Magnetic moments of odd nuclei plotted against J. Circles represent experimental values. Solid lines are upper and lower limits as obtained in this paper if only the lowest partition quantum numbers are taken into account. Dotted lines are limits obtained by Schmidt on the basis of a one-particle model.

[4] H. Margenau, Phys. Rev. **57**, 383 (1940). This calculation shows that the relativistic corrections to the magnetic momenta are too small to explain the deviation of the measured momenta from the curves of Fig. 1.

[5] W. Elsasser, J. de phys. et rad. **4**, 549 (1933); **5**, 389 635 (1934); H. Margenau, Phys. Rev. **46**, 613 (1934); F. Hund, reference 3.

[6] H. A. Bethe, Phys. Rev. **54**, 436 (1938).

[7] Recent measurements of W. H. Barkas, E. C. Creutz, L. A. Delsasso and M. G. White and of R. O. Haxby, W. E. Shoupp, W. E. Stephens and W. H. Wells (cf. also Bull. Am. Phys. Soc., New York meeting, February, 1940) show that the Coulomb energy difference is a much smoother function of the atomic mass than appeared at the time reference 6 was written. This applies, according to a kind personal communication of Dr. Stephens, particularly for nuclei with a mass number greater than 9.

This has been attempted before by K. Way[8] using an extreme form of the liquid drop model. She assumed that all particles participate about equally in the orbital motion so that the g factor ($2\,Mc/\hbar e$ times μ/J) for the orbital motion is $n_p/(n_p+n_N)$. This appears quite reasonable. Way assumes a similar g factor for the spin moment also. This would correspond to a very broad distribution of the spin angular momenta over all possible values—an assumption which is hardly acceptable. In the present paper, the g factor of the spin angular momentum will be calculated with a "symmetric Hamiltonian." This will give, essentially, the same g factor for the spin which obtains in Schmidt's model. This part of the model is, thus, to a large degree independent of the assumption that the moment is due to a single particle. For the g factor of the orbital moment, on the other hand, our result is identical with that of K. Way. Assuming Russell-Saunders coupling, we arrive at the conclusion that the magnetic moments should lie on the full lines of Fig. 1 while deviations from Russell-Saunders coupling (which are, of course, quite possible in our model) would shift the magnetic moments to the region between the full lines.

2. In describing the ground states of odd nuclei the assumption will be made that a spin-independent, symmetric Hamiltonian is a good starting point for the calculation of wave functions. In this approximation the states can be characterized by partition quantum numbers $(PP'P'')$ and the normal states of all odd nuclei are doublet states, and also the azimuthal quantum number L and $Y_t=\frac{1}{2}\sum\tau_t\sigma_z$ have sharp values.[9] Considering now interactions which do not satisfy the above requirements, states with different S, L, etc. will mix. The mixing will be much stronger between states with different L and equal S and $(PP'P'')$, than for states which differ also in S and $(PP'P'')$. The reason for this is that states with different L can be very close to the normal state[10] while states with higher S or $(PP'P'')$ belong to a different "supermultiplet" and lie necessarily much higher in first approximation. Our assumption for the normal state will be, that the state has $S=\frac{1}{2}$ and the lowest possible partition quantum numbers (cf. further below), while for L only the assumption will be made that it can give, together with $S=\frac{1}{2}$, the total J of the nucleus. Thus, the wave function will contain both an $L=J-\frac{1}{2}$ and an $L=J+\frac{1}{2}$ part. These assumptions will make the spin moment equal to the value assumed by Schmidt.

In the following two sections, we shall carry out the calculations which were outlined above. Assuming a symmetric Hamiltonian, we could assume that the wave function has the lowest possible partition quantum numbers. This would allow us to calculate the magnetic moments, as outlined above. However, it would not permit us to estimate the deviation from this magnetic moment which is caused by an admixture of states with other partition quantum numbers to the original wave function. This, however, is quite necessary because the $(PP'P'')$ cannot be expected to be good quantum numbers for heavy nuclei. In spite of this, most of the heavy nuclei, also, fall between our two curves. This can be understood on the basis of the above picture only if moderate deviations from the assumed wave functions do not give very large changes in the magnetic moment, i.e., if the magnitude of μ is not changed very strongly even when $(PP'P'')$ loses its strict significance as a quantum number. This will indeed turn out to be the case. In view of this, it should be noted, even the fact that the moments of *all* light nuclei are between the two curves does not *prove* that $(PP'P'')$ is a very good quantum number for them.

3. The so-called magnetic moment of the nucleus, μ, is the component M_Z of the magnetic moment in a direction Z in which the component of the total angular momentum J_Z is equal to the total angular momentum J. The magnetic moment consists of two parts, the orbital magnetic

[8] K. Way, Phys. Rev. **55**, 963 (1939).

[9] E. Wigner, Phys. Rev. **51**, 106 (1937); F. Hund, Zeits. f. Physik **105**, 202 (1937). In explanation of the terminology here used it may be stated that $(PP'P'')$ is the name of a supermultiplet, just as S in atomic spectra labels a multiplet. P is the highest value which either S_z, T_t, or Y_t can take, just as, for ordinary multiplets, S is the highest value which S_z can take. P' is the highest value of one of the remaining pair (e.g. S_x or Y_t if $T_t=P$); P'' is the highest possible value of the remaining operator (e.g., Y_t if $T_t=P$, $S_x=P'$). Mathematically, S_z, T_t and Y_t play entirely identical roles. The normal state of a nucleus has as small values of P, P', P'' as possible. Since $P\geq P'\geq P''$, the best choice for P is the value of T_t. Thus, for the lowest state, $P=T_t$, and P' and P'' are as small as possible. For the low excited states we still have $P=T_t$, but P' and P'' are somewhat greater than for the ground state.

[10] E. Teller and J. A. Wheeler, Phys. Rev. **53**, 778 (1938).

moment Λ_z and the spin magnetic moment Σ_z. It has been discussed repeatedly[11] whether it is permissible to consider the magnetic moment as the sum of the orbital and spin moments of the different particles. We shall assume here that this is permissible within the accuracy of our calculations.

We shall consider first the orbital magnetic moment which is, in units of the Bohr nuclear magneton, equal to the Z component of the orbital momenta of the protons, in units of $\hbar$. As mentioned before, it is not possible to carry out the calculation of this quantity rigorously but we shall adduce a plausibility argument for the correctness of the value assumed by Way.

Let us decompose the total wave function Ψ into parts with definite L and S

$$\Psi=\sum a_{LS}\Psi_{LS}. \tag{1}$$

If Russell-Saunders coupling could be assumed, (1) would consist of only one term. The Ψ_{LS} are assumed to be normalized, the sum of the squares of the $|a_{LS}|$ is 1. Since the total orbital angular momentum does not commute with the Z component of the orbital proton momentum, there will appear in the calculation of $(\Psi, \Lambda_z\Psi)$ certain cross terms between Ψ_{LS} and $\Psi_{L'S}$. These are generally small in comparison with the diagonal terms and will here be disregarded. Justification for this procedure will be given at the end of this section. Thus the orbital magnetic moment for Ψ will be taken to be the sum of the magnetic moments of the different parts of Ψ in (1):

$$(\Psi, \Lambda_z\Psi)=\sum_{LS} |a_{LS}|^2(\Psi_{LS}, \Lambda_z\Psi_{LS}). \tag{2}$$

The Ψ_{LS} in (1) have a definite Z component of the total angular momentum J_z but no definite Z components of L and S. We can denote the functions with definite Z components of L and S, out of which Ψ_{LS} is compounded, by $\Psi_{LSm\mu}$ where m and μ are the Z components L_z and S_z of L and S, respectively. We can then define a g factor for every one of these functions by the equation

$$(\Psi_{LSm\mu}, \Lambda_z\Psi_{LSm\mu})=g_\Lambda(LS)m. \tag{3}$$

The g_Λ do not depend on m or μ but depend, of course, on all other quantum numbers. The matrix elements for Ψ_{LS} can be calculated from the g_Λ by the well-known Landé-Goudsmit formula

$$(\Psi_{LS}, \Lambda_z\Psi_{LS}) = J_z\frac{J(J+1)+L(L+1)-S(S+1)}{2J(J+1)}g_\Lambda(LS). \tag{4}$$

Our task is therefore to calculate the $g_\Lambda(LS)$. For this purpose we can further decompose each $\Psi_{LSm\mu}$ into parts in which the total orbital momenta of the protons and neutrons alone have definite values, l and l':

$$\Psi_{LS}=\sum_{ll'} b_{LSll'}\Psi_{LSll'}. \tag{5}$$

Again the sum of $|b_{LSll'}|^2$ over l and l' is 1, and the matrix element $(\Psi_{LS}, \Lambda_z\Psi_{LS})$ can be calculated as the sum of the matrix elements of Λ_z for the different $\Psi_{LSll'}$ separately. Formulas derivable from the vector addition principle yield immediately (since the g factor for protons is 1, for neutrons 0)

$$g_\Lambda(LS)=\sum_{ll'} |b_{LSll'}|^2\frac{L(L+1)+l(l+1)-l'(l'+1)}{2L(L+1)}. \tag{6}$$

The summation in (6) must be carried out, in general, over all values of l and l' which can give a total L according to the vector addition model. Eqs. (4) and (6) give the average value of Λ_z for the wave function Ψ_{LS} in terms of the probabilities for this L being composed in the different possible ways out of orbital momenta of protons and neutrons, l and l'. At this point it is necessary to make some assumption concerning these probabilities. For a nucleus with an equal number of neutrons and protons, it follows from the symmetry of the Hamiltonian with respect to protons and neutrons that the probability for the angular momenta l and l' for protons and neutrons, is equal to the probability for the momenta l' and l. This means $|b_{LSll'}|^2=|b_{LSl'l}|^2$ and, under this condition, (6) can be summed up and gives $\frac{1}{2}$. This is in agreement with Way's value $n_P/(n_p+n_N)$. It can be shown, furthermore, that for $n_P\neq n_N$, the deviation of (6) from $\frac{1}{2}$ is proportional to the neutron excess. This is also in agreement with Way's assumption. It is not possible to show, in general, that the proportionality constant is $\frac{1}{2}(n_P+n_N)^{-1}$; in fact, it could be different for

[11] Cf. W. E. Lamb and L. I. Schiff, Phys. Rev. **53**, 651 (1938); D. R. Inglis, reference 2.

different isotopic spin multiplets. However, it clearly has this value if $n_P=0$ (in this case $l=0$ in (6)) and we shall assume it henceforth.

Schmidt's assumption, on the other hand, would amount to $b_{LSll'}=0$ unless $l'=0$ in case of an odd n_P, and $b_{LSll'}=0$ unless $l=0$ in case of odd n_N. Although, as mentioned before, this gives results which are in closer agreement with experimental data than our results are, we could not satisfy ourselves that it conforms with the picture of nuclear structure formed on the basis of other lines of evidence. It should be mentioned, however, that the nuclear moment does not depend critically on the validity of these assumptions since the whole orbital magnetic moment plays only a subordinate role in the total moment. Thus our curves do not differ greatly from Schmidt's.

Our final result for the orbital part of the magnetic moment is

$$(\Psi, \Lambda_Z\Psi)=\sum_{LS}|a_{LS}|^2\frac{n_P}{n_P+n_N}J_Z \times\frac{J(J+1)+L(L+1)-S(S+1)}{2J(J+1)}. \quad (7)$$

The $|a_{LS}|^2$ will be determined later.

We have neglected some cross terms in Eq. (2) and we wish now to give an estimate for them. Their exact calculation would, of course, necessitate the use of a specific nuclear model which would yield the coefficients $b_{LSll'}$, whose number is unlimited. Each cross term involves a summation of the type

$$\sum_{ll'} b_{LSll'}{}^* b_{L'Sll'}(\Psi_{LSll'}, \Lambda_Z\Psi_{L'Sll'}).$$

These cross terms vanish, of course, unless $L'=L\pm1$. For their evaluation it is important to note that the proton and neutron wave functions ψ_l and $\psi_{l'}$ out of which $\Psi_{LSll'}$ is composed, are in general different from the wave functions ψ_l' and $\psi_{l'}'$ out of which $\Psi_{L'Sll'}$ is composed. However, the matrix elements of Λ_Z are largest if $\psi_l=\psi_l'$ and $\psi_{l'}=\psi_{l'}'$ and are otherwise proportional to the scalar products of these wave functions. These scalar products must be expected to be quite small. Furthermore, the b will vary quite irregularly as to sign and magnitude, and since the sum of their squares is unity, the result of the summation is further diminished. (The Hartree model would be quite unsuited for the calculation of the above sums since it gives only a small number of b's and since the above ψ_l, $\psi_{l'}$ are closely related to the ψ_l', $\psi_{l'}'$.)

4. For the calculation of the spin magnetic moment we decompose the wave function into parts which have definite partition quantum numbers $(PP'P'')$ and definite angular momenta L

$$\Psi=\sum c_{PL}\Psi_{PL}. \quad (8)$$

P is an abbreviation for $(PP'P'')$ (the (STY) of reference 9). The Ψ_{PL} are assumed to be normalized, the sum of the squares of $|c_{PL}|$ is 1. If the "first approximation" of reference 9 could be assumed to be valid, (8) would contain only one term, corresponding to a single partition and a single L. Actually, it will be necessary to assume that terms corresponding to more than one value of L, at least, occur in (8). The operator for the magnetic moment is

$$\begin{aligned}\Sigma_Z&=\mu_P\sum_i\tfrac{1}{2}(1-\tau_{\mathfrak{z}i})\sigma_{Zi}+\mu_N\sum_i\tfrac{1}{2}(1+\tau_{\mathfrak{z}i})\sigma_{Zi}\\&=\tfrac{1}{2}(\mu_P+\mu_N)\sum_i\sigma_{Zi}+\tfrac{1}{2}(\mu_N-\mu_P)\sum_i\tau_{\mathfrak{z}i}\sigma_{Zi}.\end{aligned} \quad (9)$$

Here, $\tau_{\mathfrak{z}i}$ is the isotopic spin coordinate for the ith particle. Its value is 1 for neutrons, -1 for protons. The σ_{Zi} are the usual matrices for the Z components of the spin angular momenta, with characteristic values $+1$ and -1. The μ_P and μ_N are the magnetic moments of proton and neutron. If we again express all magnetic moments in nuclear Bohr magnetons $e\hbar/2Mc$, (9) becomes

$$\Sigma_Z=0.855S_Z-4.715Y_{\mathfrak{z}}, \quad (9a)$$

where

$$S_Z=\tfrac{1}{2}\sum_i\sigma_{Zi};\quad Y_{\mathfrak{z}}=\tfrac{1}{2}\sum_i\tau_{\mathfrak{z}i}\sigma_{Zi}.$$

Since (9a) does not depend on space coordinates, it has no matrix elements between parts of the wave function which belong to different L or to different partitions. Its mean value is, therefore

$$(\Psi, \Sigma_Z\Psi)=\sum_{PL}|c_{PL}|^2(\Psi_{PL}, \Sigma_Z\Psi_{PL}), \quad (10)$$

i.e., simply the sum of the magnetic moments of the different parts of Ψ. In atomic spectra, the partition quantum number completely determines the total spin angular momentum S, and

conversely S determines the partition quantum number so that it is sufficient to specify one of these. In nuclear problems, on the other hand, because of the existence of the isotopic spin, we have "supermultiplets" and, except for special cases, several S values belong to one supermultiplet and have the same energy if we disregard spin dependent forces. Nevertheless, S can be specified simultaneously with $(PP'P'')$, J, J_z and L. Hence, Ψ_{PL} can be decomposed again:

$$\Psi_{PL}=\sum_S c_S{}^{PL}\Psi_{PLS}, \tag{11}$$

where again

$$\sum_S |c_S{}^{PL}|^2=1.$$

TABLE I. *Magnetic moments of nuclei with odd proton and with odd neutron.*

	J	μ	SOURCE
	Odd Proton		
H^1	1/2	2.79	1
Li^7	3/2	3.25	2
B^{11}	3/2?	2.682	3
F^{19}	1/2	2.62	2
Na^{23}	3/2	2.216	4
Al^{27}	5/2	3.628	5
Cl^{35}	5/2?	1.365?	6
K^{39}	3/2	0.391	4
K^{41}	3/2	0.22	7
Sc^{45}	7/2	4.4–4.8	8
Mn^{55}	5/2	3.0	9
Co^{59}	7/2	3.5	10
Cu^{63}	3/2	2.43	11
Cu^{65}	3/2	2.54	11
Ga^{69}	3/2	2.11	12, 32
Ga^{71}	3/2	2.69	12, 32
As^{75}	3/2	1.5	13
Rb^{85}	5/2	1.34	6
Rb^{87}	3/2	2.74	6
Ag^{107}	1/2	−0.10	14
Ag^{109}	1/2	−0.19	14
In^{115}	9/2	6.4	15
Sb^{121}	5/2	3.7	16
Sb^{123}	7/2	2.8	16
I^{127}	5/2	2.8	17
Cs^{133}	7/2	2.57	4
La^{139}	7/2	2.8	16
	Odd Proton		
Eu^{151}	5/2	3.4	16
Eu^{153}	5/2	1.5	16
Lu^{175}	7/2	2.6	18
Au^{197}	3/2?	0.2	16
Tl^{203}	1/2	1.45	19
Tl^{205}	1/2	1.45	19
Bi^{209}	9/2	4.0	20
	Odd Neutron		
Be^9	3/2?	−1.175	21
Zn^{67}	5/2	0.9	22
Kr^{83}	9/2?	−1.	23
Sr^{87}	9/2	∼−1.1	24
Cd^{111}	1/2	−0.65	25
Cd^{113}	1/2	−0.65	25
Sn^{117}	1/2	−0.89	26
Sn^{119}	1/2	−0.89	26
Xe^{129}	1/2	−0.9	23
Xe^{131}	3/2	0.7	27, 23
Ba^{135}	3/2	0.9	28
Ba^{137}	3/2	0.9	28
Yb^{171}	1/2	0.45	30
Yb^{173}	5/2	−0.65	30
Pt^{195}	1/2	0.6	31
Hg^{199}	1/2	0.5	29
Hg^{201}	3/2	−0.6	29
Pb^{207}	1/2	0.6	23

[1] Kellogg, Rabi, Ramsey, Zacharias, Phys. Rev. **56**, 728 (1939).
[2] Rabi, Millman, Kusch, Zacharias, Phys. Rev. **55**, 526 (1939).
[3] Millman, Kusch, Rabi, Phys. Rev. **56**, 165 (1939).
[4] Kusch, Millman, Rabi, Phys. Rev. **55**, 1176 (1939).
[5] S. Millman and P. Kusch, Phys. Rev. **56**, 303 (1939).
[6] P. Kusch and S. Millman, Phys. Rev. **56**, 527 (1939).
[7] J. H. Manley, Phys. Rev. **49**, 921 (1936).
[8] H. Kopfermann and H. Wittke, Zeits. f. Physik **105**, 16 (1937).
[9] R. A. Fisher and E. R. Peck, Phys. Rev. **55**, 270 (1939).
[10] K. R. More, Phys. Rev. **46**, 470 (1934).
[11] Tolanski and Forester, Proc. Phys. Soc. **50**, 826 (1938).
[12] Schüler and Korsching, Zeits. f. Physik **103**, 424 (1936).
[13] Schüler and Marketu, Zeits. f. Physik **102**, 703 (1936).
[14] D. A. Jackson and H. Kuhn, Proc. Roy. Soc. **158**, 372 (1937).
[15] Millman, Rabi, Zacharias, Phys. Rev. **53**, 384 (1938).
[16] Schmidt, Zeits. f. Physik **108**, 408 (1938).
[17] Schmidt, Zeits. f. Physik **112**, 199 (1939).
[18] Gollnow, Zeits. f. Physik **103**, 443 (1936).
[19] Schüler and Schmidt, Zeits. f. Physik **104**, 468 (1937).
[20] A. B. McLay and M. F. Crawford, Phys. Rev. **44**, 986 (1933).
[21] Kusch, Millman and Rabi, Phys. Rev. **55**, 666 (1939).
[22] Lyshede and Rasmussen, Zeits. f. Physik **104**, 434 (1937).
[23] H. A. Bethe and R. F. Bacher, Rev. Mod. Phys. **8**, 82 (1936).
[24] Heyden and Kopfermann, Zeits. f. Physik **108**, 232 (1938).
[25] Schüler and Keyston, Zeits. f. Physik **71**, 413 (1931).
[26] Schüler and Westmeyer, Naturwiss. **21**, 660 (1933).
[27] Kopfermann and Rindal, Zeits. f. Physik **87**, 460 (1934).
[28] A. Benson and R. A. Sawyer, Phys. Rev. **49**, 867 (1936).
[29] Schüler and Jones, Zeits. f. Physik **74**, 631 (1932).
[30] Schüler and Korsching, Zeits. f. Physik **111**, 386 (1939).
[31] Schmidt, Zeits. f. Physik **101**, 486 (1936).
[32] N. A. Renzetti, Phys. Rev. **57**, 753 (1940).

Introducing this into (10) we obtain

$$(\Psi,\Sigma_z\Psi)=\sum_{PLS}|c_{PL}|^2|c_S{}^{PL}|^2(\Psi_{PLS},\Sigma_z\Psi_{PLS}), \tag{12}$$

plus nondiagonal matrix elements in which Ψ_{PLS} is combined with a $\Psi_{PLS'}$. We shall neglect the latter, for reasons which will be apparent later. In order to calculate the $(\Psi_{PLS},\ \Sigma_z\Psi_{PLS})$, we can go over from the wave functions Ψ_{PLS} in which J, J_z, L, S are specified, to wave functions $\psi_{PLSm\mu}$ in which J, L, S, $L_z=m$, $S_z=\mu$ are specified. We define in analogy to (3)

$$(\Psi_{LSm\mu},\Sigma_z\Psi_{LSm\mu})=g_S(PS)\mu. \tag{13}$$

Since the operator Σ_z contains only spin quantities, its matrix elements are uniquely given if the dependence of $\Psi_{LSm\mu}$ on the ordinary and isotopic spin coordinates is known; that is, they are given by the partition quantum numbers $(PP'P'')$ and S. In particular, g_S is independent of L and the same for all wave functions with the same $(PP'P'')$ and S. For (12) we have according to the oft-quoted Landé-Goudsmit formula,

$$(\Psi_{PLS},\Sigma_z\Psi_{PLS})=J_z\frac{J(J+1)+S(S+1)-L(L+1)}{2J(J+1)}g_S(PS). \tag{14}$$

The calculation of the spin part of the magnetic moment is thus reduced to the calculation of the $|c_{PL}|^2$, the $|c_S{}^{PL}|^2$, and the $g_S(PS)$. The only approximation made so far is the neglect of the off-diagonal elements mentioned after Eq. (12).

The partition which has the lowest energy in the approximation in which the spin dependent forces are neglected is[12] $(PP'P'')=(T_t\tfrac{1}{2}\pm\tfrac{1}{2})$ where $T_t=\frac{1}{2}(n_N-n_P)$ is the isotopic spin. We thus obtain to this approximation for the elements with isotopic spin T_t only one S, namely $S=\frac{1}{2}$. Hence the L values in (10) which are compatible with a definite J are $J-\frac{1}{2}$ and $J+\frac{1}{2}$. If we assume that this partition alone is present in Ψ, (10) contains only two terms, P assuming only one and L only two values. For both of these, (11) contains only one term, corresponding to $S=\frac{1}{2}$, and there are, of course, no off-diagonal elements in addition to the terms (12) so that (14) holds in this case rigorously.

[12] E. Wigner, Phys. Rev. **51**, 947 (1937).

The value of $g_S(PS)$ can be obtained rigorously also. The first part of Σ_z in (9a) gives simply 0.855μ in (13). The second part gives $-4715\cdot\frac{1}{2}$ if $\mu=S_z=\frac{1}{2}$ and if we have a $(T_t\frac{1}{2}\frac{1}{2})$ multiplet. It gives $+4715\cdot\frac{1}{2}$ if $\mu=\frac{1}{2}$ and we have a $(T_t\frac{1}{2}-\frac{1}{2})$ multiplet. This is evident even from the definition of the $(PP'P'')$ symbols: P is the maximum possible value of the isotopic spin T_t for the supermultiplet. $P'=\frac{1}{2}$ is the maximum value of S_z, compatible with the value P for T_t (it is because of this that S is uniquely given). P'', finally, is the maximum value of Y_t (in our case the only value) which is compatible with the maximum values of P and P'. Hence we obtain for

$$g_S((T_t\tfrac{1}{2}\pm\tfrac{1}{2}), L, \tfrac{1}{2})=0.855\mp4.715. \quad (15)$$

The sum $P+P'+P''$ has the form $2k-\frac{1}{2}(n_N+n_P)$ with an integer k. In our case, furthermore, $P=\frac{1}{2}(n_N-n_P)$ so that $P'+P''$ has the form $2k-n_N$. Since $P'=\frac{1}{2}$, we have $P''=+\frac{1}{2}$ if the number of neutrons is odd, $P''=-\frac{1}{2}$ if the number of neutrons is even, that of the protons therefore odd. In the former case the upper sign holds in (15), in the latter case the lower. The g_S which one obtains in this way, -3.86 and 5.57 are $2\mu_N$ and $2\mu_P$, i.e., the g factors for a single neutron and proton. This had to be expected as soon as it was established that the g_S can be calculated uniquely on the basis of our assumptions and are, thus, to a large degree independent of a special model. In consequence hereof, the g factor can be calculated using any special model compatible with the validity of the first approximation of reference 9. Such a model is, e.g., that consisting of one extra particle outside a closed, unmagnetic shell which contains an even number of protons and neutrons. The g factor for such a model is evidently that for the single particle outside the shell. Thus the mean value of Σ_z is identical with the one postulated by Schmidt.

We can now easily calculate the mean value of Λ_z also. If one assumes Russell-Saunders coupling, L can be either $J-\frac{1}{2}$ or $J+\frac{1}{2}$, and thus either $|a_{J-\frac{1}{2}}|^2$ or $|a_{J+\frac{1}{2}}|^2$ is one in (7), while all the other a_{LS} become zero. The whole magnetic moment should correspond, therefore, to one of these possibilities, represented by the full lines of Fig. 1. However, it was pointed out in the introduction that one hardly can expect strict

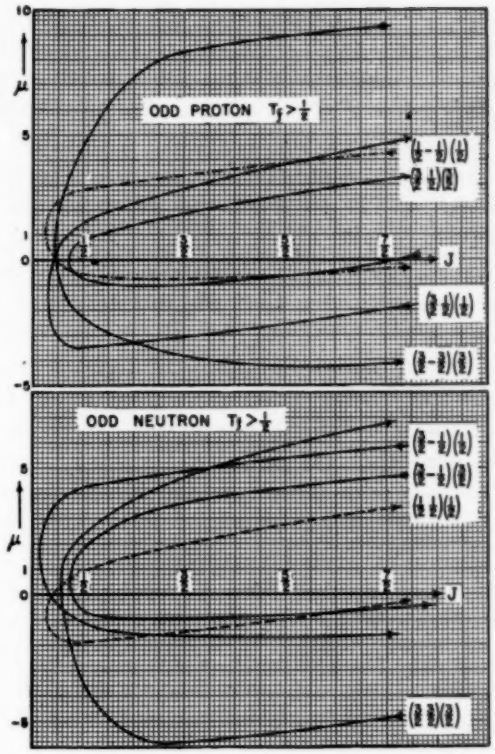

FIG. 2. Solid lines represent limits of magnetic moments for states of higher partition quantum numbers. Parentheses mean $(P'P'')(S)$. The two branches of the curves correspond to $L=|J-S|$ and $L=J+S$; the arrow points in the direction from $|J-S|$ to $J+S$. The broken lines are identical with the full lines of Fig. 1.

L–S coupling, and this makes the whole region between the full lines possible. Schmidt's curves are given as broken lines. Table I contains the experimental material used in preparing these figures.

5. Figure 1 shows that most magnetic moments lie in the region expected under the assumption that the partition of the wave function is $(T_t\frac{1}{2}+\frac{1}{2})$.[13] This does not prove, of course, that this assumption is correct because it remains possible that the magnetic moments lie in this region even if other partitions are also present. In order to decide this point, it would be necessary to calculate the magnetic moment without the above assumption. This, however, is clearly impossible, as long as the coefficients in (10) are unknown. We have adopted, therefore, the following procedure.

[13] The elements whose magnetic moments do not fall between the full lines in Fig. 1 are: In^{115} (odd proton), Kr^{83} and Sr^{87} (odd neutron). They all have $J=9/2$.

Equation (12) shows that the total spin magnetic moment $(\Psi, \Sigma_z\Psi)$ is the average of the spin magnetic moments of the different Ψ_{PLS} with weights $|c_{PLC_S}{}^{PL}|^2$ which are the probabilities for the corresponding partition, azimuthal and spin quantum numbers. In this, only the terms omitted in (12) are neglected which are always relatively small. The same thing holds for the orbital magnetic moment, given by (7). We have, therefore, calculated the total magnetic moment assuming that only one P, S and L occur in the total wave function but permitting various possibilities for these. The real magnetic moment would be a weighted average of the magnetic moments obtained in this way.

The results of these calculations are given in the Fig. 2. The broken lines are identical with the full lines of Fig. 1 and correspond to the partition $(T_t\frac{1}{2}\pm\frac{1}{2})$. The other lines correspond to higher multiplets $(PP'P'')$, all with $P=T_t$ while $(P'P'')(S)$ are given in brackets. The S is, naturally, always smaller than or equal to P'. The two branches of the curves correspond to $L=|J-S|$ and $L=J+S$, the arrow points in the direction from $|J-S|$ to $J+S$. The values of the magnetic moment for intermediate values of L are in all cases between the two branches of the curve.

For (7), $n_p/(n_p+n_N)=\frac{1}{2}$ was assumed. In order to calculate the spin magnetic moment by (12) and (14) the $g_S(PS)$ of (13) must be known. These consist of two parts, corresponding to the two parts of Σ_z in (9a). The first part is evidently 0.855. The second part depends on the matrix elements of Y_t.

In all the partitions considered, every S occurs only once in every supermultiplet for $T_t=P$. This means that although several terms are united to a supermultiplet, all these terms have different S. The g_S for the largest $S=P'$ is given by the fact that the matrix element of Y_t is P'' for the wave function with $T_t=P$, $S_z=S=P'$. For this S, therefore, the value of g_S is $4.715P''/P'$. The sum of the matrix elements of Y_t for $S_z=P'-1$ can be obtained from Fig. 1 of reference 9 as the sum of the possible values of Y_t for this value of S_z and T_t. If we subtract from this value the matrix element corresponding to the state $S_z=S-1$, $S=P'$, which is $P''(S-1)/S$, we obtain the matrix element for the state $S_z=S=P'-1$ and this gives the g_S for $S=P'-1$ if there is such a state. The matrix elements of Y_t and hence the g_S and hence all the matrix elements of the spin magnetic moment can be determined in this way. The calculation was carried out for those $(PP'P'')$ which give, according to Eqs. (10), (15) of reference 12 the lowest energies.

The fact that all moments of light nuclei and practically all moments of the other elements lie between the limits valid for the $(T_t\frac{1}{2}+\frac{1}{2})$ multiplet indicates, at any rate, that this multiplet plays a preponderant role in the normal state of odd elements.

6. We wish to point in conclusion to an experimental finding which gives reason to more serious doubts in the considerations presented here than anything mentioned above. According to the preceding considerations, the magnetic moments are expected to be distributed between the two lines of Fig. 1 in a rather random fashion. We cannot see any reason, however, why two isotopes with equal total angular momenta should have exactly equal magnetic moments. In fact we fail to see any model which would explain such a result.[14] In spite of this, so nearly equal moments for isotopes seem to have been found in at least three cases (Cu, Re, In) that it does not appear possible to blame this on a chance coincidence. We are unable to give an explanation for this phenomenon.

[14] H. Schüler and H. Korsching, Zeits. f. Physik **105**, 168 (1937).

On the Theory of the Thermal Diffusion Coefficient for Isotopes

R. CLARK JONES
Research Laboratory of Physics, Harvard University, Cambridge, Massachusetts

(Received May 4, 1940)

Enskog's general theory of thermal diffusion holds for a gas of spherically symmetrical molecules which is sufficiently dilute that collisions of more than two molecules at a time are of negligible importance. The first approximation to the thermal diffusion constant of a mixture of two isotopes is derived from this theory. The result is presented in terms of suitably defined cross-section integrals, in which the intermolecular forces are not yet specialized. This general formula for the thermal diffusion constant α is then worked out explicitly for several well-known molecular models: the elastic sphere model, the inverse power model, the Sutherland model, and the Lennard-Jones model. The various limitations on the accuracy of the theory are discussed, and the theoretical results are compared with the very few experimental data which are as yet available. The comparison indicates that the customary molecular models of kinetic theory are hardly adequate to give a satisfactory account of thermal diffusion. These models are relatively satisfactory for the elementary free-path phenomena to which they are usually applied, but they are not sufficiently precise to meet the more exacting test of thermal diffusion. The best check between theory and experiment is obtained for neon with the Sutherland model. The use of this model, however, places the entire burden of accounting for the observed decrease of α with temperature on the attractive part of the intermolecular forces, whereas in view of the smallness of this attractive force as determined by other methods, it can hardly be doubted that the decrease is actually due to the increased "softness" of the repulsive force at low temperatures.

THE importance of the phenomenon of thermal diffusion has recently been enhanced by the striking success of its use in separating isotopes.[1,2] With this success has come the need for a more complete knowledge of the value of the thermal diffusion coefficient for a mixture of isotopes. The theoretical value of this coefficient for two simple molecular models has already been stated,[3,4] but the relation of these results to the general theory of thermal diffusion has not been given. It is the purpose of this paper to indicate the general expression for the coefficient of thermal diffusion in the case of isotopes, and to derive from this general expression the results which have previously been stated without proof. We shall also derive the theoretical value of the coefficient for certain other molecular models, and compare these theoretical results with the small amount of experimental data which is available.

[1] K. Clusius and G. Dickel, Zeits. f. physik. Chemie **44**, 397 (1939).
[2] R. Clark Jones and W. H. Furry, Rev. Mod. Phys., to be published.
[3] W. H. Furry, R. Clark Jones, and L. Onsager, Phys. Rev. **55**, 1083 (1939).
[4] R. Clark Jones and W. H. Furry, Phys. Rev. **57**, 547L (1940).

NOTATION AND DEFINITIONS

The phenomenon of thermal diffusion consists in the fact that a temperature gradient in a mixture of two gases gives rise to a gradient of the relative concentration of the two constituents. We shall discuss here only the case of a mixture of two isotopes of the same gas. Let c_1 be fractional *particle* density of the lighter molecules, and c_2 the corresponding quantity for the heavier molecules. The concentrations c_1 and c_2 are thus also the fractional partial pressures of the two species. We clearly have

$$c_1+c_2=1. \tag{1}$$

Let $\mathbf{v}_1$ be the *convection* velocity of the lighter molecules, and $\mathbf{v}_2$ the convection velocity of the heavier molecules. The convection velocity of the gas as a whole is given by

$$\mathbf{v}=c_1\mathbf{v}_1+c_2\mathbf{v}_2. \tag{2}$$

The coefficient of ordinary diffusion, D_{12}, and the coefficient of thermal diffusion, D_T, are then defined as the quantities which appear in the equation of diffusion

$$\begin{aligned} c_1(\mathbf{v}_1-\mathbf{v}) &= c_1c_2(\mathbf{v}_1-\mathbf{v}_2) \\ &= -D_{12}\,\text{grad}\,c_1+D_T\,\text{grad}\log T. \end{aligned} \tag{3}$$

Unlike the coefficient of ordinary diffusion, the

coefficient of thermal diffusion is proportional to the product c_1c_2. We are therefore led to introduce another quantity, the thermal diffusion constant α, which is related to D_T by

$$\alpha = D_T/(D_{12}c_1c_2). \tag{4}$$

In the remainder of this paper we shall refer to α rather than D_T.

Qualitative Remarks

To a far greater extent than is the case with the three ordinary gas coefficients, the value of the thermal diffusion constant is sensitive to the molecular model. The free-path arguments of elementary kinetic theory are quite inadequate to give either its existence or its sign. Chapman[5] has dwelt at some length on the difficulties which beset any attempt to explain the effect upon elementary grounds. Recently, however, Frankel[6] has shown that it is possible to derive by means of a dimensional argument all of the essential features of the coefficient for the important special case of the inverse power model. This will be discussed in more detail later on when we examine this model.

The history of the theoretical development of thermal diffusion is rather interesting, but it will not be discussed here because it is presented elsewhere—briefly in reference 2, and more completely in reference 9.

The theory of thermal diffusion appears as a by-product of any sufficiently complete and rigorous kinetic theory of the phenomena of thermal conductivity, viscosity, and diffusion in gases. Two correct presentations of such a theory are now available. The first was given by Enskog[7] in his doctoral dissertation, as supplemented by an article[8] which appeared later. The second is in the recent book by Chapman and Cowling.[9] The former is more abstract and rather difficult to read. The latter has the disadvantage that its notation differs from that used by Enskog and most other recent writers on this subject. Chiefly because it is more concise, the notation of Enskog will be used in this article. The relation of the notation used by Chapman and Cowling to that used here, will, however, be indicated.

The theory of Enskog holds for a gas of spherically symmetrical molecules which is sufficiently dilute that triple collisions are of negligible importance in comparison with collisions of two molecules. The general expression obtained for α is the ratio of an infinite determinant to one of its minors; the elements of the determinants are integrals over the velocity spaces of the two molecules. The result which we shall present in this paper is the first approximation to the exact result.

The case of isotopes represents a simplification in the value of α as compared with the case of dissimilar molecules which is analogous to the simplicity of the coefficient of self-diffusion as compared with the coefficient of diffusion for two dissimilar gases. This simplification occurs because in the case of a gas consisting of a mixture of isotopes, we may suppose that the force fields of all the molecules are identical, since the field of force is determined only by the electronic configuration, and not by the mass of the nucleus.

Detailed Theory

The exact result is expressible in terms of integrals over the orbit of a molecule of species 1 as it moves in the field of a molecule of species 2. If the force fields of the molecules fall off with distance with sufficient rapidity for the gas to have an equation of state which is independent of the shape of its container, it is always possible to define an impact parameter and a relative velocity at infinity for a collision between two molecules. Let the impact parameter be indicated by b, and the relative velocity at infinity by g. Enskog then changes the scale of b and g according to the transformation:

$$g = (2kT/m)^{\frac{1}{2}}\gamma, \tag{5}$$

$$b = s\sigma(\gamma)\beta, \tag{6}$$

where $m = m_1m_2/(m_1+m_2)$ is the reduced mass, s is an arbitrary constant length, and $\sigma(\gamma)$ is an arbitrary function of γ and therefore of g. This method of factorization of the impact

[5] S. Chapman, Phil. Mag. **7**, 1 (1929).
[6] S. P. Frankel, Phys. Rev. **57**, 661L (1940).
[7] D. Enskog, Doctoral Dissertation, Upsala, 1917.
[8] D. Enskog, Arkiv f. Mat., Astron., och Fysik **16**, No. 16 (1922).
[9] S. Chapman and T. G. Cowling, *The Mathematical Theory of Non-uniform Gases* (Cambridge, 1939).

parameter, b, leads in practice to a considerable simplification of the formulae, provided that s and $\sigma(\gamma)$ are suitably chosen.

Let $\theta(\beta, \gamma)$ be the angle of deflection suffered by either molecule when it is deflected by the field of force of another, as measured in the center of gravity coordinate system. We may now define the quantities

$$\Theta^{(l)}(\gamma) = \int_0^\infty \{1 - P_l(\cos\theta)\}\beta d\beta \tag{7}$$

and in turn the quantities

$$\Omega^{(l,k)} = \int_0^\infty e^{-\gamma^2}\sigma^2(\gamma)\gamma^k\Theta^{(l)}(\gamma)d\gamma. \tag{8}$$

The Ω's are dimensionless collision cross sections suitably averaged over β and γ. Enskog would write s, σ, $\Theta^{(l)}$, and $\Omega^{(l,k)}$ with the subscript 12. Since we shall have little occasion to refer to these quantities except when they refer to a collision between a molecule of species 1 and a molecule of species 2, we shall continue to omit the subscript. Note that it is not $\Omega^{(l,k)}$, but rather $s^2\Omega^{(l,k)}$ which is independent of the choice of s and σ. The expression (12) for α is independent of s, but this is not true of the expressions for the coefficients of viscosity and diffusion.

The procedure of Chapman and Cowling[9] is similar. They define the quantities

$$\phi^{(l)} = \int_0^\infty \{1 - \cos^l\theta\} g b db \tag{9}$$

and

$$\Omega^{(l)}(r) = \pi^{\frac{1}{2}}\int_0^\infty e^{-\gamma^2}\gamma^{2r+2}\phi^{(l)}d\gamma. \tag{10}$$

The relation between the two sets of quantities is thus

$$\begin{aligned} &\phi^{(1)} = s^2\sigma^2 g\Theta^{(1)}; \quad \phi^{(2)} = \tfrac{2}{3}s^2\sigma^2 g\Theta^{(2)}, \\ &\Omega^{(1)}(r) = s^2(2\pi kT/m)^{\frac{1}{2}}\Omega^{(1,\,2r+3)} \\ &\Omega^{(2)}(r) = \tfrac{2}{3}s^2(2\pi kT/m)^{\frac{1}{2}}\Omega^{(2,\,2r+3)}. \end{aligned} \tag{11}$$

There are no one-to-one relations of the type (11) for values of l greater than two.

We have already stated that the exact expression for α which is valid for a mixture of any two gases whose molecules are spherically symmetrical comes out of the theory as the ratio of two infinite determinants. In the case of isotopes, we may consider that the force fields of all the molecules are identical, since the force fields are determined entirely by the electronic configuration of the atoms or molecules. The first approximation to the exact expression, which is given by Enskog* and Chapman and Cowling,† may then be developed in a series of ascending powers of $(m_2-m_1)/(m_2+m_1)$. Only the first term of this series is important for most pairs of isotopes.

In the notation of Enskog, the first term of this series expansion is

$$\alpha = \frac{45}{2}\frac{m_2-m_1}{m_2+m_1}\frac{(2\Omega^{(1,7)}-5\Omega^{(1,5)})(15\Omega^{(1,5)}+2\Omega^{(2,7)})}{\Omega^{(2,7)}(165\Omega^{(1,5)}-60\Omega^{(1,7)}+12\Omega^{(1,9)}+16\Omega^{(2,7)})}. \tag{12}$$

Since this expression is homogeneous and of order zero in the $\Omega^{(l,k)}$'s, the expression for α in terms of the $\Omega^{(l)}(r)$'s used by Chapman and Cowling will differ only in the substitution of $(3/2)\Omega^{(2)}(2)$ for $\Omega^{(2,7)}$, and of $\Omega^{(1)}(r)$ for $\Omega^{(1,2r+3)}$.

We now proceed to the evaluation of this expression for certain simple molecular models, namely: elastic spheres, the inverse power model, the Sutherland model, and the Lennard-Jones model. The values of $\Theta^{(l)}$ which we shall use are sprinkled through the literature in a variety of notations. In the case of the elastic sphere and inverse power models, the derivations of the quantities $\Theta^{(l)}$ will be presented, not because the derivations are elsewhere unavailable, but because they may be given so simply and briefly that it seems worth while to give them as illustrations of the concrete meaning of the formulae.

The Elastic Sphere Model

We shall suppose each molecule to behave as a smooth, rigid, elastic sphere of diameter s. The molecules of species 1 have the mass m_1, and the molecules of species 2 have the mass m_2, where $m_1 < m_2$.

Let us observe the collision between one molecule of species 1 and another of species 2.

* Reference 8, p. 51.
† Reference 9, p. 253.

We shall imagine ourselves at rest in the center of gravity system at a point removed a short distance from the place where the collision is about to occur. The spheres will enter our field of view moving in opposite directions along straight lines which are necessarily parallel. The perpendicular distance between the two lines is the impact parameter b. If b is greater than s, no collision will occur, and the angle of deflection θ is zero. For the case in which b is less than s, let us indicate the angle between the line of centers at the moment of impact and the previous direction of motion by χ. We clearly have

$$\sin\chi = b/s = \beta, \tag{13}$$

if we identify the diameter s with the s which appears in (6), and set $\sigma(\gamma)=1$. Since we are in the center of gravity coordinate system, the conservation of energy and momentum now requires that the spheres bounce off in a direction such that the angle between the new and old directions of motion is 2χ. This is perhaps most easily seen by noting that the components of velocity parallel to the line of centers at impact must be reversed in the collision, whereas the perpendicular components are unaltered. The angle of deflection is thus

$$\begin{aligned} \theta &= \pi - 2\chi, & \beta &\leqslant 1 \\ &= 0, & \beta &\geqslant 1. \end{aligned} \tag{14}$$

The integral in (7) is most easily evaluated by changing the variable of integration from β to $x=\cos\theta$. From (13) and (14) we have $dx=\frac{1}{4}\beta d\beta$, so that in this case the expression (7) for $\Theta^{(l)}$ becomes

$$\Theta^{(l)} = \tfrac{1}{4}\int_{-1}^{+1} \{1-P_l(x)\}dx = \tfrac{1}{2}, \quad l>0. \tag{15}$$

The integral of the latter term in the curly bracket vanishes for l greater than zero, since for this range of integration, the Legendre polynomials are orthogonal to $P_0(x)=1$.

The expression (8) for $\Omega^{(l,k)}$ with $\sigma=1$, $\Theta^{(l)}=\frac{1}{2}$, becomes simply

$$\Omega^{(l,k)} = \tfrac{1}{4}[\tfrac{1}{2}(k-1)]! \tag{16}$$

The expression corresponding to (16) in the notation of Chapman and Cowling† is

$$\Omega^{(l)}(r) = \frac{s^2}{8}\left[2-\frac{1+(-1)^l}{l+1}\right]\left(\frac{2\pi kT}{m}\right)^{\frac{1}{2}}(r+1)! \tag{17}$$

The substitution of (16) in (12) then yields for the elastic sphere model

$$\alpha = \frac{105}{118}\frac{m_2-m_1}{m_2+m_1}. \tag{I}$$

This result was first given by Furry, Jones and Onsager.[3]

The Inverse Power Model

In this model the molecules are considered to be centers of a repulsive force which falls off as the inverse νth power of the distance of separation; the repulsive force is given by

$$F = \kappa/r^\nu, \tag{18}$$

where κ is a constant which determines the strength of the repulsion at a given distance.

In order to discuss the details of a collision between two such molecules, let us use a polar coordinate system r, ϕ, with its plane in the plane of motion of the molecules, and with its origin at one of the two molecules. In terms of the reciprocal radius $u=1/r$, the equation of motion is then[9a]

$$\left(\frac{du}{d\phi}\right)^2 = \frac{1}{b^2} - u^2 - \frac{2}{mg^2b^2}\int_r^\infty F dr, \tag{19}$$

where, as in (5), m is the reduced mass. We now subject g and b to the transformations (5) and (6), with

$$s = (\kappa/2kT)^{1/(\nu-1)}, \quad \sigma(\gamma) = \gamma^{-2/(\nu-1)}. \tag{20}$$

These transformations, along with the substitution $x=bu$ and the relation (18), reduce (19) to the form

$$\left(\frac{dx}{d\phi}\right)^2 = 1 - x^2 - \frac{2}{\nu-1}\left(\frac{x}{\beta}\right)^{\nu-1}. \tag{21}$$

The value of x which corresponds to the value of r at the distance of closest approach is the smallest positive root of

$$1 - x^2 - (2/(\nu-1))(x/\beta)^{\nu-1} = 0. \tag{22}$$

† Reference 9, p. 168.

[9a] W. F. Osgood, *Mechanics* (Macmillan, 1937), p. 109.

Let this root be indicated by $x_0(\beta)$. Then the angle which is swept out by the molecule as it moves from infinity to the point of closest approach is, according to (21),

$$\chi=\int_0^{x_0}\{1-x^2-(2/(\nu-1))(x/\beta)^{\nu-1}\}^{-\frac{1}{2}}dx. \quad (23)$$

This angle will be the same when measured in the center of gravity system. The angle of deflection θ is now, as in the case of elastic spheres, the quantity $\pi-2\chi$. By (23), the angle θ depends only on ν and β, and therefore $\Theta^{(l)}$ is a number which depends only on ν and l. Following Enskog,[8] we set

$$\Theta^{(l)}=A_l^{(\nu)}. \quad (24)$$

The numbers $A_l^{(\nu)}$ have been evaluated by Chapman[10] for $l=1$ and 2, and $\nu=3$, 5, 7, 9, 11 and 15, by means of numerical integration. The values obtained by Chapman are tabulated in Table I, except that the values for $\nu=9$ are those obtained by Hassé and Cook.[11]

There is a variety of notations for the quantities which we have indicated by $A_l^{(\nu)}$:

Enskog[8]		Chapman and Cowling[9]		Jeans,[12] Chapman[10]
$A_1^{(\nu)}$	=	$A_1(\nu)$	=	$I_1(\nu)/2\pi$
$A_2^{(\nu)}$	=	$3A_2(\nu)/2$	=	$3I_2(\nu)/2\pi$.

The quantities A_1 and A_2 which were used by Maxwell are the same as $I_1(5)$ and $I_2(5)$.

TABLE I. *Quantities for the inverse power model.*

ν	$A_1^{(\nu)}$	$A_2^{(\nu)}$	$f(\nu)$	$6f(\nu)/5$	$C(\nu)$
3	0.8115	1.825	1.500	1.800	0.714
4.5				1.58	0.80
5	0.4220	0.6541	1.2918	1.5501	0.8156
6				1.512	0.831
7	0.3855	0.5349	1.2335	1.4802	0.8431
8				1.454	0.854
9	0.3808	0.4956	1.1930	1.4316	0.8648
10				1.412	0.874
11	0.3835	0.4778	1.1631	1.3957	0.8823
12				1.382	0.890
13				1.370	0.896
14				1.359	0.901
15	0.3931	0.4642	1.1248	1.3498	0.9064
∞	0.5000	0.5000	1.0000	1.2000	1.0000

[10] S. Chapman, Memoirs and Proc. of the Manchester Lit. and Phil. Soc. **66**, No. 1 (1922).
[11] H. R. Hassé and W. R. Cook, Proc. Roy. Soc. **125**, 196 (1929).
[12] J. H. Jeans, *Dynamical Theory of Gases* (Cambridge, fourth edition, 1925).

By virtue of (20) and (24), we now have

$$\Omega^{(l,k)}=\tfrac{1}{2}A_l^{(\nu)}\Gamma\left(\frac{k+1}{2}-\frac{2}{\nu-1}\right). \quad (25)$$

As we have noted before, the expression (12) for α is homogeneous and of order zero in the Ω's. This means that we may multiply $\Omega^{(l,k)}$ as given by (25) by any quantity whatever which does not depend on the indices l and k. One of the simple choices for such a multiplying factor is $(\Omega^{(1,5)})^{-1}$, which leads to

$$\begin{aligned}&\Omega^{(1,5)}\to 1;\\ &\Omega^{(1,7)}\to 3-2/(\nu-1);\\ &\Omega^{(1,9)}\to\{4-2/(\nu-1)\}\{3-2/(\nu-1)\};\\ &\Omega^{(2,7)}\to 3f(\nu),\end{aligned} \quad (26)$$

where

$$f(\nu)=\{1-2/(3(\nu-1))\}A_2^{(\nu)}/A_1^{(\nu)}. \quad (27)$$

Substitution of (26) in (12) now yields for the inverse power law

$$\alpha=\frac{105}{118}\frac{m_2-m_1}{m_2+m_1}\frac{\nu-5}{\nu-1}C(\nu), \quad (II)$$

where

$$C(\nu)=\frac{59}{21}\frac{(15/f)+6}{43+16\{f-1/(\nu-1)+1/(\nu-1)^2\}} \quad (28)$$

is a function of ν whose value lies between 0.8 and 0.9 for values of ν between 5 and 15. The behavior of most gases corresponds to a value of ν within this range. The functions $f(\nu)$ and $C(\nu)$ are tabulated in Table I, as is also the function $(6/5)f(\nu)$ because of its importance in the determination of the coefficient of self-diffusion D, which is also important in the theory of separating isotopes by thermal diffusion. The inverse power model predicts

$$D=(6/5)f(\nu)\eta/\rho, \quad (29)$$

where η and ρ are the coefficient of viscosity and the density, respectively.

The result (II) was first obtained by Jones and Furry.[4]

Probably the most interesting aspect of (II) is the vanishing of α for $\nu=5$, that is, for Maxwellian molecules. For values of ν greater than

TABLE II. *Values for various gases of n, of R_T according to the inverse power model, and of the Sutherland constant C.*

GAS	REFERENCE	T°K	n	$R_T(n)$	C
A	a	221	0.89	0.18	138
		333	0.80	0.34	147
		423	0.76	0.41	142
		498	0.71	0.51	150
		979	0.62	0.70	140
He	a	48	0.644	0.64	6
		123	0.646	0.64	21
		210	0.652	0.63	37
		333	0.669	0.59	66
		423	0.667	0.59	83
		1022	0.645	0.64	173
Ne	a	244	0.668	0.59	34
		333	0.657	0.62	61
		423	0.644	0.64	70
		498	0.644	0.64	82
		1030	0.623	0.69	128
Xe	b	347	0.92	0.13	250
		425	0.91	0.15	303
		525	0.83	0.29	254
Br_2	c	330	0.833	0.28	162
		475	0.985	0.02	496
Cl_2	c	293–523	~1.0	~0	~400
I_2	c	420	0.92	0.13	301
		482	1.04	−0.06	590
HCl	a	293–523	~1.0	~0	~350
HI	c	294–524	~1.0	~0	~400
O_2	d	333	0.775	0.38	126
		398	0.735	0.46	122
		448	0.731	0.47	132
		498	0.655	0.62	91
H_2	d	333	0.666	0.60	66
		398	0.694	0.54	96
		448	0.667	0.60	90
		498	0.679	0.57	108
N_2	d	333	0.737	0.46	102
		398	0.713	0.50	107
		448	0.687	0.55	103
		498	0.645	0.64	85
NH_3	d	291–573	~1.0	~0	~550
NO	g	308	0.79	0.36	128
		498	0.64	0.66	121
N_2O	f	325	0.97	0.05	277
		349–551	~0.87	~0.22	~255
CH_4	e	308	0.860	0.23	174
		348	0.825	0.30	168
		398	0.795	0.35	166
		448	0.769	0.40	165
		498	0.728	0.48	146
C_2H_6	e	308	0.958	0.07	260
		498	0.801	0.34	213
C_3H_8	e	308	0.965	0.06	267
		498	0.830	0.29	244
CO_2	f	325	0.92	0.13	240
		525	0.85	0.25	281
CO	h	347	0.72	0.49	96
		450	0.69	0.55	103
		525	0.63	0.68	98
SO_2	i	287–472	~1	~0	~425

a M. Trautz and H. Binkele, Ann. d. Physik **5**, 561 (1930).
b M. Trautz and R. Heberling, Ann. d. Physik **20**, 118 (1934).
c M. Trautz and H. Winterkorn, Ann. d. Physik **10**, 511 (1931).
d M. Trautz and R. Heberling, Ann. d. Physik **10**, 155 (1931).
e M. Trautz and K. Sorg, Ann. d. Physik **10**, 81 (1931).
f M. Trautz and F. Kurtz, Ann. d. Physik **9**, 981 (1931).
g M. Trautz and E. Gabriel, Ann. d. Physik **11**, 606 (1931).
h M. Trautz and A. Melster, Ann. d. Physik **7**, 409 (1930).
i M. Trautz and W. Weizel, Ann. d. Physik **78**, 305 (1925).
Note: Further data for high temperatures may be found in Tables 17 to 30 of M. Trautz and K. Sorg, Ann. d. Physik **7**, 427 (1930).

5, α is positive, whereas for values of ν less than 5, α is negative. It is very pleasing that this rather mysterious behavior may be explained by the elementary dimensional argument which is advanced by Frankel;[6] his argument shows that α is zero for Maxwellian molecules, and that the coefficient changes sign at $\nu=5$, being positive for ν greater than 5. Frankel's argument is no small achievement, since an elementary argument to show the existence and sign of the effect has long been desired.

The inverse power model, which is quite successful in explaining the temperature dependence of the elementary coefficients for most gases, is less successful in the case of thermal diffusion because the latter phenomenon is so much more sensitive to the molecular model; the value and sign of the thermal diffusion coefficient depend essentially on the nature of the intermolecular forces, and approximations which are adequate for the treatment of free-path phenomena do not suffice for thermal diffusion. Equation (II) indicates that α should be independent of the temperature; this is not confirmed, even approximately, by experiment.

Because no other model has the simplicity of this one, however, we shall probably continue to use it for some time to obtain an estimate of the value of α. In comparing the results of various molecular models, it is convenient to consider the ratio of the experimental or predicted value of α to that predicted by (I) for

hard spheres. This ratio will be denoted by R_T. In the case of the inverse power model, we have

$$R_T=\frac{\nu-5}{\nu-1}C(\nu). \tag{30}$$

An estimate of an appropriate value of ν for a given gas may be obtained from its second virial coefficient, or more conveniently from the temperature variation of the viscosity. If the viscosity varies as T^n, a dimensional argument suffices to show that n and ν are related by

$$\nu=(2n+3)/(2n-1). \tag{31}$$

In terms of n, (30) becomes

$$\begin{aligned} R_T&=2(1-n)C((2n+3)/(2n-1)) \\ &\leqq 1.7(1-n). \end{aligned} \tag{32}$$

Using the relation (32), Brown[13] has in this manner given an estimate of the value of R_T for a number of gases. Brown's table, with rather extensive changes and additions, is given as Table II. The more precise of the relations (32) is tabulated in Table III.

The predictions of Table II should not be taken too seriously, particularly in those cases where very small values of R_T are predicted; in such cases the inverse power model is completely inadequate.

TABLE III. *R_T as a function of n according to the inverse power model.*

n	$\nu=\frac{2n+3}{2n-1}$	$R_T=2(1-n)C(\nu)$	n	$\nu=\frac{2n+3}{2n-1}$	$R_T=2(1-n)C(\nu)$
1.1	4.33	−0.159	0.85	6.71	0.252
1.075	4.48	−0.120	0.8	7.67	0.340
1.05	4.65	−0.081	0.75	9	0.432
1.025	4.81	−0.040	0.7	11	0.529
1.0	5	zero	0.675	12.42	0.580
0.975	5.21	0.041	0.65	14.32	0.632
0.950	5.44	0.082	0.6	21	0.74
0.925	5.71	0.124	0.55	41	0.86
0.9	6	0.166	0.5	∞	1.000

INTERMOLECULAR FORCES

It is now thought that the best simple approximation to the forces exerted between molecules of the noble gases can be expressed as the sum of an inverse seventh power attraction and an exponential repulsion.[14] For the range of radii which are concerned in molecular collisions at ordinary temperatures, a force of this kind can be approximated quite well by an equation of the form

$$F=\kappa/r^{\nu}-\kappa'/r^{\nu'}. \tag{33}$$

An equation of this form has been used by Lennard-Jones[15] in the theoretical interpretation of the equation of state observed for various gases. The implication in kinetic theory of such a law of force has never been completely worked out, however, because of the enormous mathematical complexity to which it leads. The special cases of $\nu=\infty$ and $\nu'=3$ have been worked out as far as terms of the first order in the attractive force. These cases are, respectively, the Sutherland and the Lennard-Jones model.

THE SUTHERLAND MODEL

The molecules are considered to be smooth elastic spheres of diameter s, surrounded by an attractive field of force which decreases as the inverse νth power of the distance. The attractive force between two molecules is taken to be

$$F=-\kappa/r^{\nu}. \tag{34}$$

It follows from the work of James[16] that for this case

$$\Theta^{(1)}=\tfrac{1}{2}\{1+2i_1(\nu)\epsilon/(kT\gamma^2)\} \tag{35}$$

and

$$\Theta^{(2)}=\tfrac{1}{2}\{1+3i_2(\nu)\epsilon/(kT\gamma^2)\}, \tag{36}$$

[13] Harrison Brown, Phys. Rev. **57**, 242L (1940).
[14] R. H. Fowler and E. A. Guggenheim, *Statistical Thermodynamics* (Cambridge, 1939).
[15] J. E. Lennard-Jones, Proc. Roy. Soc. **106**, 463 (1924).
[16] C. G. F. James, Proc. Camb. Phil. Soc. **20**, 447 (1921).

where $i_1(\nu)$ and $i_2(\nu)$ are functions of ν defined by

$$i_1(\nu)=2\int_0^1 y^{3-\nu}(1-y^2)^{\frac{1}{2}}\int_0^y x^{\nu-1}(1-x^2)^{-\frac{1}{2}}dxdy$$
$$=\tfrac{1}{2}-4(\nu-1)\sum_r \frac{r+1}{(2r+\nu)(2r+1)(2r+3)(2r+5)} \qquad r=0,\ 1,\ 2,\ \cdots \tag{37}$$

and

$$i_2(\nu)=4\int_0^1 y^{3-\nu}(2y^2-1)(1-y)^{\frac{1}{2}}\int_0^y x^{\nu-1}(1-x^2)^{-\frac{1}{2}}dxdy$$
$$=\tfrac{1}{3}-8(\nu-1)\sum_r \frac{r+1}{(2r+\nu)(2r+3)(2r+5)(2r+7)} \qquad r=0,\ 1,\ 2,\ \cdots \tag{38}$$

and where

$$\epsilon=\kappa/\{(\nu-1)s^{\nu-1}\} \tag{39}$$

is the negative potential energy of two molecules at the moment of contact. The s and σ of (6) have the same values as in the case of simple elastic spheres.

The insertion of (35) and (36) in (8) then yields

$$\Omega^{(1,k)}=\frac{1}{4}\left\{\left(\frac{k-1}{2}\right)!+2i_1(\nu)(\epsilon/kT)\left(\frac{k-3}{2}\right)!\right\} \tag{40}$$

and

$$\Omega^{(2,k)}=\frac{1}{4}\left\{\left(\frac{k-1}{2}\right)!+3i_2(\nu)(\epsilon/kT)\left(\frac{k-3}{2}\right)!\right\}. \tag{41}$$

The last two expressions, as well as (35) and (36), are valid only to terms in the first order of ϵ/kT. Our results will therefore be correct only when ϵ/kT is small compared with unity.

The relation obtained by substituting (40) and (41) in (12) is, for the Sutherland model

$$\alpha=\frac{105}{118}\frac{m_2-m_1}{m_2+m_1}\frac{(1-i_1(\nu)\epsilon/kT)(1+\{(5i_1(\nu)+2i_2(\nu))/7\}\epsilon/kT)}{(1+i_2(\nu)\epsilon/kT)(1+\{(39i_1(\nu)+16i_2(\nu))/59\}\epsilon/kT)}. \tag{III}$$

To terms of the first order in ϵ/kT, Eq. (III) is equivalent to

$$\alpha=\frac{105}{118}\frac{m_2-m_1}{m_2+m_1}(1-F(\nu)\epsilon/kT), \tag{III'}$$

where

$$F(\nu)=\{391i_1(\nu)+407i_2(\nu)\}/413, \tag{42}$$

whence

$$R_T=1-F(\nu)\epsilon/kT. \tag{43}$$

The error involved in ignoring higher powers of ϵ/kT is probably less in (III) than in (III').

The quantities $i_1(\nu)$ and $i_2(\nu)$ have been evaluated by Enskog[7] and James,[16] and are tabulated along with $F(\nu)$ in Table IV. The notation used here is that of Chapman and Cowling, which is related to that of Enskog according to

$$\alpha(\nu)=i_1/i_2, \quad \delta(\nu)=3i_2/2. \tag{44}$$

The table of $i_1(\nu)$ and $i_2(\nu)$ given by Chapman and Cowling contains errors which are here corrected.

The Lennard-Jones Model

In this model the molecules interact according to a force law of the form (33), with $\nu'=3$. This choice of ν' is made not because of its physical appropriateness ($\nu'=7$ would be a better choice),

TABLE IV. *Quantities for the Sutherland model.*

ν	$i_1(\nu)$	$i_2(\nu)$	$F(\nu)$
2	$1/3=0.3333$	$4/15=0.2667$	0.5784
3	$(12-\pi^2)/8=0.2663$	$(\pi^2-8)/8=0.2337$	0.4824
4	$3-4\log 2=0.2274$	$8(3\log 2-2)/3=0.2118$	0.4240
5	$(3\pi^2-28)/8=0.2011$	$3(10-\pi^2)/2=0.1956$	0.3831
6	0.182	0.183	0.353
7	$1/6=0.1667$	$5(9\pi^2-88)/24=0.1722$	0.3275
9	$13/90=0.1444$	$7/45=0.1556$	0.2900

TABLE V. *Quantities for the Lennard-Jones model.*

ν	$B_1^{(\nu)}$	$B_2^{(\nu)}$	$g(\nu)$	$D(\nu)$
3	−0.812	−1.825	1.000	1.000
5	(−0.331)	−0.7244	0.589	0.653
7	−0.173	−0.4137	0.299	0.376
9	−0.077	−0.2474	0.126	0.218
11	−0.016	−0.1430	0.025	0.125
15	+0.0564	−0.0266	−0.081	0.088
∞	+0.2662	+0.3506	−0.266	−0.216

but because of its mathematical convenience. It follows from the work of Lennard-Jones,[17] and Chapman and Cowling, that

$$\Theta^{(l)}=A_l^{(\nu)}+B_l^{(\nu)}\kappa'/\{\kappa^{2/(\nu-1)}(2kT\gamma^2)^{(\nu-3)/(\nu-1)}\}, \tag{45}$$

where the A's are the quantities already introduced in (24), and the B's are quantities which must be determined by numerical quadrature. The $B_1^{(\nu)}$ and $B_2^{(\nu)}$ used here are related to the quantities used by Chapman and Cowling according to

$$B_1^{(\nu)}=B_1(\nu), \quad B_2^{(\nu)}=3B_2(\nu)/2. \tag{46}$$

The values of $B_1^{(\nu)}$ tabulated in Table V were determined by Chapman and Cowling, and the values of $B_2^{(\nu)}$ by Lennard-Jones.[17] The values of $B_1^{(5)}$, $B_1^{(3)}$, and $B_2^{(3)}$ are not given by the writers mentioned, but the latter two must clearly be the negatives of $A_1^{(3)}$ and $A_2^{(3)}$. The value of $B_1^{(5)}$ was then determined by interpolation in the expression $B_2/(B_1-0.05)$, which is nearly constant for $\nu=3$, 7, 9, and 11. It is assumed in stating (45) that s and σ have the same values as for the inverse power model.

From (8) and (45) we now have

$$\Omega^{(l,k)}=\tfrac{1}{2}A_l^{(\nu)}\Gamma\left(\frac{k+1}{2}-\frac{2}{\nu-1}\right)+\tfrac{1}{2}B_l^{(\nu)}\frac{\kappa'}{\kappa^{2/(\nu-1}2kT^{(\nu-3)/(\nu-1)}}\left(\frac{k-3}{2}\right)! \tag{47}$$

and substitution of this expression in (12) gives for the Lennard-Jones model

$$\alpha=\frac{105}{118}\frac{m_2-m_1}{m_2+m_1}C(\nu)\left(\frac{\nu-5}{\nu-1}+\frac{\kappa' g(\nu)}{\kappa^{2/(\nu-1)}(2kT)^{(\nu-3)/(\nu-1)}}\right)\left(1+\frac{\kappa D(\nu)}{\kappa^{2/(\nu-1)}(2kT)^{(\nu-3)/(\nu-1)}}\right), \tag{IV}$$

where

$$g(\nu)=-B_1/\{A_1\Gamma(3-2/(\nu-1))\} \tag{48}$$

and

$$D(\nu)=g(\nu)\left\{\frac{10B_2/(B_1 f)-15}{15+6f}+\frac{117+32B_2/B_1}{177+48\{f-1/(\nu-1)+1/(\nu-1)^2\}}\right\} \tag{49}$$

and $f(\nu)$ is the same function that arose in the case of the inverse power model. The functions $g(\nu)$ and $D(\nu)$ are also tabulated in Table V. Equations (45), (47) and (IV) are correct only to the first order in $\kappa'/\{\kappa^{2/(\nu-1)}(2kT)^{(\nu-3)/(\nu-1)}\}$.

Equation (IV) has the property that it predicts α to be independent of temperature for a value of ν slightly less than 15; for smaller values of ν, it indicates that α will *increase* as the temperature decreases.

THE LIMITATIONS INVOLVED IN EQUATION (12)

It has already been stated that (12) is the first approximation to the exact result as given by the ratio of two infinite determinants. We may obtain a rough estimate of the error involved in the first approximation by the following considerations.

[17] J. E. Lennard-Jones, Proc. Roy. Soc. **106**, 441 (1924).

It was shown by Enskog[18] in 1912 that for the case in which both the mass and the concentration of the lighter molecules are negligible in comparison with the corresponding quantities for the heavier particles, the *exact* value of α for the inverse power model is

$$\alpha=\frac{1}{2}\frac{\nu-5}{\nu-1}. \tag{50}$$

On the other hand, it is shown by Chapman and Cowling that the value of α given by the first approximation is in this case

$$\alpha=\frac{\nu-5}{\nu-1}\Big/\left\{5-\frac{4}{5}\frac{(3\nu-5)(\nu+1)}{(\nu-1)^2}\right\}. \tag{51}$$

Comparison of (50) and (51) indicates that the first approximation gives 10/13 of the exact result for elastic spheres, 8/9 of the exact value for $\nu=9$, and a vanishing error as ν approaches 5.

This limiting case, the Lorentzian case, is a particularly bad case for all of the coefficients which refer to a mixture of two gases, however. The first approximation gives a result which for elastic spheres is about 98 percent of the exact result for the coefficients of conductivity, viscosity, and self-diffusion of a simple gas, whereas in the Lorentzian case, the first approximation is in error by 8, 12, and 15 percent, respectively. If, then, one wishes to draw an analogy between the coefficient of self-diffusion and the thermal diffusion coefficient of isotopes, one might make the slightly enlightened guess that the expression (12) is about 5 percent low for elastic spheres, with a smaller error for smaller values of ν. This is at best only a guess.

The theory of Enskog which we have been using is, of course, a purely classical theory. The introduction of quantum mechanics changes the statistics obeyed by the molecules, and requires that the general theory of Enskog be redone from the beginning. This has been done by Hellund and Uehling.[19] The difference between classical and quantum statistics is, however, of negligible importance for gases at ordinary temperatures and pressures. The chief change brought about by quantum mechanics lies in the calculation of the collision cross sections, and this change is easily made within the framework of Enskog's theory; the quantities $\Theta^{(l)}$ and $\Omega^{(l,k)}$ which are to be inserted in (12) should be computed quantum-mechanically. Even here the difference between the classical and quantum cross sections is small, except possibly for hydrogen and helium. The most important quantum-mechanical effect is the fact that the wave functions for a collision between identical and nonidentical particles must have different symmetries, with the result that the cross sections for a collision between identical and between nonidentical particles are not equal. This effect was pointed out by Hellund and Uehling.[19]

Professor Mott-Smith (University of Illinois) has worked out the details of this symmetry effect for elastic spheres (private communication), and the writer hopes that he will soon publish his interesting considerations.

Comparison with Experiment

Direct experimental determinations of the thermal diffusion coefficient of isotopes are very few in number. Nier[20,21] has measured the value of α over two temperature ranges for methane, and over three temperature intervals for neon. His results are shown in Table VI. The quantity R_T is the ratio of the observed value of α to that predicted by (I).

Hassé and Cook[11] give viscosity data for neon at nine temperatures in the range 91.66°–717.6°K. The values of n obtained from these data for the temperature ranges 91.66°–194.7°, 91.66°–288.1°, and 288.1°–575.1°, are, respec-

Table VI. *Values of α determined experimentally by Nier.*

Species 1	Species 2	Temp. Range	α	R_T
$C^{12}H_4$	$C^{13}H_4$	296°–728°	0.0080±~5%	0.30
		296°–573°	0.0074±~5%	0.27
Ne^{20}	Ne^{22}	283°–617°K	0.0302± 2%	0.71
		90°–294°K	0.0188± 2%	0.44
		90°–195°K	0.0165± 8%	0.39

[18] D. Enskog, Ann. d. Physik **38**, 731 (1912).
[19] E. J. Hellund and E. A. Uehling, Phys. Rev. **56**, 818 (1939).
[20] A. O. Nier, Phys. Rev. **56**, 1009 (1939).
[21] A. O. Nier, Phys. Rev. **57**, 338 (1940).

tively, 0.745, 0.716, and 0.676. According to the inverse power model the values of R_T which correspond to these values of n, are by Table III, 0.44, 0.50, and 0.58. These values are to be compared with the experimental values of R_T for roughly the same temperature ranges: 0.39, 0.44, and 0.71. Of course, the fact that n varies with temperature at all indicates that the inverse power model is lacking.

The value of R_T as predicted by viscosity data may also be obtained from the Sutherland model. According to the work of James,[16] the constant C which appears in the Sutherland equation for the viscosity is given by

$$C=i_2(\nu)\epsilon/k. \tag{52}$$

If we assume $\nu=7$, the value predicted by the quantum theory of van der Waals forces, we find from (III) and (52) that

$$R_T=\frac{(1-0.9679\ C/T)(1+0.9771\ C/T)}{(1+C/T)(1+0.9110\ C/T)}, \tag{53}$$

$$\cong\frac{1-0.98\ C/T.}{1+0.92\ C/T}. \tag{54}$$

The experimental data of Hassé and Cook for neon may be fitted rather well over the entire range of temperature by the Sutherland relation with $C=60°$. With this value of C, the values of R_T predicted by (54) for the temperatures 142°, 192°, and 450°, are, respectively, 0.42, 0.54, and 0.77. These values agree with experiment somewhat better than in the case of the inverse power model. The same difficulty faces us here, however, that has led to the rejection of the Sutherland model as being more than a convenient interpolation formula; namely, the fact that the value of $\epsilon/k=350°$, which by (52) corresponds to $C=60°$, is much larger than the value which is indicated by other and more reliable measurements of this quantity, such as the latent heat of vaporization of the crystalline solid, and measurements of the second virial coefficient. According to Buckingham,[22] such considerations point quite definitely to a value of ϵ/k of about 30° or 40°.

[22] R. A. Buckingham, Proc. Roy. Soc. **168**, 264 (1938).

Buckingham has been able to fit the experimental measurements of the second virial coefficient of neon by a formula of the Lennard-Jones type (33) with $\nu'=7$, and with a value of ν which may vary in the range 9 to 15. For all of these values of ν, however, the Lennard-Jones model (with $\nu'=3$) predicts that α will fall or at least not rise as the temperature increases. Since this behavior is not at all in agreement with experiment, we must conclude that the Lennard-Jones model is not useful in connection with thermal diffusion in the case of neon. Whether this failure is due to the choice of $\nu'=3$, or whether the difficulty is more deeply seated, the writer is unable to say or guess.

The methane molecule does not possess a spherically symmetrical field of force, and we should therefore not expect that the theory of Enskog, which holds only for spherically symmetrical molecules, would give results in close agreement with experiment. The inverse power model is particularly inappropriate in application to methane, inasmuch as the value of n varies between 1.028 and 0.728 in the temperature range 91.5°–522.8°K. From Table II, we find that for the temperatures 448° and 498°, the values of n are 0.77 and 0.73; we then find from Table III that the corresponding values of R_T are 0.40 and 0.49. These values may be compared with the experimental results 0.27 and 0.30. The Sutherland equation fits the viscosity data much better, with C equal to about 160°. With this value of C, the values of R_T predicted by (54) for the temperatures 430° and 512° are 0.48 and 0.54, which are in very poor agreement with experiment.

The comparison of theory with experiment is sufficiently good in the case of neon to encourage us that we are on the right track, but on the other hand is sufficiently poor to indicate that much remains to be done. In particular, we are faced with the task of working out the predictions of more complicated molecular models than those which have been considered up to the present time. The models discussed in the present paper have proved quite satisfactory for the treatment of free-path phenomena, but they are not sufficiently precise to meet the test of thermal diffusion.

ACKNOWLEDGMENT

On the same day that the manuscript of the present paper was handed to the secretary for retyping, Professor W. H. Furry of this department received a letter from Professor H. M. Mott-Smith (University of Illinois) which contained much of the material in this paper. In subsequent correspondence it was suggested by Professor Mott-Smith that the writer proceed with publication.

The writer would like to thank Professor W. H. Furry for helpful comments on the manuscript.

JULY 15, 1940 PHYSICAL REVIEW VOLUME 58

On Directional Correlation of Successive Quanta

DONALD R. HAMILTON*
Harvard University, Cambridge, Massachusetts
(Received May 6, 1940)

A theoretical investigation shows that there should be a correlation between the directions of propagation of the quanta emitted in two successive transitions of a single radiating system. This correlation is described by a function $W(\theta)$ which gives the relative probability that the second quantum will be emitted at an angle θ with the first; W is determined by the angular momenta of the three levels involved in the two transitions and by the multipole order of the radiation emitted in these transitions. The explicit forms of W for all angular momenta and for dipole and quadrupole radiation are given; experimental determination of W in any given case should limit these factors to a small number of possibilities. This has particular interest as a means of investigating the nuclear energy levels involved in γ-radiation; here W should be observable by measuring the variation with θ of gamma-gamma coincidence counting rates.

INTRODUCTION

IT has been suggested by Dunworth[1] that there might be some correlation between the directions of emission of two successive gamma-quanta emitted by a nucleus when this nucleus passes from an excited level A to the ground level C, by way of a definite intermediate level B. This suggestion was pointed out to the author by Dr. I. A. Getting in connection with the latter's search for such a correlation by means of gamma-gamma coincidence experiments. The present paper is a theoretical discussion of the question.

The problem of resonance radiation[2] is basically similar to the present one, since both are concerned with the radiation from an excited level in which a system finds itself as the result of an anisotropic process. This process is, in the first case, an absorption from a unidirectional (and usually polarized) beam of light; in the second, an emission of a quantum in one particular direction.

An explicit formulation involves the transitions between the $(2J+1)$ m-states of each level. ($\mathbf{J}$ is total angular momentum of a level, the m are the eigenvalues of J_z.) We designate the states of the nucleus as A_l, B_n, C_p; subscripts are values of m. For a given multipole order of the transition AB (or BC), the angular distribution of quanta emitted in a transition A_lB_n (or B_nC_p) depends only on $|\Delta m|$, where $\Delta m \equiv (p-n)$ or $(n-l)$; hence we write these distributions as $\varphi_{|n-l|}(\theta)$ and $f_{|p-n|}(\theta)$. The relative probabilities of the various transitions A_lB_n and B_nC_p are denoted by g_{ln} and G_{np}, respectively. Now suppose that the nuclei are initially oriented at random—i.e., all states A_l equally populated for any arbitrary axis of quantization. In the transition AB, the sum of the probabilities of all components A_lB_n with a given Δm is independent of Δm; hence the probability that a quantum emitted at an angle θ_1 with the axis has been emitted in a transition with given Δm is proportional to $\varphi_{|\Delta m|}(\theta_1)$. The relative populations of the B_n are then $\sum_l g_{ln}\varphi_{|n-l|}(\theta_1)$ and the angular distribution of radiation from the decay of state B_n alone is $\sum_p G_{np}f_{|p-n|}(\theta_2)$.

* Society of Fellows.
[1] J. V. Dunworth, Rev. Sci. Inst. **11**, 167 (1940).
[2] V. F. Weisskopf, Ann. d. Physik **9**, 27 (1931).

Thus one might at first sight take as the total angular distribution of the second quantum the weighted sum of the angular distributions from each state B_n, given by

$$W(\theta_2)=\sum_n[\sum_l g_{ln}\varphi_{|n-l|}(\theta_1)]\times[\sum_p G_{np}f_{|p-n|}(\theta_2)]. \quad (1)$$

However, Eq. (1) seems incorrect since it has $W(\theta_2)$ depending not on the angle between the quanta, but on their directions with respect to the axis. This deeply offends one's sense of spectroscopic stability, according to which the choice of axis should affect the ease of a calculation but not the final result. As will be shown later, the point overlooked in obtaining Eq. (1) is the fact that if the first quantum is emitted in a definite direction then the phases of the states B_n are related; hence these states do not radiate independently of each other and the last step in obtaining Eq. (1) is based on a fallacy.

The same difficulty with phases beset the older quantum-theory calculations of the polarization of resonance radiation. There it was found that a physically reasonable result was obtained for one particular choice of axis (parallel to the electric vector of incident plane polarized light, or parallel to the direction of propagation of a circularly polarized beam); this was later justified quantum mechanically. Analogously, it will be shown that in our case the "naive" theory gives the correct result if one takes Oz, the axis of quantization, along the direction of propagation of the first quantum, since in this case the phases of the B_n are random. Furthermore, with this choice of axis the observed quanta are emitted only in transitions for which $\Delta m=\pm 1$. (Proposition 2a, later.) Hence, on setting $\theta_1=0$ and $\theta_2=\theta$, and dropping the constant factor $\varphi_1(0)$, the relative probability that the second quantum will be emitted at an angle θ with the first is

$$W(\theta)=\sum_n(g_{n+1,n}+g_{n-1,n})(\sum_p G_{np}f_{|p-n|}(\theta)). \quad (2)$$

We have discussed the naive treatment because, although incorrect, it suggests a simplified form (Eq. (2)) of the result of the exact treatment (Eq. (10)) which reduces by at least one order of magnitude the labor required for explicit calculation of $W(\theta)$, as well as providing additional physical insight.

Theory

The exact treatment is based on the time dependent Schrödinger equation (Eq. (4)) which deals with the interdependence of probability amplitudes rather than of their absolute squares.

Emission or absorption of a quantum constitutes a transition between two states of the system nucleus-plus-quantized-radiation-field, and is caused by the small matter-radiation coupling, H, in the Hamiltonian of the whole system. Since the velocities of the heavy particles in the nucleus are small compared with the velocity of light we take

$$H=-\int \mathbf{i}\cdot\mathbf{A}dv=-c^{-1}\int \rho\mathbf{t}\cdot\mathbf{A}dv,$$

where ρ and $\mathbf{i}$ are the charge and current densities associated with the given transition of the nucleus. The radiation field vector potential, $\mathbf{A}$, is taken in the gauge in which the scalar potential is zero.

This radiation field is quantized by quantizing the amplitudes of its normal modes. These modes might, for example, be plane or spherical waves; the particular form is a matter of convenience and depends on arbitrarily chosen boundary conditions. Running plane waves are the most straightforward in dealing with directions of propagation. The radiation field, then, is represented by an assembly of simple harmonic oscillators, each of which corresponds to a running plane wave of frequency ν, direction of propagation $\boldsymbol{\kappa}_0$, and polarization $\mathbf{e}$. (The latter are both unit vectors.) The vector potential of such an oscillator is given by $\mathbf{A}=q\mathbf{e}\exp(i\boldsymbol{\kappa}\cdot\mathbf{r})$ where $\boldsymbol{\kappa}=\kappa\boldsymbol{\kappa}_0=2\pi\nu c^{-1}\boldsymbol{\kappa}_0$. The time dependent amplitude of the oscillator, q, is independent of $\mathbf{r}$. The matrix elements of H for a given transition are calculated from

$$H=-qc^{-1}\mathbf{e}\cdot\int \rho\mathbf{t}\exp(i\boldsymbol{\kappa}\cdot\mathbf{r})dv, \quad (3)$$

where $\boldsymbol{\kappa}_0$ and $\mathbf{e}$ refer to the quantum emitted in the transition.

(The procedure now followed, from Eq. (4) to Eq. (7) inclusive, is very similar to that used in reference 2; we therefore omit many details.)

Let n_i be the occupation number of the ith field oscillator. Then if the first and second quanta are emitted into the ρth and σth field oscillators, respectively, the necessary states of the system may be specified, and their probability amplitudes written, as follows:

State	Probability amp.
$(A_l, n_1 \cdots n_\rho \cdots n_\sigma \cdots)$	a_l
$(B_n, n_1 \cdots n_\rho+1 \cdots n_\sigma \cdots)$	$b_{n\rho}$
$(C_p, n_1 \cdots n_\rho+1 \cdots n_\sigma+1 \cdots)$	$c_{p\rho\sigma}$.

The time dependence of the probability amplitudes is given by

$$-i\hbar\dot{a}_j=\sum_k H_{jk}a_k+E_ja_j, \tag{4}$$

where a_j and a_k are any of the above a_l, $b_{n\rho}$, or $c_{p\rho\sigma}$. Writing $(A_l \cdots n_\rho \cdots | H | B_n \cdots n_\rho+1 \cdots) \equiv (A_l|H_\rho|B_n)$, etc., Eq. (4) becomes

$$-i\hbar\dot{a}_l=\sum_{n,\rho}(A_l|H_\rho|B_n)b_{n\rho}, \tag{5a}$$

$$-i\hbar\dot{b}_{n\rho}=\sum_l(A_l|H_\rho|B_n)^*a_l+\sum_{\sigma,p}(B_n|H_\sigma|C_p)c_{p\rho\sigma}+h(\nu_\rho-\nu_{AB})b_{n\rho}, \tag{5b}$$

$$-i\hbar\dot{c}_{p\rho\sigma}=\sum_n(B_n|H_\sigma|C_p)^*b_{n\rho}+h(\nu_\rho+\nu_\sigma-\nu_{AC})c_{p\rho\sigma}. \tag{5c}$$

Here $h\nu_{AB}=E_A-E_B$, etc., and E_A is taken as zero. The following solutions to (5) are then assumed, subject to determination of the unknown quantities therein so that (5) is satisfied:

$$a_l=\alpha_l \exp[-2\pi\Gamma(A_l)t], \quad b_{n\rho}=\sum_l \beta_{ln\rho}(\exp[-2\pi\Gamma(A_l)t]-\exp[-2\pi\Gamma_\rho(B_n)t]), \tag{6a, b}$$

$$c_{p\rho\sigma}=\sum_l \epsilon_{lp\sigma}(\exp[-2\pi\Gamma(A_l)t]-\exp[-2\pi\Gamma_{p\sigma}(C_p)t])$$
$$+\sum_n \delta_{np\rho\sigma}(\exp[-2\pi\Gamma_\rho(B_n)t]-\exp[-2\pi\Gamma_{p\sigma}(C_p)t]). \tag{6c}$$

Substitution of Eq. (6) into Eq. (5) (most conveniently carried out by working upwards from Eqs. (5c) and (6c)) gives the following results:

$$\begin{aligned}
&\Gamma(A_l)=\gamma(A_l), \quad \Gamma_\rho(B_n)=i(\nu_{AB}-\nu_\rho)+\gamma(B_n), \quad \Gamma_{p\sigma}(C_p)=i(\nu_{AC}-\nu_\rho-\nu_\sigma),\\
&h\beta_{ln\rho}=\alpha_l(A_l|H_\rho|B_n)^*/(i[\Gamma(A_l)-\gamma(B_n)]+\nu_{AB}-\nu_\rho)\\
&h\epsilon_{lp\sigma}=\sum_n \beta_{ln\rho}(B_n|H_\sigma|C_p)^*/[\nu_{AC}-\nu_\rho-\nu_\sigma+i\Gamma(A_l)],\\
&h\delta_{np\rho\sigma}=-(B_n|H_\sigma|C_p)^*\sum_l \beta_{ln\rho}/[\nu_{AC}-\nu_\rho-\nu_\sigma+i\Gamma_\rho(B_n)].
\end{aligned} \tag{7}$$

The α_l are entirely undetermined, corresponding to the fact that their values constitute the initial conditions of the problem. The $\gamma(A_l)$ are given by $h^2\gamma(A_l)=\sum_n \pi F_{ln}(\nu_{AB})$ where $F_{ln}(\nu)d\nu=\sum_\rho|(A_l|H_\rho|B_n)|^2$. ($\sum_\rho$ indicates summation from $\nu_\rho=\nu$ to $\nu+d\nu$, and over all directions and polarizations.) Hence $4\pi\gamma(A_l)$ is the probability of radiative transition from the state A_l. An exactly analogous statement holds for $\gamma(B_n)$. The $\gamma(A_l)$ and $\gamma(B_n)$ are independent of l and n, as would be expected from symmetry considerations.

From Eq. (3),

$$(A_l|H_\rho|B_n)=-c^{-1}(n_\rho|q|n_\rho+1)(A_l|H(\kappa_0{}^\rho, \mathbf{e}^\rho)|B_n)$$

where

$$(A_l|H(\kappa_0{}^\rho, \mathbf{e}^\rho)|B_n)\equiv\mathbf{e}^\rho\cdot(A_l|\dot{\mathbf{r}}\exp(i\boldsymbol{\kappa}^\rho\cdot\mathbf{r})|B_n). \tag{8}$$

(Similarly for $(B_n|H_\sigma|C_p)$.) H_ρ and $H(\kappa_0\rho, \mathbf{e}\rho)$ are effectively independent of ν_ρ over the line breadth range of frequencies. Remembering this and calculating a_l, $b_{n\rho}$, and $c_{p\rho\sigma}$ by substitution of Eq. (7) into Eq. (6), we find that each probability amplitude is the product of two factors. The first depends

on t and some or all of ν_ρ, ν_σ, $\gamma(B_n)$ and $\gamma(A_l)$. The second depends on the initial conditions and on the matrix elements of $H(\kappa_0, \mathbf{e})$. As a result $W_{\rho\sigma}$, the probability of emission of quanta into the oscillators σ and ρ, will be the product of two factors of the same type. ($W_{\rho\sigma}$ is given by limit $(t\to\infty)\sum_p\langle|c_{p\rho\sigma}|^2\rangle_{Av}$.) In calculating $W(\kappa_0', \mathbf{e}', \kappa_0'', \mathbf{e}'')$, the probability of emission of two quanta characterized, respectively, by $\kappa_0', \mathbf{e}'$ and $\kappa_0'', \mathbf{e}''$, one integrates $W_{\rho\sigma}$ over ν_ρ and ν_σ. The second factor in $W_{\rho\sigma}$ is unaltered by this, and the integration of the first factor introduces no new dependence on $\kappa_0', \mathbf{e}', \kappa_0'', \mathbf{e}''$, since the frequency distribution of oscillators is independent of κ_0 and $\mathbf{e}$. Hence the first factor in $W_{\rho\sigma}$ and its parents, the first factors in the probability amplitudes, are useless since we are interested only in the *relative* variation of $W(\kappa_0', \mathbf{e}', \kappa_0'', \mathbf{e}'')$ with $\kappa_0', \mathbf{e}', \kappa_0'', \mathbf{e}''$. We therefore drop these factors and write the abbreviated probability amplitudes as a_l, b_n, c_p:

$$a_l=\alpha_l, \quad b_n=\sum_l \alpha_l(A_l|H(\kappa_0', \mathbf{e}')|B_n)^*, \tag{9a, b}$$

$$c_p=\sum_n b_n(B_n|H(\kappa_0'', \mathbf{e}'')|C_p)^*=\sum_l \alpha_l[\sum_n(A_l|H(\kappa_0', \mathbf{e}')|B_n)^*(B_n|H(\kappa_0'', \mathbf{e}'')|C_p)^*]. \tag{9c'} \tag{9c''}$$

The α_l specify the initial distribution of nuclei among the states A_l. Normally this will be completely random. This is equivalent to saying that $\alpha_l=\exp(i\delta_l)$ (omitting normalization) where the δ_l are random—that is, where $\langle\exp[i(\delta_{l_1}-\delta_{l_2})]\rangle_{Av}=\delta_{l_1 l_2}$. ($\langle\ \rangle_{Av}$ hereafter indicates an averaging over all nuclei, i.e. over all values of the δ_l.) Any result is to be averaged over the δ_l. Furthermore, to each κ_0 there correspond two arbitrary orthogonal $\mathbf{e}$'s; and since a γ-ray counter cannot differentiate between these two polarizations any final result must be summed over $\mathbf{e}'$ and $\mathbf{e}''$.

Thus at any given time the relative probability of two quanta having been emitted in the directions κ_0', κ_0'', in the solid angles $d\omega'$, $d\omega''$, is $Wd\omega' d\omega''$ where

$$W=\sum_{p, e', e''}\langle|c_p|^2\rangle_{Av}=\sum_{l, p, e', e''}|\sum_n(A_l|H(\kappa_0', e')|B_n)^*(B_n|H(\kappa_0'', e'')|C_p)^*|^2 \tag{10}$$

by Eq. (9c''). Since W is not an absolute probability, we shall occasionally drop constant factors from it without further comment.

The interference of probabilities mentioned in the Introduction is evident in Eq. (10). A nucleus may pass from the state A_l to C_p by way of several intermediate states B_n; but the probability of the transition A_lC_p is not the sum of the individual transition probabilities for the several routes $A_lB_nC_p$. The interference arises because the contributions to c_p from these different routes are summed before squaring rather than afterwards. If W is written down using Eq. (9c') instead of Eq. (9c'') it will be seen that the cross terms vanish when $\sum_{e'}\langle b_n b_k^*\rangle_{Av}=0$ for $n\neq k$, i.e. when the phases of the b_n are random.

We now state two propositions (previously referred to) which enable us to reduce Eq. (10) to Eq. (2), and which hold for all multipole orders (proofs in Appendix I):

1. The value of W is independent of the direction which we choose for the axis of quantization, hence we may choose this direction to suit our convenience.

2. If we take the axis along the direction of propagation of the first quantum, then: (2a) $l-n=\pm1$; (2b) $\sum_{e'}\langle b_n b_k^*\rangle_{Av}=0$ for $n\neq k$.

Proposition (1) involves simply a slight generalization of the principle of spectroscopic stability. (2a) is useful in proving (2b) as well as in calculating W; its physical significance was mentioned in the introduction. It might be noted that while (2b) makes the phases of the b_n random when we do not observe the polarization of the first quantum, they are also random if the first quantum is circularly polarized.

These propositions enable us to put $\kappa_0=\mathbf{k}$ and write

$$W=\sum_{nlpe'e''}|(A_l|H(\mathbf{k}, \mathbf{e}')|B_n)|^2|(B_n|H(\kappa_0'', \mathbf{e}'')|C_p)|^2, \quad l=n\pm1. \tag{11}$$

The interference has been removed. (In a sense one may say that the degeneracy of level B has been removed, since if B_n were nondegenerate there would have been no interference in the first

TABLE I. *R/Q, for both transitions dipole.*

	$\Delta J=-1$	$\Delta J=0$	$\Delta J=1$
$\Delta j=-1$	$\frac{1}{13}$	$\frac{-(2J-1)}{(14J+13)}$	$\frac{J(2J-1)}{(26J^2+67J+40)}$
$\Delta j=0$	$\frac{-(2J+3)}{(14J+1)}$	$\frac{(2J-1)(2J+3)}{(12J^2+12J+1)}$	
$\Delta j=1$	$\frac{(J+1)(2J+3)}{(26J^2-15J-1)}$		

TABLE II. *R/Q, for first transition quadrupole, second dipole.*

	$\Delta J=1$	$\Delta J=0$	$\Delta J=-1$
$\Delta j=2$	$\frac{-3}{29}$	$\frac{3(2J+3)}{(26J-3)}$	$\frac{-3(J+1)(2J+3)}{(58J^2-23J+3)}$
$\Delta j=1$	$\frac{3(J-5)}{(55J+61)}$	$\frac{-3(2J+3)(J-5)}{(58J^2+49J-15)}$	$\frac{3(2J+3)(J-5)}{(110J^2-49J+15)}$
$\Delta j=0$	$\frac{(2J-3)(2J+5)}{(36J^2+92J+61)}$	$\frac{-(2J-3)(2J+5)}{5(4J^2+4J-1)}$	$\frac{(2J-3)(2J+5)}{(36J^2-20J+5)}$
$\Delta j=-1$	$\frac{3(2J-1)(J+6)}{(110J^2+269J+174)}$	$\frac{-3(2J-1)(J+6)}{(58J^2+67J-6)}$	$\frac{3(J+6)}{(55J-6)}$
$\Delta j=-2$	$\frac{-3J(2J-1)}{(58J^2+139J+84)}$	$\frac{3(2J-1)}{(26J+29)}$	$\frac{-3}{29}$

place.) The quantities $\sum_{e'}|(A_l|H(\kappa_0'\mathbf{e}')|B_n)|^2$ and $\sum_{e''}|(B_n|H(\kappa_0''\mathbf{e}'')|C_p)|^2$ contain in their dependence on κ_0' and κ_0'' the angular distributions of quanta emitted in the transitions A_lB_n and B_nC_p, and when integrated over all directions of emission are proportional to the total probabilities of these transitions. Hence

$$\sum_{e'}|(A_l|H(\kappa_0',\mathbf{e}')|B_n)|^2 \leqq g_{ln}\,\varphi_{|n-l|}(\theta_1), \quad \sum_{e''}|(B_n|H(\kappa_0'',\mathbf{e}'')|C_p)|^2 \leqq G_{np}\,f_{|p-n|}(\theta_2). \tag{12}$$

(φ and f normalized to any convenient constant.) Putting Eq. (12) into Eq. (11), setting $\theta_1=0$ and $\theta_2=\theta$, and dropping the constant $\varphi_1(0)$, we obtain Eq. (2) as was promised.

The g_{ln}, G_{np}, and $f_{|p-n|}(\theta)$ depend on the multipolarity of the transition to which they refer, and this multipolarity is in turn determined by the predominating term in the expansion of $\exp(i\kappa\cdot\mathbf{r})$ in $H(\kappa_0,\mathbf{e})$. In Appendix II the expanded form of $H(\kappa_0,\mathbf{e})$ is given and the method of calculating the $f_{|p-n|}(\theta)$ is outlined. The resulting angular distributions (of course identical with those obtained by various other methods[3]) are as follows:

Dipole radiation: $f_1(\theta)=1+\cos^2\theta$, $f_0(\theta)=2(1+\cos^2\theta)$.

Quadrupole radiation: $f_2(\theta)=1-\cos^4\theta$, $f_1(\theta)=1-3\cos^2\theta+4\cos^4\theta$, $f_0(\theta)=6(\cos^2\theta-\cos^4\theta)$.

(Note that in accordance with proposition (2a), $f_0(0)=f_2(0)=0$.) The g_{ln} and G_{np} for dipole or quadrupole transitions may be obtained from the matrix elements in reference 3, pp. 63 or 95.

CALCULATIONS

We designate the angular momenta of the levels A, B and C as $J-\Delta j$, J, and $J+\Delta J$, respectively, so that the angular momentum changes in the first and second transitions are Δj and ΔJ.

The g_{ln} are usually given as functions of the initial quantum numbers $J-\Delta j$ and l but are more convenient for use here as functions of J and n. Making this change and defining

$$d_n=g_{n+1,n}+g_{n-1,n}, \quad D_n=G_{n,n+1}+G_{n,n-1}, \quad E_n=G_{n,n+2}+G_{n,n-2},$$

we have

$$W=f_0(\theta)\sum_n d_nG_{nn}+f_1(\theta)\sum_n d_nD_n+f_2(\theta)\sum_n d_nE_n.$$

[3] E. U. Condon and G. H. Shortley, *Theory of Atomic Spectra* (Cambridge University Press, 1935), for example, Chap. IV.

TABLE III. *R/Q, for both transitions quadrupole.*

	$\Delta J=0$	$\Delta J=-1$	$\Delta J=-2$
$\Delta j=-2$	$\frac{-(2J-3)(2J+1)}{(2J+3)(6J+5)}$	$\frac{(J+3)}{(17J+15)}$	$\frac{1}{8}$
$\Delta j=-1$	$\frac{(5J-2)(2J-3)(2J+5)}{(20J^3+52J^2+41J+6)}$	$\frac{-(17J^2+17J-30)}{(35J^2+35J+6)}$	$\frac{(J-2)}{(17J+2)}$
$\Delta j=0$	$\frac{-(2J-3)(4J^2+4J-7)(2J+5)}{(2J-1)(2J+3)(4J^2+4J-1)}$	$\frac{(5J+7)(2J-3)(2J+5)}{(20J^3+8J^2-3J+3)}$	$\frac{-(2J+1)(2J+5)}{(2J-1)(6J+1)}$
$\Delta j=1$		$\frac{-(2J+3)(17J^3+69J^2-77J-105)}{(70J^4-9J^3-73J^2-27J-9)}$	$\frac{(2J+3)(J^2+18J+5)}{(34J^3-57J^2+8J+3)}$
$\Delta j=2$			$\frac{(J+1)(2J+3)(2J^2-9J+1)}{(2J-1)(16J^3-42J^2+29J+3)}$

	$\Delta J=2$	$\Delta J=1$
$\Delta j=-2$	$\frac{J(2J-1)(2J^2+13J+12)}{(2J+3)(16J^3+90J^2+161J+84)}$	$\frac{(2J-1)(J^2-16J-12)}{(34J^3+159J^2+224J+96)}$
$\Delta j=-1$		$\frac{-(2J-1)(17J^3-18J^2-164J-24)}{(70J^4+289J^3+374J^2+188J+24)}$

TABLE IV. *S/Q, for both transitions quadrupole.*

	$\Delta J=0$	$\Delta J=-1$	$\Delta J=-2$
$\Delta j=-2$	$\frac{4(J-1)(2J-3)}{3(2J+3)(6J+5)}$	$\frac{-4(2J-3)}{3(17J+15)}$	$\frac{1}{24}$
$\Delta j=-1$	$\frac{-16(J-1)(2J-3)(2J+5)}{3(20J^3+52J^2+41J+6)}$	$\frac{16(2J-3)(2J+5)}{3(35J^2+35J+6)}$	$\frac{-4(2J+5)}{3(17J+2)}$
$\Delta j=0$	$\frac{16(J-1)(J+2)(2J-3)(2J+5)}{3(2J-1)(2J+3)(4J^2+4J-1)}$	$\frac{-16(J+2)(2J-3)(2J+5)}{3(20J^3+8J^2-3J+3)}$	$\frac{4(J+2)(2J+5)}{3(2J-1)(6J+1)}$
$\Delta j=1$		$\frac{16(2J-3)(2J+3)(J+2)(2J+5)}{3(70J^4-9J^3-73J^2-27J-9)}$	$\frac{-4(2J+3)(J+2)(2J+5)}{3(34J^3-57J^2+8J+3)}$
$\Delta j=2$			$\frac{(J+1)(2J+3)(J+2)(2J+5)}{3(2J-1)(16J^3-42J^2+29J+3)}$

	$\Delta J=2$	$\Delta J=1$
$\Delta j=-2$	$\frac{J(2J-1)(J-1)(2J-3)}{3(2J+3)(16J^3+90J^2+161J+84)}$	$\frac{-4(2J-1)(J-1)(2J-3)}{3(34J^3+159J^2+224J+96)}$
$\Delta j=-1$		$\frac{16(2J-1)(J-1)(2J-3)(2J+5)}{3(70J^4+289J^3+374J^2+188J+24)}$

If the second transition is dipole,

$$W=\sum_n d_n(D_n+2G_{nn})+\cos^2\theta\sum_n d_n(D_n-2G_{nn})\equiv Q+R\cos^2\theta, \tag{13a}$$

while if it is quadrupole,

$$W=\sum_n d_n(D_n+E_n)+\cos^2\theta\sum_n d_n(\tfrac{2}{7}^{(6)}G_{nn}-3D_n)$$
$$+\cos^4\theta\sum_n d_n(-\tfrac{2}{7}^{(6)}G_{nn}+4D_n-E_n)\equiv Q+R\cos^2\theta+S\cos^4\theta. \tag{13b}$$

Dropping a constant factor, our correlation function for calculation is

$$\mathbf{W(\theta)=1+(R/Q)\cos^2\theta+(S/Q)\cos^4\theta.}$$

The g_{ln}, G_{np}, d_n, D_n and E_n are linear functions of n^2 for dipole transitions and quadratic functions of n^2 for quadrupole transitions, so that the summations indicated may involve $\sum_n 1$, n^2, n^4, n^6, n^8 where $n=-J,\cdots J$. These sums (for n integral or half-integral) are given by[4]

[4] The author is indebted to Dr. J. R. Stehn for a derivation of the formulae for Σn^6 and Σn^8.

$$\sum 1=2J+1,\quad 3\sum n^2=J(J+1)(2J+1),\quad 15\sum n^4=J(J+1)(2J+1)(3J^2+3J-1),$$
$$21\sum n^6=J(J+1)(2J+1)(3J^4+6J^3-3J+1),$$
$$45\sum n^8=J(J+1)(2J+1)(5J^6+15J^5+5J^4-15J^3-J^2+9J-3).$$

In Q, R, and S, each of these sums occurs multiplied by a polynomial in J. When the summations are completed for the most complicated case (both transitions quadrupole), Q, R and S are nearly always of the form $J(J+1)(2J+1)$ times a sixth-degree polynomial in J. These polynomials are found to contain a number of linear factors such that R/Q and S/Q are ratios of much smaller polynomials.

Since the coupling term is Hermitian, it is obvious from Eq. (10) that if two pairs of transitions are each other's inverses, i.e., differ by an interchange of initial and final angular momenta and radiation processes, and have the same intermediate angular momentum, then their correlation functions are identical. However, the processes of calculating W for a sequence and for its inverse are distinctly different; this provides a valuable check on the calculations. $1\to2\to0$ (dipole, quadrupole) and $0\to2\to1$ (quadrupole, dipole), for example, are two such sequences. For the second of these, (13a) shows that there is no $\cos^4\theta$ term in W; for the first, this may be shown only by proving explicitly that $S=0$.

The functions R/Q and S/Q are given in Tables I to IV. Any sequence not shown is to be obtained from its inverse. These functions are shown graphically in Figs. 1 to 5. Each curve begins at the lowest value of J permitted by the selection rules. (See Appendix II.) Beyond $J=7$, each curve is connected by an oblique line to its asymptote.

Discussion

Some generalizations to higher multipole orders may be made. Electric and magnetic multipoles of the same order will not be distinguishable, since the g, G, f and φ are the same for each. $W(\theta)$ will in general be a polynomial in $\cos^2\theta$ of degree l, where the lowest multipole present is a 2^l-pole. It will be noted that for dipole and quadrupole radiation $W(\theta)$ is a constant for $J=0, \frac{1}{2}$, and is linear in $\cos^2\theta$ for $J=1, 3/2$; one suspects that for all multipoles $\cos^{2k}\theta$ may appear only when $J\geqslant k$.

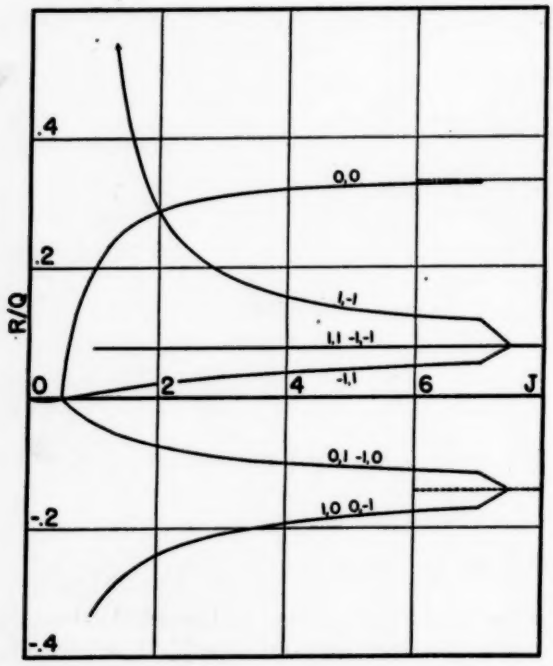

Fig. 1. R/Q as function of J; both transitions dipole. Curves labeled $\Delta j, \Delta J$. Point not shown: on $(1,-1)$ curve, $J=1$, $R/Q=1$.

Our procedure is changed only formally, and the final results not at all, if one or both transitions are absorptions rather than emissions. Thus, for example, W should give the angular distribution of resonance radiation excited by a unidirectional unpolarized beam of light.

We have tacitly assumed that during τ, the lifetime of level B, J_z is constant. But, for example, the atomic electrons produce at the nucleus a field $\mathbf{H}$ oriented at random with respect to $\varkappa$; $\mathbf{J}$ precesses about $\mathbf{H}$ with the Larmor precession frequency $\nu=\mu H/Jh$. Roughly, J_z will change by $\pm\hbar$ for half the nuclei when $\mathbf{J}$ has precessed through an angle $(3\pi/4J)$, i.e., in time $t=(3/8J\nu)=(3h/8\mu H)$ sec. The hyperfine structure splitting of an atomic level is $\Delta\nu\sim(3\mu H/hc)\sim1/tc$ cm^{-1}; for $\Delta\nu\leq1$ cm^{-1} (which is usually true), $t\geqslant3\times10^{-11}$ sec. For three levels

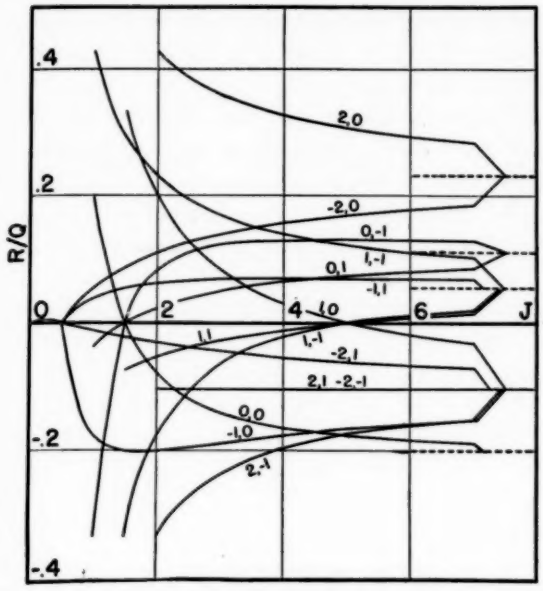

FIG. 2. R/Q as function of J; first transition quadrupole, second dipole. Curves labeled Δj, ΔJ.

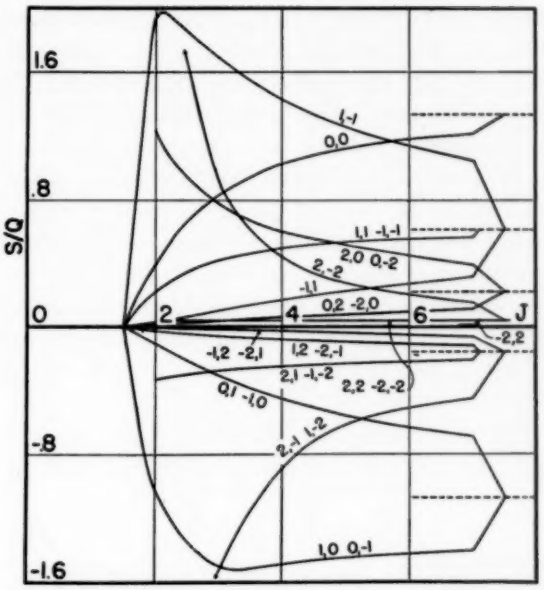

FIG. 4. S/Q as function of J; both transitions quadrupole. Curves labeled Δj, ΔJ. Points not shown: on $(2, -2)$ curve, $J=2$, $S/Q=4$; on $(2, -1)$, $(1, -2)$ curve, $J=2$, $5/2$, $S/Q=-16/3$, $-80/33$.

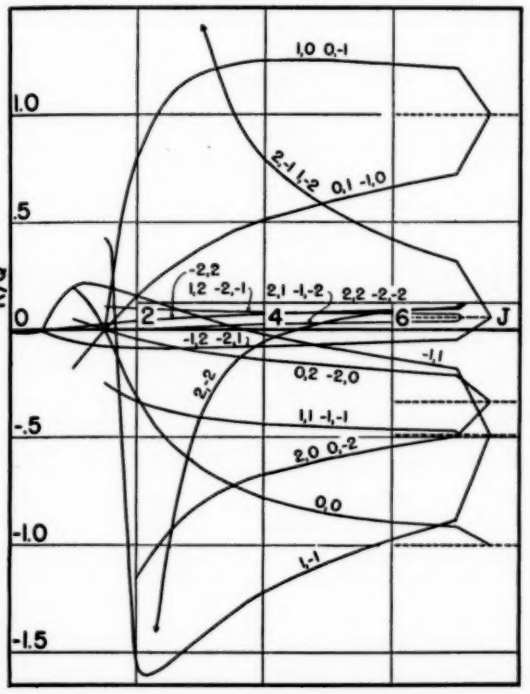

FIG. 3. R/Q as function of J; both transitions quadrupole. Curves labeled Δj, ΔJ. Points not shown: on $(2, -2)$ curve, $J=2$, $R/Q=-3$; on $(2, -1)$, $(1, -2)$ curve, $J=2$, $5/2$, $R/Q=5$, $25/11$.

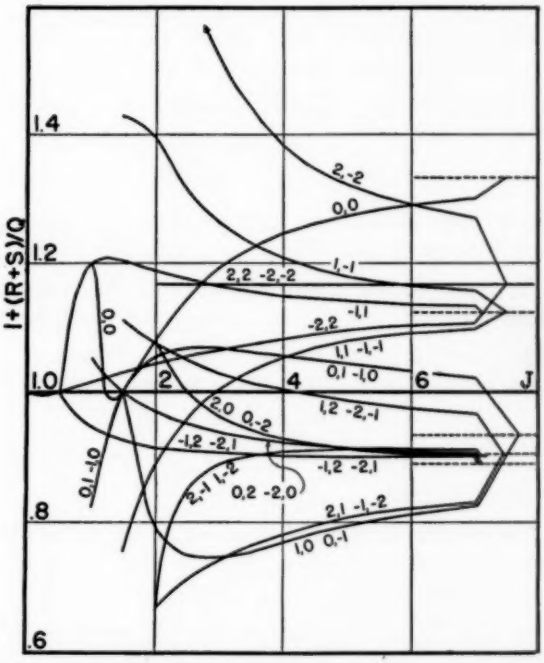

FIG. 5. $1+(R+S)/Q=W(0 \text{ or } \pi)/W(\pi/2)$, as function of J; both transitions quadrupole. Curves labeled Δj, ΔJ. Point not shown: on $(2, -2)$ curve, $J=2$, $1+(R+S)/Q=2$.

of RaC′ and ThC′ for which τ is known to be of the order of 5×10^{-13} sec.,[5] it is then probably true that $t \gtrsim 60\tau$, which is satisfactory. However, a nucleus of mass 200 emitting a 1-Mev quantum recoils with 2.5 volts energy and if unimpeded

[5] H. A. Bethe, Rev. Mod. Phys. **9**, 69 (1937).

would travel 8×10^{-8} cm, or two atomic diameters, in the above τ. It is hard to judge the effect of this motion on the time average **H**. As regards light nuclei, the γ-lifetimes of five excited states formed by proton capture[5] are much shorter and recoil energies much higher (by factors 10^{-2} to 10^{-4} and 10^{2} to 10^{4}, respectively) than in the above cases; the distances traveled in τ range from 0.08 to 4.5×10^{-8} cm. Reorientation is very improbable here unless the fields encountered in the recoil motion are larger, by 10^{3} to 10^{5}, than the static field indicated by hyperfine structure.

The condition $t\gg\tau$ (criterion that $J_z=$ constant, as discussed above) is identical with the condition that the splitting of level B under the influence of **H** be much less than the radiation width of B.

As already mentioned, an attempt is being made by Getting to observe the angular correlation effect, using the γ-rays M and X of ThPb.[6] The counting rates involved are low because of the inefficiency of γ-ray counters and because each counter subtends a comparatively small solid angle at the source; during the necessarily long runs the characteristics of the counters change so that no final results are yet available.

The author is greatly indebted to Professor J. H. Van Vleck for several discussions of important aspects of the questions here treated.

Appendix I

Proposition (1)

a_l, b_n, c_p are probability amplitudes of eigenstates with a fixed axis of quantization; let the corresponding probability amplitudes for some arbitrary axis be α_l, β_n, γ_p. (α, β, γ are not the quantities previously designated by these letters!) We first indicate the proof that $\sum_p|c_p|^2=\sum_p|\gamma_p|^2$ if the α_l which enter into the calculation of the γ_p are determined by a unitary transformation from the initially given a_l. The usual form of the principle of spectroscopic stability (reference 3, Eq. (2²25)), applied to our case, only shows that the total transition probability is independent of the axis of quantization when the states of the initial level have equal amplitudes and random phases; thus it only tells us that $\langle\sum_n|b_n|^2\rangle_{Av}=\langle\sum_n|\beta_n|^2\rangle_{Av}$. For the transition BC we need a generalized form for arbitrary initial states. Following Condon and Shortley[3] it is easily shown that

$$\sum_p|\gamma_p|^2=\sum_{n,k,p}b_n^*b_k(B_n|H|C_p)(B_k|H|C_p)^*=\sum_p|c_p|^2,$$

which may be written in their notation by putting $b_n=(\Gamma_b'|)$, $\beta_n=(\Delta_b'|)$, $c_p=(\Gamma_c'|)$, $(B_n|H|C_p)=(\Gamma_b'|H|\Gamma_c')$, etc.

As concerns the unitary transformation from the a_l to the α_l, this is trivial for our particular initial conditions; it is physically obvious, or may be shown by making the transformation, that if $\langle a^*_{l_1}a_{l_2}\rangle_{Av}=\delta_{l_1l_2}$ then $\langle\alpha^*_{l_1}\alpha_{l_2}\rangle_{Av}=\delta_{l_1l_2}$. Hence the α_l also are equal in amplitude and random in phase and averages of any quantity over the phases of the a_l or of the α_l are equivalent processes. Thus $W=\sum\langle|c_p|^2\rangle_{Av}=\sum\langle|\gamma_p|^2\rangle_{Av}$ where the γ_p are calculated from the α_l in the same way as were the c_p from the a_l.

Proposition (2a)

Physically, $l-n=\pm1$ means that whenever a system is observed to emit a quantum in a particular direction, the projection of **J** on this direction has changed by $\mp\hbar$; therefore the projection of the angular momentum of the quantum on its direction of propagation is $\pm\hbar$. The latter result follows from Heitler's treatment of the eigenwaves of the radiation field in a spherical hohlraum.[7] Heitler chooses the set of eigenwaves which, when quantized, have definite values of the total angular momentum and its projection on Oz; these eigenwaves correspond to the various multipole radiation fields emitted in transitions of radiating matter between eigenstates of $\mathbf{J}^2$ and J_z. The angular dependence of the field strengths of these eigenwaves shows that the flow of energy along the axis of quantization Oz vanishes for all eigenwaves except those for which the projection of the angular momentum on the axis is $\mp\hbar$, and which therefore were emitted in a transition $\Delta J_z=\Delta m=\pm\hbar$.

[6] F. Oppenheimer, Proc. Camb. Phil. Soc. **32**, 328 (1936).
[7] W. Heitler, Proc. Camb. Phil. Soc. **32**, 112 (1936).

The proposition may also be proved easily for the explicit form of H given in Eq. (8):

$$(A_l|H(\kappa_0', \mathbf{e}')|B_n)=\mathbf{e}'\cdot(A_l|\mathbf{t}\exp(i\kappa'\cdot\mathbf{r})|B_n)=\mathbf{e}'\cdot\sum_{D,s}(A_l|\mathbf{t}|D_s)(D_s|\exp(i\kappa'\cdot\mathbf{r})|B_n).$$

(D_s indicates all states except those of levels A and B.) As is permitted by proposition (1), we make Oz coincide with κ_0'. Then $i\kappa\cdot\mathbf{r}=i\kappa z$; z, and hence $\exp(i\kappa z)$, is diagonal in J_z, therefore $(D_s|\exp(i\kappa z)|B_n)=0$ unless $s=n$. Except when $l-n=\pm1$, $\mathbf{e}\cdot(A_l|\mathbf{t}|D_n)$ is zero since $\mathbf{e}$ lies in the xy plane. Hence $(A_l|H(\kappa_0', \mathbf{e}')|B_n)=0$ unless $l-n=\pm1$.

Proposition (2b)

By Eqs. (8) and (9b),

$$\sum_{e'}\langle b_n^*b_k\rangle_{Av}=\sum_l(A_l|\mathbf{t}\exp(i\kappa'\cdot\mathbf{r})|B_n)\cdot(\mathbf{e}_1'^*\mathbf{e}_1'+\mathbf{e}_2'^*\mathbf{e}_2')\cdot(A_l|\mathbf{t}\exp(i\kappa'\cdot\mathbf{r})|B_k)^*,$$

which is to be evaluated for $\kappa_0'=\mathbf{k}$. The vectors $\mathbf{e}_1'$ and $\mathbf{e}_2'$ are the two arbitrary unit orthogonal (in general complex) polarization vectors associated with κ_0'. $\mathbf{e}_1'$ and $\mathbf{e}_2'$ lie in the xy plane; it may easily be shown that $\mathbf{e}_1'^*\mathbf{e}_1'+\mathbf{e}_2'^*\mathbf{e}_2'\equiv\mathbf{ii}+\mathbf{jj}$. Since $(A_l|H(\kappa_0', \mathbf{e}')|B_n)=0$ for $\kappa_0'=\mathbf{k}$ unless $n=l\pm1$, we have $\langle b_n^*b_k\rangle_{Av}=0$ for $n\neq k$ unless $k=n\pm2$. The only quantity to be investigated, then, is

$$\begin{aligned}\sum_{e'}\langle b_{l+1}^*b_{l-1}\rangle_{Av}&=(A_l|\mathbf{t}\exp(i\kappa z)|B_{l+1})\cdot(\mathbf{ii}+\mathbf{jj})\cdot(A_l|\mathbf{t}\exp(i\kappa z)|B_{l-1})^*\\&=\{\textstyle\sum_D(A_l|\dot{x}|D_{l+1})(D_{l+1}|\exp(i\kappa z)|B_{l+1})\}\{\sum_D(A_l|\dot{x}|D_{l-1})^*(D_{l-1}|\exp(i\kappa z)|B_{l-1})^*\}\\&\quad+\{\textstyle\sum_D(A_l|\dot{y}|D_{l+1})(D_{l+1}|\exp(i\kappa z)|B_{l+1})\}\\&\qquad\times\{\textstyle\sum_D(A_l|\dot{y}|D_{l-1})^*(D_{l-1}|\exp(i\kappa z)|B_{l-1})^*\}.\end{aligned}\tag{14}$$

Now $(A_l|\mathbf{t}|D_{l\pm1})=2\pi i\nu_{AD}(A_l|\mathbf{r}|D_{l\pm1})$. From the matrices of x and y (e.g. reference 3, p. 63) one may verify that if $(A_l|x|D_{l+1})\equiv\alpha(l)$ then $(A_l|y|D_{l+1})=i\alpha(l)$; $(A_l|x|D_{l-1})^*=-\alpha^*(-l)$; and $(A_l|y|D_{l-1})^*=i\alpha^*(-l)$. From this it follows that the terms in x in Eq. (14) exactly cancel those in y; hence $\sum_{e'}\langle b^*{}_{l+1}b_{l-1}\rangle_{Av}=0$ as was to be shown.

Appendix II

Expanding,
$$\begin{aligned}H(\kappa_0, \mathbf{e})&=\mathbf{e}\cdot\mathbf{t}\exp(i\kappa\cdot\mathbf{r})=\mathbf{e}\cdot\mathbf{t}+2\pi i\nu c^{-1}\mathbf{e}\cdot\mathbf{t}\mathbf{r}\cdot\kappa_0+\cdots\\&=\mathbf{e}\cdot\mathbf{t}+\pi i\nu c^{-1}[\mathbf{e}\cdot(\mathbf{t}\mathbf{r}+\mathbf{r}\mathbf{t})\cdot\kappa_0+\mathbf{e}\cdot(\mathbf{t}\mathbf{r}-\mathbf{r}\mathbf{t})\cdot\kappa_0]+\cdots.\end{aligned}$$

Since $(N'|\mathbf{t}|N'')=2\pi i\nu_{N'N''}(N'|\mathbf{r}|N'')$, N' and N'' any two states of the nucleus, it follows easily that $(N'|\mathbf{t}\mathbf{r}+\mathbf{r}\mathbf{t}|N'')=2\pi i\nu_{N'N''}(N'|\mathbf{r}\mathbf{r}|N'')$. By classical or quantum-vector analysis,

$$(N'|\mathbf{t}\mathbf{r}-\mathbf{r}\mathbf{t}|N'')\cdot\kappa_0=(N'|\mathbf{r}\times\mathbf{t}|N'')\times\kappa_0.$$

The multipole moments of a system with charge and current densities ρ and $\mathbf{i}$ are defined thus:

$$\begin{aligned}&\text{electric dipole moment}&&=\mathbf{P}=\textstyle\int\rho\mathbf{r}dv,\\&\text{electric quadrupole moment}&&=\mathfrak{N}=\textstyle\int\rho\mathbf{r}\mathbf{r}dv,\\&\text{magnetic dipole moment}&&=\mathbf{M}=(1/2c)\textstyle\int\rho\mathbf{r}\times\mathbf{t}dv=(\frac{1}{2})\int\mathbf{r}\times\mathbf{i}dv\end{aligned}$$

and in terms of these, $H(\kappa_0, \mathbf{e})\sim\mathbf{e}\cdot(\mathbf{P}+\mathbf{M}\times\kappa_0+i\pi\nu c^{-1}\mathfrak{N}\cdot\kappa_0+\cdots)$.

The vector part of the matrix elements of $\mathbf{P}$ and $\mathbf{M}$ (reference 3, p. 63) is one of three orthonormal vectors $\mathbf{T}(\Delta m)$. ($\mathbf{T}(i)\cdot\mathbf{T}(j)=\delta_{ij}$.) The J selection rule is $\Delta J=0, \pm1$ with $0\to0$ forbidden. Similarly the matrix elements of $\mathfrak{N}$ (reference 3, p. 95) are proportional to one of five "orthonormal" dyadics $\mathfrak{R}(\Delta m)$ (i.e. $\mathfrak{R}(i):\mathfrak{R}(j)=\delta_{ij}$); and the selection rule on J is here $\Delta J=0, \pm1, \pm2$, with $0\to0$, $\frac{1}{2}\to\frac{1}{2}$, $1\rightleftharpoons0$ forbidden. The angular distributions of radiation emitted by these multipoles depend only on Δm and are proportional to $\sum_e|\mathbf{e}\cdot\mathbf{T}(\Delta m)|^2$, $\sum_e|\mathbf{e}\cdot\mathbf{T}(\Delta m)\times\kappa_0|^2$ and $\sum_e|\mathbf{e}\cdot\mathfrak{R}(\Delta m)\cdot\kappa_0|^2$. Since $\mathbf{e}_1^*\mathbf{e}_1+\mathbf{e}_2^*\mathbf{e}_2\equiv\mathbf{I}-\kappa_0\kappa_0$, ($\mathbf{I}\equiv\mathbf{ii}+\mathbf{jj}+\mathbf{kk}$, the identity dyadic), these functions may be written $\mathbf{T}^*(\Delta m)\cdot(\mathbf{I}-\kappa_0\kappa_0)\cdot\mathbf{T}(\Delta m)$, etc. Use of the explicit forms for $\mathbf{T}(\Delta m)$ and $\mathfrak{R}(\Delta m)$ gives the results in the text.

The Theoretical Constitution of Metallic Beryllium

CONYERS HERRING* AND A. G. HILL
George Eastman Laboratory of Physics, Massachusetts Institute of Technology, Cambridge, Massachusetts

(Received May 13, 1940)

Calculations of total energy as a function of lattice constant, and of some other properties, have been made for metallic beryllium, by a self-consistent field method. Since such calculations have not been made before for any but monovalent metals, the principal object was to find out how far the various assumptions which are usually made in them remain valid for higher valencies, and to test the practicability of certain methods of making the calculations. The theoretical values of binding energy, lattice constant, and compressibility agree reasonably well with experiment. The calculated work function, however, could be made to coincide with the experimental value only by assuming a surface double layer of over 5 volts, which seems impossibly large. This suggests a very large deviation of the exchange energy from the value for completely free electrons. An investigation of the behavior of the exchange energy yields an expression for the deviation from the free electron value which is valid for low electron densities, but not for those which occur in beryllium. The distribution of the electronic states in energy is found to be of the sort needed to account for the diamagnetism of beryllium. Concerning methods of calculation, it is shown that a rather complicated procedure is necessary to obtain quantitative results when a Hartree ion core field is used (as was done in the present case), and that construction of an empirical field is preferable. The assumption $E_k = E_0 + \alpha\hbar^2k^2/2m$, for the energy of an electron with wave vector k, cannot be used for calculations of lattice constant or compressibility for a divalent metal; it is therefore necessary to calculate directly the energies of states near the Fermi surface. This was done by the "orthogonalized plane wave" method, which is shown by tests to be capable of fairly high accuracy, though laborious. This method suggests a simple qualitative way of understanding a number of features of the electronic energy spectrum of a metal and its manner of variation with lattice constant. Incidental results include a proof that the interaction of the $1s$ shells is entirely negligible, and a calculation of the electrostatic interaction energy of the ions as a function of the c/a ratio.

1. INTRODUCTION

THE quantum theory of metals, in the form developed by Wigner and Seitz,[1] has proved rather successful in the explanation and quantitative calculation of a number of properties of alkali metals, such as binding energy, lattice constant, compressibility,[2] and work function.[3] So far no attempt has been made to calculate any of these properties for a divalent metal;[4] moreover, all the metals for which calculations of electronic energy bands[4] have been made have been cubic. The present work on beryllium was undertaken with several objects, of which the most important was that of finding out how far the various assumptions usually made in the application of the theory to monovalent metals remain valid for higher valencies. We also wanted to become familiar with the technique of calculating electronic energies in a crystal of this sort, and in particular to see what additional difficulties are introduced by the fact that the metal is divalent, and by the fact that it has a hexagonal lattice. Finally, we hoped to make a fairly detailed test of the practicability and accuracy of the "orthogonalized plane wave" method of calculating electronic energies and wave functions in crystals, recently described by one of us.[5]

Since the calculations which had to be made for beryllium were considerably more complicated than those which have been made for monovalent metals, and were in addition of an unfamiliar sort, it was not thought wise to try to carry them through with as high a precision as can be attained for alkalis. Nevertheless, sufficient accuracy had to be maintained so that a comparison of the results with experiment

* National Research Fellow, 1937–39. At Princeton University during completion of this work, 1939–40.

[1] E. Wigner and F. Seitz, Phys. Rev. **43**, 804 (1933) and **46**, 509 (1934); F. Seitz, Phys. Rev. **47**, 400 (1935).

[2] J. Bardeen, J. Chem. Phys. **6**, 367, 372 (1938).

[3] E. Wigner and J. Bardeen, Phys. Rev. **48**, 84 (1935); J. Bardeen, Phys. Rev. **49**, 653 (1936).

[4] In addition to the calculations which have been referred to, there are in the literature calculations of the electron energy levels of a number of solids, made by the cellular method of Slater, Phys. Rev. **45**, 794 (1934). Two of these are for metals with more than one valence electron per atom: M. F. Manning and H. Krutter, Phys. Rev. **51**, 761 (1937), (Ca); M. F. Manning and M. I. Chodorow, Phys. Rev. **56**, 787 (1939) (W). However, in none of these cases has an attempt been made to calculate the total energy of the crystal.

[5] C. Herring, Phys. Rev. **57**, 1169 (1940).

would throw light on the validity of some of the more fundamental assumptions made in the course of the work. It was therefore thought at the beginning that the most convenient thing to do would be to make a Hartree self-consistent field solution for the electrons in the metal by using for the core wave functions the $1s$ wave functions given by Hartree and Hartree[6] for Be^{++}. This self-consistent field solution was obtained, and our final results are based on it; however, the calculation of the total energy from the Hartree wave functions turned out to be rather more laborious than we had anticipated, and in fact both theory and computation would have been much simplified by constructing at the outset an empirical field of the sort used by Seitz[1] for lithium. Section 2 consists in the derivation of the formula (28) for the total energy of a beryllium crystal, in the Hartree approximation; if an empirical field had been used these lengthy calculations would not have been necessary. Section 3 describes the approximately self-consistent potential field used for the calculations. The next four sections are devoted to the problem of finding the Hartree energy parameters E_k for the continuous distribution of valence electron states. The quantities directly calculated for this purpose are: (1) the energy E_0 of the lowest valence electron state, obtained by the method of Wigner and Seitz;[1] (2) $\alpha=(m/\hbar^2)[\partial^2E_k/\partial k^2]_{k=0}$, obtained by the method of Bardeen;[2] and (3) energies E_k of a number of states near the surface of the Fermi distribution, obtained by the orthogonalized plane wave method.[5] The distribution of the electronic states in energy can be estimated from these quantities by a graphical method. It is of less interest to know the number of states per unit range of E than the number per unit range of the quantity η defined by (29), since the latter is more closely connected with the ionization energies of the individual electronic states; consequently the distributions are calculated in Section 7 for η rather than for E. The difference between η_k and E_k consists of a number of terms, which can be calculated if the wave function φ_k is known. The graphical calculations of Section 7 are aided by the use of rough values of $\beta=(m/\hbar^2)(\partial^2E_k/\partial k^2)$, computed for the same wave vectors $\mathbf{k}$ for which the energies E_k mentioned above were calculated. In Section 8 a brief investigation is made of the validity of the assumption, usually made in calculations of this sort, that the exchange energy of the valence electrons in the metal is the same as that of a free electron gas of the same density. Section 9 contains all the results of the present work, and a discussion of their significance.

2. Total Energy in the Hartree Approximation

The notation employed in this and the following sections is for the most part the same as that of reference 5. Atomic units will be used, energies being measured in rydberg units and distances in units of the Bohr radius $\hbar^2/me^2$. For mathematical convenience periodic boundary conditions will be imposed:[7] it will be assumed that the crystal is of practically infinite extent, but that all the wave functions, potentials, etc. are trebly periodic in space, with periods $N_a\mathbf{t}_a$, $N_b\mathbf{t}_b$, $N_c\mathbf{t}_c$, where $\mathbf{t}_a$, $\mathbf{t}_b$, $\mathbf{t}_c$, are three fundamental translations of the crystal lattice, and N_a, N_b, N_c, are three very large integers. The parallelepiped defined by $N_a\mathbf{t}_a$, $N_b\mathbf{t}_b$, $N_c\mathbf{t}_c$, will be called the "fundamental volume" Ω; we assume it to consist of N unit cells each of volume Ω_0 and each containing n atoms ($n=2$ for beryllium). It will be assumed that each unit cell can be divided up into "atomic cells" each of volume Ω_0/n and all alike except for orientation. Mention will frequently be made of an "s sphere": this is a sphere with center at an atomic position and radius r_s so chosen that its volume equals the volume of an atomic cell. The symbol (ψ_1, ψ_2) will be used for the scalar product $\int_\Omega \psi_1^*\psi_2 d\tau$ of any pair of wave functions.

When periodic boundary conditions are employed one cannot speak of the electrostatic potential due to a charge distribution unless the integral of the charge density over Ω vanishes. So if we want to break up the electrostatic potential in the crystal, or the electrostatic self-energy, into contributions from different sources, we must use some artifice. For the potential due to any charge distribution satisfying our periodic

[6] D. R. Hartree and W. Hartree, Proc. Roy. Soc. London **A149**, 210 (1935); **A150**, 9 (1935).

[7] M. Born, Ency. Math. Wiss. 5, iii, p. 587; M. Born and J. H. C. Thompson, Proc. Roy. Soc. **A147**, 594 (1934).

boundary conditions we shall accordingly use what may be called the "neutralized potential" of the distribution.[8] If ρ is such a charge distribution and $\bar{\rho}$ is its average value over Ω, the neutralized potential Φ due to ρ is defined as that solution of

$$\nabla^2\Phi = -4\pi(\rho-\bar{\rho}),$$

which satisfies the periodicity conditions and has average value 0. In other words, Φ is the potential due to the combination of ρ with a homogeneous charge distribution of such sign and density as to neutralize ρ over Ω. It is not hard to see that the final electrostatic energy per atom of a neutral crystal will be independent of whether neutralized or ordinary potentials are used in calculating it. To make the analogy with the usual electrostatic potential as close as possible, we shall write $2Z/D(\mathbf{r})$ for the neutralized potential, in rydbergs per electron, due to a charge Z times the electronic charge located at the origin: thus $D(\mathbf{r})$ is practically the same as r whenever r is small compared with the dimensions of the fundamental volume.

If V_j is the neutralized potential due to the charge distributions of all the Hartree eigenfunctions except φ_j, the Hartree functions φ_j will satisfy

$$(H_0+V_j)\varphi_j = E_j\varphi_j, \tag{1}$$

where

$$H_0 = -\nabla^2 - \sum_\nu 2Z/D(\mathbf{r}-\mathbf{R}_\nu) + c; \tag{2}$$

here Z is the nuclear charge (4 for beryllium), $\mathbf{R}_\nu$ runs over the position vectors of all nuclei in the fundamental volume, and c is a constant fixing the zero for E_j, which we are free to choose as we please. It will be a sufficiently good approximation to assume that when j is a core state φ_j is the same as the Hartree $1s$ function for a free Be^{++} ion (hence that φ_j is localized about a particular atom); when j is a valence electron state φ_j will be taken to be a Bloch wave[9] of the form $\exp(i\mathbf{k}_j\cdot\mathbf{r})u_{k_j}(\mathbf{r})$, where u_{k_j} has the translational periodicity of the lattice. In both cases φ_j is assumed normalized to 1 over Ω, which for the core state is practically infinite. With wave functions of this form V_j is practically the same for all valence electron states, but is different for the core states. Wigner and Seitz have pointed out that the potential for a valence electron inside any s sphere is approximately

$$v(r)+(3X/r_s - Xr^2/r_s^3), \tag{3}$$

where $v(r)$ is the potential due to the ion at the center, and where the second term is the potential due to a charge of X electrons uniformly distributed over the volume of the s sphere ($X=2$ for beryllium). When j is a valence electron state we may write

$$(H_0+V_j) = -\nabla^2 + U_0. \tag{4}$$

The average value of U_0 is equal to c, and it will be convenient to choose c equal to the average of (3) over an s sphere: this may be written

$$c = \frac{3}{4\pi r_s^3}\int_s [v(r)+2X/r]d\tau - 3X/5r_s, \tag{5}$$

provided we assume $v(r) = -2X/r$ for $r \geq r_s$.

Since the φ_j for valence electron states are eigenfunctions of a single Hamiltonian, they are all orthogonal to one another. But since the Hamiltonian for the core states is different, the φ_j for valence electron states will not be orthogonal to those for the core states. The customary procedure[10] in determining the total energy by the Hartree method commences by replacing the Hartree eigenfunctions by a set of orthogonal linear combinations of them. Accordingly we shall define the functions

$$\psi_j = \varphi_j + \Delta\varphi_j \tag{6}$$

to be such an orthogonal and normal set. We may specify $\Delta\varphi_j = 0$ when j is a core state (this implies neglect of the small overlap of core functions of different atoms[11]); and when j is a

[8] This conception is similar to that used when electrostatic potentials are calculated by the method of Ewald. See for example the article of M. Born and M. Göppert-Mayer in the *Handbuch der Physik* (Berlin, 2nd ed., 1933), Vol. 24/2, p. 711. We use periodic boundary conditions and neutralized potentials, rather than working with a finite crystal, because it is desirable to be able to break up the electrostatic energy into parts without the danger that some of the parts may depend on the size and shape of the crystal.

[9] F. Bloch, Zeits. f. Physik **52**, 555 (1929).

[10] D. R. Hartree and M. M. Black, Proc. Roy. Soc. London **A139**, 311 (1933).

[11] The effect of such overlapping on the total energy gives just the Heitler-London value for the potential energy of the repulsive force between the ions. It is shown in Appendix I that this repulsive force must be negligible, although no attempt has been made to calculate it for the Hartree wave functions.

valence electron state

$$\psi_j(\mathbf{r}) = \frac{\varphi_j(\mathbf{r}) - \sum_\nu a_j(\nu)\varphi_{1s}(\mathbf{r}-\mathbf{R}_\nu)}{1-\sum_\nu |a_j(\nu)|^2}, \tag{7}$$

where $a_j(\nu) = (\varphi_{1s\nu}, \varphi_j)$ is the scalar product of the $1s$ function on the νth nucleus with φ_j. In the Hartree approximation the total energy W_H relative to widely separated Be^{++} ions and electrons consists of three parts: the kinetic energy of the valence electrons, the electrostatic energy of the crystal relative to the decomposed state, and the exchange energy minus the exchange energy in the decomposed state. Each of these three must be calculated with the ψ_j.

In calculating the sum of these three terms we need not for the present restrict ourselves to the case of beryllium, and accordingly Eq. (13) below will hold for any values of Z, X, and n. The electrostatic term may be broken up into the neutralized interaction energy of the ions, that of the valence electrons, and that of the ions with the valence electrons. In calculating the neutralized interaction energy of two different ions μ and ν, it is convenient to picture each ion as composed of a positive point charge equal to the charge X carried by an ion, and a neutral distribution consisting of the core electrons and a positive point charge $(Z-X)$. The interaction energy of the neutral distributions of μ and ν is zero, if we neglect overlapping. The energy of the neutral distribution of μ in the neutralized potential due to the point charge X at $\mathbf{R}_\nu$ is

$$\int_\infty \frac{X}{\Omega}[v(|\mathbf{r}-\mathbf{R}_\mu|)+2X/|\mathbf{r}-\mathbf{R}_\mu|]d\tau,$$

where $-X/\Omega$ is the constant charge density used in forming the neutralized potential of the point charge X, and the quantity in brackets is the negative of the (ordinary, not neutralized) potential due to the neutral distribution on μ. Adding twice this to the interaction energy $2X^2/D(\mathbf{R}_\mu-\mathbf{R}_\nu)$ of the point charges gives the neutralized interaction energy of the two ions. We can now write

$$\begin{aligned}\text{Electrostatic part of } W_H = {} & \tfrac{1}{2}\sum_{\mu\neq\nu}\left\{2X^2/D(\mathbf{R}_\mu-\mathbf{R}_\nu)+2X/\Omega\int[v(r)+2X/r]d\tau\right\} \\ & +\tfrac{1}{2}\sum_{i,j\ \text{valence}}\int_\Omega\int_\Omega \frac{\psi_j^*(\mathbf{r})\psi_i^*(\mathbf{r}')2\psi_j(\mathbf{r})\psi_i(\mathbf{r}')d\tau d\tau'}{D(\mathbf{r}-\mathbf{r}')} \\ & +\sum_{j\ \text{valence}}\int_\Omega |\psi_j(\mathbf{r})|^2\sum_\nu\left[\frac{-2Z}{D(\mathbf{r}-\mathbf{R}_\nu)}+\sum_{i\ \text{core on}\ \nu}\int_\Omega \frac{2|\psi_i(\mathbf{r}')|^2}{D(\mathbf{r}-\mathbf{r}')}d\tau'\right]d\tau. \end{aligned} \tag{8}$$

In the summations in (8) and henceforth, unless otherwise stated, states i or j with the same orbital wave function but different spins are to be counted separately.

Let us introduce the abbreviations $C_{ij}(\psi)$ for the double integral in the second term of (8), and $A_{ij}(\psi)$ for the corresponding exchange integral. Then remembering (1), (2), and (5), the total energy is

$$\begin{aligned} W_H = {} & \sum_{j\ \text{valence}}(\psi_j, H_0\psi_j)+\Big[\tfrac{1}{2}\sum_{i,j\ \text{valence}}+\sum_{\substack{i\ \text{core}\\ j\ \text{valence}}}\Big]C_{ij}(\psi) \\ & -\Big[\tfrac{1}{2}\sum_{\substack{i,j\ \text{valence}\\ \text{spins}\ \|}}+\sum_{\substack{i\ \text{core}\\ j\ \text{valence}\\ \text{spins}\ \|}}\Big]A_{ij}(\psi)+\tfrac{1}{2}\sum_{\mu\neq\nu}2X^2/D(\mathbf{R}_\mu-\mathbf{R}_\nu)+3nNX^2/5r_s. \end{aligned} \tag{9}$$

We shall now investigate the consequences of inserting (6) in (9). In the first term of (9) we have, using (1)

$$\begin{aligned}(\psi_j, H_0\psi_j) &= (\psi_j, \{H_0+V_j-V_j\}\psi_j) \\ &= -(\varphi_j, V_j\varphi_j)-2\Re(\Delta\varphi_j, V_j\varphi_j)-(\Delta\varphi_j, V_j\Delta\varphi_j) \\ &\quad +E_j[1+2\Re(\varphi_j, \Delta\varphi_j)]+(\Delta\varphi_j, \{H_0+V_j\}\Delta\varphi_j), \end{aligned} \tag{10}$$

where the symbol $\Re$ means "real part of." Since ψ_j and φ_j are both normalized

$$2\Re(\varphi_j, \Delta\varphi_j) = -(\Delta\varphi_j, \Delta\varphi_j). \tag{11}$$

The second term of (9) is, with neglect of terms containing three or more $\Delta\varphi$'s,

$$\Big[\tfrac{1}{2}\sum_{i,j\ \text{valence}} + \sum_{\substack{i\ \text{core}\\ j\ \text{valence}}}\Big]C_{ij}(\psi) = \Big[\tfrac{1}{2}\sum_{i,j\ \text{valence}} + \sum_{\substack{i\ \text{core}\\ j\ \text{valence}}}\Big]C_{ij}(\varphi) + 2\Re\sum_{j\ \text{valence}}(\Delta\varphi_j, V_j\varphi_j) + \sum_{j\ \text{valence}}(\Delta\varphi_j, V_j\Delta\varphi_j) + \tfrac{1}{2}\sum_{i,j\ \text{valence}}\int_\Omega\int_\Omega \frac{2[2\Re\Delta\varphi_i(\mathbf{r}')\varphi_i^*(\mathbf{r}')][2\Re\Delta\varphi_j(\mathbf{r})\varphi_j^*(\mathbf{r})]}{D(\mathbf{r}-\mathbf{r}')}d\tau d\tau', \tag{12}$$

where $C_{ij}(\varphi)$ is a double integral like the one in (8), but with the ψ's replaced by φ's. Thus the first term of (12) is just

$$\sum_{j\ \text{valence}}(\varphi_j, V_j\varphi_j).$$

The combination of (9), (10), (11), and (12) gives, to the order of accuracy of (12)

$$W_H = \sum_{j\ \text{valence}} E_j - \tfrac{1}{2}\sum_{i,j\ \text{valence}} C_{ij}(\varphi) - \tfrac{1}{2}\sum_{\substack{i,j\ \text{valence}\\ \text{spins}\ \|}} A_{ij}(\psi) - \sum_{\substack{i\ \text{core}\\ j\ \text{valence}\\ \text{spins}\ \|}} A_{ij}(\psi) + \sum_{j\ \text{valence}}(\Delta\varphi_j, \{H_0+V_j-E_j\}\Delta\varphi_j) + Q + \tfrac{1}{2}\sum_{\mu\neq\nu} 2X^2/D(\mathbf{R}_\mu-\mathbf{R}_\nu) + 3nNX^2/5r_s, \tag{13}$$

where Q stands for the last term of (12). In (13), which applies to any metal with sufficiently compact core wave functions, the first three terms are the only ones which would be present if the Hartree field were used in the same way as the empirical fields used by Wigner and Seitz[1] for sodium, and by Seitz[1] for lithium. The fourth term is the exchange between valence electrons and cores. The fifth term, whose physical meaning is less directly obvious, will be shown below to give important contributions to the binding energy of beryllium. Moreover, since it contains two $\Delta\varphi$'s, which vary with lattice constant on account of the normalization of the wave functions, this term has quite an important effect on lattice constant and compressibility. The term Q was expected for the same reason to have an appreciable effect on the compressibility; numerical calculation however showed it to be almost negligible. The neglected terms with three and four $\Delta\varphi$'s are smaller still.

We shall now specialize to the case of beryllium, and with the aid of a few approximations which are safe in this case it will be possible to put the fourth, fifth, and sixth terms of (13) into a form which can be used for numerical calculation. The exchange energy $A_{ij}(\psi)$ of a valence electron state ψ_j with a core state ψ_i may be evaluated by expanding ψ_j into spherical harmonics about the nucleus on which ψ_i is localized. The part involving each spherical harmonic gives a contribution to $A_{ij}(\psi)$ which can be expressed as a double integral containing the radial coefficient of that spherical harmonic.[12] We shall retain only the terms $l=0$ and 1, writing

$$\psi_j = \varphi_j + \Delta\varphi_j = R_0(r) + \sum_{m=-1}^{1} R_{1m}(r)P_1^m(\cos\theta)\exp(im\varphi) \tag{14}$$

plus terms in higher harmonics which we neglect. Now the negative potential near the nucleus is practically spherically symmetrical, and is large compared with the width of the valence electron band and large compared with the variation of the potential with lattice constant. It is therefore reasonable to expect that near the nucleus the s part of φ_j can be well approximated by a constant

[12] The method of calculating these exchange terms has been described by J. C. Slater, Phys. Rev. **34**, 1293 (1929).

times a fixed function φ_{00} independent of j and of lattice constant. For φ_{00} we shall choose the eigenfunction of the lowest valence electron state, for the observed value of the lattice constant; in the approximation of Wigner and Seitz, which we use in Section 4, this wave function is simply a $2s$ function whose radial derivative vanishes on the boundary of the s sphere. Since the quantity $a_j(\nu)$ occurring in (7) depends only on the s part of φ_j around the νth atom, and since in all cases the $a_j(\nu)$ are so small that the second term of the denominator of (7) is $\lesssim 0.01$, we may set in (14)

$$R_0(r)=\frac{\varphi_j(0)}{\varphi_{00}(0)}\psi_{00}(r), \tag{15}$$

where ψ_{00} is the function obtained by putting $\varphi_j=\varphi_{00}$ in (7). Numerical calculations have shown that the error in the approximation (15) affects the contribution of R_0 to $A_{ij}(\psi)$ in the most unfavorable cases by only a few percent. We may approximate to R_{1m} near the nucleus by a similar expression:

$$R_{1m}(r)=\left[\lim_{r'\to 0}\frac{R_{1m}(r')}{R_p(r')}\right]R_p(r), \tag{16}$$

where $R_p(r)$ is the radial part of some standard solution, with $l=1$, of the wave equation in the central field which approximates the field around the nucleus. We shall choose for R_p the radial part of the p function calculated in the same central field used for φ_{00} with an energy parameter so chosen that the boundary condition $R_p'=0$ is satisfied on the surface of the s sphere for the observed lattice constant; the scale of R_p will be made definite by assuming that

$$2N/3\int_0^{r_s}4\pi r^2R_p^2dr=1$$

for $r_s=2.37$ Bohr units, corresponding to the observed lattice constant. This corresponds roughly to assuming that a function defined in each atomic cell as $R_p\cos\theta$ is normalized to 1 over Ω.

If the higher harmonics as in (14) are neglected, the approximations (15) and (16) yield,[12] for any valence electron state j,

$$\sum_{\substack{i\ \text{core}\\ \text{spin}\,\|\,j}}A_{ij}(\psi)=2s_jG_0+\tfrac{2}{3}p_jG_1. \tag{17}$$

Here

$$s_j=\text{average on }\nu\text{ of }\left|\frac{\varphi_j(\mathbf{R}_\nu)}{\varphi_{00}(\mathbf{R}_\nu)}\right|^2; \tag{18}$$

$$p_j=\text{average on }\nu\text{ of }\sum_{m=-1}^{1}\left|\lim_{\mathbf{r}\to\mathbf{R}_\nu}\frac{R_{1m}(|\mathbf{r}-\mathbf{R}_\nu|)}{R_p(|\mathbf{r}-\mathbf{R}_\nu|)}\right|^2, \tag{19}$$

where $R_{1m}(|\mathbf{r}-\mathbf{R}_\nu|)$ is meant to refer to the p part of ψ_j near the νth nucleus; and

$$G_0=\int_0^\infty\int_0^\infty\frac{P_{1s}(r)P_{2s}^0(r')P_{1s}(r')P_{2s}^0(r)}{r_b}drdr', \tag{20}$$

$$G_1=\int_0^\infty\int_0^\infty P_{1s}(r)P_{2p}(r')P_{1s}(r')P_{2p}(r)\frac{r_a}{r_b^2}drdr', \tag{21}$$

where r_a and r_b are, respectively, the smaller and larger of r and r', and where

$$P_{1s}(r)=r(4\pi)^{\frac{1}{2}}\varphi_{1s}(r),\quad P_{2s}^0(r)=r(8\pi N)^{\frac{1}{2}}\psi_{00}(r),$$

and

$$P_{2p}(r)=r(8\pi N/3)^{\frac{1}{2}}R_p(r)$$

are the radial s and p functions. Thus

$$\int_0^\infty P_{1s}^2 dr = 1;$$

P_{2s}^0 and P_{2p} are normalized to

$$\int_0^{2.37} P^2 dr = 1$$

and the former has been orthogonalized to P_{1s}.

An approximation of the same nature as (15) may also be used in the fifth term of (13). If we neglect the second term in the denominator of (7),

$$\Delta\varphi_j = -\sum_\nu a_j(\nu)\varphi_{1s}(\mathbf{r}-\mathbf{R}_\nu), \tag{22}$$

and if the s part of φ_j is nearly a constant multiple of φ_{00} near each nucleus,

$$a_j(\nu) = \frac{\varphi_j(\mathbf{R}_\nu)}{\varphi_{00}(\mathbf{R}_\nu)}(\varphi_{1s\nu}, \varphi_{00}).$$

If we set

$$a/(2N)^{\frac{1}{2}} = (\varphi_{1s\nu}, \varphi_{00}) \tag{23}$$

and use (18), the fifth term of (13) becomes (neglecting of course overlap of core functions on different atoms)

$$a^2 \sum_{j \text{ valence}} s_j(\varphi_{1s}, \{-\nabla^2 + U_0 - E_j\}\varphi_{1s}). \tag{24}$$

We shall assume φ_{1s} to be localized about an atom at the origin, and shall use the approximate expression (3) for U_0,[13] with

$$v(r) = -2Z/r + 2v_{1s},$$

where v_{1s} is the potential due to one $1s$ electron on the free Be^{++} ion. If $-\epsilon$ is the Hartree $1s$ energy parameter for the free ion, we have

$$(-\nabla^2 + U_0 - E_j)\varphi_{1s} = (-\nabla^2 - 2Z/r + v_{1s} + \epsilon + v_{1s} - \epsilon + 6/r_s - 2r^2/r_s^3 - E_j)\varphi_{1s}.$$

Since φ_{1s} is the Hartree eigenfunction for the free ion, the first four terms in the parenthesis operate on it to give zero. The integral of $v_{1s}|\varphi_{1s}|^2$ is just twice the quantity $F_0(1s, 1s)$ calculated by Hartree and Hartree,[6] and the integral of $2r^2/r_s^3|\varphi_{1s}|^2$ is so small that it can be neglected. Therefore

$$\text{Fifth term of (13)} \approx a^2 \sum_{j \text{ valence}} s_j(-\epsilon - E_j + 2F_0 + 6/r_s). \tag{25}$$

The small sixth term of (13) can be transformed by using approximations of the same nature as those which we have described for the two preceding terms. As the term is unimportant we shall give only the result:

$$Q = 16Na^2\bar{s}^2 B, \tag{26}$$

where

$$\bar{s} = 1/4N \sum_{j \text{ valence}} s_j$$

is the average of s_j over all occupied states, and where

$$B = 2\int_0^{r_s} \left[\frac{\int_0^r (P_{1s}P_{2s} - 3ar_1^2/r_s^3)dr_1}{r} \right]^2 dr, \tag{27}$$

[13] This approximation gives rise to only a very small error. Cf. Wigner and Seitz, reference 1, Appendix II.

with P_{1s} as defined under (20) and (21), while $P_{2s}(r)=r(8\pi N)^{\frac{1}{2}}\varphi_{00}$ is the radial $2s$ wave function *not* orthogonalized to P_{1s}.

We are now ready to combine the expressions for the various terms of (13). The most useful way of grouping the terms would be to find out how much the energy is changed by removal of an electron from each state j, and then to express the total energy as a sum of these "ionization" energies plus whatever additional terms are necessary. If this has been done one can for example find the location of the Fermi surface from the requirement that the ionization energies of all electrons on the Fermi surface must be the same, and the requirement that the number of quantum states with ionization energies below that of the Fermi surface must equal the number of electrons. Now to find the precise ionization energies of the different states the change in the second and third terms of (13) due to removal of a particular electron would have to be calculated. To a good approximation the second term of (13) is zero, because it is the self-energy of the almost uniform charge distribution of the valence electrons minus its average value.[14] So it will not do much harm to neglect the change of this term when an electron is removed. But the third term of (13) is more troublesome. If the electron wave functions were plane waves and the filled region a sphere in momentum space, the change of this term on removal of an electron could be calculated rather easily: it is a function of the momentum of the electron, which has been given explicitly by Brillouin.[15] It will be shown in Section 8, however, that the exchange contributions to the ionization energies of the various electrons probably differ quite appreciably from these free electron values, and the differences are hard to calculate. We shall therefore leave untouched the third term of (13), as well as the second, and shall define a quantity η_j as the contribution of all the other terms of (13) to the ionization energy of the jth electron. From (13), (17), (25), and (26) we find

$$W_H=\sum_{j\text{ valence}}\eta_j-\tfrac{1}{2}\sum_{i,j\text{ valence}}C_{ij}(\varphi)-\tfrac{1}{2}\sum_{\substack{i,j\text{ valence}\\ \text{spins }\|}}A_{ij}(\psi)-16Na^2\beta^2B+\tfrac{1}{2}\sum_{\mu\neq\nu}\frac{8}{D(\mathbf{R}_\mu-\mathbf{R}_\nu)}+24N/5r_s \quad (28)$$

where

$$\eta_j=E_j+s_j[a^2(-\epsilon-E_j+2F_0+6/r_s+8B\beta)-2G_0]-\tfrac{2}{3}p_jG_1. \quad (29)$$

Of the quantities occurring in (28) and (29), five are independent of the lattice constant and of which quantum states are occupied, and it will be convenient to list their numerical values here; ϵ and F_0 are given by Hartree and Hartree,[6] and the others are calculated from the $2s$ and $2p$ wave functions of Section 4:

$$a=0.096 \qquad F_0=2.278$$
$$\epsilon=11.344 \qquad G_0=0.0284$$
$$G_1=0.0364.$$

To obtain the binding energy we must first subtract from W_H the "correlation energy"[16] due to the fact that the electrons tend to avoid one another in a way not taken into account by the Hartree or Fock approximation; the binding energy per atom of the crystal is then the difference between the resulting total energy, divided by $2N$, and the energy of a neutral beryllium atom relative to the doubly ionized state. Now it would not be correct to take for this energy difference between Be^{++} and Be the value given by a Hartree field calculation, if we include the correlation term in the energy of the crystal, since the tendency of the two valence electrons to avoid each other is not taken into account in the Hartree calculation for the atom. On the other hand, the correlation term is much too important to be omitted from the energy of the crystal. We shall therefore take for the energy difference between Be^{++} and Be the experimental value 2.024 rydbergs. This will tend to make our calculated binding energy too small, since it includes, in addition to correlation between the valence electrons, the effect of all other imperfections in the Hartree method.

---

[14] The deviation of this term from zero is roughly estimated in Appendix II.
[15] L. Brillouin, J. de phys. et rad. **5**, 413 (1934).
[16] E. Wigner, Phys. Rev. **46**, 1002 (1934); Trans. Faraday Soc. **34**, 678 (1938).

TABLE I. *The potential due to an ion and an s sphere.*

r	$-U_1(r, 2.37)$	r	$-U_1(r, 2.37)$	r	$-U_1(r, 2.37)$
0.04	182.7	0.28	15.44	0.92	2.067
0.08	83.14	0.36	10.46	1.08	1.446
0.12	50.48	0.44	7.59	1.40	0.667
0.16	34.59	0.60	4.556	1.72	0.256
0.20	25.35	0.76	3.008	2.04	0.057
				2.36	0.000

TABLE II. *Values of $E_0(r_s)$ and α.*

r_s	$E(U_1, r_s)$	$E_0(r_s)$	γ	α
2.07	0.167	0.333	1.154	0.422
2.37	0.100	0.102	1.124	0.616
2.67	0.067	−0.017	1.104	0.697

3. THE FIELD

If we define $v(\mathbf{r})$ to be $-4/D(\mathbf{r})$ for $r \gtrsim r_s$, instead of $-4/r$ as before, the potential U_0 defined by (4) may be written

$$U_0 = \sum_\nu v(\mathbf{r}-\mathbf{R}_\nu) - \frac{6}{5r_s} + \mathrm{v}_{\mathrm{val}}, \tag{30}$$

where $\mathrm{v}_{\mathrm{val}}$ is the neutralized potential due to the valence electron distribution. It would undoubtedly be sufficiently accurate to assume $\mathrm{v}_{\mathrm{val}}=0$ in (30), since the charge distribution of the valence electrons is almost uniform; if necessary, a first-order perturbation correction could be applied to the energies calculated using this assumption.

What was actually done was to get a rough approximation to $\mathrm{v}_{\mathrm{val}}$ for $r_s=2.37$, and for other values of r_s to assume $\mathrm{v}_{\mathrm{val}}$ to vary in the same way near each ion as for $r_s=2.37$. More explicitly, for $r_s=2.37$ the valence electron distribution in a given s sphere was assumed to consist of a charge of one electron distributed with a density proportional to $|\varphi_{00}|^2$, plus a charge of one electron with a density proportional to $|R_p|^2$, where φ_{00} and R_p are the functions mentioned in the preceding section. The potential due to an ion and an s sphere containing the charge distribution just described will be called $U_1(r, 2.37)$. This function, values of which may be found from Table I, was determined so that the φ_{00} and R_p calculated from it were the same as those used in it: in this sense it is "self-consistent." If we define v_1 as the difference between $U_1(r, 2.37)$ and the neutralized potential due to a sphere of radius 2.37 containing a charge of two electrons uniformly distributed, we have

$$\begin{aligned} v_1(\mathbf{r}) &= U_1(r, 2.37) - 6/2.37 + 2r^2/2.37^3 \quad \text{for } r \lesssim 2.37 \\ &= -4/D(\mathbf{r}) \quad \text{for } r \gtrsim 2.37. \end{aligned} \tag{31}$$

The potential U which was actually used in calculating[17] the valence electron φ_j and E_j is now defined for all values of r_s by

$$U(\mathbf{r}) = \sum_\nu v_1(\mathbf{r}-\mathbf{R}_\nu) - \frac{6}{5r_s}, \tag{32}$$

and we have for the zeroth Fourier coefficient

$$U[0] = \frac{1}{(4/3)\pi r_s^3} \int_\alpha \left[v_1(r) + \frac{4}{r} \right] d\tau \approx c = U_0[0], \tag{33}$$

as a comparison with (5) shows. Since (32) differs slightly from (30), especially when $r_s \neq 2.37$, there will be a correction to the total energy resulting from the first-order perturbation corrections to the E_j; this is roughly estimated along with the Coulomb energy in Appendix II.

4. DETERMINATION OF E_0 AND α

Wigner and Seitz[1] have shown that the energy parameter E_0 for the lowest valence electron state in a metal can be determined with remarkable accuracy by integrating the radial wave equation

[17] The potential (32) is used directly in Sections 5 and 6; in Section 4 the wave functions are calculated in the field $U_1(r, 2.37)$ and their energies then corrected for the difference between this and (32).

for an s function in a single atomic cell, and finding the energy for which the radial derivative of the wave function vanishes at the radius r_s. Accordingly, s functions φ_0 were determined for several energies by numerical integration, in the field $U_1(r, 2.37)$ of the preceding section, and the energies for which the radial derivative vanished at $r_s = 2.07$, 2.37, and 2.67 were found by graphical interpolation. These energies are listed in Table II in the column headed $E(U_1, r_s)$.

The desired energy parameter $E_0(r_s)$ is rather accurately given by $E(U_1, r_s)$ plus the average over an atomic cell of $|\varphi_0|^2 U$ minus the average over an s sphere of $|\varphi_0|^2 U_1(r, 2.37)$. As it will be of interest in Section 6 to have a rather precise value of E_0 to compare with the value calculated by the orthogonalized plane wave method, we shall evaluate this energy correction with greater accuracy than is needed for the other purposes of this paper. In analogy to (31) let us define for $r \leqslant r_s$

$$U_1(r, r_s) = v_1(r) + 6/r_s - 2r^2/r_s^3. \tag{34}$$

By (33) the average of U over an atomic cell then equals the average of $U_1(r, r_s)$ over an s sphere. Also

$$\text{spherical average of } U = U_1(r, r_s) + \left[\sum_\nu{}' v_1(\mathbf{R}_\nu) - \frac{36}{5r_s}\right], \tag{35}$$

the constant term in brackets being small (it is calculated numerically in Section 9). If φ_0 is normalized over an s sphere we can now write

$$E_0(r_s) = E(U_1, r_s) + \int_{\text{atomic cell}} [|\varphi_0|^2 - |\varphi_0(r_s)|^2] U d\tau + |\varphi_0(r_s)|^2 \int_{\text{atomic cell}} U d\tau - \int_{s\text{ sphere}} |\varphi_0|^2 U_1(r, 2.37) d\tau.$$

The region of integration in the second term can be changed to the s sphere without much harm, since the integrand is nearly zero in the region between the cell and the sphere; then (35) can be used. In the second integral we may replace U by $U_1(r, r_s)$ and change the region of integration to the s sphere. The result is

$$E_0(r_s) = E(U_1, r_s) + \int_{s\text{ sphere}} |\varphi_0|^2 [U_1(r, r_s) - U_1(r, 2.37)] d\tau + (\gamma - 1)\left[\sum_\nu{}' \frac{4}{D(\mathbf{R}_\nu)} + \frac{36}{5r_s}\right] \tag{36}$$

where

$$\gamma = |\varphi_0(r_s)|^2 \cdot \frac{4\pi}{3} r_s^3$$

is the ratio of the square of the wave function at r_s to its mean value. The quantity

$$\left[\sum_\nu{}' \frac{4}{D(\mathbf{R}_\nu)} + \frac{36}{5r_s}\right]$$

depends on the c/a ratio of the crystal. The observed c/a ratio for beryllium is 1.58; however, no appreciable error in any of the quantities being calculated in this paper is apt to result from using the value 1.63 (corresponding to ideal close packing of spheres), and as some of the numerical work is simpler if this value is used, all the calculations of this paper have been made assuming $c/a = 1.63$. For this case

$$\left[\sum_\nu{}' \frac{4}{D(\mathbf{R}_\nu)} + \frac{36}{5r_s}\right] \text{ has the value } \frac{0.0317}{r_s}.$$

The integral in (36) was evaluated numerically for $r_s = 2.07$ and 2.67. The resulting values of $E_0(r_s)$ are given in the third column of Table II; γ, which appears also in the expression (38) for α, is given in the fourth column.

The general form for an electron eigenfunction in the trebly periodic potential field of a crystal is[9]

$$\varphi_{\mathbf{k}}=\exp(i\mathbf{k}\cdot\mathbf{r})u_k, \tag{37}$$

where the function u_k possesses the same translational periodicity as the crystal; $\mathbf{k}$ is called the wave vector of the eigenfunction φ_k. The assignment of a wave vector to a given wave function is unique only to within 2π times an arbitrary vector of the reciprocal lattice; to make it unique one may define the "reduced wave vector" as the shortest wave vector which can be associated with the given eigenfunction. Also, an infinite number of eigenfunctions can be found for any value of $\mathbf{k}$. The energy E_0 which we have just calculated is the third lowest of those going with wave vector zero (the lowest belong to the functions of the $1s$ core band, and there are two such orbitals because there are two atoms in the unit cell).

For wave vectors close to zero there exist energies close to E_0, whose expansion in powers of k for a hexagonal crystal is of the form

$$E_k=E_0+\alpha_\perp(k_x^2+k_y^2)+\alpha_{11}k_z^2+0(k^4).$$

Here k_z is the component of $\mathbf{k}$ along the hexagonal axis, and k_x and k_y are the components along any axes perpendicular to this. It can be shown that $\alpha_\perp$ and α_{11} must be very nearly the same when the c/a ratio for the crystal is 1.63, which, as described above, is the value assumed in the present calculations.

With $\alpha_{11}=\alpha_\perp=\alpha$, the value of α can be calculated from the formula

$$\alpha=\gamma\left[\frac{r}{f}\frac{df}{dr}-1\right]_{r=r_s} \tag{38}$$

given in the first paper of Bardeen.[2] Here $f(r)$ is the radial p function obtained by outward integration in the field $U_1(r, r_s)$ using the energy E_0. This formula, though an approximation, seems to be a very good one, both for the absolute value of α and for the manner of its variation with r_s. The values of α listed in Table II were calculated from the field $U_1(r, 2.37)$ for all values of r_s, but only a negligible correction would result from changing the field to $U_1(r, r_s)$.

5. Excited Energies

Because of the fact that the occupied region of $\mathbf{k}$ space extends in beryllium out to and beyond the first planes of energy discontinuity, the parabolic approximation $E_k=E_0+\alpha k^2$, which usually suffices for monovalent metals, is quite inadequate as a representation of the energies of most of the occupied quantum states. In fact, the calculations of Section 9, (3) show that with this approximation no stable state of the crystal exists anywhere near the observed lattice constant. We therefore calculate in this section the energy parameters of a number of states near the Fermi surface, using the orthogonalized plane wave method. An approximation to the energy parameter of such a state is obtained by solving a secular equation

$$\det(\chi_k, H\chi_{k'})-E(\chi_k, \chi_{k'})=0, \tag{39}$$

where the functions χ_k are defined by Eq. (4) of reference 5. It is obvious that by taking a sufficient number of rows and columns in (39) a very good approximation to the desired energy could be obtained; it will be shown in this section and the next that fairly accurate energy values result even if only a few rows and columns are used. The matrix elements occurring in (39) are given by (13) and (14) of reference 5. For our case these take the form

$$\begin{aligned}(\chi_k, H\chi_{k'})=k^2\delta_{kk'}&+U(\mathbf{k}'-\mathbf{k})-\{E_{1s}-F(0,0)\}A_{1s}(k)A_{1s}(k')\{1+\exp[i(\mathbf{k}'-\mathbf{k})\cdot\mathbf{t}]\}\\&-\{A_{1s}(k)I_{1s}(\mathbf{k}')+A_{1s}(k')I_{1s}^*(\mathbf{k})\}\{1+\exp[i(\mathbf{k}'-\mathbf{k})\cdot\mathbf{t}]\}\\&+A_{1s}(k)A_{1s}(k')\sum_{\nu'\neq\nu}\sum_{\nu}^{\text{cell}}\{E_{1s}S(\nu,\nu')+F(\nu,\nu')\}\exp[-i\mathbf{k}\cdot\mathbf{R}_\nu+i\mathbf{k}'\cdot\mathbf{R}_{\nu'}]\end{aligned} \tag{40}$$

and

$$(\chi_k, \chi_{k'}) = \delta_{kk'} - A_{1s}(k)A_{1s}(k')\{1+\exp[i(\mathbf{k}'-\mathbf{k})\cdot\mathbf{t}] - \sum_{\nu'\neq\nu}\sum_{\nu}^{\text{cell}} S(\nu,\nu')\exp[-i\mathbf{k}\cdot\mathbf{R}_\nu + i\mathbf{k}'\cdot\mathbf{R}_{\nu'}]\}, \quad (41)$$

where $\mathbf{t}$ is a vector joining the atom at the origin of coordinates to one of its nearest neighbors in the layer above or below it when the hexagonal axis is vertical. To use (40) and (41) we need to know values of the coefficients $A_{1s}(k)$, the Fourier coefficients $U[\mathbf{K}]$ of the potential (32), and the various overlap integrals.

For the field which was called $V(r)$ in reference 5 we chose the field $U_1(r, 2.37)$. The $1s$ eigenfunction was determined by numerical integrations, and its energy was found to be $E_{1s} = -4.55$ rydbergs. The integral which gives $\Omega_0^{\frac{1}{2}}A_{1s}(k)$ (Eq. (5) of reference 5) was calculated numerically for $k=0$ and two other values of k; for values of k smaller than the larger of these $A_{1s}(k)$ was determined graphically, and for greater values of k it was assumed that $A_{1s}(k)$ could be represented by an expression of the type of (29) of reference 5, which would be exactly correct for a hydrogenic core function. It was found, in fact, that by properly choosing the value of b in this expression, the three directly calculated values of $A_{1s}(k)$ could be fairly well represented.

To calculate the Fourier coefficients $U[\mathbf{K}]$, an integral similar to that in (18) of reference 5 was calculated numerically for eight values of $\mathbf{K}$, so spaced that the value of the integral for any other value of $\mathbf{K}$ could be fairly accurately estimated graphically. Table III contains the Fourier coefficients of U for the case $c/a = 1.63$. The argument of each U in the first column is a vector of the reciprocal lattice, designated by four indices according to the Bravais-Miller notation.[18] Not all the Fourier coefficients of U are real, and for those which are complex only the absolute magnitude is given. The phase of each Fourier coefficient $U[\mathbf{K}]$ is that of the quantity[19] $-[1+\exp(i\mathbf{K}\cdot\mathbf{t})]$ where $\mathbf{t}$ is as described under (40) and (41), and where the minus sign is due to the fact that $U(r)$ is everywhere negative.

TABLE III. *Fourier coefficients of U for c/a = 1.63.*

r_s	2.07	2.37	2.67
$U[000, 0]$	−0.6624	−0.5634	−0.4893
$U[000, 2]$	−0.3759	−0.3197	−0.2779
$U[000, 4]$	−0.1106	−0.0940	−0.0782
$\lvert U[1\bar{1}0, 0]\rvert$	0.2087	0.1783	0.1557
$\lvert U[1\bar{1}0, 1]\rvert$	0.2898	0.2459	0.2135
$\lvert U[1\bar{1}0, 2]\rvert$	0.1046	0.0900	0.0781
$\lvert U[1\bar{1}0, 3]\rvert$	0.1438	0.0974	0.0845
$\lvert U[1\bar{1}0, 4]\rvert$	0.047	0.039	0.034
$U[2\bar{1}\bar{1}, 0]$	−0.1552	−0.1398	−0.1138
$U[2\bar{1}\bar{1}, 2]$	−0.120	−0.100	−0.085
$\lvert U[2\bar{2}0, 0]\rvert$	0.0611	0.0514	0.0446
$\lvert U[2\bar{2}0, 1]\rvert$	0.100	0.085	0.071
$\lvert U[2\bar{2}0, 2]\rvert$	0.050	0.042	0.035

A number of the higher Fourier coefficients not listed in Table III occur in the expressions for the energies of some of the states which perturb the ones we are interested in. As the energies of the occupied states are rather insensitive to these Fourier coefficients, they were estimated by a rough extrapolation from the coefficients in the table.

The small overlap integrals given by (10), (11) and (12) of reference 5 could have been calculated with fair accuracy by methods similar to those mentioned there. However, we did not feel that the accuracy aimed at in this work was great enough to require a complete and accurate inclusion of overlap terms. It was considered sufficient to make use of an estimate of the overlap terms in (40) which is almost certainly too great. A comparison of the energies of the eigenfunction calculated with and without these overestimated overlap terms shows whether or not the uncertainty due to our ignorance of correct values of the overlap integrals is dangerous. In making this "overestimate" we shall neglect the $S(0, \nu)$, and the $F(0, \nu)$[20] for $\nu \neq 0$. For the eigenfunctions considered in this section this neglect does very little harm, because the quantities are small and, for the $\mathbf{k}$ vector we shall use, their coefficients in (40) turn out to

[18] Cf. N. F. Mott and H. Jones, *Theory of the Properties of Metals and Alloys* (Oxford, 1936), p. 159.

[19] Cf. Eq. (18), reference 5.

[20] In Section 6 a calculation of E_0 is given from more accurate values of the overlap terms, and values for $S(0\nu)$ are given.

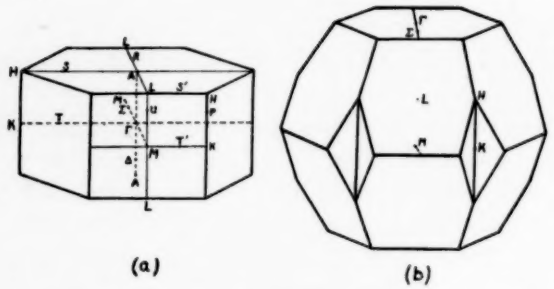

FIG. 1. First and second Brillouin zones for the close-packed hexagonal lattice.

be small. Since the chief contribution to the integral for $F(0, 0)$ comes from near the nucleus, we shall assume that $(U-V)$ is constant in this integral and equal to its value at the nucleus. This gives

$$F(0, 0) \approx (U-V)_{r=0} = 6\left(\frac{1}{r_s} - \frac{1}{2.37}\right). \quad (42)$$

The quantity $I_{1s}(\mathbf{k})$ is more difficult to approximate adequately. If we make the same assumption regarding the constancy of $(U-V)$ we have

$$I_{1s}(\mathbf{k}) = 6\left(\frac{1}{r_s} - \frac{1}{2.37}\right) A_{1s}(k). \quad (43)$$

More accurately calculated values for $I_{1s}(0)$ are given in the next section, and a comparison shows that the expression (43) is numerically too large by a factor 1.6 for $r_s=2.07$, and a factor 1.3 for $r_s=2.67$. For large values of $\mathbf{k}$, the contribution to the $I_{1s}(\mathbf{k})$ integral from the region close to the nucleus is relatively more important, however, since at a distance from the nucleus the phase of the exponential is different in different directions. So we may expect the approximation (43) to be a little less bad for the wave vectors to be considered in this section, than for $\mathbf{k}=0$. If (42) and (43) are inserted into (40) and the $S(0, \nu)$ and $F(0, \nu)$ for $\nu \neq 0$ are neglected, the resulting expression for $(\chi_k, H\chi_{k'})$ has the form which would be obtained by replacing E_{1s} by $(E_{1s}+6/r_s-6/2.37)$ and disregarding all the overlap terms. The energies E which will be given later on in Table V are obtained by calculating all matrix elements of the Hamiltonian in this way.

Before beginning on the detailed calculation of the energies of the various states, it will be worth while to consider what the occupied states for beryllium would be like in the approximation of almost free electrons.[21] In this approximation $\mathbf{k}$-space is divided up into Brillouin zones, across the boundaries of which discontinuities in energy occur. The boundaries of the various Brillouin zones are the planes which bisect perpendicularly the vectors from the origin to the various points of the reciprocal lattice, each multiplied by 2π. The first Brillouin zone is, in general, the space which can be reached from the origin by crossing just one plane, etc. We shall adhere to this definition here, although on account of the presence of a twofold screw axis in the space group there is no discontinuity in energy across the top and bottom boundaries of the first Brillouin zone.[22] The first and second Brillouin zones are shown in Fig. 1, and a number of wave vectors are indicated by letters.[23] Since there are just enough electrons present to fill the first two zones, we may expect that a Fourier analysis of the true crystal eigenfunction of a state near the Fermi surface would show it to be composed principally of one or more plane waves of wave vectors near the boundary of the second Brillouin zone.

Now the eigenfunctions in a crystalline field can be classified according to symmetry types, corresponding to the various irreducible repre-

TABLE IV. *Symmetry types for each lettered point in Fig. 1.*

POINT	NO. OF PLANE WAVES OF SAME KINETIC ENERGY AND SAME REDUCED WAVE VECTOR	SYMMETRY TYPES
M	2	M_1^+, M_2^-
L	4	L_1, L_1
K	3	K_1, K_5
H	6	H_1, H_2, H_3
Σ	2	Σ_1, Σ_3
Γ	2	Γ_3^+, Γ_4^-

[21] See the article of Sommerfeld and Bethe, *Handbuch der Physik* (Berlin, 2nd ed., 1933), Vol. 24/2, p. 385.

[22] That there cannot be a discontinuity in energy across these planes was first shown by F. Hund, Zeits. f. Physik **99**, 119 (1936); cf. also C. Herring, Phys. Rev. **52**, 361 (1937).

[23] It will be noted that the second zone in Fig. 1 differs from the zone (there designated as the "first zone") in Fig. 65 of Mott and Jones, *Theory of the Properties of Metals and Alloys* (Oxford, 1936), in that we have included wedge-shaped pieces around the sides. The volume of these wedge-shaped pieces is just sufficient to make the whole zone hold exactly two electrons per atom.

sentations of the space group.[24] Suppose we take all the plane waves which have the same reduced wave vector, and the same kinetic energy, as the one corresponding to a particular lettered point in Fig. 1; with the aid of character tables for the irreducible representations of the close-packed hexagonal space group[25] we can find all the symmetry types which occur among the linear combinations of these plane waves. These symmetry types are listed, for each lettered point, in Table IV, the notation being that of reference 25. In the approximation of almost free electrons the symmetry types of those eigenfunctions at the lettered points which belong to the first and second zones must of course be among the listed types. It is reasonable to expect that the same holds true for the actual crystal eigenfunctions, i.e., that if we select the two valence electron states nearest the Fermi surface which have reduced wave vector corresponding to a given one of the lettered points, the symmetry types of these states will be among those listed for the given point in Table IV. It turns out that this is indeed the case, although it is of course necessary to investigate eigenfunctions of other symmetry types, which arise in the free electron approximation from higher energy plane waves, and to make sure that none of these have energies near the Fermi level.

For each symmetry type in Table IV the appropriate plane wave combination was set up. Similarly out of plane waves of higher energies linear combinations were formed having each of these symmetry types. These linear combinations of plane waves were then made orthogonal to the core functions, just as was done for a single plane wave in (4) of reference 5. Such a linear combination of plane waves, orthogonalized to the cores, will be referred to as a "constituent χ state" of the eigenfunction of the same symmetry type.

For certain symmetry types of Table IV it happens that the plane wave combination is itself orthogonal to the 1*s* core functions, so that no multiples of the core functions need to be added to get the constituent χ-state. This is the case for all symmetry types except those (labeled (*s*) in Table IV) which occur among the Bloch waves formed from the core functions. For each symmetry type we chose the several constituent χ-states of lowest average energy, and using (40) and (41) evaluated the scalar products of these with each other and the matrix of the Hamiltonian relative to them. The lowest root of a secular equation gave an approximate value for the Hartree energy parameter of the crystal eigenfunction.

The energy parameters so obtained are the quantities E_j listed in Table V. We have included

TABLE V. *Hartree energy parameters of the crystal eigenfunction.*

STATE	r_s=2.07 E_j	ΔE_j	2.37 E_j	2.67 E_j	ΔE_j	No. CONSTITUENT χ-FUNCTIONS
(*s*) M_1^+	0.764	0.006	0.547	0.401	−0.004	4
(*s*) M_2^-	1.010	−0.012	0.702	0.492	−0.016	4
(*s*) L_1	0.888	−0.003	0.650	0.489	0.001	3
K_1	0.967		0.712	0.537		5
(*s*) K_3	1.197	−0.008	0.852	0.623	−0.009	4
K_4	1.878		1.377	1.049		4
H_1	1.231		0.913	0.696		5
H_2	1.117		0.810	0.604		6
(*s*) Σ_1	1.419	0.011	1.012	0.726	−0.035	4
Σ_3	0.975		0.713	0.537		5
Γ_3^+	0.721		0.507	0.370		6
(*s*) Γ_4^-	1.45	0.05	1.00	0.68	−0.04	3

[24] L. P. Bouckaert, R. Smoluchowski and E. Wigner, Phys. Rev. **50**, 58 (1936).
[25] C. Herring, to be published in another place.

TABLE VI. *Values of E_0 calculated by the orthogonalized plane wave method. $\bar{E}_0$ is the average energy of the wave function χ_0 with inclusion of all overlap terms except the $F(0\nu)$ for $\nu \neq 0$. The four perturbations listed, and $E_0^{(1)}$, are calculated with inclusion of overlap terms and assuming $I_{1s}(\mathbf{k})/A_{1s}(k) = I_{1s}(0)/A_{1s}(0)$. $E_0^{(2)}$ is calculated with inclusion of overlap terms, using (42), and (43) for $\mathbf{k} \neq 0$, but using correct $I_{1s}(0)$. $E_0^{(3)}$ is calculated including only the $I_{1s}(\mathbf{k})$ and $F(0, 0)$ overlap terms, and assuming (42) and (43) for all $\mathbf{k}$. $E_0^{(4)}$ is calculated omitting all overlap terms. E_0^{WS} is taken from Table II.*

r_s	2.07	2.37	2.67
$I_{1s}(0)$	0.076	−0.0027	−0.049
$F(0, 0)$	0.342	0.0000	−0.269
$S(0, \nu)$	0.00159	0.00051	0.00016
$\bar{E}_0$	0.3771	0.1208	−0.0065
pert. $(1\bar{1}0, 0)$	0.004_2	0.0005	0.0002
$(1\bar{1}0, 1)$	0.024_4	0.0085	0.0017
$(000, 2)$	0.005_7	0.0015	0.0000
$(1\bar{1}0, 2)$	0.002_4	0.0017	0.0034
$E_0^{(1)}$	0.340	0.108	−0.012
$E_0^{(2)}$	0.355	0.109	−0.014
$E_0^{(3)}$	0.307	0.110	0.001
$E_0^{(4)}$	0.382	0.110	−0.028
E_0^{WS}	0.333	0.102	−0.017

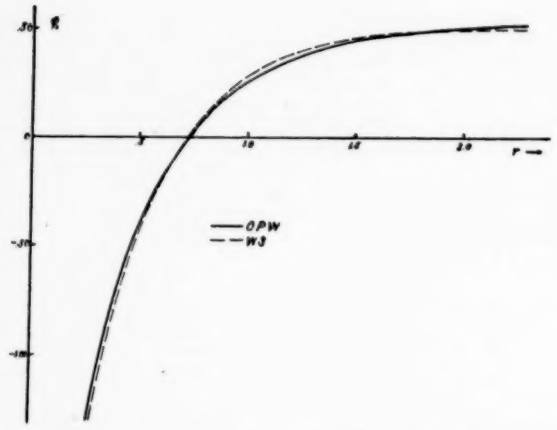

FIG. 2. Comparison of the orthogonalized plane wave and Wigner-Seitz wave functions for $\mathbf{k}=0$, $r_s=2.37$. The former (OPW) goes at $r=0$ to the value -4.21, the latter (WS) to -4.01.

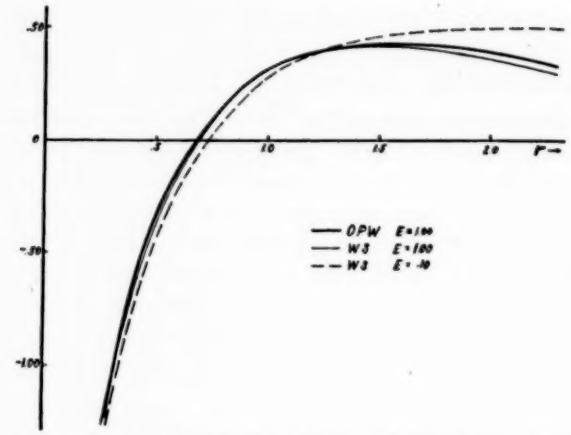

FIG. 3. Comparison of the s part of the orthogonalized plane wave function for Γ_4^- with central field functions, for $r_s=2.37$. The former (OPW) curve goes at $r=0$ to the value -4.4, the $E=0.10$ curve to -4.01, and the $E=1.00$ curve to -3.8.

here the lowest energy state of symmetry K_6 in addition to the states listed in Table IV. The quantities ΔE_j were obtained by subtracting the listed value of E_j from the value which resulted when all the overlap terms in (40) and (41) were neglected. Thus we may expect the solution of the correct secular equation to lie between E and $E+\Delta E$; probably about halfway. The last column of Table V gives for each symmetry type the number of constituent χ-functions used in the secular equation; we have neglected the perturbations due to the small matrix elements of the Hamiltonian connecting the constituent χ-functions with the core functions.

The differences between the E_j's in the table and the average energies $\bar{E}_j$ for the lowest constituent χ-state are quite small, of the order 0.03 to 0.06 Ry, for the states not designated (s). The corresponding differences for the (s) states are as high as 0.20 Ry. Because of the rough perturbation method used the energy parameters are probably inaccurate to 0.01 Ry or more. However, the third figure listed in the table is significant in taking the differences δE_j and $\delta^2 E_j$, between the E_j's for the three values of the lattice constant, which are used in computing the lattice constant and compressibility. The quantities $\delta^2 E_j - \delta^2 \bar{E}_j$ are only a few thousandths of a Rydberg unit for all the non-(s) states except K_6. For the (s) states these quantities may be as high as 0.05 Ry.

6. TESTS OF THE ORTHOGONALIZED PLANE WAVE METHOD

Since our results will depend considerably upon the calculations of the preceding section, and since these calculations are the first to be published using the orthogonalized plane wave method, a check on the accuracy of the method is desirable. The most obvious test to make is to calculate E_0 by the orthogonalized plane wave method, and compare the result with the value obtained by the method of Wigner and Seitz. Another kind of test which can be made is to calculate the wave function for any state by the orthogonalized plane wave method, and then to compare the s and p parts of this wave function with the s and p functions for the same energy obtained by integrating the wave equation with the spherically symmetric potential $U_1(r, r_s)$ of

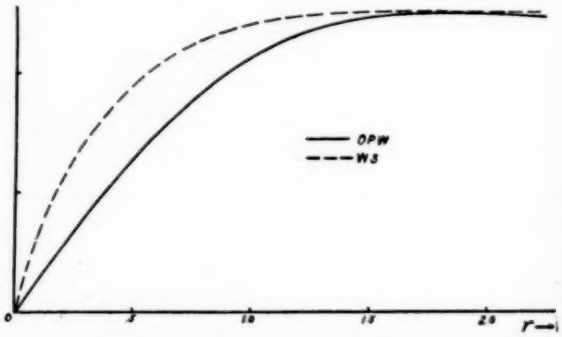

FIG. 4. Comparison of the p part of the orthogonalized plane wave function for Γ_3^+ with the central field function of the same energy, $r_s=2.37$.

Section 3. The radial functions obtained by these two methods should be the same to within a constant factor as long as r is sufficiently small so that the deviation of the true field U from spherical symmetry is negligible.

The results of the calculation of E_0 by the orthogonalized plane wave method are given in Table VI. As it is of interest to see how well E_0 can be calculated when all the overlap terms in (40) and (41) are taken accurately into account, values of $I_{1s}(0)$ and of $S(0, \nu)$ for nearest neighbors were calculated from (23), (24), (25), and (26) of reference 5; these are given in the first three rows of Table VI, along with accurate values of $F(0, 0)$ which were used here instead of the approximation (42).

Of the energies $E_0^{(1)} \cdots E_0^{(4)}$ calculated in various ways, one would expect $E_0^{(1)}$ to be the most accurate, with $E_0^{(2)}$ next. The energies $E_0^{(3)}$, and $E_0^{(4)}$ are calculated with the same approximations which were used for E and $E+\Delta E$, respectively, in Table V; the differences are much larger here because most of the (s) functions in Table V are rather smaller near a nucleus than the wave function φ_0 of Table VI, and also because $A_{1s}(k)$ is smaller for larger k values. The deviation of $E_0^{(1)}$ from E_0^{WS} is of the same order of magnitude as the uncertainty in the energies due to the uncertainty in the extrapolated values of $A_{1s}(k)$. The second differences of $E_0^{(1)} \cdots E_0^{(4)}$ and E_0^{WS} with respect to r_s, which are important for the compressibility, are, respectively, 0.112, 0.123, 0.088, 0.134 and 0.112. The perturbations listed in Table VI are the second-order perturbations due to the χ-states corresponding to the listed indices and other plane waves of the same kinetic energy.

Figure 2 shows a comparison for $r_s=2.37$ of the wave function φ_0 of Section 4 with the s part of the wave function calculated with the matrix elements used for $E_0^{(1)}$ in Table VI (omitting, however, the small perturbation by the (1–10, 0) waves). The two wave functions are drawn with the same normalization. It will be noted that the close agreement between the two functions persists even to $r=0$. The perturbations have a rather small effect on the wave function in this case, and even the unperturbed wave function χ_0 agrees fairly closely with the Wigner-Seitz function. Figure 3 shows a comparison, also for $r_s=2.37$, of the s part of the orthogonalized plane wave function for the state Γ_4^- with the s function of energy 1.00 in the field $U_1(r, 2.37)$. Since the eigenfunction cannot be accurately approximated by an s function alone, we cannot introduce a normalization requirement: the two curves have therefore been arbitrarily given the same ordinate at $r=1.24$. For comparison the Wigner-Seitz function from Fig. 2 is drawn in also, fitted to the same value at 1.24. It will be seen that the orthogonalized plane wave function resembles the central field function for $E=1.00$ much more closely than the one for $E=0.10$, although the agreement is not so good as in

TABLE VII. *Values of s_i and p_i and the derivatives of these quantities.*

STATE	s_i			p_i			η_i			w_i'	w_i''
	$r_s=2.07$	2.37	2.67	2.07	2.37	2.67	2.07	2.37	2.67		
M_1^+	0.164	0.141	0.121	1.5	0.8	0.5	0.713	0.514	0.378	0.1314	0.1651
M_2^-	0.555	0.511	0.462	1.4	0.6	0.3	0.924	0.636	0.438	0.1168	0.0734
L_1	0.007	0.009	0.014	1.7	1.0	0.5	0.847	0.625	0.476	0.2189	0.2752
K_1	0	0	0	3.2	1.9	1.2	0.888	0 666	0.509	0.0876	0.1101
K_5	0.344	0.292	0.280	0.9	0.5	0.4	1.142	0.810	0.586	0.0876	0.0184
K_6	0	0	0	2.6	1.5	1.0	1.82	1.34	1.02	0.0073	0
H_1	0	0	0	3.1	1.6	1.0	1.156	0.873	0.672	0.0876	0.1101
H_2	0	0	0	3.1	1.9	1.2	1.041	0.764	0.576	0.1460	0.1284
Σ_1	0.850	0.765	0.746	1.5	0.7	0.3	1.300	0.918	0.641	0.0146	0.0092
Σ_3	0	0	0	1.7	1.0	0.6	0.935	0.690	0.522	0.0438	0.0551
Γ_3^+	0	0	0	1.6	1.1	0.7	0.682	0.481	0.352	0.0438	0.0550
Γ_4^-	1.61	1.25	1.00	0	0	0	1.29	0.87	0.58	0.0146	0
Γ_1^+	1.617	1.000	0.654	0	0	0	0.186	0.007	−0.081		
$\left[\frac{d}{d(k^2)}\right]_{k=0}$	−2.11	−1.42	−1.00	1.69	1.16	0.81	0.563	0.714	0.769		
δ	0.58	0.40	0.29								
B	0.161	0.163	0.165								

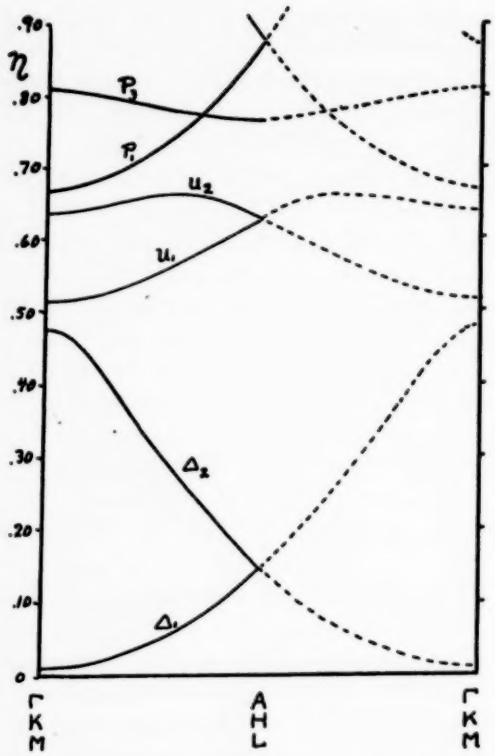

FIG. 5. η *vs.* **k** along lines of Fig. 1 parallel to the hexagonal axis, for $r_s=2.37$. The representation P_3 is two-dimensional. (The horizontal scale is different from that of Figs. 6 and 7.)

Fig. 2, especially for $r=0$. The poorer agreement is to be expected, since only three constituent χ-states were used, the smallest number for any of the states in Table V. One might expect the orthogonalized plane wave functions for the (s) states of Table V to be considerably more in error for $r_s=2.07$ or 2.67 than for 2.37, because of the crude treatment of the overlap terms. To test this curves similar to Fig. 3 were constructed for the state M_2^-, for $r_s=2.07$; the agreement with the central field function of the same average energy was found to be slightly worse for large r than in Fig. 3, but slightly better for small r.

It was pointed out in reference 5 that one would expect the orthogonalized plane wave functions to resemble the true eigenfunctions more closely in their s parts (and also in their d and higher parts) than in their p parts. This expectation is confirmed by Fig. 4, where the p part of the orthogonalized plane wave function for the Γ_3^+ state of Table V, for $r_s=2.37$, is compared with the central field p function of the same energy. The ordinates of the two curves correspond to values of the p part along a line in the direction of the hexagonal axis, and are arbitrarily chosen equal at $r=1.88$. In spite of the apparently poor agreement of the wave function here, however, the energies of the states not labeled (s) in Table V are probably accurate to 0.01 Ry. A similar plot for the H_2 wave function shows even worse agreement, which can perhaps be attributed to the fact that this function is far from a pure p function: the more of the higher harmonics there are in the wave function, the less the effect on the energy of an inaccuracy in the p part.

7. Distribution of States in Energy

As has been remarked previously, the quantities η_j defined by (29) are of more physical interest than the E_j. To obtain them we need to know the quantities s_j and p_j. The s_j defined by (18) can be calculated in a straightforward way from the approximate wave functions which correspond to the energies E in Table V. The p_j could be calculated similarly from their definition (19); however, since the p parts of these approximate wave functions differ considerably from the p parts of the true eigenfunctions near a nucleus (as shown by Fig. 4), the values of the p_j calculated in this way would be very bad. So instead, each p_j was estimated from the magnitude of the p part of the approximate wave function at a distance of 1.5 Bohr units from each nucleus. Such estimates are very

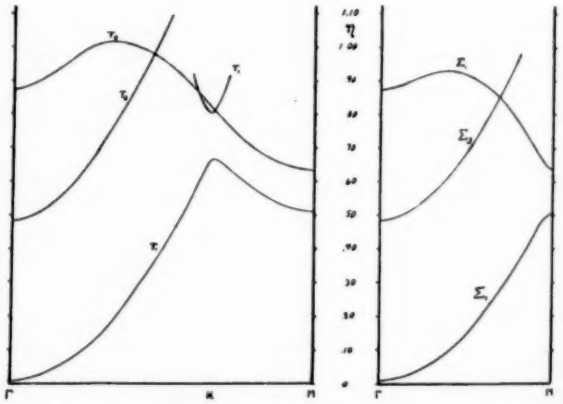

FIG. 6. η *vs.* **k** along lines in the central plane of the first Brillouin zone, for $r_s=2.37$.

rough, but are good enough for our purposes. The first two sections of Table VII give the values of the s_j and the p_j. Also given are the derivatives of these quantities with respect to k^2 at $k=0$, which can be calculated by an analysis similar to that used by Bardeen[2] to obtain α. This analysis is given in Appendix III.

The next to the last line of Table VII gives roughly estimated values of $\bar{s}$, the average of the s_j of the occupied states, which appears in (28) and (29) with a very small coefficient. The quantity which multiplies $\bar{s}$ is given in the last line. The values of the η_j, which can now be calculated from (29), are given in the third section of Table VII.

As the first step in the determination of the distribution of states in η, graphs were drawn of η against reduced wave vector along a number of lines in **k**-space. Reduced wave vectors (lying always in the first Brillouin zone) were used because the wave functions of the higher energy states did not resemble single plane waves closely enough to justify assigning unique wave vectors to them outside the first Brillouin zone. These graphs were constructed for $r_s=2.07$, 2.37, and 2.67; those for $r_s=2.37$ are reproduced in Figs. 5, 6 and 7. The symmetry types belonging to the various curves are written in, using the notation of reference 25; use has been made of the fact, pointed out there, that the line ΓK when prolonged reaches a point equivalent to M, and that similarly AH prolonged reaches a point equivalent to L.

It will be noticed that some of the curves have horizontal tangents at the symmetry points and

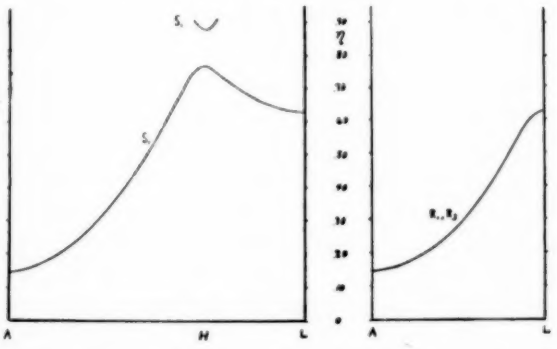

FIG. 7. η *vs.* **k** along lines in the top plane of the first Brillouin zone, for $r_s=2.37$. The representation S_1 is two-dimensional; R_1 and R_2 are one-dimensional but coincide in energy because of time-reversal symmetry.

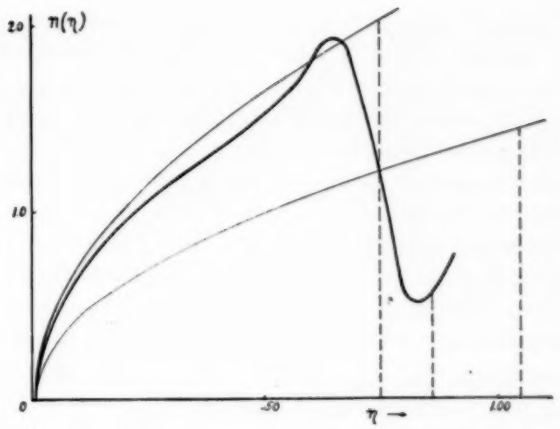

FIG. 8. Distribution of states in the energy parameter η, for $r_s=2.37$, with the scale such that $\int_{\eta_0}^{\eta_{max}} n(\eta)d\eta=1$.

that others do not, and that in the latter cases the slopes of the two curves which intersect at the point in question are equal and opposite. These facts can be deduced from the space group and time-reversal symmetry of the problem. It will be noticed also that there is a very sharp curvature at the points Γ_3^+, Γ_4^- in Fig. 5, M_1^+, M_2^-, K_1, K_5 in Fig. 6, and H_1, H_2 in Fig. 7. In each case this curvature is due to the perturbation of the curve in question by others which have the same symmetry at the general point of the line; the curvature is sharp because the chief perturbing influence comes from a curve which comes very close to the one in question. For these cases the curvature β at the symmetry point depends chiefly on the energy interval between the curves at that point, and can be calculated roughly.[26] Each of the lower curves of Figs. 5 and 6 was drawn by plotting a number of points on the parabola

$$\eta_k=\eta_0+\left[\frac{d\eta}{d(k^2)}\right]_{k=0}k^2$$

and then drawing a curve osculating this parabola at the bottom and osculating another parabola of curvature β at the top. The other curves were drawn in what seemed to be the most plausible manner, using the various β values.

With the aid of Figs. 5, 6, and 7 secondary

[26] The reasoning involved in such calculations of curvatures is discussed in more detail in Appendix IV.

graphs similar to Fig. 6 and Fig. 7 were drawn in planes $\frac{1}{3}$ and $\frac{2}{3}$ way between the plane of Fig. 6 and that of Fig. 7. In these planes none of the curves will intersect,[27] and use was made of the fact that the energy separation of two bands varies linearly with the distance in **k**-space from a "line of contact" in a plane of symmetry.[27] From all these graphs contours of constant η were drawn, and from their areas the number of states per unit range of η could be roughly determined. Figure 8 shows this distribution function; for $r_s=2.37$. The Fermi surface is represented by a vertical dotted line at $\eta=0.872$, and the distribution function is normalized to

$$\int_{0.007}^{0.872} n(\eta)d\eta=1.$$

For comparison two parabolas are also shown: the lower one shows what the distribution function would be for free electrons ($\eta_k=\eta_0+k^2$), and the upper one shows what it would be if η_k were

$$\eta_0+\left[\frac{d\eta}{d(k^2)}\right]_{k=0}k^2.$$

The Fermi surface appropriate to each of these cases is represented by a dotted line.

Table VIII gives, for three values of r_s, the energies η_{max} of the Fermi surface, and the average energies $\bar{\eta}$ of all occupied states, as determined by the graphical method just described. The differences $\delta\bar{\eta}$ and $\delta^2\bar{\eta}$ are also shown. However, one may very well doubt the accuracy of a second difference computed from three separate graphical calculations. To get an independent estimate of $\delta\bar{\eta}$ and $\delta^2\bar{\eta}$, one may try averaging the differences of the η_j, with appropriate weights w_j (such a procedure neglects the effect on $\delta^2\bar{\eta}$ of the change of the shape of the Fermi surface with lattice constant). For a choice of weights to be "reasonable," it should assign to each of the lower energy levels listed in Table VII a weight approximately proportional to the number of *distinct* wave functions belonging to the listed energy value, and to each of the higher levels a weight smaller than this number, to take account of the fact that levels near and above the Fermi surface affect the average energy of the filled region less than the lower levels. It is less easy to decide how much weight should be given to $[d\eta/d(k^2)]_{k=0}$. Figure 9 illustrates the difficulty.

TABLE VIII. *The energies of the Fermi surface and the average energies of all occupied states for three values of r_s.*

	$r_s=2.07$	2.37	2.67
η_{max} from graphs	1.18	0.87	0.64
$\bar{\eta}$ from graphs	0.701	0.480	0.337
$\delta\bar{\eta}$ from graphs		−0.221	−0.143
$\delta^2\bar{\eta}$ from graphs		0.078	
$\delta\bar{\eta}$ from w_j'		−0.257	−0.176
$\delta^2\bar{\eta}$ from w_j'		0.081	
$\delta\bar{\eta}$ from w_j''		−0.241	−0.165
$\delta^2\bar{\eta}$ from w_j''		0.076	
parabolic $\delta\bar{\eta}$		−0.193	−0.156
parabolic $\delta^2\bar{\eta}$		0.037	

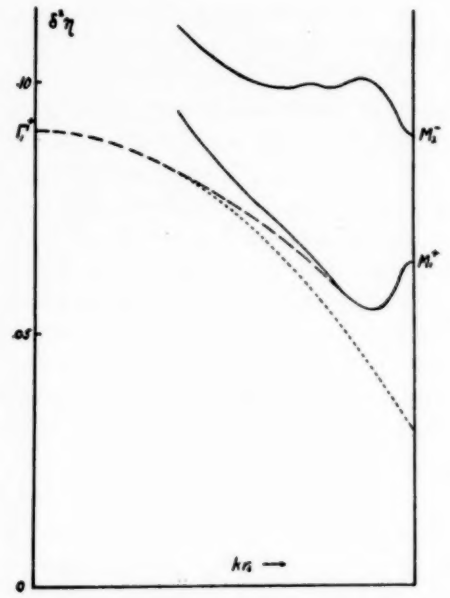

FIG. 9. Variation of $\delta^2\eta$ with kr_s.

Here $\delta^2\eta_k$ is plotted against kr_s along the line ΓM. If η_k were simply $\eta_0+k^2[d\eta/d(k^2)]_{k=0}$, the graph for the lower band would be the dotted parabola. Actually it must end at the value belonging to the M_1^+ state. The value of $\delta^2\bar{\eta}$ will depend quite seriously on whether or not the true curve follows the parabola nearly to the end, so it is important to decide just how the curve should be drawn. The rough β-values calculated in Appendix IV yield a sharp downward curvature at the M_1^+ end. Now β is the second-order part of a root of a second-degree secular equation; if the energy gap at the right hand end is sufficiently small, the exact solution

[27] See C. Herring, Phys. Rev. **52**, 365 (1937).

of this secular equation can be shown to yield a curve of $\delta^2\eta_k$ against k of the rather complicated form shown by the lower full curve. The true curve must deviate from this one by an amount which varies smoothly near the M_1^+ end, since it comes from matrix elements of $\partial/\partial x$ connecting the M_1^+ state with states a considerable distance from it. From the other end, it can be shown (see Section 9, Part (7)) that the curve of $\delta^2\eta_k$ against k must deviate from the parabola in the upward direction by a fairly appreciable amount if we neglect the perturbations due to the Fourier coefficients of the potential. We may therefore expect the true curve to look something like the dashed curve. Except for the dip near the end this is very much the type of curve we would draw if we were given the $\delta^2\eta$ values for Γ_1^+ and M_1^+, and knew nothing about $d\eta/d(k^2)$ or about any of the fine points just discussed. It should be noted, moreover, that in the next higher band the curve (upper full curve) has sharp variations which are almost the mirror image of those of the lower band, and if a small region near M_2^- in the higher band is occupied, $\delta^2\bar{\eta}$ will have about the same value as if the curves for both bands had been drawn smoothly.

Accordingly we may conclude that $\delta^2\bar{\eta}$ is probably about equal to the "reasonably weighted" average of the $\delta^2\eta_j$, to within the accuracy with which this average can be determined. In the last two columns of Table VII are given two sets of weights, w_j' and w_j''; the w_j'' are less "reasonable" than the w_j', having been chosen so as to give a value of $\delta^2\bar{\eta}$ which may be regarded as a lower limit. The $\delta\bar{\eta}$ and $\delta^2\bar{\eta}$ calculated from the w_j', from the w_j'', and from the parabolic assumption $\eta_k=\eta_0+k^2[d\eta/d(k^2)]_{k=0}$, are given in Table VII.

8. Error in Assuming Free Electron Exchange

The term $\frac{1}{2}\sum A_{ij}(\psi)$ in (28) is the exchange energy of the valence electrons. Order-of-magnitude calculations made by Seitz[1] have indicated that for alkali metals it is a rather good approximation to set this exchange energy per electron equal to $0.916X^1/r_s$, which is the exchange energy, per electron, of a perfect free electron gas whose density equals the density of valence electrons in the metal. For beryllium with $r_s=2.37$, this would give 0.482 rydberg per electron, or 304 kilocalories per gram atom. The largeness of this term, and the fact that the higher energy eigenfunctions for beryllium differ considerably from single plane waves, give us good reason to worry about the legitimacy of using the free electron value. As the actual exchange energy is very hard to calculate, however, we shall in this section merely give two lines of reasoning from which the limiting behavior of the exchange energy for low and high electron densities can be calculated; these make possible an estimate of the order of magnitude of the deviation from the free electron value for the actual case of beryllium.

The integral $A_{ij}(\psi)$ may be interpreted as twice the neutralized self-energy of the charge distribution $\psi_i^*\psi_j$ (if $j\neq i$ the neutralizing charge is zero). Let

$$\psi_i^*(\mathbf{r})\psi_j(\mathbf{r})=\sum_{\mathbf{K}}\gamma_K(i,j)\exp\left[i(\mathbf{k}_j-\mathbf{k}_i+\mathbf{K})\cdot\mathbf{r}\right], \tag{44}$$

where $\mathbf{k}_i$ and $\mathbf{k}_j$ are the reduced wave vectors of ψ_i and ψ_j, and where $\mathbf{K}/2\pi$ runs over all vectors of the reciprocal lattice. Then the neutralized potential due to $\psi_i^*\psi_j$ is, if $i\neq j$,

$$4\pi\sum_{\mathbf{K}}\frac{\gamma_K(i,j)}{|\mathbf{k}_j-\mathbf{k}_i+\mathbf{K}|^2}\exp\left[i(\mathbf{k}_j-\mathbf{k}_i+\mathbf{K})\cdot\mathbf{r}\right] \tag{45}$$

(if $i=j$ the term $\mathbf{K}=0$ must be omitted). Since the $i=j$ term contributes only an amount of order $1/N$ to the energy per atom, it may be neglected; we then have from (45),

$$\frac{1}{2}\sum_{\substack{i,j\ \text{valence}\\ \text{spins}\ ||}}A_{ij}(\psi)=8\pi\Omega\sum_{\mathbf{K}}\sum_{\substack{i\neq j\\ \text{orbitals}}}\frac{|\gamma_K(i,j)|^2}{|\mathbf{k}_j-\mathbf{k}_i+\mathbf{K}|^2}, \tag{46}$$

where in the summation on the right i and j run over the orbital wave functions only, states with different spins being no longer distinguished.

Suppose now that we have a fictitious metal, for which the wave functions ψ_j of the various quantum states are the same as for the actual metal, but for which the number of valence electrons to occupy these states is less than for the actual metal by a factor ξ^3; the actual metal corresponds to $\xi=1$. Thus as $\xi\to 0$ the radius of the occupied region of k space is asymptotically proportional to ξ. The $\mathbf{K}=0$ term in (46) is of order ξ^4, while all the terms for which $\mathbf{K}\neq 0$ are of order ξ^6. For small ξ we can expand the wave function of any occupied state in a series in powers of the three rectangular components of its wave vector:

$$\psi_k=\exp(i\mathbf{k}\cdot\mathbf{r})[\psi_0+\sum_{\mu=1}^{3} ik_\mu v_\mu+\sum_{\mu,\nu=1}^{3}(ik_\mu)(ik_\nu)w_{\mu\nu}\cdots]. \tag{47}$$

We may choose ψ_0 real: then the v_μ, $w_{\mu\nu}$ will be real. This gives

$$\gamma_0(i,j)=\frac{1}{\Omega}\int_\Omega[|\psi_0|^2+i\psi_0\sum_{\mu=1}^{3}(k_{j\mu}-k_{i\mu})v_\mu+\sum_{\mu,\nu=1}^{3}k_{j\mu}k_{i\nu}v_\mu v_\nu-\psi_0\sum_{\mu,\nu=1}^{3}(k_{j\mu}k_{j\nu}+k_{i\mu}k_{i\nu})w_{\mu\nu}\cdots]d\tau. \tag{48}$$

Now the normalization of ψ_k requires that v_μ be orthogonal to ψ_0 and that

$$2\int_\Omega \psi_0 w_{\mu\nu}d\tau=\int_\Omega v_\mu v_\nu d\tau.$$

For cubic crystals

$$\int_\Omega v_\mu v_\nu d\tau=\lambda\delta_{\mu\nu}, \tag{49}$$

where

$$\lambda=\int_\Omega v_\mu^2 d\tau=\tfrac{1}{3}\int_\Omega[\sum_{\mu=1}^{3}v_\mu^2]d\tau; \tag{50}$$

it is probably a good approximation to assume that this is also true for hexagonal crystals with c/a close to 1.63 (this is similar to the assumption $\alpha_{||}=\alpha_\perp$ made in Section 4). Using these relations, (48) becomes

$$\gamma_0(i,j)=\frac{1}{\Omega}\left[1-\frac{\lambda}{2}|\mathbf{k}_j-\mathbf{k}_i|^2+0(\xi^4)\right]. \tag{51}$$

The $\mathbf{K}=0$ term of (46) is therefore

$$\frac{8\pi}{\Omega}\sum_{\substack{i\neq j\\ \text{orbitals}}}\left[\frac{1}{|\mathbf{k}_j-\mathbf{k}_i|^2}-\lambda+0(\xi^2)\right]. \tag{52}$$

If the filled region of **k**-space is asymptotically spherical, as is always the case for cubic crystals, and as we are assuming for beryllium, it can easily be shown that

$$\frac{8\pi}{\Omega}\sum_{\substack{i\neq j\\ \text{orbitals}}}\frac{1}{|\mathbf{k}_j-\mathbf{k}_i|^2}=NnX\xi^3\left[\frac{0.916\xi}{r_e}\right]+0(\xi^5). \tag{53}$$

Here $NnX\xi^3$ is just the number of electrons in Ω, for our fictitious crystal, and

$$\frac{r_e}{\xi}=\left(\frac{3}{4\pi NnX\xi^3}\right)^{\frac{1}{3}}$$

is the radius of a sphere whose volume equals the volume per electron. The first term of (53) is just the exchange energy, in rydbergs, of a free electron gas.[28] If the filled region of $\mathbf{k}$-space were asymptotically ellipsoidal instead of spherical, the leading term in (53) would of course be different, and the remaining terms would be $0(\xi^6)$ instead of $0(\xi^8)$. In the terms of (46) with $\mathbf{K}\neq 0$ we have, using (47),

$$\gamma_K(i,j)=\gamma_K(0,0)+\sum_{\mu=1}^{3}(k_{j\mu}-k_{i\mu})f_{K\mu}+0(\xi^2),$$

where $f_{K\mu}$ is a Fourier coefficient of $i\psi_0 v_\mu$. Also,

$$\frac{1}{|\mathbf{k}_j-\mathbf{k}_i+\mathbf{K}|^2}=\frac{1}{K^2}-\frac{2(\mathbf{k}_j-\mathbf{k}_i)\cdot\mathbf{K}}{K^4}+0(\xi^2).$$

Inserting these in (46), the terms linear in $(\mathbf{k}_j-\mathbf{k}_i)$ drop out on summation, and we have

$$8\pi\Omega\sum_{\mathbf{K}\neq 0}\sum_{\substack{i\neq j\\ \text{orbitals}}}\frac{|\gamma_K(i,j)|^2}{|\mathbf{k}_j-\mathbf{k}_i+\mathbf{K}|^2}=8\pi\Omega\left(\frac{NnX\xi^3}{2}\right)^2\sum_{\mathbf{K}\neq 0}\frac{|\gamma_K(0,0)|^2}{K^2}+0(\xi^8). \tag{54}$$

We may note that

$$8\pi\Omega\sum_{\mathbf{K}\neq 0}\frac{|\gamma_K(0,0)|^2}{K^2}=C_{00}(\psi)$$

is just twice the neutralized self-energy of the charge distribution $|\psi_0|^2$. Combining (46), (52), (53), and (54) gives finally

$$\tfrac{1}{2}\sum_{\substack{i,j\ \text{valence}\\ \text{spins}\ \|}}A_{ij}(\psi)=NnX\xi^3\left[\left(\frac{0.916}{r_s}\right)\xi+\left(\frac{NnX}{4}C_{00}(\psi)-\frac{3\lambda}{2r_s^3}\right)\xi^3+0(\xi^5)\right]. \tag{55}$$

The bracketed quantity in (55) is the exchange energy per electron; for small values of ξ the second term gives the correction to be applied to the free electron value represented by the first term.

To calculate this correction numerically for beryllium we may note that the functions v_μ occurring in (47) are the same as those occurring in the corresponding expansion of φ_k in powers of the k_μ. Bardeen[2] has shown that in each atomic cell it is a good approximation to set

$$v_\mu=-x_\mu\varphi_0+\frac{x_\mu}{r^2}\left(\frac{r_s^2\varphi_0(r_s)}{f(r_s)}\right)f(r), \tag{56}$$

where f is the radial p function calculated in the same field used for φ_0, with the same energy E_0. We have already calculated f for use in (38). If we replace each atomic cell by an s sphere, the integral on the right of (50) can thus be expressed in terms of a radial integral of a known function. The resulting values of λ are given in the first line of Table IX. The second line of Table IX gives the values of $\frac{1}{4}NnXC_{00}(\psi)$, which can be calculated by radial integrations of the sort used in Appendix II. The third line represents the correction to the exchange energy per electron which would obtain if the $0(\xi^5)$ in (55) could be neglected even for $\xi=1$. The second derivative of this term with respect to r_s is quite appreciable, as is to be expected from the occurrence of r_s^3 in the denominator. Actually, of course, the $0(\xi^5)$ in (55) becomes appreciable (for beryllium) when ξ is still rather smaller than 1, and we cannot trust the last line of Table IX to give anything more than the order of magnitude of the correction to be added to the free electron exchange energy. For monovalent metals, however, (55) might give a good approximation.

[28] Cf. Wigner and Seitz, reference 1.

To get an expression valid for larger values of ξ, one might try to evaluate higher terms in the expansion of the exchange energy in powers of ξ, just as the first two were obtained above. This does not seem impossible, although the next term would be much harder to calculate than the first two. However, when the Fermi surface extends beyond the first planes of energy discontinuity in **k**-space, we can no longer expect such a formal power series to be valid for $\xi=1$.

Two other possible lines of attack suggest themselves, but they both appear even less valid than the preceding. One is to start from a free electron gas, and treating the potential U as a small perturbation, to find the second-order change in the exchange energy. This second-order change can be expressed as a rapidly convergent series of terms containing the squares of the Fourier coefficients $U[\mathbf{K}]$. But the rapidity of the convergence is misleading: it can be shown that each term is positive, so that in the second order the perturbation increases the exchange energy, for any value of ξ; this does not agree with the result obtained for beryllium above (Table IX) that for small ξ the exchange energy is less than for free electrons. This is not surprising, since the wave functions obtained by applying a small perturbation to plane waves do not resemble the true wave functions at all in the regions near nuclei.

The second possibility is to use a Fermi-Thomas model, assuming a large number of electrons to be present in a region in which U changes only slightly (ξ very large). For this model the exchange energy per electron in a given region of space is $0.916/\rho_e(\mathbf{r})$ where $(4\pi/3)[\rho_e(\mathbf{r})]^3$ is the reciprocal of the electron density at the point $\mathbf{r}$. Multiplying this by the electron density and integrating give the total exchange energy. The final result is

$$\text{Average exchange energy per electron}=\frac{0.916\xi}{r_s}\left\{\frac{\frac{1}{\Omega}\int_\Omega (E_m-U)^2 d\tau}{\left[\frac{1}{\Omega}\int_\Omega (E_m-U)^{3/2}d\tau\right]^{4/3}}\right\}, \tag{57}$$

where E_m is the energy of the highest occupied state, which is of order ξ^2 as $\xi\to\infty$. The coefficient of $0.916\xi/r_s$ is always >1, so here again the exchange energy is greater than for free electrons. If (57) were assumed to hold for $\xi=1$, this coefficient would be roughly 1.9; however, most of the contribution to this value comes from regions within a few tenths of a Bohr unit from each nucleus, where for $\xi=1$ the Fermi-Thomas model is completely inapplicable.

9. Results and Discussion

(1) Binding energy

If we insert in (28) the free electron values for the Coulomb and exchange energies, use the precise value (see Part (6) of this section) for the electrostatic interaction energy of the ions, and then add to (28) the free electron value of the correlation energy, for which Wigner[16] has given the expression $1.16/(r_s+5.1)$ rydbergs per electron, we obtain for the energy per atom of the crystal

$$\frac{W}{2N}=2\bar{\eta}-\frac{7.077}{r_s}-\frac{1.46}{r_s+6.4}-0.074\delta^2 B. \tag{58}$$

Inserting in (58) the observed value of 2.37 for r_s and the graphically determined value of $\bar{\eta}$ from Table VIII, and subtracting the observed energy -2.024 rydbergs of the neutral Be atom, there results a binding energy of 0.170 rydberg per atom, or 53 kilocalories per gram atom. If we were to assume the deviation from the free electron value of the exchange energy per electron to be as given by the last line of Table IX, this correction would decrease the above value

Table IX.

	$r_s=2.07$	2.37	2.67
λ	0.165_0	0.135_2	0.109_5
$\frac{NnX}{4}C_{00}(\psi)$	0.003	0.002	0.002
$\left(\frac{NnX}{4}C_{00}(\psi)-\frac{3\lambda}{2r_s^3}\right)$	−0.053	−0.028	−0.015

TABLE X. *Values of r_s and $1/\kappa$ as obtained in various ways.*

	r_s	$(1/\kappa)\times10^{-12}$
from graphs	2.23	0.87
from w_j'	2.57	1.32
from w_j''	2.45	1.00
experimental[29]	2.37	1.25

of the binding energy to 36 kilocalories. However, there seems to be both theoretical and empirical evidence (see Part (5) below) that the exchange energies of electrons near the Fermi surface are numerically greater than the free electron values, so that the average deviation from the free electron exchange energy is probably less than that given in Table IX, perhaps even of the opposite sign. The deviation of the Coulomb energy from the free electron value, whose order of magnitude is estimated in Appendix II, increases the binding energy by about 2 kilocalories.

(2) The experimental value of the binding energy

The only direct determination of the binding energy of beryllium is that of Baur and Brunner.[30] These authors by measuring the slope of a vapor pressure curve find 53.5 kcal./g-atom for the heat of sublimation at around 2000°K; the heat of sublimation at 0°K, which is to be compared with the binding energy calculated above, should be at most a few kilocalories greater than this. Such a value would agree nicely with the theory, but we feel that it cannot be correct. For it is possible to calculate the heat of sublimation from the vapor pressure at a single temperature, if the latent heat of fusion is known, together with specific heats of the solid and liquid phases over the entire temperature range. To obtain a heat of sublimation as small as 53.5 kcal. at any of the temperatures at which Baur and Brunner measured the vapor pressure one would have to assume a specific heat for molten beryllium of nearly 20 cal./g-atom/°C. If instead a value of 8 cal. is assumed the heat of sublimation at 2111°K is around 80 kcal./g-atom if the Baur and Brunner value of the vapor pressure at this temperature is used. This would mean a value of about 85 kcal./g-atom at 0°K which value we feel is nearer the truth. This is also more in line with the estimate of 75 kcal./g-atom given by Bichowsky and Rossini.[31]

(3) Lattice constant and compressibility

The energies given by (58) for the three values 2.07, 2.37, and 2.67 of r_s can be fitted to a parabola, whose minimum gives the theoretical equilibrium value of r_s. The compressibility in c.g.s. units is given by

$$\frac{1}{\kappa}=\frac{3.88\times10^{12}}{r_s}\left[\frac{d^2}{dr_s^2}\left(\frac{W}{2N}\right)-\frac{2}{r_s}\frac{d}{dr_s}\left(\frac{W}{2N}\right)\right], \quad (59)$$

where r_s is still to be measured in Bohr units, $W/2N$ in rydbergs. The second term vanishes at the equilibrium lattice constant. We shall calculate $1/\kappa$ for $r_s=2.37$, and since this is not the theoretical equilibrium lattice constant, there will be a small contribution from the second term.

Table X gives the values of r_s and $1/\kappa$ resulting from (58) and (59) for each of the estimates of $\delta\bar{\eta}$ and $\delta^2\bar{\eta}$ in Table VIII. No values of r_s and $1/\kappa$ are given corresponding to the parabolic assumption, because when the resulting $\delta\bar{\eta}$ and $\delta^2\bar{\eta}$ are used the curve of W against r_s is concave downward. If the last line of Table IX were used for the deviation from the free electron value of the exchange energy, the values of $1/\kappa$ would be increased by about 0.3. The deviation from the free electron value of the Coulomb energy will introduce a correction of only a few percent into the calculated values of $1/\kappa$, and will have a negligible effect on r_s.

Bardeen[2] has pointed out that a relation

$$W=A(r_0/r_s)^3+B(r_0/r_s)^2-C(r_0/r_s) \quad (60)$$

suggested by some work of Fröhlich,[32] holds rather well for alkali metals. Bardeen chose the constants A, B, C, to fit the observed binding energy, lattice constant, and compressibility at zero pressure; he then calculated the variation of compressibility with volume and found it in good agreement with experiment. The same procedure applied to beryllium gives a pressure coefficient of compressibility about two-thirds

[29] At room temperature. Compressibility from P. W. Bridgman, Proc. Am. Acad. Arts and Sciences **68**, 27 (1937).

[30] E. Baur and R. Brunner, Helv. Chim. Acta **17**, 958 (1934).

[31] F. R. Bichowsky and F. D. Rossini, *The Thermochemistry of the Chemical Substances* (Reinhold, 1936).

[32] H. Fröhlich, Proc. Roy. Soc. **A158**, 97 (1937).

the observed value.[33] This is sufficiently close so that we can use (60) to estimate the amount of error in the assumption, used above, that W varies parabolically with r_s. In this way it can be concluded that the r_s values given in Table X are too large by something like 0.05 Bohr unit, and that the $1/\kappa$ values are too large by ten or fifteen percent.

(4) Diamagnetism

Beryllium is known to be rather strongly diamagnetic,[34] whereas magnesium and calcium, the two metals which ought to resemble it most closely in electronic structure, are paramagnetic. The chief cause of this may very well be the low density of electronic states near the Fermi surface, which is shown by the heavy curve in Fig. 8. This abnormally low density causes the paramagnetic contribution which the spins of the electrons make to the total susceptibility to be only a fraction of the value it would have if the electrons were free.

(5) Work function

The work function ϕ is the change in the energy of the crystal when one electron is removed; if starting from (28) we follow the line of reasoning used by Wigner and Bardeen,[3] and include the correlation energy as in (58) above, we obtain

$$-\phi=\eta_{\max}-\frac{4}{3}\frac{(2)^{\frac{1}{3}}0.916}{r_s}-\frac{0.73}{r_s+6.4}-\frac{0.73r_s}{3(r_s+6.4)^2}-D, \quad (61)$$

where D is the discontinuity in the potential energy of an electron (measured in rydbergs) which occurs at the surface of the crystal because of the double layer, and where the exchange energy per electron has been assumed to have the free electron value $0.916/r_s=(2)^{\frac{1}{3}}0.916/r_s$. Inserting 2.37 for r_s in (61) and taking $\eta_{\max}$ from Table VIII, we find

$$\phi=-0.14+D.$$

Now experimentally ϕ is about 3.9 volts,[35] or 0.29 rydberg. There is thus 0.43 rydberg to be accounted for by the double layer and by the deviation from the free electron values of exchange and correlation energy. The correlation terms in (61) are rather small, so it is reasonable to put most of the blame on the double layer and the exchange. For the alkali metals D is known to be small, of the order of a few hundredths of a rydberg.[3] For beryllium it should be larger, because there are two electrons per atom and because the electrons move faster; but a value as large as 0.43 rydberg would be very unreasonable. Probably, therefore, one must assume that the exchange energies of electrons at the Fermi surface are considerably greater than the corresponding free electron values. This is not unreasonable, although a very large effect is needed to remove the discrepancy on the work function. For the wave functions considered in Section 8, for example, some of the terms $A_{ij}(\psi)$ can become quite large, although the large part tends to cancel out on summation. Of course, the possibility should not be entirely eliminated that a pure beryllium surface would have a very low work function, and that in spite of careful precautions the observed values are due to oxygen contamination.

(6) Electrostatic energy of the ions and its variation with c/a.

The quantity $\sum_\nu{}'4/D(\mathbf{R}_\nu)$ which occurs in (28) and (36) represents the neutralized potential, at the position of an ion at the origin, due to all the other ions. The deviation of this quantity from $-36/5r_s$ was needed in Section 4. Moreover, the success of the theory of Fuchs[36] in predicting the elastic constants of the alkali metals leads one to suspect that the behavior of this electrostatic term may be important in determining the equilibrium value of the ratio c/a, and possibly in determining the relative stability of different lattice types.[37] In Fig. 10 the ratio of $\sum_\nu{}'1/D(\mathbf{R}_\nu)$ to $1/r_s$, as calculated

[33] P. W. Bridgman, reference 31, corrected for the improved pressure-volume relation for iron, which was used as a reference material, Phys. Rev. **57**, 235 (1940).

[34] M. Owen, Ann. d. Physik **37**, 657 (1912).

[35] M. M. Mann and L. A. DuBridge, Phys. Rev. **51**, 120 (1937).

[36] K. Fuchs, Proc. Roy. Soc. **A153**, 622 (1936) and Proc. Roy. Soc. **A157**, 444 (1936).

[37] H. B. Huntington, Phys. Rev. **57**, 60 (1940), has shown that the elastic constants of divalent hexagonal metals as determined from electrostatic energy of the ions do not agree nearly so well with experiment as do those for the alkali metals. So the electrostatic energy of the ions is probably only one of a number of factors determining the equilibrium c/a for beryllium.

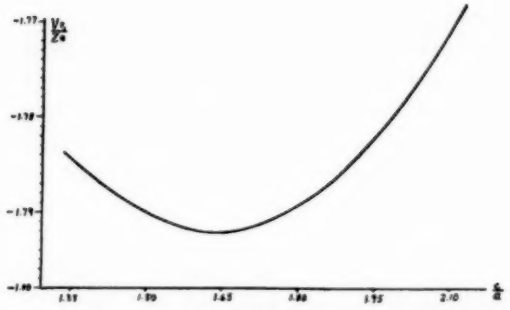

FIG. 10. Variation with c/a of the neutralized potential $\bar{V}$ produced at an ionic position by all other ions.

by the method of Ewald,[8] is plotted against c/a. The minimum electrostatic energy comes very close to $c/a=1.63$, although there seems to be no symmetry requirement which would cause the minimum to occur at exactly this point. At $c/a=1.63$,

$$\sum_{\nu}{}' \frac{4}{D(\mathbf{R}_\nu)} + \frac{36}{5r_s} = \frac{0.031_7}{r_s};$$

for the face-centered and body-centered cubic lattices this quantity has the values $0.03312/r_s$ and $0.03256/r_s$, respectively.[36] The differences between these quantities represent the differences in rydbergs per atom, between the electrostatic energies of the three lattice types; the electrostatic energy for the hexagonal lattice is thus lower than for either of the cubic types, but by an amount which is probably too small to be significant in determining the stable type.

(7) Remarks on the calculations

Apart from the deviation of the exchange and correlation energies from the free electron values, the principal uncertainties in the calculations of the above quantities arise from the use in Section 5 of an insufficient number of constituent χ-states and of a very crude estimate of the overlap integrals. The neglect of the perturbation of the valence electron states by the matrix elements connecting them with the core states ((16) and (17) of reference 5) is less serious. From Fig. 4 one can estimate that the energy given in Table V for the Γ_3^- state is too high by something like 0.01 Ry; this has been confirmed by a more accurate solution of the secular equation for this state. The other energies may be expected to be in error by a similar amount. This would account for a part, but probably only a part, of the difference between our calculated binding energy and the probable true value. The overlap uncertainty, whose order of magnitude is indicated by the ΔE's in Table V, is negligible for $r_s=2.37$, so it does not affect the binding energy. Its effect on the lattice constant and compressibility may be appreciable, but we do not think it can be very great, as some of the ΔE's in Table V are positive and some negative. Moreover, the lattice constant and compressibility will not be much affected by the neglect of the higher constituent χ-states, since most of the contribution to the variation of the E's with r_s in Table V comes already from the unperturbed $\bar{E}$'s. Combining these facts with what has been said in (1), (3), and (6) above, and in Section 8, it may be concluded that the exchange correction is probably fairly important for the binding energy, lattice constant, and compressibility, and apparently very important for the work function. The correlation energy probably differs from the free electron value by only a fraction of the latter, and probably varies less rapidly with r_s than does the exchange. The comparison of theory with experiment cannot make possible any stronger assertions about correlation than these, since for beryllium exchange is larger relative to correlation than for the alkalis and deviates so strongly from the free electron value that it largely masks the behavior of the correlation energy. However, *a priori* one might expect the polarization of the core by the valence electrons to have a serious effect, especially for the compressibility. The approximate agreement between theory and experiment tends to show that this effect must be small.

The orthogonalized plane wave method of calculating energy values provides an illuminating interpretation of the way in which E_k varies with $\mathbf{k}$. If $\mathbf{k}$ is not too near the boundary of the Brillouin zone, the principal term in E_k is the average energy of the wave function χ_k obtained by orthogonalizing a plane wave to the core functions. For beryllium, if we neglect overlap effects, this term is

$$\bar{E}_k = \frac{k^2 + U[0] + 9.1A_{1s}^2(k)}{1 - 2A_{1s}^2(k)} \quad \text{(cf. (40) and (41))}. \quad (62)$$

Now $A_{1s}^2(k)$ is $1/r_s^3$ times a function of k which decreases monotonically toward zero as k increases. So (62) shows why α is less than 1, why α decreases with decreasing r_s, and why the curve of E_k against k tends to deviate in the upward direction from the osculating parabola $E_k=E_0+\alpha k^2$. This upward deviation is of course often nullified by the influence of Bragg reflections.

In conclusion the authors wish to express their thanks to Professors J. C. Slater, E. Wigner and F. Seitz for discussions of various parts of this paper.

Appendix I

A rough upper limit to the interaction energy of two beryllium ion cores can be obtained quickly by considering a pair of fictitious atoms, each consisting of a nucleus of charge $2e(Z/2)^{\frac{1}{2}}$, and two "electrons" each of mass m and charge $e(Z/2)^{\frac{1}{2}}$. The fictitious atom is thus simply a helium atom with the electronic charge increased by $(Z/2)^{\frac{1}{2}}$, making the potential energy of an electron in the field of the nucleus the same function of r for the fictitious atom as for the actual ion core. Since the electrons in the fictitious atom repel each other more strongly than those in the ion core, we may expect the electron distribution of the former to be more spread out than that of the latter, hence the repulsive exchange force at large distances will be greater for the fictitious atoms than for the ion cores. The increased interaction of the electrons will also cause the van der Waals attraction between the fictitious atoms to be greater than that between the ion cores. Therefore, if both types of force are negligible for the fictitious atoms, the interaction of the ion cores can be neglected.

If $w(r)$ is the interaction energy of two helium atoms a distance r apart, dimensional considerations show that the interaction energy of a pair of our fictitious atoms must be $\frac{1}{4}Z^2w(\frac{1}{2}Zr)$. Now for $r_s=2.07$ Bohr units, nearest neighbor atoms in the beryllium lattice are 3.74 Bohr units apart, and at twice this distance the van der Waals term for helium predominates over the repulsive one. Using the expression for w given by Margenau[38] we have

$$4w(2\times 3.74)=-0.00007 \text{ rydberg},$$

which is quite negligible.

Appendix II

The Coulomb energy correction to the total energy values used in Section 9 consists of two parts: the sum

$$\frac{-1}{2Nn}\sum_{i,j\ \text{valence}} C_{ij}(\varphi),$$

and the correction to $2\bar{\eta}$ required by the fact that we have calculated the η's using the potential (32) instead of (30). Thus to the energy values we have used should be added

$$\frac{\Delta W_H}{nN}=-\tfrac{1}{2}\int_{\text{atomic cell}}\rho v_{\text{val}}d\tau+\int_{\text{atomic cell}}\rho(\mathbf{r})\sum_\nu[v(\mathbf{r}-\mathbf{R}_\nu)-v_1(\mathbf{r}-\mathbf{R}_\nu)]d\tau+\int_{\text{atomic cell}}\rho v_{\text{val}}d\tau,$$

where ρ is the charge density of valence electrons.

Since $[v-v_1]$ differs from zero only inside the radius r_s,

$$\frac{\Delta W_H}{nN}=\tfrac{1}{2}\int_{\text{atomic cell}}\rho v_{\text{val}}d\tau+\int_{\text{atomic cell}}\rho[v-v_1]d\tau. \tag{A}$$

In the regions between a cell and an s sphere ρv_{val} is nearly constant and $[v-v_1]$ is negligible, so in both integrals the region of integration may be changed to the s sphere without sensible error.

To obtain ρ and v_{val} accurately, it would be necessary to calculate the charge distributions due to all the various eigenfunctions, and average them. However, the order of magnitude of the cor-

[38] H. Margenau, Phys. Rev. **56**, 1000 (1939), Eq. (20).

rection can be estimated for $r_s=2.37$ by using as a rough approximation to ρ a distribution ρ_1 consisting of a charge of two electrons distributed with a density proportional to $|\varphi_{00}|^2+\frac{1}{3}R_p^2$. As described in Section 3, the neutralized potential due to this distribution is just $[v-v_1]$. For $r_s=2.37$ we have therefore

$$\frac{\Delta W_H}{nN}\approx-\tfrac{1}{2}\int_{s\text{ sphere}}\rho_1[v_1-v]d\tau=-\tfrac{1}{2}\int_{s\text{ sphere}}(\rho_1-\tilde{\rho}_1)[v_1-v]d\tau, \tag{B}$$

where $\tilde{\rho}_1=3/2\pi r_s^3$ may be introduced because $[v_1-v]$ has average value 0. If we define $Z_0(r)$ as $4\pi\int_0^r(\rho_1-\tilde{\rho})r^2dr$, the right of (B) becomes

$$-\tfrac{1}{2}\int[v_1-v]dZ_0=\tfrac{1}{2}\int Z_0d[v_1-v]=-\int_0^{r_s}\left(\frac{Z_0}{r}\right)^2dr. \tag{C}$$

Evaluation of this integral gives $\Delta W_H/nN\approx-0.0063$. A rough upper bound for the rate of variation of this correction with r_s can be obtained by noting that if the contributions to the integral on the right of (C) are almost entirely from small values of r, the first integral on the right of (A) will be roughly proportional to r_s^{-6}, the second to r_s^{-3}. If this were assumed we should have

$$\frac{\Delta W_H}{nN}\approx0.0063\left(\frac{2.37}{r_s}\right)^3\left[\left(\frac{2.37}{r_s}\right)^3-2\right]. \tag{D}$$

Direct calculations of $C_{00}(\varphi)$ and $C_{00}(\psi)$ which were made for different lattice constants showed that the former is roughly proportional to r_s^{-6}, but that the latter varies much less rapidly (see Table IX). It is likely that (A) also varies rather less rapidly than (D).

The self-energy $\frac{1}{2}C_{00}(\psi)$ of ψ_0 is needed in Section 8. This may be reduced to an integral like that on the right of (C), a rough evaluation of which yielded the values listed in Table IX.

Appendix III

To find s_k and p_k for small values of k, let us set

$$\varphi_k=e^{i\mathbf{k}\cdot\mathbf{r}}[\varphi_0+\sum_{\mu=1}^{3}ik_\mu v_\mu+\sum_{\mu,\nu=1}^{3}(ik_\mu)(ik_\nu)w_{\mu\nu}+\cdots], \tag{A}$$

$$E_k=E_0+\alpha k^2+\cdots. \tag{B}$$

Inserting (A) and (B) in the Schrödinger equation and setting to zero each term of the resulting power series in the components of $\mathbf{k}$, we have a sequence of wave equations, the first three of which are

$$(-\nabla^2+U-E_0)\varphi_0=0, \tag{C}$$

$$(-\nabla^2+U-E_0)v_\mu-2\partial\varphi_0/\partial x_\mu=0, \tag{D}$$

$$(-\nabla^2+U-E_0)w_{\mu\nu}-\left(\frac{\partial v_\mu}{\partial x_\nu}+\frac{\partial v_\nu}{\partial x_\mu}\right)+(\alpha-1)\delta_{\mu\nu}\varphi_0=0. \tag{E}$$

The boundary conditions are that φ_0, v_μ, and $w_{\mu\nu}$ must all have the periodicity of the lattice. Bardeen has shown[2] that a good approximation to v_μ in each atomic cell is

$$v_\mu=\frac{x_\mu}{r}\left[-r\varphi_0+\frac{r_s^2\varphi_0(r_s)}{f(r_s)}\frac{f}{r}\right], \tag{F}$$

where f is a radial p function satisfying $d^2f/dr^2+[E_0-2/r^2-U]f=0$. The first term of (F) is a particular solution of (D); the second is a solution of the associated homogeneous equation, so

chosen as to make v_μ vanish on the surface of the s sphere. Expanding the exponential in (A) and using (F), we have

$$p \text{ part } \varphi_k = \frac{i\mathbf{k}\cdot\mathbf{r}}{r}\left[\frac{r_s^2\varphi_0(r_s)}{f(r_s)}\frac{f}{r}+0(k^3)\right]. \tag{G}$$

From (19) therefore

$$p_k = k^2\left[\frac{r_s^2\varphi_0(r_s)}{f(r_s)}\right]^2\cdot\frac{4\pi}{3}\frac{f^2}{P_{2p}{}^2}+0(k^4). \tag{H}$$

Putting (A) into (18), s_k is defined for small k by

$$s_k = \left|\frac{\varphi_0(0)-\sum_{\mu,\nu=1}^{3}k_\mu k_\nu w_{\mu\nu}(0)}{\varphi_{00}(0)}\right|^2+0(k^4) \tag{I}$$

$$=\frac{\varphi_0(0)^2-\frac{2}{3}\varphi_0(0)w(0)k^2}{|\varphi_{00}(0)|^2}+0(k^4),$$

where

$$w=\sum_{\mu=1}^{3}w_{\mu\mu}.$$

An approximate expression for w can be obtained by steps similar to those used in obtaining (F). It can readily be verified that a particular solution of (E) is

$$w_{\mu\nu}{}^{(0)} = -\frac{(x_\mu v_\nu+x_\nu v_\mu)}{2}-\frac{x_\mu x_\nu}{2}\varphi_0-\frac{\alpha}{\delta_{\mu\nu}}\frac{\partial\gamma}{\partial E}\Big]_{E=E_0}, \tag{J}$$

where in the last term $\gamma(E, \mathbf{r})$ may be any function which satisfies the wave equation (C) with E_0 replaced by E, and which varies continuously with E in such manner that $\gamma(E_0, \mathbf{r})=\varphi_0$. We shall take for γ the $2s$ function obtained by outward integration starting from the value $\varphi_0(0)$. The general solution of (E) is thus $w_{\mu\nu}{}^{(0)}+w_{\mu\nu}{}^{(1)}$, where $w_{\mu\nu}{}^{(1)}$ satisfies the homogeneous equation. We must choose $w_{\mu\nu}{}^{(1)}$ so that this sum satisfies the boundary conditions and the normalization condition

$$\int_{\Omega_0}[v_\mu v_\nu-2\varphi_0 w_{\mu\nu}]d\tau=0. \tag{K}$$

We are here interested only in the function w which occurs in (I). Let us set

$$w^{(0)}=\sum_{\mu=1}^{3}w_{\mu\mu}{}^{(0)}, \quad w=w^{(0)}+w^{(1)}.$$

It can be verified that $w^{(0)}$ is almost spherically symmetrical, and almost satisfies the boundary conditions. Therefore w will be almost spherically symmetrical and so if we take the trace of Eq. (K) it will be permissible to change the region of integration in the resulting equation from a cell to an s sphere:

$$\int_{s\text{ sphere}}[\sum_{\mu=1}^{3}v_\mu{}^2-2\varphi_0 w]d\tau=0. \tag{L}$$

We need only the s part of w in (I), and this can now be determined from (L). Since $w^{(1)}$ satisfies the same wave equation as φ_0,

$$s \text{ part of } w^{(1)}=b\varphi_0$$

and b can be determined by substituting $w=w^{(0)}+w^{(1)}$ in (L). The result is most conveniently

expressed if φ_k is considered to be normalized to 1 over an atomic cell, instead of over Ω as in the text. It is

$$2b=3\lambda+\int_{s\text{ sphere}}\varphi_0\left\{2\sum_{\mu=1}^{3}x_\mu v_\mu+r^2\varphi_0+\alpha\frac{\partial\gamma}{\partial E}\right]_{E=E_0}\Bigg\}d\tau, \tag{M}$$

where

$$\lambda=\int_{s\text{ sphere}}v_\mu^2 d\tau$$

is the same as the quantity defined by (50). The integration in (M) can easily be reduced to a radial integral and evaluated numerically. Since $w(0)=w^{(1)}(0)=b\varphi_0(0)$, we have from (I)

$$\frac{d}{d(k^2)}\left(\frac{s_k}{s_0}\right)\Bigg]_{k=0}=-\tfrac{2}{3}b. \tag{N}$$

Appendix IV

A direct calculation of the variation of η_k with $\mathbf{k}$ near a symmetry point of Fig. 1 would be rather involved, since to the calculated variation of E_k would have to be added that of all the other terms in (29). These other terms may change quite considerably in a short distance from the symmetry point, since the form of the wave function varies rapidly with k near a small energy gap. However, a fair approximation to the behavior of η_k near such a point can be obtained by noting that the η_k are roughly the energy parameters which would occur in the solution of a wave equation formed with some potential U', different from U, but independent of $\mathbf{k}$.

Let $\boldsymbol{\Theta}$ be one of the symmetry points in Fig. 1, and let $\varphi_{j\boldsymbol{\Theta}}$, $\eta_{j\boldsymbol{\Theta}}$ be the complete set of wave functions and energies going with reduced wave vector $\boldsymbol{\Theta}$. Let $j=1$ and $j=2$ correspond to the states of the two lowest valence electron bands, and suppose for simplicity that the levels $\eta_{1\boldsymbol{\Theta}}$ and $\eta_{2\boldsymbol{\Theta}}$ are nondegenerate, so that $\partial\eta_k/\partial\mathbf{k}=0$ at Θ for the bands 1 and 2. For any $\boldsymbol{\kappa}$ we can write for the wave function of band 1 the infinite series

$$\varphi_{\boldsymbol{\Theta}+\boldsymbol{\kappa}}=e^{i\boldsymbol{\kappa}\cdot r}\sum_j b_j\varphi_{j\boldsymbol{\Theta}}. \tag{A}$$

The chief contribution to the summation in (A) will come from small values of j; if the separation of bands 1 and 2 at $\boldsymbol{\Theta}$ is small compared with the distance of band 1 from any other band, the terms $j=1$ and 2 will be much more important for small κ than any others. If (A) is substituted in the wave equation $(-\nabla^2+U'-\eta_{\boldsymbol{\Theta}+\boldsymbol{\kappa}})\varphi_{\boldsymbol{\Theta}+\boldsymbol{\kappa}}=0$, there results the secular equation

$$\det\left[2\boldsymbol{\kappa}\cdot\mathbf{F}_{ij}+(\eta_{j\boldsymbol{\Theta}}+\kappa^2-\eta_{\boldsymbol{\Theta}+\boldsymbol{\kappa}})\delta_{ij}\right]=0, \tag{B}$$

where $\mathbf{F}_{ij}=-i(\varphi_{i\boldsymbol{\Theta}},\nabla\varphi_{j\boldsymbol{\Theta}})$. If κ is very small this can be solved by the Schrödinger perturbation method. When κ is so large that $\boldsymbol{\kappa}\cdot\mathbf{F}_{12}$ is of the same order of magnitude as $(\eta_{2\boldsymbol{\Theta}}-\eta_{1\boldsymbol{\Theta}})$, however, this procedure must be modified by first finding two functions φ_a, φ_b, which are orthogonal linear combinations of $\varphi_{1\boldsymbol{\Theta}}$ and $\varphi_{2\boldsymbol{\Theta}}$ and which diagonalize the part $i,j=1,2$ of the matrix in brackets in (B). After this has been done we may set up the secular equation relative to these two new functions and the remaining functions $\varphi_{3\boldsymbol{\Theta}}$, $\varphi_{4\boldsymbol{\Theta}}\cdots$, and solve this by the perturbation method. This procedure will work for values of κ which are an appreciable fraction of the diameter of the Brillouin zone, provided $\eta_{3\boldsymbol{\Theta}}$, $\eta_{4\boldsymbol{\Theta}}$ are separated from $\eta_{1\boldsymbol{\Theta}}$ by amounts of the order of magnitude of those which would be encountered for almost free electrons. Let η_a, η_b be the energies corresponding to φ_a, φ_b: they are the roots of the second-degree secular equation obtained by taking only $i,j=1,2$ in (B). Thus $\eta_{\boldsymbol{\Theta}+\boldsymbol{\kappa}}$ for band 1 is η_a plus perturbations from the higher states.

The second-order perturbations from $\varphi_{3\boldsymbol{\Theta}}$, $\varphi_{4\boldsymbol{\Theta}}$, $\cdots$ may vary rapidly with κ, since φ_a and φ_b vary rapidly with κ when κ is small; however, the sum of these second-order perturbations will always be less than some function $c\kappa^2$, where c is of the order of 1. They can therefore

be neglected in rough calculations of the manner of variation of $\eta_{\Theta+\kappa}$ with κ for small κ, since as will be shown presently the variation of η_a with κ is on a rather larger scale than $c\kappa^2$. We have

$$\eta_a=\tfrac{1}{2}(\eta_{1\Theta}+\eta_{2\Theta}) +\kappa^2-\tfrac{1}{2}[(\eta_{2\Theta}-\eta_{1\Theta})^2+16|\boldsymbol{\kappa}\cdot\mathbf{F}_{12}|^2]^{\frac{1}{2}}, \quad \text{(C)}$$

while η_b has the same form with a plus sign before the radical. Successive differentiations of (C) with respect to K, and with respect to r_s holding Kr_s constant, establish the existence of the maxima and minima shown in Fig. 9, provided the difference $(\eta_{2\Theta}-\eta_{1\Theta})$ is sufficiently small.

The quantities

$$\beta_\Theta=\tfrac{1}{2}\frac{\partial^2\eta_{\Theta+\kappa}}{\partial\kappa^2}\Big]_{K=0}\approx\tfrac{1}{2}\frac{\partial^2\eta_a}{\partial\kappa^2}\Big]_{\kappa=0}$$

are easily obtained from (B) or (C). The required matrix elements $\mathbf{F}_{12}$ were calculated for several points Θ, using for the wave functions the best approximation which could be obtained from two constituent χ-functions (for most of the (s) states it turned out that the wave function could not be well approximated by a single constituent χ-function, but could be by two). These matrix elements were found to be within about 25 percent of the values they would have for almost free electrons.

JULY 15, 1940 PHYSICAL REVIEW VOLUME 58

Design and Preliminary Performance Tests of the Westinghouse Electrostatic Generator

W. H. WELLS, R. O. HAXBY,* W. E. STEPHENS,* AND W. E. SHOUPP*
Westinghouse Research Laboratories, East Pittsburgh, Pennsylvania

(Received May 3, 1940)

Design and performance characteristics of the Westinghouse electrostatic generator are discussed. Steady voltages of 1.3 Mv at atmospheric pressure and up to a maximum to date of 3.7 Mv at about 75 lb./sq. in. have been used to accelerate hydrogen ions. The maximum steady voltage is limited mainly by sparking along the belts. The voltage remains constant to within 0.5 percent for observing times of several minutes, and at times to within 0.2 percent for a half-minute or so.

INTRODUCTION

DURING the past three years, a large electrostatic generator of the belt type, using compressed air insulation, has been constructed at the Westinghouse Research Laboratories in East Pittsburgh. It has been in satisfactory operation for nearly a year as a source of high energy protons for research in nuclear physics. This paper gives an account of the design features and a preliminary account of its performance. Details of the researches in nuclear physics carried out to date will be published soon in other papers.

The first successful utilization of air under high pressure as insulating medium for an endless-belt electrostatic generator was made by Barton, Mueller, and L. C. Van Atta[1] but they did not apply the potential to an accelerating tube. Herb, Parkinson, and Kerst,[2] using a somewhat similar generator successfully applied 400 kv to a vacuum tube to accelerate hydrogen ions. A larger generator was then constructed by them[3] and the performance of these generators indicated that further development to larger dimensions was a practical method of obtaining a beam of high energy ions having energy

* Westinghouse Research Fellow.

[1] H. A. Barton, D. W. Mueller, L. C. Van Atta, Phys. Rev. **42**, 901 (1932).
[2] R. G. Herb, D. B. Parkinson, D. W. Kerst, Rev. Sci. Inst. **6**, 261 (1935).
[3] R. G. Herb, D. B. Parkinson, D. W. Kerst, Phys. Rev. **51**, 75 (1937); D. B. Parkinson, R. G. Herb, E. J. Bernet, J. L. McKibben, Phys. Rev. **53**, 642 (1938).

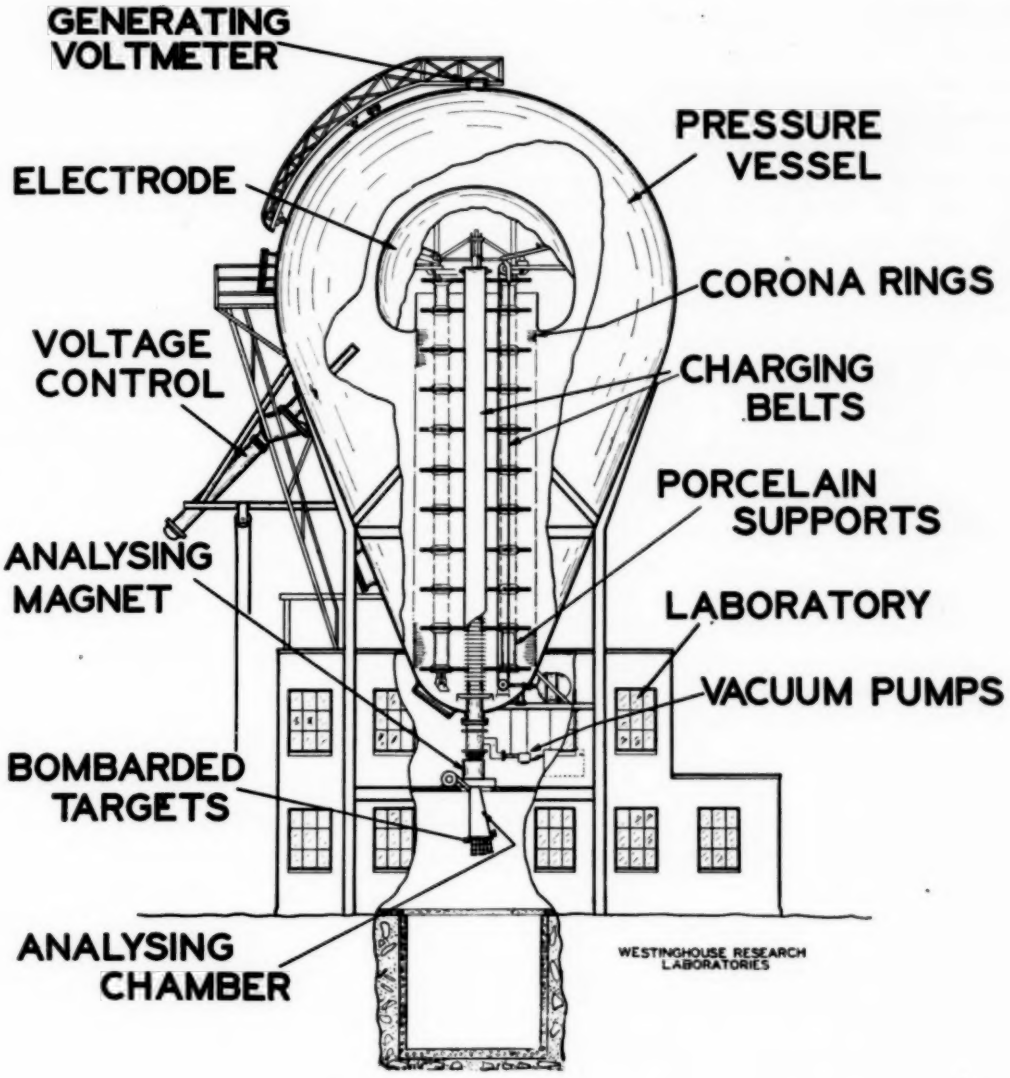

FIG. 1. Elevation view of generator.

homogeneous to a fraction of a percent which is the performance of electrostatic generators at atmospheric pressure.[4]

PRESSURE VESSEL

Large spherical and cylindrical gas containers have been fabricated for a number of years, and the use of a large spherical container for a disk electrostatic machine was suggested by M. A. Tuve, L. R. Hafstad, and O. Dahl.[5] The pear-shaped pressure vessel inside which the generator is built is shown in Fig. 1. This vessel[6] is made up of two sections of spherical surfaces of 30 and 10 feet in diameter joined by a conical section to give a total vertical height of 47 feet. It is mounted on a tower structure so that the lower nozzle of the vessel is 14 feet from the ground in the center of the second floor of the associated laboratory building, as shown in Fig. 1.[7] This shape was chosen for the saving in

[4] M. A. Tuve, L. R. Hafstad, O. Dahl, Phys. Rev. **48**, 315 (1935); L. C. Van Atta, D. L. Northrup, C. M. Van Atta, R. J. Van de Graaff, Phys. Rev. **49**, 761 (1936).

[5] M. A. Tuve, L. R. Hafstad, O. Dahl, Naturwiss. **24**, 625 (1936).

[6] Constructed in 1937 by Chicago Bridge and Iron Works, C. H. Jennings, The Welding Engineer **24**, Dec. (1939).

[7] W. H. Wells, J. App. Phys. **9**, 677 (1938); W. H. Wells, Phys. Rev. **5**, 599A (1939); W. H. Wells, R. O. Haxby, W. E. Shoupp, W. E. Stephens, Phys. Rev. **57**, 347A (1940).

weight of steel over that necessary to make a spherical or cylindrical vessel with the same minimum clearances from high voltage cap to the pressure vessel, both through the air gap and along the support insulators and belts. Since the best voltage distribution for highest total voltage along the belts and support towers is approximately linear, the clearances radially from tank wall to tower were made to vary linearly with height.

Maximum voltage difference for a given field strength at the inner electrode is obtained with concentric electrodes at a ratio of diameters of 2 for spheres and of $e(=2.718)$ for infinitely long cylinders. For the same diameter of inner electrode, the field strength at the surface of the inner electrode for concentric spheres is twice the value for the field strength with concentric cylinders when the condition for maximum voltage difference is fulfilled. Hence, in our design, the insulator length was increased by a factor of about three over that used in the larger generator at the University of Wisconsin, and the diameter of the inner electrode was increased by roughly a factor of 6.

The vessel was tested pneumatically so as to give an adequate safety factor over its maximum working pressure of 120 lb./in.^{2}. The lower shell is made of $\frac{5}{8}$-inch plate, twice the necessary thickness, so as to reduce stresses due to loading by the support tower and to permit drilling through the shell later for electrical leads or other purposes. There are three 30-inch diameter manholes provided as shown in Fig. 1. Each of these is provided with a 3-inch diameter sight-glass mounted to give a linear angle of view of about 90°. The lower manhole gives access to the inside of the support tower. A 12-inch nozzle at the top of the vessel is used to mount a generating voltmeter in a symmetric position with respect to the high voltage electrode. The vacuum tube comes out of the vessel through a 14-inch nozzle at the bottom of the vessel. The top dome of the vessel is of $\frac{7}{8}$-inch steel plate, and the upper conical plates are $1\frac{3}{4}$ inch thick with the lower conical plates of decreasing thickness. These plates were welded in position with the inner surfaces held flush and the welds then ground flush with the plate surfaces.

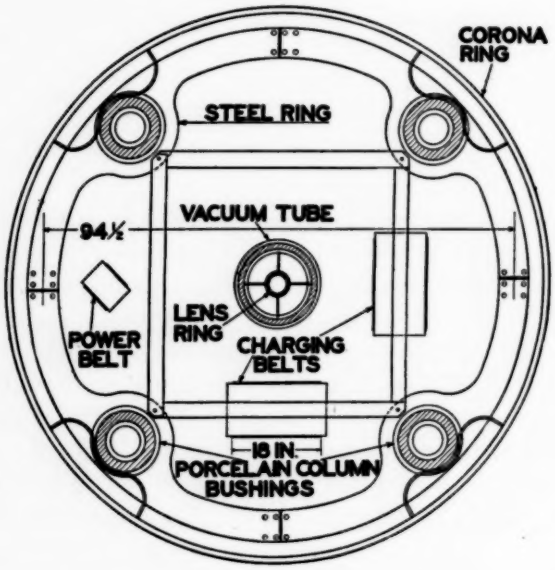

FIG. 2. Plan view of support tower showing location of belts, vacuum tube, corona rings, and removable channel irons.

HIGH VOLTAGE ELECTRODE

The high voltage electrode is supported on a porcelain and steel insulating tower, as shown in Fig. 1. The upper part of the electrode has a radius of 7.5 feet. The lower half of the electrode curves in more rapidly than the upper spherical surface, as shown in Figs. 1 and 4, as the radial distance from the pressure vessel increases along the conical portion. This permits some gain in the support tower and charging belt length.

The electrode is of $\frac{3}{16}$-inch steel plate dished at the factory and welded in the field. The welds and all weld beads remaining were ground off. The electrode has irregularities of the surface due to difficulties which showed up in dishing this thin plate, and is out-of-round in some places by as much as $\frac{1}{8}$ of an inch in 3 or 4 inches. However, there has been no consistent sparking at atmospheric pressure from any one place on the electrode.

SUPPORT TOWER

The support tower is constructed as shown in the two views Figs. 2 and 3. It is made with sufficient flexibility in the flat steel rings to limit the mechanical stresses in the porcelains to a low

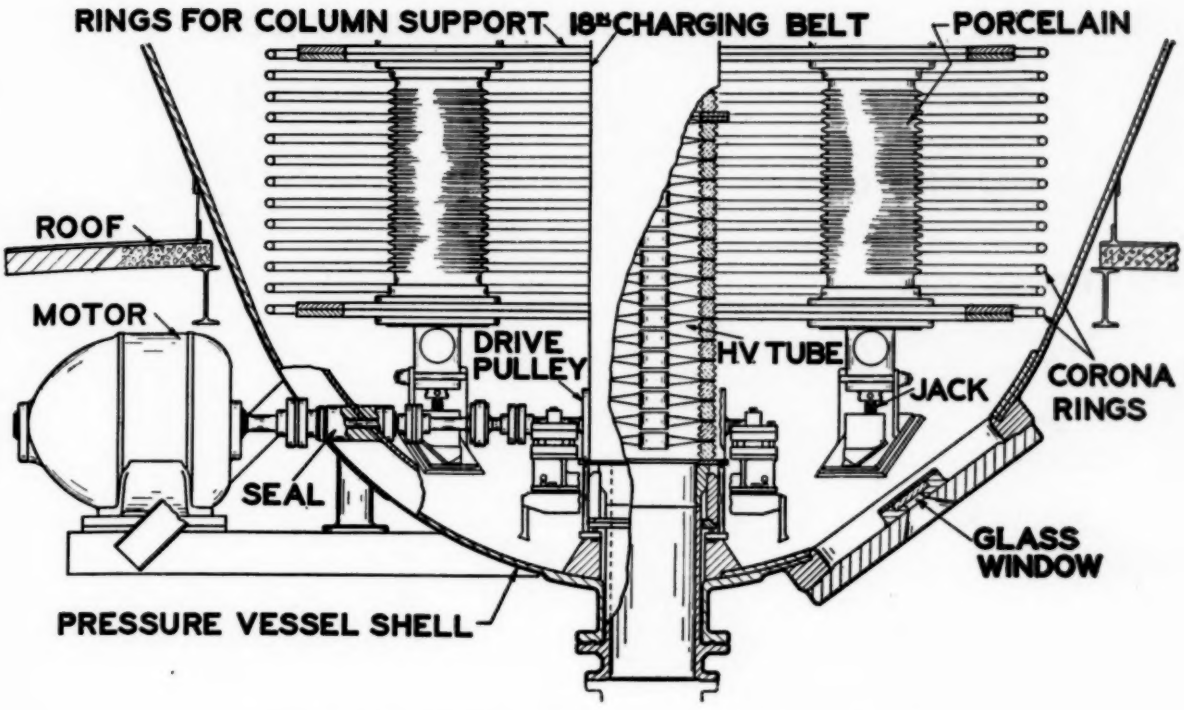

FIG. 3. Vertical section of base of pressure vessel and support tower.

value.[8] The tower is made up of a series of ten separate sections, nine of which are 3 feet in height while the upper one is 2 feet in height. Each section consists of two flat steel rings bolted to and held apart by four porcelain bushings. The flat steel rings are made up of four quadrant pieces for economy of fabrication and ease of assembly. The sections are stacked with the bushings in line vertically, to transmit the vertical load directly in compression. The successive sections are bolted together only at points halfway between the bushings with $\frac{1}{16}$-inch shims inserted between sections both below the bushings and at the points of bolting between sections.

Application of a lateral force to the upper end of the tower will cause the steel rings to deflect in bending and twist, thus limiting the tensile stresses in the bushings to low values. This design also avoids large stresses in the bushings due to temperature gradients between the sections, and due to errors in machining of the ring or assembly of the tower. The natural period of the tower is 0.77 second. From the measured damping, it was computed that a 150-lb. man swaying through an amplitude of 1 ft. in resonance with the tower could build up an amplitude of the tower about equal to that produced by a 450-lb. force statically applied, and the bending stress in the porcelain bushings at this value of lateral force is less than 50 lb. per sq. in., which is quite safe. The tower is

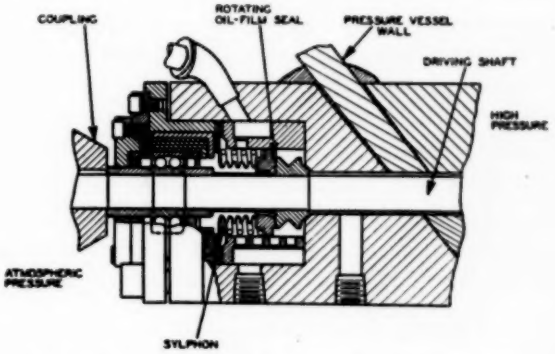

FIG. 4. Rotary oil film seal on driving shafts for the fabric belts.

We wish to express our appreciation of the help given by the Mechanics Department of the Westinghouse Research Laboratories in the many mechanical problems which arose in the design and construction; in particular, to Dr. A. M. Wahl for calculations on the support tower design; and to Mr. B. F. Langer for many helpful discussions of mechanical problems.

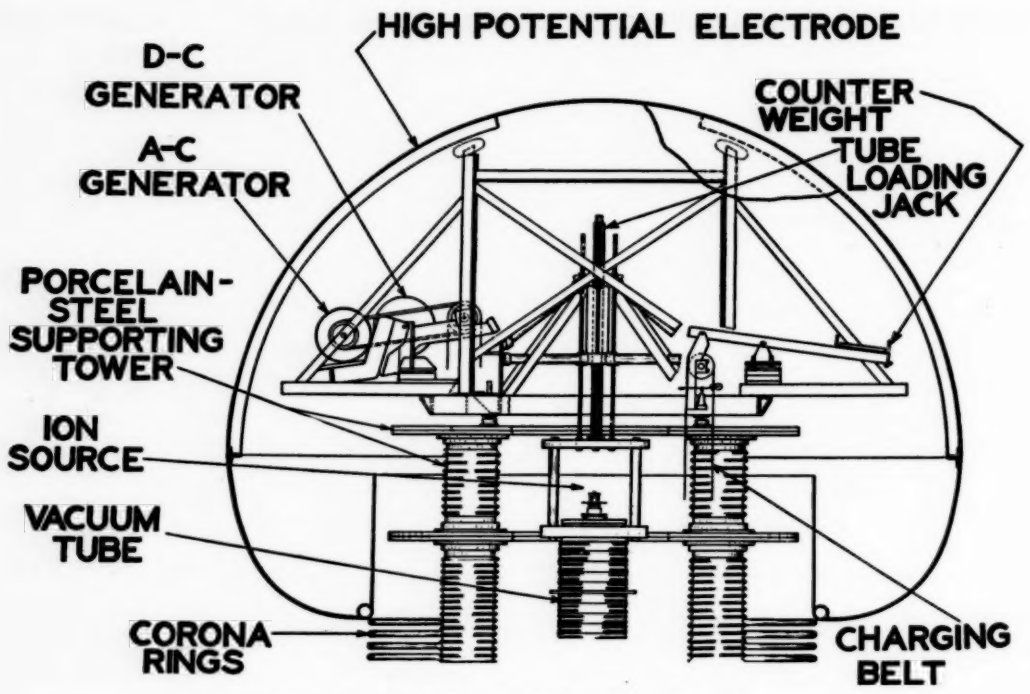

FIG. 5. Vertical section of high voltage electrode.

capable of standing erect in case of complete destruction of a bushing.

As shown in Fig. 3, the lower end of the tower rests on four jack screws to permit lateral adjustment of the tower after erection. Movement of over an inch vertically for one jack is permissible because of the flexibility of the towers. Likewise, four independent vertical jacks support the electrode on the tower to give a further vertical adjustment. The lower jacks are mounted on 12″ by 12″ pads welded to the pressure vessel wall to distribute the loading on the shell.

The porcelain bushings were fabricated at the Derry Works of the Westinghouse Electric and Manufacturing Company. The bushings have corrugations one inch deep both inside and outside with a central hole varying from 6 to 7 inches, and an outside diameter of 12 inches at the base where they were cemented to the end caps. The flat steel rings were machined smooth and the end caps of the bushings were likewise machined.

BELTS, PULLEYS, AND MOTORS

Two charging belts, each 18 inches in width, run at right angles to each other in the positions shown in Fig. 2. The lower driving pulleys are $10\frac{1}{2}$ inches in diameter and 20 inches in length, with crowning of 0.01 inch per inch over the outer 3 inches. All of the pulleys are made of steel tubing welded to end plugs attached to the shafts and the assembly then dynamically balanced. The charging belts are driven by Westinghouse Type SK 15 hp, d.c. motors with speed variable between 400 r.p.m. and 2000 r.p.m. with the rotors dynamically balanced. The motors are mounted outside the vessel, as shown in Fig. 3, with the driving shaft passing through the pressure vessel wall. The pressure seals used are of the type used for refrigerator units[9] (see Fig. 4). Test showed only a small air leakage which was negligible considering the size of the pressure vessel. Three flexible Thomas couplings are used in each shaft, as shown in Fig. 3. The upper pulleys for the charging belts are $6\frac{3}{8}$ inches in diameter with the same crowning as the lower pulleys. The pulleys are mounted on the counter weight system, as shown in Fig. 5 so as to give a constant force of 200 lb. for each run of a belt, permitting of stretch of each run of a belt of more than 12 inches. The center-to-

[9] Obtainable from Clifford Manufacturing Company, Boston, Mass.

center pulley distance is about 31½ feet for new belts. The exact stretching for the different belt materials under this load has not been measured, but in general we are able to use the same belts for several months after they are once in alignment, without further adjustment. However, since the insertion of the aluminum tubes (as described later) close to the surfaces of the belts, it has been necessary to limit the lateral movement of the upper pulley so as to keep the belts from rubbing against the tubes. A belt six inches wide of the same material as the charging belts transmits power to the electrode. One 2-kw, 220-volt, a.c. generator and one 2-kw, 220-volt, d.c. generator are driven by the upper pulley of the six-inch belt. through intermediate V-belts. These generators supply power for the belt charging systems, ion source, and lights in the high voltage electrode.

Both the lower and upper pulleys for the charging belts are mounted on Micarta blocks to insulate them from ground and the electrode, respectively. We have used them as inductor plates, but burned out the shaft insulator when the lower pulley was -20 kv to ground and the points horizontally opposite the center of the pulley at $+20$ kv. The spray points were then moved to a position several inches above the pulley. Variacs are used to control the spray voltage on a set of office pins spaced ½ inch apart and about ¼ inch from the belts, at both ground and high voltage end of the belts. Under pressure, with the different belt materials used, it has been necessary to adjust the charge on the two runs of the belt to obtain maximum voltage. Raising the spray voltage on one run of a belt above this best value causes sparking on this run of the belt near the high voltage electrode. This seems to imply that at maximum voltage the charge density is the same on each run of a belt. At this balanced condition a lower voltage is necessary for negative corona points spraying charge on the belts than is necessary for positive points.

The first belt material tried was Goodyear Zeppelin fabric, which gave, at a speed of 5000 feet per minute, a charging current including both belts of about 500 microamperes, measured from the electrode to ground through a microammeter at atmospheric pressure. To eliminate the lap joint of these thin belts, a commercial belting of fabric and latex, called brown Tontex[10] was tried with a vulcanized smooth splice of thickness the same as the rest of the belt. These gave a lower charging current of about 300 microamperes. They were injured by sparks along the belts. A series of aluminum tubes was then installed, as described later in this paper, giving an increase in the maximum voltage obtainable, but rips due to sparking at these higher voltages soon necessitated removal of the Tontex belts. The next belts tried were a commercial black latex coated belting of the kind used by Professor J. G. Trump.[11] They have a smooth spliced joint. These belts were also injured by sparks and one of the charging belts was split down the center line for one-half of its length. Next, Balata[12] belts were tried. These have two of the fabric layers on the outside surface, with the Balata material and one fabric layer between them. The charge transported was about 300 microamperes again. All types of belting take many hours in dry air to dry out after exposure to humid air. We have found that a somewhat higher voltage can be obtained near 45 lb./in.^{2} air pressure after running these belts for about a hundred hours, than was the case with any of the other kinds of heavy belting used.

Air-Drying System

Air for the pressure vessel is dried by two activated alumina[13] drying beds in series. Valves are arranged with a blower whose capacity is about 200 cubic feet per minute at 3 lb., so that the air initially in the pressure vessel can be circulated through the towers and back into the vessel. The towers also dry the incoming air at a rate of about 250 cubic feet per minute, with no change in the relative humidity in the pressure vessel that is not explainable as a temperature effect.

It is necessary to reduce the relative humidity in the pressure vessel to about 40 percent to obtain high voltage on the electrode. No apparent

[10] Tontex belts are obtainable from Tontex Corporation, Grand Rapids, Michigan.
[11] Private communication from Professor Trump.
[12] Balata belts are obtainable from Victor Balata and Textile Co., New York, New York.
[13] Design information can be obtained from the Aluminum Ore Co., East St. Louis, Illinois.

gain in maximum voltage was obtained in one series of tests when the relative humidity was below 10 percent for several days.

Corona Ring System

A system of metal rings surrounding the support tower was provided as in the design of R. G. Herb and associates.[2] A set of gaps between adjacent rings, consisting of four negative points opposite a plane, act to produce corona current down the ring system. One hundred rings of 1.25 inch diameter Al tubing held by brackets in the corrugations of the bushings are spaced at about one inch average clearance. This clearance varies somewhat because of the flexibility of mounting. At the ends of the porcelain bushings the clearance from the bushing caps to the nearest ring is somewhat larger. One corona ring is attached to the center of the flat steel rings of the support tower to shield their surfaces. The corona rings have a mean diameter of 108 inches.

With this choice of corona rings, the average axial field strength at the surface of a ring was estimated to be about one-half of the field strength at the spherical surface of the high voltage electrode. This seemed sufficient to prevent the ring system from being a limitation to the maximum voltage of the generator.

Voltage Control

As a control for voltage on the electrode, a "poker" is mounted on a nozzle at one side of the pressure vessel, as is shown in Fig. 1. It can be made to approach the electrode or recede back into the vessel wall by a reversible drive controlled from the control panel for the generator. A friction drive is used to avoid damage to the apparatus. A set of points on the end of the "poker" controls the voltage by varying the corona-current drain from the high voltage electrode. The position of the "poker" is indicated on the control panel by means of Westinghouse Type ADS position indicator motors. The direction chosen for the poker is at about 45° upward, so that corona from the points would affect the generating voltmeter as little as possible. There has, as yet, been no indication of such an effect.

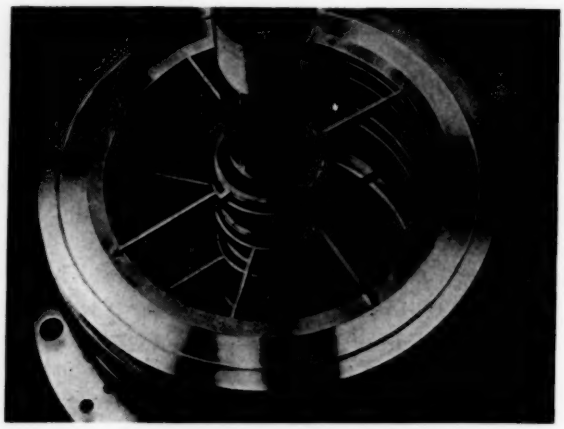

Fig. 6. Photograph taken during assembly of a section of the accelerating tube.

The voltage is also controlled by adjustment of the spray voltages used for the charging belts. An increase in the voltage on the ion-source probe decreases the voltage on the high voltage electrode since this increases the output of the ion source.

Accelerating Tube and Vacuum System

The accelerating vacuum tube occupies a central position inside the support column as shown in Figs. 1 and 2. It is made up of 130 flat porcelain rings, 15 inches mean diameter, 1 inch minimum wall thickness, and $2\frac{1}{8}$ inches in height.[14] Two flanges 1 inch in depth were made on both inside and outside walls, to increase the surface creepage path. The rings were ground flat and then coated with a platinum alloy glaze giving a metallic end surface in intimate contact with the porcelain to prevent concentration of electrical stress where the porcelain joins the gasket.

The structure of the tube is shown in the photograph (Fig. 6). Flat rings of $\frac{1}{8}$-inch brass, extending about $\frac{1}{2}$ inch inside and outside of the porcelain ground surfaces, hold a 5-inch outside diameter ring of $\frac{1}{8}$-inch wall, one inch in height in the center, by means of 4 radial webs. All joints were silver soldered. The majority of the electrodes which form the focusing gaps of the tube are $2\frac{1}{8}$ inches in height made from $\frac{1}{4}$-inch wall brass tube with 4-inch outside diameter.

[14] Made at the Derry Works of the Westinghouse Electric & Manufacturing Company.

The electrodes are supported from the 5-inch diameter brass ring by four steel Allen screws forced into the brass at time of assembly. The tube was assembled with $\frac{3}{32}$-inch diameter tin wire gaskets and aligned on a mandrel in sections consisting of 18 porcelains with the associated brass electrode structures. Steel end rings which remained with each section were used to transport and to compress the section by means of tie rods. The end rings were doweled to insure correct alignment of the tube in final position. The upper lens ring in each section was made longer to preserve the lens gap of about $\frac{3}{8}$ inch between successive electrodes.

With cover plates and rods to prevent overloading of the gaskets, each section was tested to 180 lb./in.^{2} external pressure. The tin wire gaskets have an elastic limit on short time tensile test of 1300 lb./in.^{2}. The full pressure load on the top of the tube at 120 lb./in.^{2} could probably be supported without much more flow by the gaskets when they reach a radial width of $\frac{3}{16}$ inch due to friction gripping of the thin gasket by the ground porcelain surface. It was decided, however, to provide a large jack screw to increase the compressive force on the tube when necessary, and also to provide four tie rods opposing the action of the jack screw to prevent most of the extra compressive force due to pressures above atmospheric from being applied to the gaskets. This arrangement can be seen in Fig. 5. The tube is braced laterally to the support column at three places, $\frac{1}{3}$ and $\frac{2}{3}$, and at the upper end of its height since calculation showed that the unbraced structure would be close to the buckling limit.

In the assembly of a section of the tube, the gasket seals were compressed to about one-half their final thickness, painted with thinned glyptal by means of hypodermic needles, and the remainder of the compression was then taken up. The vacuum system contains over 1000 feet of this type of seal, and can be pumped down with our present pumping system to below 2×10^{-5} mm Hg. The lower end of the vacuum tube rests on the top of a flanged pipe which forms the seal from inside the pressure vessel to the space outside. This has a thick lead gasket which was compressed eccentrically to compensate for final misalignment of the tube with respect to the support column. The gross adjustment due to misalignment of the lower nozzle axis was taken up by welding together the flange and the outlet pipe with their axes at a small angle.

As shown in Fig. 1, the vacuum pumps and analyzing magnet are located in the second floor room of the laboratory building. The analyzing chamber with nozzles for attachment of targets is at the center of the first floor room. A four-inch all-metal diffusion pump with a speed of 240 liters per second backed by a Hypervac 20 is used. The diffusion pump is of the self-fractionating type supplied by the Distillation Products Corporation, Rochester, New York. When first attached by means of a 12-inch length of straight 4-inch pipe to the main vacuum tube and without a baffle, trouble was experienced due to back streaming of the pump oil into the main tube, causing the oil to run down to the target position. This back streaming was not eliminated by insertion of the baffle, which came with the pump, but was eliminated by inserting a 12-inch vertical section of 4-inch pipe between the diffusion pump and the main vacuum tube. This cuts down the pumping speed approximately half, but the pipe attached to the main vacuum tube has remained dry for the last several inches before entering the main tube. After continuous pumping for several months, about $\frac{1}{3}$ of the oil in the diffusion pump disappeared. It did not appear to be condensed in either the main vacuum system so as to impair its ability to stand high voltage, nor did it appear in a buffer tank used between the diffusion pumps and the mechanical pump, and so probably had been pumped away as volatile products formed from the oil.

Controls

The controls necessary to operate the generator, excepting the belt motor controls, have been put on two relay rack panels mounted on a wheeled table. About 100 control wires from the panel are connected to the panels in the form of 22 prong plugs, so that the controls can be moved to another part of the building when necessary. Seven position indicator motors[15] are

[15] Type ADS position indicator motors made by Westinghouse Electric and Manufacturing Company.

mounted on the panel and connected to seven others inside the pressure vessel. Strings go up from these to the high voltage electrode to adjust Variacs on spray voltage, ion source filament, ion source high voltage supplies, and a needle valve controlling the gas flow for the ion source. The panel also contains the lower spray voltage control for the charging belts. Controls are also provided for the deflecting magnet and for the generating voltmeter, voltage control "poker," and main tube vacuum measurements.

An illuminated meter panel in the high voltage electrode shows the ion source performance and upper spray voltage for the belts. A telescope is used to view this panel from the first floor of the laboratory through a sight glass in the lower manhole.

Voltage Tests and Belt Performance

The maximum voltage obtainable at atmospheric pressure is about 1.4 Mv. This is limited by sparking from the electrode to the pressure vessel wall and down the corona ring system. A beam of particles can be maintained for hours at 1.25 Mv.

When first operated at pressures above atmospheric, the maximum sparking voltage was limited by sparking along regions of the charging belts, vacuum tube, and corona rings. A representative set of values is given by the points for curve *A* in Fig. 7. As the pressure was increased, a region was reached in which the maximum voltage obtainable began to fall with increasing pressure. A similar effect at a somewhat higher pressure has been reported by Herb and Bernet.[16] This region was characterized by shorter and more frequent sparks along the belts and corona ring system than occurred at lower pressures. During these tests the belts were damaged in many places by sparks which ripped out fabric and latex, and in some cases, split the belts.

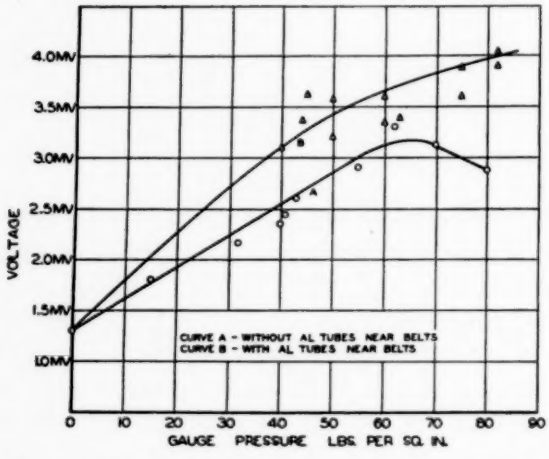

FIG. 7. Maximum sparking voltage of the generator as a function of air pressure, with and without aluminum tubes near the belts.

The charging belt surfaces have a minimum clearance of about 10 inches from the vacuum tube and parts of the support column. Trump and Van de Graaff[17] have made a small belt machine operating in air under pressure, in which a series of metal tubes was placed parallel to and near the surfaces of the belts to reduce the horizontal voltage difference between a point at the belt and a nearby point on the vacuum tube or high voltage electrode supports. Following this idea, we inserted a series of aluminum tubes of $\frac{3}{4}$ inch diameter placed on each run of the belts every 3 feet. It was also necessary to place these tubes along the power belt, after which the maximum obtainable voltage at a given pressure was higher as given by the points for curve *B* in Fig. 7. The limitation was still sparking of the same general character as before.

The corona gaps between the corona rings along the support tower each consist of four negative points opposing a positive plane. The maximum voltage obtainable with the generator occurs for gap spacing of about $\frac{3}{4}$ to 1 inch. In general, it is possible to maintain an ion beam focused on the target at voltages a few hundred kilovolts below the maximum voltage at which sparking occurs. The highest sparking voltage obtained is 4 million volts, as shown in Fig. 7. The highest voltage at which an ion beam has been maintained is 3.7 million volts.

Ion Source

The ion source now being used is shown in Fig. 8. It is an adaptation from one described by Tuve, Hafstad, and Dahl[18] with changes in

[16] R. G. Herb and E. J. Bernet, Phys. Rev. **52**, 379 (1937).

[17] J. G. Trump and R. J. Van de Graaff, Phys. Rev. **55**, 1160 (1939).

[18] M. A. Tuve, L. R. Hafstad, and O. Dahl, Phys. Rev. **48**, 315 (1935).

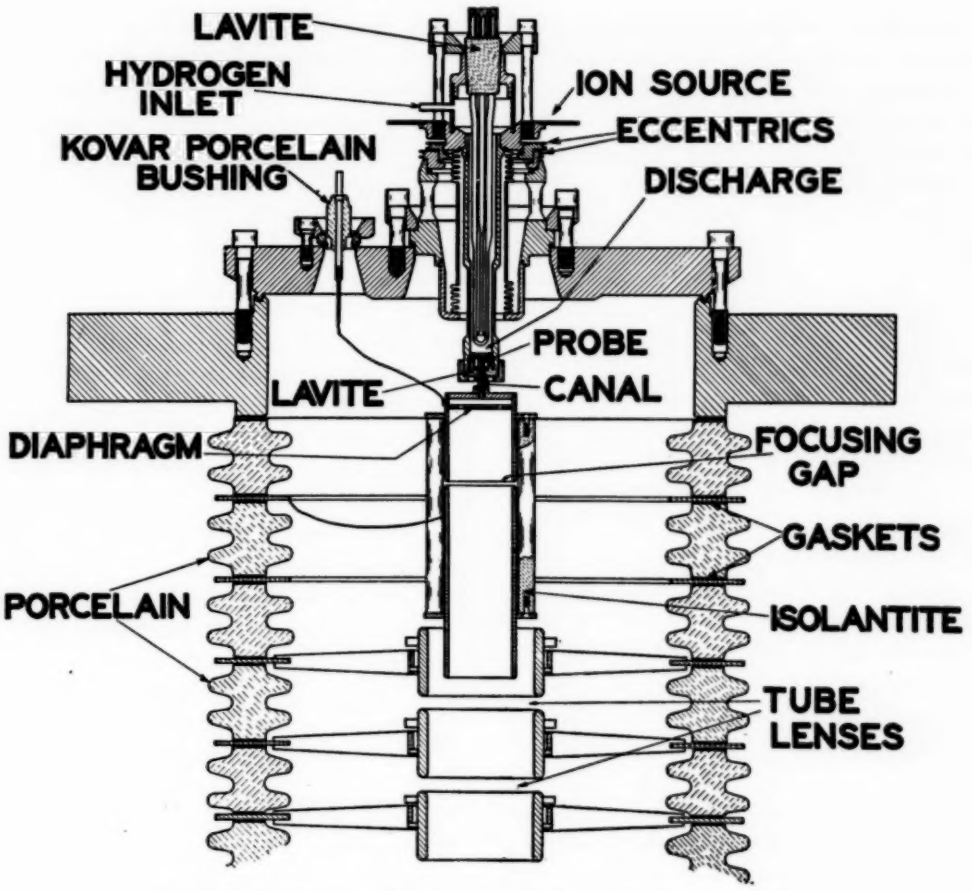

FIG. 8. Ion source and first few accelerating gaps of vacuum tube.

the probe mounting and in the first focusing gap. Satisfactory filament life of several hundred hours is obtained at about 200 milliamperes discharge current. The filament is made of 10-mil tungsten wound with 5-mil nickel, coated with a BaO and SrO mixture and a binding agent. The discharge voltage drop is between 50 and 100 volts with hydrogen pressure of 2 to 3×10^{-2} mm Hg. With voltage of about 2 kv on the probe, an output current of 50 to 80 microamperes of ions was obtained as measured below the probe to the rest of the tube as a Faraday cage.

To get some idea of the total effective focusing action of the large number of electrostatic lenses which make up the main part of the tube, calculations were made by the method of Hansen and Webster.[19] From the general theory of lens action together with the experimental potential distribution found by Kirkpatrick and Beckerley[19] the formula for the focal length of each individual lens is

$$f=16.5R(V/\Delta)^2.$$

Here R is the radius of the cylindrical electrodes, V is the potential in volts of the first cylinder of a lens relative to the potential of the ion source, and Δ is the potential difference between the two cylinders constituting the lens. In deriving the formula, it is supposed that the gap between the cylinders is small compared to R, that the length of each cylinder is long compared to R, and that Δ is small compared to V. Actually in our case the length of the cylinders is not long compared to R so the actual focal length will be much greater than that given by the formula. If Z is the coordinate of a particle measured along the tube axis and r is its distance

[19] W. W. Hansen and D. L. Webster, Rev. Sci. Inst. 7, 17 (1936). (See especially fine print paragraphs at end of paper.) P. Kirkpatrick and J. G. Beckerley, Rev. Sci. Inst. 7, 24 (1936).

from the axis, then the method of Hansen and Webster gives the following equation for the average trajectory of a particle through a succession of lenses spaced a distance l apart, using the above approximation for the focal length of each lens and assuming that Δ is the same for each lens (uniform voltage distribution along tube),

$$d^2r/dz^2 = -(l/16.5R)r/z^2.$$

This differs slightly from the formula as printed by Hansen and Webster because of some numerical misprints in their paper. Although this equation may have solutions of oscillatory type (corresponding to a succession of focal points along the length of the tube) if $l/R > 4.1$, with our dimensions $l/R = 1.25$, so the non-oscillatory case is the one that applies here. This is even more the case when it is remembered that the formula for f overestimates the power of the individual lenses.

With the method indicated, it appears that the aggregate focusing action of the tube is such that a beam that is parallel 1/13 of the tube length from the ion source end will be brought to a focus at the target ten feet beyond the end of the lens system. This is such a weak contribution to the focusing that it is evident that the first few lenses near the ion source must be relied upon to do the focusing. This result from theory is in accord with our experience and that of other workers with whom we have discussed the question.

The first focusing gap must be considered as a thick lens since the increase in voltage between the cylinders is not small compared to the voltage on the first, or probe, cylinder. Useful data giving the constants for such a lens over a considerable range of voltage ratios are given by Klemperer and Wright.[20]

That a large fraction of the ions had a spread in direction after coming from the probe so that they were not focused by the present lens arrangement was shown by inserting a diaphragm 5 mm below the probe canal with a 1 mm diameter central opening and several side openings for gas flow. The current from the probe canal measured as before was now about 5 microamperes, and total ion currents of the same order of magnitude are obtained at the target in a well-focused spot. The currents obtained in the beams of different masses are about 0.3, 0.5, 0.5 microamperes of H^+, H_2^+, H_3^+, respectively, and commercial tank hydrogen is used, the hydrogen supply line being kept at a pressure of 15 lb./in.^{2} above that used inside the pressure vessel. Between successive electrodes of the accelerating tube 1000-megohm IRC resistances are connected. These resistances are connected electrically to the corona ring system only at the two lateral places where there are braces to insure mechanical stability of the tube as already mentioned. These are located at points $\frac{1}{3}$ and $\frac{2}{3}$ of the way along the length of the tube. It is necessary to keep the vacuum at the lower end of the vacuum tube below about 10^{-4} mm Hg in order to maintain high voltage on the tube.

Voltage Measurement and Steadiness

Voltage on the high voltage electrode is measured with a generating voltmeter installed in the 12-inch nozzle at the top of the pressure vessel. The voltmeter was calibrated by using the value of 0.862 Mv for one of the prominent resonances for gamma-ray production from fluorine bombarded by protons. This value was determined by Bernet, Herb, and Parkinson.[21] By bombarding a thin tantalum fluoride target with the H^+, H_2^+, and H_3^+ beams, the generating voltmeter was shown to be linear using the voltages at which the 0.862-Mev resonance was a maximum as 1.724 Mv for the H_2^+ beam and 2.586 Mv for the H_3^+ beam.

The generating voltmeter is used as a null instrument.[22] A measured voltage is applied to an adjacent sectored plate of the voltmeter until the field due to this plate is the same as the field produced by the high voltage at the pick-up plate. The induced voltage produced on the pick-up plate is amplified and viewed on an oscilloscope. The wave form for the balance point is easily reproduced. The voltage on the high voltage electrode remains constant at a

[20] Klemperer and Wright, Proc. Phys. Soc. London **51**, 296 (1939).

[21] E. J. Bernet, R. G. Herb, and D. B. Parkinson, Phys. Rev. **54**, 398 (1938).

[22] G. P. Harnwell and S. N. Van Voorhis, Rev. Sci. Inst. **4**, 540 (1933).

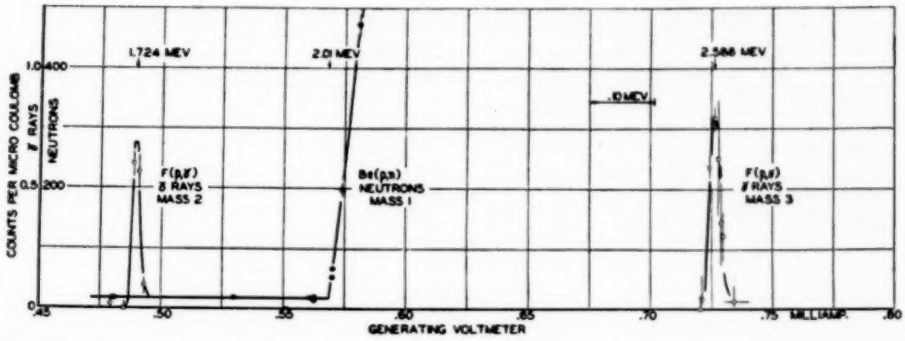

FIG. 9. Curve showing fluorine gamma-ray resonances used for voltage calibration and a typical run to determine the (p,n) threshold for beryllium.

given voltage to within 0.5 percent for observing times of several minutes. Sometimes the voltage remains constant to within 0.2 percent for one-half minute or so.

The generator is especially suitable for the investigation of nuclear reactions in which it is desirable to know the homogeneity in energy at a given energy to within limits of a few tenths of a percent. It is possible to vary the voltage of the generator from below 1 Mv up to 3.7 Mv and at different voltages within these limits to obtain focused ions which are homogeneous in energy to within 0.2 percent.

The apparatus is being used for accurate measurements of the thresholds of several light elements for emission of neutrons under proton bombardment. This work is now being completed and will be published soon in another paper. As an indication of the steadiness of the apparatus, Fig. 9 shows the gamma-ray resonances from a thin tantalum fluoride target with H_2^+ and H_3^+ ions and also the yield of neutrons obtained on proton bombardment of beryllium. The threshold value, 2.01 Mev,[22] is obtained by linear interpolation between the two fluorine resonance peaks. Although the fluorine resonance peaks seem narrower than the widths previously reported by Herb, we do not feel entirely sure of this until it is checked again. Critical discussion of this threshold value and others obtained on proton bombardment of lithium, boron, and carbon will be presented later.

We wish to express our appreciation for the cooperation and assistance given to this work by many members of the staff of the Westinghouse Research Laboratories, and in particular to Dr. L. W. Chubb, Director, and Drs. E. U. Condon and J. Slepian, Associate Directors of the Laboratories. The technical assistance of Mr. J. W. W. Ow in the drafting work connected with the generator has been an important contribution to its successful construction and operation.

[22] This value, given by a sample run, is not to be taken as our final result. This generating voltmeter scale could be read only to ½ or ¼ percent. Hence the error in this comparison is approximately one percent.

Orientation of Liquid Crystals by Heat Conduction

G. W. STEWART, D. O. HOLLAND AND L. M. REYNOLDS
State University of Iowa, Iowa City, Iowa

(Received April 18, 1940)

This is a new phenomenon in heat conduction in which the "liquid crystals" of para-azoxyanisol acquire a preferred orientation under the action of heat conduction in the liquid. A temperature gradient of but 1° or 2°C per cm, at a temperature of approximately 125°C, is sufficient to give a marked effect. The orientation is indicated by the variation in intensity in the x-ray diffraction halo. Both the effect and its magnitude are rather surprising, and it is anticipated that the explanation may rest in the dominance of acoustic waves of inertia and viscosity in heat conduction in liquids, as described by Lucas.

IN a comparison[1] of the x-ray diffraction intensity distributions with para-azoxyanisol in the liquid crystalline and isotropic states, the first author found a new conduction of heat phenomenon. A temperature gradient of 1° or 2°C per cm, the temperature decreasing downward, produced a preferred horizontal orientation of the elongated bundles or swarms of molecules. The direction of "orientation" is taken to be that of the longest axis of a swarm, the axis possessing the greatest induced magnetic moment. The direction of preferred orientation just mentioned was perpendicular to that produced by vertical convection currents.

This new heat conduction effect is somewhat surprising, for in view of the temperature, approximately 400°K, any kind of anticipated effect produced by a gradient a degree or two per cm would be rather small. Herewith is presented briefly the concordant results of three different experimental tests of the phenomenon, with a suggestion of the possible causes of the orientation effect.

EXPERIMENTAL RESULTS

I. The first experiments were those to which reference has already been made. A very thin-walled glass cylindrical tube 1.0 cm in diameter and 9.0 cm in length was surrounded by a loosely-fitting paper jacket and placed in an oven having an internal diameter of 7.3 cm and height of 16.0 cm. This jacket prevented convection currents in the air immediately surrounding the tube. Even the introduction of an air circulating fan into the oven did not produce any alterations in the temperature gradient at the tube as indicated by two thermocouples spaced 1.8 cm apart vertically just outside. A number of tests with different temperature gradients were made, and the x-ray intensity results (obtained by an ionization chamber) and the gradients plotted. These showed that unquestionably any increase in temperature gradient, temperatures decreasing downward, affected the intensity as if by an increase in horizontal preferred orientation. In these experiments the angular diffraction of x-rays in one plane only could be measured.

II. The second set of experiments were made by Donald O. Holland. An oven was constructed so as to provide the passage of a small parallel pencil of x-rays and the diffraction halo was produced on a photographic film. A vertical, thin-walled glass tube was used as before, but now an oven similar to that of Fig. 1 (which was actually used in the third experiment) was constructed. The ends of the tube were surrounded by brass blocks to insure their temperatures as measured by external thermocouples and the tube was surrounded by a brass cylinder to assist in securing a temperature gradient with horizontal isothermal levels. With this type of apparatus the halos completely corroborated the experiments recorded in "I" above. At the nearest attainable uniform temperature throughout, there always remained a slight convection as evidenced by the asymmetry of the circular halo, the alteration in density on the film showing a small preferred vertical orientation of the swarms. With increasing temperature gradient, tempera-

[1] G. W. Stewart, J. Chem. Phys. **4**, 231–236 (1936).

ture higher at the top of the tube, the asymmetry in the halo at first disappeared and then appeared again, but as if the halo were rotated through 90°. This indicated the disappearance of one preferred swarm orientation (vertical) and the appearance of another (horizontal). At each selected temperature gradient it was necessary to hold the temperatures constant for several hours to insure a steady condition. A sample of the nature of the change in the diffraction ring with increasing temperature gradient is indicated by the later photographs of Reynolds in Fig. 2.

These experiments were followed by others with the tube in a horizontal position. For a temperature gradient along the tube in either direction, convection currents always existed. Nevertheless the heat conduction phenomenon was in evidence and all the results were interpretable by the combined convection and temperature gradient effects.

III. The third series of experiments was by Leon M. Reynolds. At first an oven was tried where the sample tube was not so completely surrounded by copper blocks at its ends. In this oven, a uniform temperature gradient and strictly horizontal isothermal levels were not successfully secured, convection currents persisted, and the preferred orientation remained dominantly vertical. The conduction of heat phenomenon did not appear. But when the oven in Fig. 1 was substituted, results similar to those of Holland at once appeared. This third set of experiments in which was used the best oven of the three, confirmed the reality of the heat conduction phenomenon and also showed how carefully convection must be reduced if the new phenomenon is to be brought into evidence.

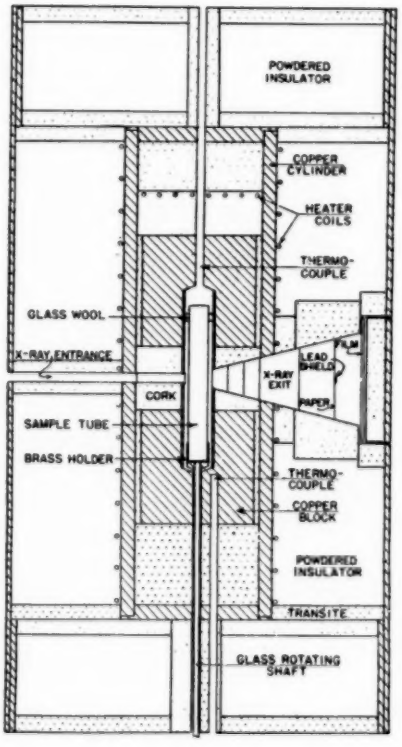

FIG. 1. Oven used by Reynolds in the third group of experiments. Cross section parallel to x-ray path.

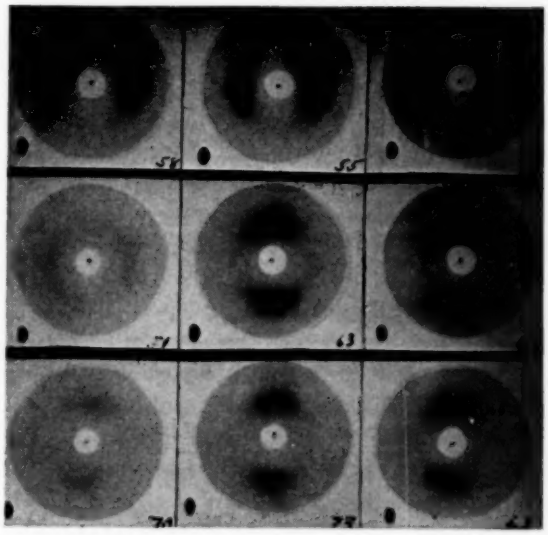

FIG. 2. Diffraction halos, x-ray beam horizontal, photographic film vertical. Sample, para-azoxyanisol at 119° to 130°. Temperature gradients are in degrees C/cm, reading from left to right, top line first, 0°, 0.05°, 0.13°, 0.27°, 0.32°, 0.65°, 0.83°, 1.10°, 1.46°.

Typical results of Reynolds and Holland are shown in Fig. 3. By photometric measurement the ratio of scattered x-ray intensities at the two points of each halo may be obtained. With I_h as the intensity produced by horizontal orientation of the swarms and I_v by vertical orientation, the ratio I_v/I_h is plotted for the two experimenters. If I_v only is plotted, a curve of a similar general shape is obtained but, by using the ratio, the error introduced by variation in development of the film is eliminated.

Reynolds determined the effect of rotation of the sample upon the preferred orientation of the swarms. This is shown in Fig. 4.

Discussion

In Fig. 3 the general course of the curves is similar to the results obtained in x-ray diffraction experiments with a magnetic field.[2] In each case the effect is caused by the orientation of the swarms or bundles of molecules. In Fig. 3, the greater orientation in the Reynolds' experiments is accounted for by the improvement in the horizontality of the isothermal levels. The results of Fig. 4 also confirm the interpretation of the experiments. Rotation of the containing cylinder about a vertical axis would, through irregularities in the tube and in the motion, coupled with viscosity, cause a shear in the horizontal plane perpendicular to the radius of the cylinder. This would produce an effect similar to a horizontal circular convection current, namely, that of a preferred orientation of the bundles in the direction of the velocity stream. Hence one would expect the rotation of the tube to give a preferred orientation in the horizontal plane, or to increase the effect of the temperature gradient. This is shown to be the case of Fig. 4.

Thus all the experiments are consistent with the view that there is a new conduction of heat phenomenon in addition to the well-known magnetic and convection effects in the liquid crystal form of para-azoxyanisol. Although the effect of such a small heat conduction is surprising, yet

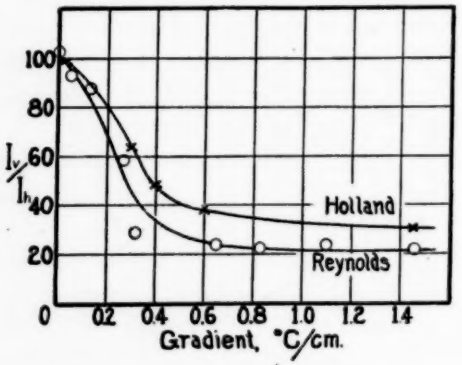

Fig. 3. Alteration in orientation with temperature gradient, temperature decreasing downwards. Circles; Reynolds, corresponding to the nine photographs in Fig. 2. Crosses; Holland. Scale for ordinates modified to give value 100 at zero gradient.

[2] G. W. Stewart, Phys. Rev. **38**, 931 (1931).

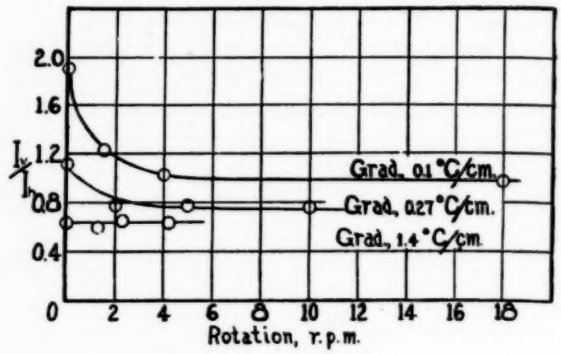

Fig. 4. Rotation increases the effect of heat conduction.

one must remember that the orientation of these bundles in a magnetic field is relatively easy. A field of 2200 gauss will give practically complete orientation and 1300 gauss but a few percent less. The swarms or bundles are relatively large,[3] containing approximately one million molecules, the size probably having a considerable variation. This accounts for the relative ease of orientation at any ordinary temperature. Orientation by convection is probably produced by the shearing effect of a velocity gradient perpendicular to the convection velocity. Orientation by conduction might be caused by radiation pressure of the acoustic waves. But it seems more simple in accord with the experiments and calculations of Lucas,[4] to regard the important transverse waves of inertia and viscosity in the fluid as effective in producing by their displacements a torque on the bundles. This may cause a preferable orientation in the plane containing these displacements and perpendicular to the direction of flow of heat energy.

At the moment, the possible importance of the new heat conduction effect would seem to be as a tool in the study of liquid crystal bundles or swarms, of the cause of the exerted torque whether momentum or transverse displacement velocity gradient, and of the acoustic waves, both longitudinal and transverse, which are responsible for heat conduction in liquids.

[3] Evidence also in Ornstein and Kast, Faraday Society Discussion, 1933, p. 931.

[4] R. Lucas, J. de phys. et rad. **7**, 40 (1937).

LETTERS TO THE EDITOR

Prompt publication of brief reports of important discoveries in physics may be secured by addressing them to this department. Closing dates for this department are, for the first issue of the month, the eighteenth of the preceding month, for the second issue, the third of the month. Because of the late closing dates for the section no proof can be shown to authors. The Board of Editors does not hold itself responsible for the opinions expressed by the correspondents.

Communications should not in general exceed 600 words in length.

Radioactivity Produced by Bombarding Thallium

Previously published data on the activities produced in thallium show several periods: 4 ± 0.5,[1] 4.1,[2] and 5[3] min. produced by slow and fast neutrons, 97 min. by slow neutrons[1,4] and 50 min. by fast neutrons.[3] The similarity between the short period and the half-life, 4.76 min., of the naturally radioactive isotope of Tl, actinium C″ (Tl^{207}) led to a careful comparison of the two activities, since the latter could be made from Tl only by the unknown (D, β^+) reaction.

The thallium used for bombardment was purified by the following successive processes: recrystallization of thallous nitrate and sulfate, oxidation to thallic chloride, extraction with ether, conversion to thallous sulfate, electrolytic deposition as thallium metal. The metal was fused in a current of hydrogen and rolled into a thin sheet.

The activity obtained by short bombardment of the Tl, with slow and fast neutrons and deuterons, had an average half-life of 4.23 ± 0.03 min. Actinium C″ was separated chemically from the active deposit of actinium, and the average value, 4.77 ± 0.05 min. was obtained under the same conditions of measurement with the Lauritsen electroscope. The difference between the two values is much beyond the experimental error, leaving no doubt that they are not identical.

In order to make certain the chemical nature of the 4.23-min. period, the very active material from the deuteron bombardments was separated chemically, using the insolubility of thallous iodide, chromate and chloride, the solubility of thallic chloride in ether and of thallous sulfide in dilute acid. In all cases the activity followed the reactions of thallium.

The activity is produced by neutrons from the Be+D and Li+D reactions, both when wrapped in cadmium and when surrounded by 10 cm of paraffin. It is thus induced by both slow and fast neutrons and this in intensities of the same order of magnitude. Since the two stable isotopes of Tl are present in the amounts: 203 — 29.5 percent, 205 — 70.5 percent, the evidence supports the conclusion of Heyn,[2] that the isotope is Tl^{204}, produced from Tl^{203} by neutron capture and from Tl^{205} by the $(n, 2n)$ reaction.

The range of the negative β-particles in Al is 0.75 ± 0.05 g/cm², which gives 1.6 ± 0.1 Mev as the energy (using the relation $R=0.526E-0.094$). Sargent[5] gives the similar value 0.68 g/cm² for the range of the β-rays from AcC″, from which the energy 1.47 Mev follows. The γ-ray or bremstrahlung background of the Tl^{204} is about 0.01 percent of the total activity.

Intense slow neutron bombardments, lasting up to four hours, have not shown any period of the order of the 97-min. half-life. However, 1 to 2-hour deuteron bombardments produce a weak activity, about five times the background of the Geiger-Mueller counter used, which has been chemically identified as thallium. It shows a decay in 2½ months corresponding to a half-life of 1 to 2 years. A similar decay is shown by an activity produced by 4-hour slow neutron bombardments, with intensities about equal to the background. This seems to indicate that the activity is due to Tl^{206}, produced from Tl^{205} by (D, p) and (n, γ) reactions.

Bombardment of thallium by deuterons also produced a strong activity with a period of 52 ± 1 hours which has been chemically identified as lead by several reactions: the precipitation of lead sulfide, chromate and sulfate, and the solution of the latter two in acetate and alkali. A fractional precipitation of lead sulfate was carried out by acidifying a solution of lead sulfate in sodium acetate. The activity per milligram of the three fractions obtained was the same within the experimental error of about five percent.

The absorption curve of this lead activity in Al shows a β-activity with a range of 0.11 ± 0.01 g/cm² indicating an energy of 500 kev, accompanied by a γ-ray activity equal in intensity to six percent of the total. The energy of this has not yet been determined.

Pb^{204} and Pb^{206} are the two possible isotopes of lead which could be produced from Tl^{203} and Tl^{205} by the usual (D, n) reaction. Both of these are, however, stable. The results would suggest that the activity is due to a metastable state in one of them which emits a γ-ray that is internally converted into the observed β-rays.

We wish to thank Professor J. M. Cork and other members of the Physics Department for their interest and help in making the bombardments with the cyclotron. This work has been made possible by a grant from the Horace H. Rackham Trust Fund.

KASIMIR FAJANS
ADOLF F. VOIGT

Chemistry Department,
University of Michigan,
Ann Arbor, Michigan,
July 2, 1940.

[1] P. Preiswerk and H. von Halban, Comptes rendus 201, 722 (1935).
[2] F. A. Heyn, Nature 139, 842 (1937).
[3] M. L. Pool, J. M. Cork and R. L. Thornton, Phys. Rev. 52, 239 (1937).
[4] J. C. McLennan, L. G. Grimmett and J. Read, Nature 135, 505 (1935).
[5] B. W. Sargent, Can. J. Research 17A, 82–102 (1939).

The Seven-Day Uranium Activity

The production of radioactive U^{237} by fast neutron irradiation of uranium has been reported recently by Nishina *et al.*[1] The same activity has been observed independently here. It was first found in samples of uranium placed immediately behind a beryllium target bombarded by 16-Mev deuterons. These showed an activity of half-life 7.0 ± 0.2 days which could not be separated chemically from uranium. If the purification was done immediately after activation, the 23-minute uranium and its 2.3-day daughter[2] also appeared, but if the purification was done after a few hours, only the 7-day period was seen. The ratio after a short bombardment of the initial intensities of the 7-day activity to the 2.3-day activity was about $\frac{1}{4}$.

Since the 7-day period was not seen in earlier experiments of the author in which uranium layers thin enough to allow the fission products to recoil out were exposed to neutrons from a beryllium target bombarded by 8-Mev deuterons, it seemed likely that it is produced by a fast neutron reaction. In confirmation of this it was found that the intensity (with 16-Mev H^2 on Be) is greatly reduced if the sample is surrounded with paraffin during bombardment and is not affected by cadmium shields. It was also found possible to observe the 7-day period in a thin uranium layer placed immediately behind the target, and an analysis of the resulting decay curve gave the same ratio of intensities (7-day to 2.3-day) as the chemically separated fractions from a bulk sample.

The 7-day beta-particles have an absorption curve characteristic of a simple continuous distribution with an end point at 0.26 Mev. There are also soft gamma-rays with at least two components, but no annihilation radiation, in agreement with the observation of Nishina *et al.*[1] that the electrons are negative. Dr. A. C. Helmholz, using a magnetic spectrograph, could find no internal conversion lines. Since this excludes the possibility of K capture, the daughter product must be element 93. An attempt to find such an activity was made. An 80-microcurie sample of 7-day uranium was allowed to decay for 26 days, and then element 93 was extracted from it, by the method of fluoride precipitation in reducing and oxidizing media,[2] with cerium carrier. The resulting product showed no measurable activity of either beta- or alpha-rays, so the period of this substance must be very long. (It can hardly be very short, since the active uranium has no high energy beta-particles and no alpha-particles of range greater than those from U_{II}.)

I wish to express my gratitude to the Rockefeller Foundation and the Research Corporation, whose financial support made this work possible.

EDWIN MCMILLAN

Radiation Laboratory,
Department of Physics,
University of California,
Berkeley, California,
June 28, 1940.

[1] Y. Nishina, T. Yasaki, H. Ezoe, K. Kimura and M. Ikawa, Phys. Rev. **57**, 1182 (1940).
[2] E. McMillan and P. H. Abelson, Phys. Rev. **57**, 1185 (1940).

The Energy Released in the Reaction $Li^6(p,\alpha)He^3$ and the Mass of He^3

Two groups of workers in this laboratory have completed determinations of the energy released in the reaction $Li^6(p,\alpha)He^3$ using different variable-pressure absorption cells calibrated in different ways. The variable-pressure cells used were constructed with two compartments, the forward one for retarding the alpha-particles, and the rear one for collecting the ionization produced by them at the end of their range. A linear amplifier was used to detect the ionization pulses. The region from which ions were collected was defined by a perforated screen transverse to the axis of the cell, but the ionization compartment was always at the same pressure as the retarding compartment. This introduces no complications into the interpretation of the results provided that the alpha-particles, at all pressures used, come to the end of their range in the gas of the ionization compartment. Thus there was only one window for the particles to traverse, placed over a perforated screen at the entrance to the retarding compartment.

In one experiment, such a cell was placed to collect particles from thin targets of lithium and beryllium, bombarded with 370-kev protons. The range difference between the alpha-particles from $Be^9(p,\alpha)Li^6$ and $Li^6(p,\alpha)He^3$ was found to be 1.83 mm. Using the precisely known energy of the beryllium particles, from our electrostatic analyzer measurements, and the slope of the Cornell (1938) range-energy curve in this region, we find that Q for $Li^6(p,\alpha)He^3$ is 3.95 ± 0.06 Mev.

The other determination was an outgrowth of experiments on the range-energy curve of alpha-particles in the energy region 0.8–2.0 Mev. A strong source of polonium was placed near the entrance of our electrostatic analyzer, and absorption screens introduced between it and the analyzer to absorb all but the last 0.5–1.0 cm of range. A small fraction of the resulting particles, homogeneous in energy, was deflected through the electrostatic analyzer and allowed to enter an absorption cell of the previously described type. By varying the deflecting voltage, the cut-off pressures of the cell for alpha-particles from 1.09 to 1.73 Mev have been determined. This same cell, with all its auxiliary apparatus, was then placed opposite a thin lithium target and the cut-off for the alpha-particles from $Li^6(p,\alpha)He^3$ determined. The result indicated an energy release of 3.94 ± 0.05 Mev.

We have used our previous values for reaction energies in computing the mass of He^3 which is included in the following list, based on 1.00813 ± 0.00002, 2.01473 ± 2, and 4.00386 ± 7 for the masses of H, D, and He^4, respectively.

He^3	3.01685 ± 10	Be^8	8.00765 ± 15
Li^6	6.01684 ± 11	Be^9	9.01484 ± 13
Li^7	7.01814 ± 11		

The previously accepted value for the energy release in the reaction $Li^6(p,\alpha)He^3$ was 3.72 ± 0.08 Mev.

SAMUEL K. ALLISON
LEONARD C. MILLER
GILBERT J. PERLOW
LESTER S. SKAGGS
NICHOLAS M. SMITH, JR.

University of Chicago,
Chicago, Illinois,
June 19, 1940.

The Theory of the Diffuse Scattering of X-Rays from Crystals

We wish to discuss a recent paper by Zachariasen[1] on the theory of the diffuse scattering of x-rays by crystals. In this discussion we shall use the symbols and terms of Zachariasen's paper and we shall refer to an equation in his paper by placing a Z in front of the equation number, thus (Z5).

Following Zachariasen, we shall consider the unmodified (non-Compton) part of the scattered radiation from a small crystal of linear dimensions of the order 10^{-4} cm. Absorption effects in such a crystal may be neglected. We prefer to distinguish between the cases $l=l'$ and $l\neq l'$ in (Z5), (Z6) and (Z7) and we write the result in the form

$$\begin{aligned} J &= Sf^2\{N+e^{-2M}\Sigma'_l\Sigma'_{l'}\exp[2\pi i(\mathbf{k}-\mathbf{k}_0)\cdot\mathbf{r}_{ll'}]\exp P_{ll'} \\ &\leq Sf^2\{N+e^{-2M}\Sigma'_l\Sigma'_{l'}\exp[2\pi i(\mathbf{k}-\mathbf{k}_0)\cdot\mathbf{r}_{ll'}] \\ &\quad +e^{-2M}\Sigma'_l\Sigma'_{l'}P_{ll'}\exp[2\pi i(\mathbf{k}-\mathbf{k}_0)\cdot\mathbf{r}_{ll'}]\}, \end{aligned} \tag{A}$$

where $\Sigma'\Sigma'$ denotes omission of those terms for which $l=l'$. Equation (A) holds both at and away from a Laue spot. It may be simplified to

$$\begin{aligned} J &= J_0e^{-2M}+Sf^2\{N(1-e^{-2M}) \\ &\quad +e^{-2M}\Sigma'_l\Sigma'_{l'}P_{ll'}\exp[2\pi i(\mathbf{k}-\mathbf{k}_0)\cdot\mathbf{r}_{ll'}]\} \end{aligned} \tag{B}$$

where

$$J_0=Sf^2\Pi_i\frac{\sin^2[N_i\pi(\mathbf{k}-\mathbf{k}_0)\cdot\mathbf{a}_i]}{\sin^2[\pi(\mathbf{k}-\mathbf{k}_0)\cdot\mathbf{a}_i]}. \tag{C}$$

It is convenient to write (B) as

$$J=J_1+J_2 \tag{D}$$

as in (Z8). Away from the maxima of J_1, J_2 is the only term of importance, and we shall write it in the form

$$J_2=J_D+J_{\mathrm{FWZ}} \tag{E}$$

with

$$J_D=Sf^2N(1-e^{-2M}), \tag{F}$$

the Debye part, and

$$J_{\mathrm{FWZ}}=Sf^2e^{-2M}\Sigma'_l\Sigma'_{l'}P_{ll'}\exp[2\pi i(\mathbf{k}-\mathbf{k}_0)\cdot\mathbf{r}_{ll'}], \tag{G}$$

the Faxen-Waller-Zachariasen part. For an isotropic crystal at a given temperature the Debye part is a function of $(\sin\phi/2)/\lambda$ alone, while the FWZ part is a function not only of $(\sin\phi/2)/\lambda$ but also of the orientation of the crystal relative to the primary rays. The FWZ part may be either positive or negative. Now it follows from (Z26) and (Z27) that

$$\langle J_{\mathrm{FWZ}}\rangle_{\mathrm{Av}}=0 \tag{H}$$

upon averaging over a sufficient range of orientations of the crystal. Thus unless precaution be taken to use a rather perfect crystal, *what one actually measures is the Debye diffuse scattering*. This is suggested by Zachariasen[1] but not, we believe, with the proper emphasis.

Further, in all of the work of Jauncey and his collaborators the technique of Jauncey and May[2] or the Jauncey-Bruce[3] modification of this technique has been used. The purpose of this technique has been to avoid any scattered radiation which is *orientation-sensitive*. As we now know, this technique would not only avoid Laue spots but in addition the peaks of the FWZ radiation which is also *orientation-sensitive*. In view of this, together with the fact that the crystals used were imperfect* we believe that Jauncey and his collaborators have come very close to determining the Debye part of the diffuse scattering.

In the theory as developed by Jauncey and Harvey[4-7] the simplifying assumption was made that the probability of a set of displacements of the atoms of a crystal was equal to the product of the probabilities of the separate displacements. This is only true if the displacements are independent of each other. In this case $P_{ll'}=0$ and the Faxen-Waller-Zachariasen part of the diffuse scattering becomes zero. However, as Zachariasen points out, this simplifying assumption is not justified for any real crystal and so we have the Faxen-Waller-Zachariasen part as well as the Debye part of the diffuse scattering.

G. E. M. Jauncey

Washington University,
St. Louis, Missouri,

G. G. Harvey

Massachusetts Institute of Technology,
Cambridge, Massachusetts,
June 24, 1940.

[1] W. H. Zachariasen, Phys. Rev. **57**, 597 (1940).
[2] G. E. M. Jauncey and H. L. May, Phys. Rev. **23**, 128 (1924); G. E. M. Jauncey and W. D. Claus, Phys. Rev. **46**, 941 (1934).
[3] G. E. M. Jauncey and W. A. Bruce, Phys. Rev. **50**, 413 (1936).
* Had imperfect crystals not been used this technique would give values *less* than the Debye formula.
[4] G. E. M. Jauncey, Phys. Rev. **37**, 1193 (1931).
[5] G. E. M. Jauncey and G. G. Harvey, Phys. Rev. **37**, 1203 (1931).
[6] G. G. Harvey, Phys. Rev. **56**, 242 (1939).
[7] G. E. M. Jauncey, Phys. Rev. **56**, 644 (1939).

The Latitude Effect in Cosmic Rays at Far Southern Latitudes

Two meters for measuring the total cosmic-ray intensity from all directions, namely a single Geiger counter[1] and an electroscope of the type described by Millikan and Neher,[2] were operated on board the *U.S.S. North Star* during a recent trip through the Antarctic regions. The electroscope was operated on the Philadelphia-Panama-Dunedin, New Zealand-Little America run, while the counter set was operated on that from Dunedin to Little America-Valparaiso-Palmer Land-Valparaiso-Panama. The electroscope was inside a 10-cm thick lead shield, and the single Geiger counter was inside 7.5 cm of lead. The counter counts, approximately 190,000 per day, were scaled down with a conventional thyratron scale-of-four circuit[3] and then recorded on a dial recorder. The daily mean counting rate and the daily mean electroscope reading were corrected for changes in atmospheric pressure by applying the same barometer coefficient to each. The daily mean counting rate was then multiplied by an arbitrary constant to enable it to be shown on the same scale as the electroscope ionization. The corrected readings were then plotted against geomagnetic latitude and are presented in Fig. 1.

It will be observed that the cosmic-ray intensity shows the familiar "knee" at approximately geomagnetic latitude 38° south. Between the knee and 77° south the intensity rises by 3 ± 0.3 percent, this rise being shown by both the counter and the electroscope. At latitudes nearer the equator the curves obtained by the two meters are not

exactly similar, since the above routes carried the two instruments through quite different longitudes and hence through different horizontal magnetic intensities at corresponding geomagnetic latitudes. The electroscope readings, taken at longitudes further west than the counter observations, are lower at the equator. The application of an external temperature coefficient[4] of -0.15 percent per degree C to the data will cause the intensity curve to become horizontal between the knee and 77° south, the highest geomagnetic latitude reached. This may be

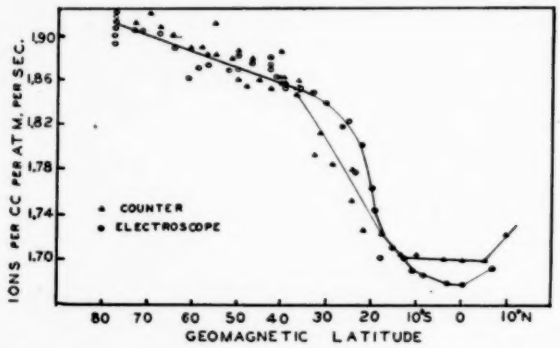

FIG. 1. Cosmic-ray intensities as measured by electroscope and counter, in southern latitudes. The differences between the curves in middle latitudes is due to longitude effect. Each point is a daily mean. The electroscope remained on board the ship at 77°S for six days before being put ashore, and the normal daily fluctuations may be judged from the corresponding six points. The data are not corrected for external temperature.

compared with a coefficient of -0.18 found by Compton.[4] These observations were made during January and March, the summer months in the Southern Hemisphere; at this season it is to be expected, from the observations of Hess,[5] that the temperature coefficient will be at a minimum.

It will be noted that the counter and electroscope measurements show the same increase with latitude above the knee. Since the counter counts the total number of rays, while the electroscope measures the total ionization, it is evident that the average specific ionization per ray at sea level remains constant with change in latitude above the knee. From this it can be shown that the ratio of electrons to mesotrons is constant.

The results will be discussed in detail in a forthcoming issue of the *Journal of the Franklin Institute*.

We wish to acknowledge the support of the Carnegie Institution of Washington in connection with the use of the Millikan-Neher meters, as well as film for these donated by the Eastman Kodak Company and batteries presented by the Burgess Battery Company.

E. T. CLARKE
S. A. KORFF

U. S. Antarctic Service and Bartol Research Foundation
The Franklin Institute,
Swarthmore, Pennsylvania
June 24, 1940.

[1] E. T. Clarke and S. A. Korff, this issue, p. 201A.
[2] R. A. Millikan and H. V. Neher, Phys. Rev. **50**, 15 (1936).
[3] C. E. Wynn-Williams, Proc. Roy. Soc. **A136**, 312 (1932).
[4] A. H. Compton and R. N. Turner, Phys. Rev. **52**, 799 (1937).
[5] V. F. Hess, Phys. Rev. **57**, 781 (1940).

The Nuclear Magnetic Moment of C^{13} *

Professor H. C. Urey's generosity has made available KCN and NaCN in which the abundance of C^{13} is about 22 percent. Since these compounds are suitable for molecular-beam magnetic-resonance experiments, they have been used to measure the magnitude of the gyromagnetic ratio[1] and to determine the sign[2] of the nuclear magnetic moment of C^{13}. In addition to minima due to N^{14} and K^{39}, there was observed in curves taken with the KCN beams a new resonance minimum, the ν/H ratio for which was constant to better than 0.3 percent for frequencies ranging from 0.7 megacycle per second to 4.8 megacycles per second. The corresponding g value was 1.401 ± 0.004. This minimum was not observed in curves taken with beams of KCN containing only the normal abundance of C^{13}. In curves taken with the NaCN beams it was difficult to see the new resonance point because of the broadness of the Na^{23} resonance curve and the proximity of the Na^{23} minimum to the new minimum. (The g value for Na^{23} is 1.476.) In these NaCN curves, nevertheless, at field values about 4 percent higher than those for the Na^{23} minimum there was observed a slight asymmetry which was not found in curves taken with a beam of ordinary NaCN. It was possible that this asymmetry was like that described by Millman[2] but when the fields were reversed, it remained on the high field side of the Na^{23} minimum and thus could not be attributed to imperfect conditions in the oscillating magnetic field. The new minimum has therefore been assigned to C^{13}. The g value given above was calculated from the minimum observed in curves taken with the KCN beams and is referred to the published[3] g value of 2.167 for Li^7 which has been used as a standard in these laboratories. The sign of the nuclear magnetic moment, as determined by Millman's method of field reversal,[2] is positive.

The value of the nuclear magnetic moment can be determined from measurements of the g value only if the spin is known. There are two theoretical predictions for the spin of C^{13}: the value $\frac{1}{2}$ derived from the Hartree model[4] and the value $\frac{3}{2}$ from the alpha-particle model.[5] C^{13} can be considered as C^{12} with an added neutron. Therefore, with the rotational angular momentum, K, equal to 1, a spin of $\frac{1}{2}$ makes a positive nuclear magnetic moment possible. If, however, the spin is taken as $\frac{3}{2}$, with K still 1, the negative magnetic moment of the extra neutron is added algebraically to the smaller moment due to the rotational angular momentum and the resultant nuclear magnetic moment is always negative. This negative sign is in direct contradiction to the positive sign which we have determined experimentally. Furthermore, D. R. Inglis has pointed out in a discussion of spin-orbit coupling in light nuclei[6] that a rough calculation of the splittings due to the Larmor and the Thomas precessions indicates that the spin-orbit coupling is negative, a conclusion which is in agreement with the predictions of the Hartree model.[4] We feel, therefore, that the spin of C^{13} is much more likely to be $\frac{1}{2}$ than $\frac{3}{2}$. The corresponding nuclear magnetic moment obtained from our measured g value is 0.700 ± 0.002 nuclear magneton. It may be objected that the

only experimentally determined value for the spin of C^{13} is $\frac{1}{2}$, which Townes and Smythe[7] obtained by investigating the alternating intensities of lines in band spectra. Examination of their results will show, however, that the value $\frac{3}{2}$ is their choice as the best of three possibilities: $\frac{1}{2}$, $\frac{3}{2}$ and $\frac{5}{2}$. The value $\frac{1}{2}$ is by no means ruled out. The disagreement between the value 0.700 nuclear magneton which we suggest for the nuclear magnetic moment of C^{13} and that of 1.05 nuclear magnetons predicted by the Hartree model[4] is about 50 percent. This is no more serious than has been the case with more than one nuclear constant.

I wish to thank Professor I. I. Rabi for suggesting this problem, and for his helpful discussions and criticism. It is a pleasure to acknowledge the generous way in which Dr. S. Millman and Dr. P. Kusch have given both valuable suggestions and time to aid the course of these experiments.

ROBERT H. HAY

Department of Physics,
Columbia University,
New York, New York,
June 27, 1940.

* Publication assisted by the Ernest Kempton Adams Fund for Physical Research of Columbia University.

[1] Rabi, Zacharias, Millman and Kusch, Phys. Rev. **53**, 318 (1938).
[2] S. Millman, Phys. Rev. **55**, 628 (1939).
[3] Rabi, Millman, Kusch and Zacharias, Phys. Rev. **55**, 526 (1939).
[4] M. E. Rose and H. A. Bethe, Phys. Rev. **51**, 205 (1937).
[5] R. G. Sachs, Phys. Rev. **55**, 825 (1939).
[6] D. R. Inglis, Phys. Rev. **56**, 1175 (1939).
[7] C. H. Townes and W. R. Smythe, Phys. Rev. **56**, 1210 (1939).

Structure of the Lower Excited Levels of the Br^{80} Nucleus

In studying the radiations emitted by the isomeric radio-bromine we established that there are many soft γ-rays with an energy of several tens of kev.[1]

Measuring the absorption of γ-rays in Al and using the method of selective filters we showed that the energy of these γ-rays is undoubtedly less than 48 kev, i.e., they are not connected with the conversion transition which had been investigated previously.[2]

The radio-bromine was obtained from the cyclotron of the Radium Institute of the Academy of Sciences of the USSR. The electrons emitted by the source were deflected by a magnetic field, so that the electromagnetic radiation only could penetrate into the G-M counter which was filled with a mixture of krypton (95 percent) and xenon (5 percent). The μ/ρ value (in Al) for the detected γ-rays was found to be 0.68, which corresponds to $E_\gamma \backsimeq 37$ kev.

The method of selective filters showed that the energy of these γ-rays lies between 35.9 and 37.4 kev. The results of these measurements are given in Table I.

The decay period of the 37-kev γ-radiation is found to be 4.5 hours. The following scheme would fit all the experimental results. The total excitation energy of the metastable Br nucleus is 85 kev. From this level there are transitions to a lower excited level which differs from the upper level by 48 kev in energy. This transition proceeds, as follows from our preliminary experiments, by internal conversion only. From this lower excited state, the energy of which exceeds by some 37 kev that of the ground state of Br^{80}, a γ-transition takes place, only partially associated with internal conversion. The conversion electrons corresponding to this second transition have been observed by Valley and McCreary.[3]

TABLE I. *Comparison of absorption coefficients* (μ/ρ).

Filter	K-limit (kev)	Theoretical value of μ/ρ (according to Johnson) for $E\gamma$ = 48 kev	38 kev	37 kev	35 kev	μ/ρ (exp.)
Nd	43.6	21.7		6.9		8±1
Ba	37.4		32.1	5.6		5±1
Cs	35.9			33.7	6.2	33±2

Using an absorbed layer of radio-bromine on silver, as a radioactive source, and the krypton-filled counter with a Cellophane window 100μ thick, and also appropriate filters, we determined the ratio of the number of x-ray quanta registered by the counter, to the number of registered soft γ-quanta. This ratio was found to be 4.1 ± 0.3.

Using this value and taking into account the relative counting coefficient for x-ray quanta with $E = 13.5$ kev and γ-quanta with $E = 37$ kev in our counter, and the fluorescence yield for the bromine atom, we estimated the value of the internal conversion coefficient α for the lower transition on the assumption that it is equal to 1 for the upper transition. The former is found to be equal to 0.5.

A theoretical calculation with the formulas given by Hebb and Uhlenbeck and by Dancoff and Morrison shows that such a value of α may be associated only with a dipole electric transition. Hence for the lower (37 kev) transition $\Delta I = 1$.

In conclusion we wish to thank Professor I. V. Kourtschatow for helpful discussions.

A. P. GRINBERG
L. I. ROUSSINOW

Physico-Technical Institute,
Leningrad, U. S. S. R.,
May 8, 1940.

[1] Roussinow and Yusephovitch. Report on the Conference on Nuclear Physics, November, 1939, Kharkov.
[2] Roussinow and Yusephovich. Comptes rendus Acad. Sci. URSS **24**, 129 (1939).
[3] G. E. Valley and R. L. McCreary, Phys. Rev. **56**, 863 (1939).

Regularities Among the Heavy Nuclei

In a recent paper on the missing heavy nuclei[1] I pointed out certain regularities that suggest that Rn, AcA, ThA, and RaA should all be beta-active as well as alpha-active. I was unaware that this conclusion had already been reached by Minder[2] by a similar argument. Just recently[3] Minder has published an account of experiments which give some evidence for the emission of beta-rays by RaA. The evidence for branching is not conclusive, however, since one cannot be sure that the observed electrons are true nuclear beta-rays. Minder's inability to detect the hypothetical $_{85}$Ekal^{218} by chemical means is not surprising in view of the work of Segrè, MacKenzie and Corson[4] on the properties of that element. Even with proper chemical procedure it will be extremely difficult to detect these atoms if my estimate of their half-life as ~0.1 sec. is correct within a factor of 100. If, however, branching does occur to the extent indicated by Minder's experiments and by those of Hulubei and Cauchois[5] in which they found x-ray lines of element 85, the fast alpha-particles

of $_{85}$Ekal^{218} should be detectable. Indeed, they should already have been found in the work on the range of alpha-particles of RaA. The alpha-particles might have escaped detection if the branching ratio is only 0.01 or so, as predicted.

Minder's unorthodox view[2] that Ra, ThX, AcX, RdTh and RdAc also emit some nuclear beta-rays can hardly be accepted without more evidence since it would involve a most extraordinary irregularity of the nuclear energy surfaces in the neighborhood of $Z=87$.

The basic assumption underlying my predictions of the radioactive properties of certain nuclei was that neighboring nuclei of even Z (or of odd Z) and of the same value of $y=A+50-3Z$ are likely to have similar radioactive properties. This is subject to the reservation that for every value of y the nuclei are beta-active above a certain value of Z and beta-stable below it. For $y=14$ and even Z's the dividing value of Z is 81, for lower values of y and even Z's it is above $Z=92$; for $y=12$ and odd Z's it is 82, for $y=10$ and odd Z's it is between 83 and 89. The validity of the assumption is strengthened by the recent discovery of two more nuclei which do have the properties which were thus predicted. McMillan and Abelson[6] have shown that $_{93}$EkaRe^{239} is beta-active, the half-life being the already known one of 2.3 days. Nishina and collaborators[7] have produced a 6.5-day beta-active U by the action of fast neutrons on U, and have naturally attributed it to U^{237}. In neither case could any activity of the disintegration products be detected so that it was concluded that the resulting $_{94}$EkaOs^{239} and $_{93}$EkaRe^{237} nuclei are alpha-active with long half-lives, as was predicted by the above method. The prediction is particularly sure for $_{94}$EkaOs^{239} for which $y=7$. All of the known nuclei of even Z having $y=9$ are beta-stable and it is even more likely that those having $y=7$ should be beta-stable. By the method outlined in reference (1) the half-life of $_{94}$EkaOs^{239} may be estimated to lie between that of Pa (3.2×10^4 yr.) and U^{235} (7.1×10^8 yr.) and somewhat closer, logarithmically, to the latter. For $_{93}$EkaRe^{237} one could not be entirely sure even though for it $y=8$ as for $_{91}$Pa^{231}, but if $_{93}$EkaRe^{237} is not beta-stable then there must either be no beta-stable isotope of EkaRe at all or $_{93}$EkaRe^{235}, isobaric with U^{235}, must be beta-stable. Both alternatives seem very unlikely. The experimental evidence concerning $_{93}$EkaRe^{237} is inconclusive, however, since McMillan and Abelson[6] have shown that the chemical properties of element 93 are different from those generally anticipated and assumed by Nishina *et al.*[7] in their endeavor to separate $_{93}$EkaRe^{237}.

I am indebted to Dr. E. Segrè for calling my attention to the work of Minder.

LOUIS A. TURNER

Palmer Physical Laboratory,
Princeton University,
Princeton, New Jersey,
June 27, 1940.

[1] L. A. Turner, Phys. Rev. **57**, 950 (1940).
[2] Minder, Helv. Phys. Acta **11**, 497 (1938).
[3] Minder, Helv. Phys. Acta **13**, 144 (1940).
[4] Segrè, MacKenzie and Corson, Phys. Rev. **57**, 1087 (1940).
[5] H. Hulubei and Y. Cauchois, Comptes rendus **209**, 39 (1939).
[6] E. McMillan and P. H. Abelson, Phys. Rev. **57**, 1185 (1940).
[7] Nishina, Yasaki, Ezoe, Kimura and Ikawa, Phys. Rev. **57**, 1182 (1940).

Initial Reignition Voltage Measurements

The voltage necessary to establish an arc in the reversed direction after arc failure increases rapidly with respect to time from an initial value. Usual measurements of this reignition voltage are made with alternating-current arcs,[1] but the time interval between arc failure and application of the voltage can only be reduced asymptotically to zero. This method also has the disadvantage that the current at which the arc fails varies, and cannot be controlled. A method has been devised to overcome these difficulties.

A direct-current arc was maintained between electrodes which could be connected instantaneously to a charged capacitor (350 μf). The capacitor was charged to various potentials of opposite sign to the arc voltage drop. As the capacitor potential is increased a value is reached at which it discharges rapidly across the arc space. This value of capacitor voltage represents the initial reignition voltage for a definite original arc current. Investigation with a cathode-ray oscillograph justified the method.

The reignition voltages measured were independent of arc supply voltage and the value of capacitance over a range of 1 to 350 μf. They were also nearly independent of arc length except for a slight maximum which was somewhat more pronounced at higher currents. However, when delay was introduced between arc failure and application of the reignition voltage, the usual sharp increase with decreasing electrode spacing was observed. Measurements of reignition voltage as a function of time gave a linear increase over the first 80 microseconds of 1.5 volts per microsecond for a 3-ampere, 3-mm Cu arc.

The striking variation of initial reignition voltage as the arc current was varied is shown in Fig. 1. At small currents the values are rather constant around 250 volts, but for most metals as the current is increased, the values decrease rather abruptly to a new nearly constant value. For some materials these values are but slightly higher than the arc voltage. The critical current seems to increase with the heat diffusivity of the electrode material. That this transition from a high to a low value may correspond to a change in the arc mechanism itself is also suggested by a transition in the arc voltage at corresponding values of

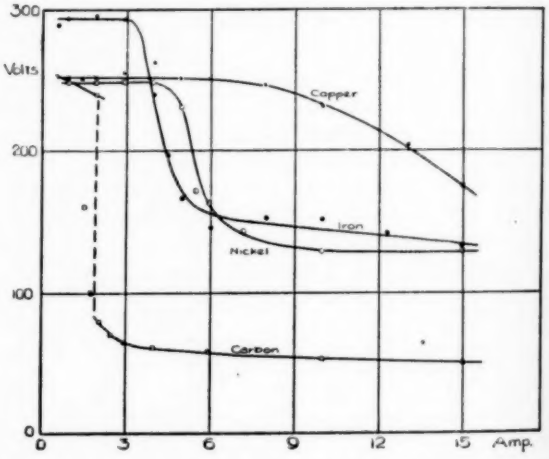

FIG. 1. Initial reignition voltage as a function of arc current.

current as reported by Cobine[2] for carbon. This has also been observed with a cathode-ray oscillograph for an arc fed with superposed alternating and direct current. Transitions in the reignition voltage have been observed for C, Co, Cr, Fe, Mn, Mo, Ni, W and Zn while Cu, Ag, and Al show only a single state over the range of current investigated (0.8–15 amp.).

MAX GARBUNY
LYNN H. MATTHIAS

Allen-Bradley Laboratory,
Milwaukee, Wisconsin,
June 19, 1940.

[1] See J. Slepian, J. A. I. E. E. October, 1928; F. C. Todd and T. E. Browne, Phys. Rev. 36, 732 (1930).
[2] J. D. Cobine, R. B. Power and L. P. Winsor, J. App. Phys. 10, 420 (1939).

A Rotational Analysis of Some CS_2 Bands in the Near Ultraviolet System

In considering the possible electron configurations of various electronic states of carbon disulphide, Mulliken concluded that the molecule, though linear in the normal state, is bent in the excited electronic state of the λ3200 absorption band system.[1]

Some time ago Jenkins[2] reported that some of the bands in this system resemble those of a linear molecule with a simple P and R branch. However, with the spectrograph used, many of the lines were not resolved. Photographs of the bands taken by the writer in the second order of a 30,000-line-per-inch grating having a practical resolving power of about 300,000, show some of the bands fairly well resolved. Both parallel and perpendicular types are present. It will be shown by Mulliken in a later paper that even if the molecule is bent in the excited electronic state, one may still expect essentially the same types of band structures as if it had remained linear. Let $\Lambda h/2\pi$ be the angular momentum along the axis in the lower state. In the upper electronic state, the angular momentum around an axis parallel to the line joining the S atoms may be characterized approximately by $Kh/2\pi$, because even a considerably bent carbon disulphide molecule approximates surprisingly closely to a symmetric top. Then there exists for practical purposes a selection rule, $(K-\Lambda)=0$ (parallel type), or ± 1 (perpendicular type).

The results obtained from the analysis of four rotational bands may be summarized as follows:

Band at λ3501, type $^1\Sigma_u^+ \leftarrow {}^1\Sigma_g^+$, $B'=0.1122$, $B''=0.1093$
Band at λ3467, type $^1\Pi_g \leftarrow {}^1\Sigma_u^+$,
$B_{PR}'=0.1044$, $B_Q'=0.106_5$, $B''=0.1016$
Band at λ3637, type $^1\Sigma_u^+ \leftarrow {}^1\Sigma_g^+$, $B'=0.1178$, $B''=0.1151$
Band at λ3601, type $^1\Sigma_u^+ \leftarrow {}^1\Sigma_g^+$, $B'=0.1120$, $B''=0.1097$

The B values are in cm^{-1}. The symbols used for the transition type are not strictly applicable to the bent molecule but represent those linear molecule types which the observed bands resemble. However, the capital Greek letters continue to represent the total angular momentum about the figure axis.

The bands at λ3501 and λ3601 have a common upper state whose rotational levels are perturbed. This perturbation has been analyzed indicating that it is of the heterogeneous type ($\Delta\Lambda=\pm 1$), the observed $^1\Sigma_u^+$ being perturbed by a $^1\Pi_u$ state. The perturbation analysis gives sufficient data to determine that the B value of the perturbing state is 0.113 cm^{-1}. The prediction by the theory that the heterogeneous type of perturbation causes a constant shift of all levels whose J values are greater than those of the perturbed levels, has been verified. The intensity distribution among the perturbed lines and the extra lines introduced by the perturbation has been calculated and verified. The lower states of these two bands differ by two quanta of the degenerate vibration ν_2. This would indicate that the value $\nu_2=397$ cm^{-1}, as given by the Raman spectra data for liquid carbon disulphide, is too low for carbon disulphide vapor.

It will be noted that the band at λ3467 has two B values for the upper state. One was obtained from the Q branch, the other from the P and R branches. This may most reasonably be explained by a splitting of the levels due to the removal of K degeneracy by asymmetry. In order for the asymmetry to be sufficiently large to produce the observed splitting, it is necessary that the apex angle be bent to about 120° in the upper state. Calculations show that in spite of this asymmetry, rotational levels in the upper state will still approximately follow a simple $J(J+1)$ formula if J is less than 25.

LEONARD N. LIEBERMANN

Ryerson Physical Laboratory,
University of Chicago,
Chicago, Illinois,
June 25, 1940.

[1] R. S. Mulliken, J. Chem. Phys. 3, 720 (1935).
[2] F. A. Jenkins, Astrophys. J. 70, 191 (1929).

Gamma-Ray Resonances from the Bombardment of Carbon by Deuterons

Gamma-rays from the bombardment of carbon by deuterons were first reported by Lauritsen and Crane.[1] Later Tuve and Hafstad[2] reported γ-rays of high intensity from carbon bombarded by 1.0-Mev deuterons. We have confirmed this high yield of γ-rays from $C^{12}+H^2$ and have further found that the curve of γ-ray intensity as a function of bombarding energy is not a continuously rising curve but exhibits resonances. This is very interesting in view of the fact that it is the first known case of resonant emission of γ-rays from deuteron bombardment. Furthermore the data on the resonances in the emission of neutrons[3] and protons[4] from $C^{12}+H^2$ indicate that the γ-rays, at least in part, come from a radiative capture of a deuteron by C^{12}.

The experiments on the γ-ray resonances have been carried out with the Rice Institute high pressure Van de Graaff machine. The γ-rays have been detected both by means of coincidences of Geiger counters and by a Wulf type electroscope filled with argon at 70 atmospheres pressure. Most of the data have been taken with the electroscope because of the greater reliability and speed of such measurements. The intensity of the γ-rays from one microampere of 1.5-Mev deuterons on a thick graphite target was found to give the same ionization in the argon-filled chamber as 5 mg of radium (filtered by 1 cm of iron). The γ-ray intensity from $C^{13}+H^2$ was found to be three

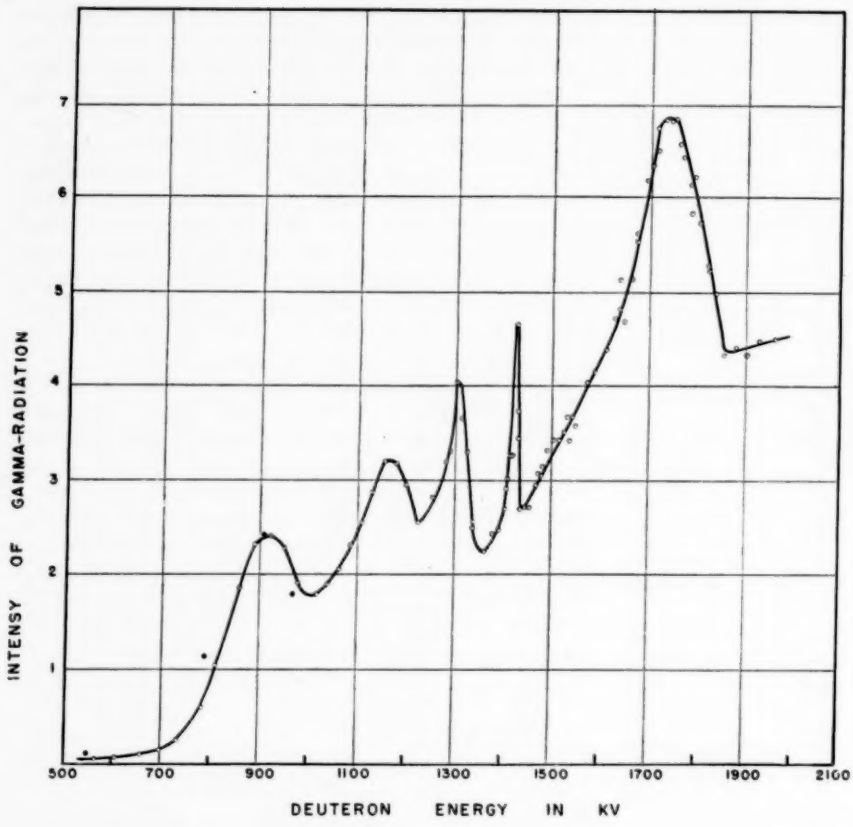

FIG. 1. The excitation curve for the emission of γ-rays from a thin target of carbon bombarded by deuterons. Open circles refer to data taken with an argon-filled ionization chamber and solid circles to data taken with coincidence Geiger counters.

times that obtained from the bombardment under similar circumstances of a thick crystal of CaF_2 by 1.5-Mev protons.

The excitation curves for the γ-rays have been carried out with thin carbon targets made by evaporation of paraffin onto silver disks. These targets were in general only a few thousand volts thick. The deuterons were magnetically analyzed by deflection through 90° before falling on the paraffin targets. Figure 1 gives the yield curve for the γ-rays from 550 kev up to 2000 kev. This curve shows resonances at 920, 1160, 1300, 1430, and 1740 kev. The experimental half-widths of the resonances vary from about 250 kev for the level at 1740 kev to 10 kev for the level at 1430 kev. The 10-kev width of this level is probably due to the spread in energy of the deuteron beam.

The γ-rays from all the resonances are hard, and although differing slightly, show about the same absorption in lead as do the γ-rays from RaTh. With poor geometrical conditions the radiation from the resonance at 1300 kev was reduced to half-value in 2.6 cm of lead.

Gamma-rays might arise from the following reactions:

$$C^{12}+H^2\rightarrow(N^{14*})\rightarrow C^{13*}+H^1+Q_1;$$
$$Q_1=2.71 \text{ Mev for ground state} \quad (1)$$

$$C^{13}+H^2\rightarrow(N^{14*})\rightarrow N^{13*}+n^1+Q_2;$$
$$Q_2=-0.25 \text{ Mev for ground state} \quad (2)$$

$$C^{13}+H^2\rightarrow(N^{14*})\rightarrow N^{14}+\gamma_1+Q_3; \qquad Q_3=10.4 \text{ Mev} \quad (3)$$

$$C^{13}+H^2\rightarrow(N^{14*})\rightarrow N^{14**}+\gamma_2+Q_3;$$
$$Q_3=10.4 \text{ Mev for ground state}$$
$$N^{14**}\rightarrow N^{14}+\gamma_3$$

$$C^{12}+H^2\rightarrow C^{12*}+H^2, \quad (4)$$
$$C^{12*}\rightarrow C^{12}+\gamma.$$

The fact that the yield of N^{13} exhibits some of the same resonances[3] as the γ-rays shows that reactions involving C^{13} could not be responsible. Considerations of the intensity of the γ-rays and of the relative abundance of the carbon isotopes ($C^{12}/C^{13}=90$) leads to the same conclusion. The observed γ-rays cannot come from reactions (2) or (4) because they would then be of very low energy. This would be impossible in view of the Geiger-counter coincidence measurements and of the absorption coefficient in lead.

Since the γ-ray resonances at 1300, 1430, and 1740 kev are not exhibited for proton emission,[4] it seems reasonable to suppose that the γ-rays from these levels are not from reaction (1), and so must be from the only remaining reaction (3). All the γ-rays would not be expected to have the maximum possible energy, but frequently the N^{14*} would return to the ground state of N^{14} in steps, as in the case of the reaction:

$$C^{13}+H^1\rightarrow(N^{14*})\rightarrow N^{14}+\gamma_1+Q_5; \quad Q_5=8.2 \text{ Mev} \quad (5)$$
$$C^{13}+H^1\rightarrow(N^{14*})\rightarrow N^{14**}+\gamma_2$$
$$N^{14**}\rightarrow N^{14}+\gamma_3.$$

Lauritsen and Fowler[5] have found γ-rays with energies of 2.8, 5.4 and 8. 1 Mev from this reaction.

Further work is in progress to investigate the energy of the γ-rays and a more detailed account of these experiments will be given after this work has been completed.

W. E. BENNETT
T. W. BONNER

The Rice Institute,
Houston, Texas,
June 27, 1940.

[1] C. C. Lauritsen and H. R. Crane, Phys. Rev. **45**, 345 (1934).
[2] M. A. Tuve and L. R. Hafstad, Phys. Rev. **48**, 106 (1935).
[3] T. W. Bonner, E. Hudspeth and W. E. Bennett, Phys. Rev., following letter.
[4] M. M. Rogers, W. E. Bennett, T. W. Bonner and E. Hudspeth, Phys. Rev., following letter.
[5] C. C. Lauritsen and W. A. Fowler, this issue, p. 193A.

Resonances in the Emission of Neutrons from the Reaction $C^{12}+H^2$

We have investigated the excitation curve for the reaction

$$C^{12}+H^2\rightarrow(N^{14*})\rightarrow N^{14}+n^1-0.25 \text{ Mev.} \qquad (1)$$

The excitation curve for the neutrons had previously been obtained by Amaldi, Hafstad and Tuve[1] using a thick carbon target. Their measurements showed no resonances because they extended to only 950 kev.

We have found that the excitation curve from a thin carbon target is not a smooth one, but shows resonances at 920, 1160, 1300, and 1825 kev. To detect the neutrons we have used a Wulf electroscope filled with hydrogen at a pressure of 7 atmospheres and we have studied the radioactivity of the N^{13} which is formed whenever a neutron is emitted according to reaction (1). The ionization measurements are much quicker, and so most of the data are of this kind. The measurements of the radioactivity of N^{13} were taken as a check on the ionization chamber data.

The hydrogen-filled electroscope would also detect neutrons from the reaction

$$C^{13}+H^2\rightarrow(N^{15*})\rightarrow N^{14}+n^1+5.2 \text{ Mev.} \qquad (2)$$

However, the yield from this reaction is only 1 percent that from reaction (1) at 800 kev.[2]

The amount of radioactive N^{13} formed in a thin paraffin target was measured by means of a thin-walled Geiger counter placed outside a thin window on the target tube. The procedure was to bombard the target for ten minutes, then shut off the high voltage and follow the activity of the target.

Figure 1 shows the excitation curves obtained from the ionization currents in hydrogen and from the radioactivity of the N^{13}. Since some of the ionization in hydrogen is due to γ-rays, corrections had to be made to compensate for this effect. By using radium filtered by 1.0 cm of lead, we found that the γ-ray sensitivity of the electroscope filled with hydrogen was only 4.75 percent that of the argon-filled chamber which was used in the γ-ray measurements. We used the same target in both experiments, so we were able to calculate that the contribution of the γ rays to the total ionization in hydrogen was 19 percent at 1525 kev. A corresponding correction was made at all other voltages. Curve (3) gives this corrected ionization due to the neutrons alone. Both curves (1) and (3) show resonances at 920, 1160, and 1300 kev. These are the same resonances as those found for the emission of γ-rays.[3] However, the γ-ray resonance at 1430 kev does not show as a resonance for neutron emission.

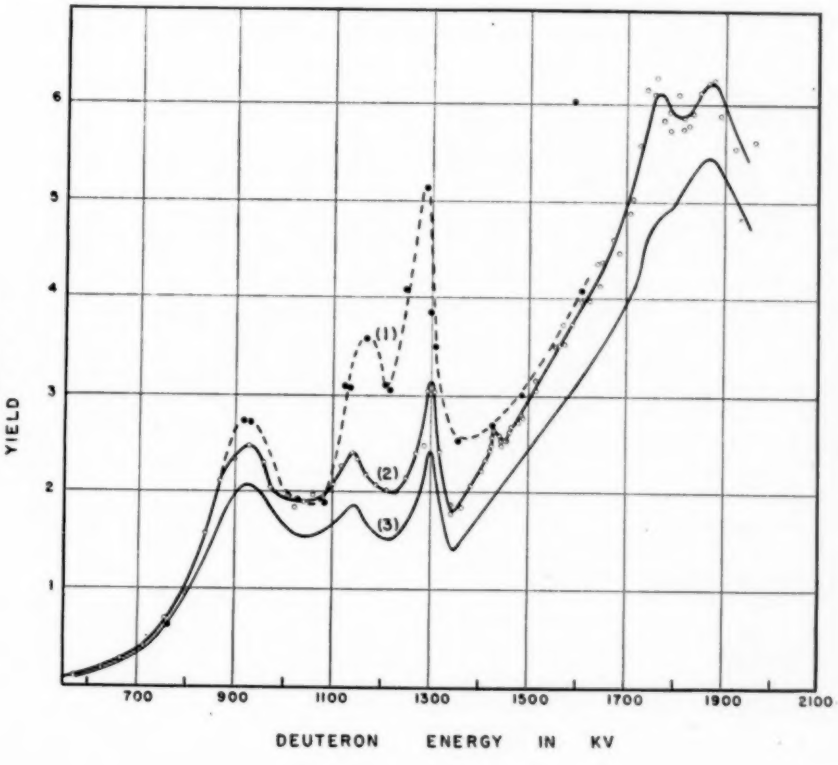

FIG. 1. Excitation curves for the emission of neutrons from a thin target of carbon bombarded by deuterons. Curve (1) gives the yield of N^{13} produced in the reaction. Curve (2) shows the ionization in a hydrogen-filled ionization chamber. Curve (3) is obtained from curve (2) by subtracting the effect produced by the γ-rays from carbon. Hence curve (3) represents the neutron yield.

Above 1430 kev the hydrogen ionization data shows a level at 1740 kev and 1825 kev. The resonance at 1740 kev disappears after the γ-ray correction is made (curve 3). The neutron resonance at 1825 kev is definitely at a higher energy than the γ-ray level at 1740 kev.

The neutron resonances at 920, 1160, 1300 and 1825 kev correspond to excited states in the intermediate N^{14} nucleus at 11.19, 11.39, 11.51, and 11.96 Mev. These excited states of N^{14} might also be expected to break up into $C^{13}+H^1$, giving resonances in the yield of protons. This prediction has been tested and the results are given in the following letter.[4]

T. W. Bonner
Emmett Hudspeth
W. E. Bennett

The Rice Institute,
Houston, Texas,
June 27, 1940.

[1] E. Amaldi, L. R. Hafstad and M. A. Tuve, Phys. Rev. 51, 896 (1937).
[2] T. W. Bonner and W. M. Brubaker, Phys. Rev. 50, 308 (1936).
[3] W. E. Bennett and T. W. Bonner, preceding letter.
[4] M. M. Rogers, W. E. Bennett, T. W. Bonner and E. Hudspeth, following letter.

Resonances in the Emission of Protons from the Reaction $C^{12}+H^2$

Since the γ-rays[1] and neutrons[2] from the bombardment of carbon by deuterons show many of the same resonances, we might expect the protons from the reaction

$$C^{12}+H^2\rightarrow(N^{14*})\rightarrow C^{13}+H^1+2.7\text{ Mev} \qquad (1)$$

also to show the same resonances. These resonances correspond to excited states in the intermediate N^{14} nucleus, and we might expect the emission of a neutron, a proton or a γ-ray to be competing processes. We have studied the excitation curve of the 15-cm protons to see if resonances occur.

The protons were detected by a 2.5-cm deep ionization chamber connected to a linear amplifier. Such a deep chamber was used so that protons could be counted far from the end of their range. This was useful because the range of the protons from reaction (1) changes with bombarding energy.

Figure 1 gives our experimental excitation curve for protons. The curve shows the same resonance at 920 kev that was exhibited for the emission of γ-rays and neutrons. The next resonance occurs at 1220 kev; this is 60 kev greater than the second resonance for the emission of γ-rays. In order to make certain whether the resonances come at different positions, we have checked the γ-ray curve immediately after obtaining the proton resonance. The γ-ray resonance came at 1160 kev. It seems possible that the resonances at 1160 and 1220 kev really are the same level in N^{14} but that the exact position of the peak depends upon the particle that is emitted. Breit[3] has predicted that the peak on such a resonance curve may be displaced as much as the width of the level, depending upon the mode of disintegration. It seems possible that

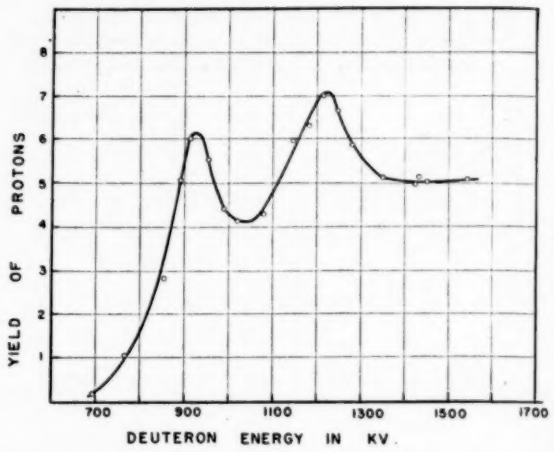

FIG. 1. The excitation curve for the emission of 15-cm protons from a thin target of carbon bombarded by deuterons.

the neutron resonance at 1825 kev may likewise be the same level in the intermediate N^{14} as the 1740-level for γ-ray emission.

The protons do not show a resonance at 1300 kev, in contrast to the neutrons and γ-rays. A careful search was made to see if the protons showed a resonance at 1430 kev. The high voltage was adjusted to be on the peak of the 1430-kev level for γ-rays and then the yield of protons observed. No increased yield was found at this voltage. The proton curve, unlike the curves for γ-rays and neutrons, does not show a rise in the region of 1350–1600 kev, indicating that the level at 1740 or 1825 kev may be missing.

The relative yield of protons and neutrons has been obtained at 920 kev, by counting the number of N^{13} atoms formed in comparison to the number of protons from the same thin target. At 90° to the bombarding direction the ratio of protons to neutrons is 1.9. This indicates that the excited intermediate N^{14} nucleus is about equally likely to break up into a proton or a neutron. The relative number of γ-rays is more difficult to obtain, but there seem to be more quanta of γ-rays than protons or neutrons.

There appear to be selection rules which prohibit the emission of protons from the 1300, 1430, and 1740-kev levels. Also there appears to be a selection rule which prohibits the emission of neutrons from the 1430-kev level. The 1430-kev level might be expected to be narrower than the other levels because it can decay only by emission of γ-rays and therefore has a longer lifetime.

M. M. Rogers
W. E. Bennett
T. W. Bonner
Emmett Hudspeth

The Rice Institute,
Houston, Texas,
June 27, 1940.

[1] W. E. Bennett and T. W. Bonner, preceding letter.
[2] T. W. Bonner, E. Hudspeth and W. E. Bennett, preceding letter.
[3] G. Breit, Science 91, 419 (1940).

Proceedings of the American Physical Society

MINUTES OF THE SEATTLE, WASHINGTON, MEETING, JUNE 18–21, 1940

THE 235th regular meeting of the American Physical Society was held at the University of Washington, Seattle, Washington. A joint session with the American Association of Physics Teachers, held on the afternoon of June 18, was addressed by R. T. Birge, W. Weniger and A. A. Knowlton, who discussed the training and employment of physicists. A symposium on Cosmic Rays, held on the morning of June 19, included the presentation by Volney Wilson of a paper by A. H. Compton, a paper by R. A. Millikan, Victor Neher and H. G. Stever (presented by Neher) and a paper by Hans Bethe. The afternoon session of June 19, a joint session with the Astronomical Society of the Pacific, was addressed by G. M. Volkoff and D. B. McLaughlin, who discussed the problem of stellar energy. On the morning of June 20 N. F. Ramsey and J. R. Zacharias presented papers on Nuclear Moments and John von Neumann discussed special cases in the Theory of Operator Rings. For this paper the American Physical Society was in joint session with the American Mathematical Society. The afternoon session of June 20 comprised an Informal Symposium on Theoretical Physics, conducted by J. R. Oppenheimer, who opened the discussions by a presentation of "The present crisis in the quantum theory of fields." Hans Bethe, G. M. Volkoff and H. Snyder also participated.

On Wednesday noon a luncheon was held at the Hotel Meany. K. K. Darrow and Frederick Bedell spoke briefly.

The forty-seven contributed papers, abstracted and indexed below, were presented in parallel sessions during the morning and afternoon of June 21. Numbers 2, 7, 18, and 29 were read by title.

PAUL KIRKPATRICK
Local Secretary for the Pacific Coast

ABSTRACTS

1. The Spatial Asymmetry of Cerenkov Radiation as a Function of Electron Energy. H. O. WYCKOFF AND J. E. HENDERSON, *University of Washington*.—The visible radiation proceeding in the form of a hollow cone from the path of a high speed electron traveling through a transparent medium was first discovered and investigated qualitatively by Cerenkov. Frank and Tamm have given a classical theoretical explanation of this asymmetry based on the fact that the electrons producing the radiation travel with a velocity greater than the velocity of the radiation they produce in the medium. They predict that $\cos\theta = 1/\beta n$ where θ is the half-angle of the cone, n the index of refraction of the medium and β is the ratio v/c. The present experiment was devised to determine the dependence of the angle of emission of the radiation upon the electron energy. Electrons from an electron tube operating at up to 815 kv impinged upon a thin sheet of mica. By measurement of the position of the radiation after reflection from a conical mirror the angle of emission in the mica was determined. All experimental points were found to lie on the theoretical curve within the experimental error between electron velocities provided by potentials from 240 kv to 815 kv. This gives strong evidence in support of the theory of Frank and Tamm.

2. Absolute f Values of Cd I and Cu I Lines. R. B. KING, *Mount Wilson Observatory*, AND D. C. STOCKBARGER, *Massachusetts Institute of Technology*.—The absolute f values of the Cd I line λ3261 ($^1S_0 - {}^3P_1$) and the Cu I resonance lines λλ3247, 3274 ($^2S_{1/2} - {}^2P_{3/2,\,1/2}$) have been measured by the method of total absorption. The metal vapors were obtained in a furnace designed for accurate temperature control and measurement to temperatures of 1400°C. The measurements were made at low vapor pressures (weak absorption lines) at temperatures in the neighborhood of 200°C for Cd and 925°C for Cu. Results: for Cd λ3261 $f = 0.0023$; for Cu λ3247 $f = 0.62$, λ3274 $f = 0.32$. The value for Cd λ3261 is in good agreement with the values 0.0019 [1] and 0.0021 [2] obtained by other investigators by different methods. Details will be published in a Mount Wilson contribution to appear in the *Astrophysical Journal* (in press).

[1] W. Kuhn, *Habilitationsschrift* (Zürich, 1926); H. D. Koenig and A. Ellett, Phys. Rev. **39**, 576 (1932).
[2] A. Ellett, Phys. Rev. **33**, 124A (1929).

3. The Positive Corona Discharge. K. S. FITZSIMMONS, L. B. LOEB AND J. M. MEEK, *University of California*.—In order to determine the conditions for streamer propagation in positive point corona measurements were made in

dry air with confocal paraboloids and have been previously reported.[1] These data, together with supplementary data, enable curves of the variation of field strength across the gap to be drawn for onset of streamers, steady burst pulse corona, and spark breakdown. A paraboloid of focal length 0.009 cm was used in conjunction with four other paraboloids of focal length 1, 2, 3 and 5 cm, respectively. As was to be expected the field strength curves for streamer onset lie within experimental error of each other. The results for the 1-cm gap were initially at fault due to the presence of excess NO_2 etc. owing to lack of adequate air circulation, a fault which was later rectified. The values of the streamer-producing field agree in a surprising measure with the criterion for streamer onset inherent in the new theory of spark discharge.[2]

[1] K. S. Fitzsimmons, Phys. Rev. **57**, 251A (1940).
[2] J. M. Meek, Phys. Rev. **57**, 722 (1940); L. B. Loeb and J. M. Meek, J. App. Phys. **11**, 438 (1940); also July issue, in press.

4. On the Structure of the Arc Spectrum of Tungsten. OTTO LAPORTE, *University of Michigan*, AND J. E. MACK, *University of Wisconsin.*—Since the last report on this spectrum[1] essential progress has been made in the interpretation of levels. Despite the fact that no pronounced coupling holds we have succeeded in considerably extending our previous identifications among the levels of the low even, middle odd, and high even groups. In the middle group the levels $d^4s(^6D)p\ ^{7,5}(PDF)$ and in the high even group the levels $d^4s(^6D)s\ ^{7,5}D$ have been identified. Using formulae published by Ostrofsky[2] it has been possible to assign most of the low levels to d^4s^2. Also numerous d^5s levels have been found for the sake of whose theoretical treatment a calculation of the electrostatic interactions in d^5 has been carried out.

[1] Phys. Rev. **52**, 249 (1937).
[2] Phys. Rev. **46**, 604 (1934).

5. Temporal Effects in Nitrogen Afterglows. JOSEPH KAPLAN, *University of California at Los Angeles*, AND SIDNEY M. RUBENS, *University of Southern California.*—Continued experiments on the difference in spectra of nitrogen afterglows taken at varying times after the interruption of the discharge have led to an hypothesis regarding the meaning of these temporal effects. By employing long tubes viewed end-on it has been possible to obtain afterglow spectra in reasonably short times. At the pressures maintained in these experiments, 10 to 20 mm Hg, the early phase of the afterglow showed intense first-negative bands as well as strong λ3467, making this the most faithful reproduction of the auroral spectrum so far achieved. The actual intensity of 3467 increases with time early in the afterglow in spite of the decrease in the total intensity of the afterglow. For equal intensity of the persistent first-positive bands, there is a great increase in intensity of 3467 with time. These results are interpreted in terms of rapid predissociation of the nitrogen molecule from a state whose population depends on the elapsed time of the glow or on the elapsed number of collisions. Evidence for this is the correspondence between the early phase of a high pressure afterglow and a later phase of a lower pressure afterglow. This rapid predissociation is proposed as the origin of forbidden lines in upper-atmospheric spectra.

6. Afterglows in Nitrogen-Helium Mixtures. SIDNEY M RUBENS, *University of Southern California*, AND JOSEPH KAPLAN, *University of California at Los Angeles.*—The spectra of afterglows have been obtained in nitrogen-helium mixtures at two different nitrogen-helium ratios. With an excess of helium the relative intensity of λ3467 early in the afterglow corresponds to that observed in the late stage of the afterglow in pure nitrogen. Tentative identification of spectra of the late phase of this afterglow indicates the presence of the nebular line near 5200 and the absence of 3467. Thus a temporal effect exists in the N_2—He glow but one different from that previously reported for pure nitrogen. Early and late spectra for N_2—He glows, in which the amounts of the two gases are about equal, show a mixture of the temporal effects for pure N_2 and the one discussed above. The remarkably large relative intensity of 3467 may be caused either by the prevention of diffusion of metastable nitrogen atoms to the walls or by the enhanced predissociation of nitrogen produced by helium. That the latter is probably predominant is indicated by the effect of helium in producing an abnormal intensity distribution in the first-positive group in the afterglow and the existence of a temporal effect different from that in pure nitrogen.

7. Note on the Polarization of Light Emitted by Electrically Exploded Wires. WILLI M. COHN, *El Cerrito-Berkeley, California.*—The polarization of light emitted by an electrically exploded wire was photographically investigated. No polarization was found, within the limits of accuracy. It is concluded that scattered and reflected light does not contribute to the emission from electrically exploded wires. This leaves temperature radiation and continuous electron radiation as the only factors causing the emission of the continuous spectrum.

8. The Sparking Threshold in Air. WILLIAM R. HASELTINE, *University of California.*—To test the streamer theory of breakdown recently developed by Loeb and Meek,[1,2] a stabilized voltage source was set up, and the breakdown potential measured between plane parallel electrodes in dry air. Automatic recording of sparks was provided. Thresholds have been measured at various values of $p\delta$ from 100 to 400. The value at $p\delta=316$, $T=15°C$ seems to be 15.4 kv. The theory contains an incompletely specified parameter, by means of which the predicted threshold can be varied about two percent. When this is assigned to fit one point, the agreement with other points is remarkable. The effect of previous sparks on the threshold is most marked. At atmospheric pressure, a series of previous sparks may lower the threshold by 600 out of 10,000. On standing, there is a slow recovery. When the chamber is continuously flushed by a slow stream of dry air, the effect is greatly reduced, but not eliminated. Also, at lower pressures (200 mm) the effect is only about one percent (50 v out of 5000). This seems to be caused, in part at least, by the formation of nitrogen oxides. When the threshold is about 12 kv, the region in which time lags and statistical fluctuations could be detected is certainly less than 50 v wide.

[1] J. M. Meek, Phys. Rev. **57**, 722 (1940).
[2] L. B. Loeb and J. M. Meek, J. App. Phys. **11**, 438 (1940); also July issue, in press.

9. Forbidden Lines in the Spectrum of PbI. S. MROZOWSKI, *Radiation Laboratory, University of California. (Introduced by F. A. Jenkins.)*—The hyperfine structure of the forbidden lines of lead (within the $6p^2$ configuration) has been studied with the purpose of establishing the intensity rules in hyperfine structure of forbidden lines. The spectrum was excited very intensely by electric standing waves in a helium atmosphere of about 5 mm pressure and saturated Pb vapor at about 850°C.[1] For the pure magnetic dipole line 4618A the intensity ratio and the ratio of the distances from the center of gravity were found to agree with the predictions of the well-known rules for electric dipole transitions. For the pure electric quadrupole line 5313A the ratios are given by the Rubinowicz formulas transcribed for the case of hyperfine structure by Opechowski.[2] In the case of the line 7330A, of mixed type, the intensities are approximately those for the electric dipole radiation, showing that this line has mostly a magnetic dipole character. An upper limit of the admixture of the electric quadrupole character can be evaluated from these measurements. The relative intensities of these three lines and of two others, 4659A and a newly found line 9250A ($^3P_2-{}^1D_2$), are being measured for the purpose of comparison with theory.

[1] H. Niewodniczanski, Acta Physica Polonica **2**, 375 (1934).
[2] S. Mrozowski, Phys. Rev. **57**, 207 (1940).

10. Raman Spectra Evidence for the Disappearance of the Cyanate Ion from an Aqueous Solution of Potassium Cyanate. FORREST F. CLEVELAND, *Armour Institute of Technology.*—In a recent study of the infra-red absorption spectrum of a saturated aqueous solution of potassium cyanate, Williams[1] found that the bands at 840 and 2180 cm^{-1} in the freshly prepared solution became weaker with age of the solution and that additional bands corresponding to characteristic absorption frequencies of NH_4 and CO_3 appeared. To supplement the infra-red data, Raman spectra of such a solution have been obtained over a ten-day period. Displacements, estimated intensities, and depolarization factors obtained from spectrograms made the first day were: 1225(6)0.6, 1315(4)0.6, and 2171(10)0.3. After three days, these lines had disappeared, three new lines, 1003(8)0.4, 1033(8)0.3, and 1064(10)0.3, had appeared, and the solution had acquired an unmistakable odor of ammonia. Since the frequencies 1064 and 1033 are known to correspond to the symmetrical breathing frequencies of the CO_3 ion in K_2CO_3 and $KHCO_3$ solutions, the conclusions drawn by Williams from the infra-red data are verified.

The assignment of the frequencies observed for the fresh solution presents some difficulty. Calculations indicate that the frequencies observed at 1225 and 1315 can hardly be fundamental frequencies of the linear $-O-C\equiv N$ group. Goubeau[2] has reported 1204 and 1307 for cyanic acid and it may be, therefore, that these lines are due to the formation of some of this acid in the solution.

[1] Dudley Williams, Phys. Rev. **57**, 1077A (1940).
[2] J. Goubeau, Ber. Deut. Chem. Ges. **68**, 912 (1935).

11. Fluorescence Method of Identifying Potato Tubers Free from Bacterial Ring Rot and Other Types of Decay. HARRY C. KELLY AND V. E. IVERSON, *Montana State College.*—The identification of potato tubers free from bacterial ring rot and other types of diseases which cause tuber breakdown has proven to be an important problem to potato seed growers. A rapid and inexpensive method of detection of some tuber diseases by examination under ultraviolet light and the resulting fluorescence is described. The method[1] has found commercial application in culling seed stock. A comparison with other methods of detecting the ring rot organism is given and the application of the new test method is illustrated.

[1] "A New Method of Identifying Potato Tubers Free from Bacterial Ring Rot and Other Types of Tuber Decay," Mimeo. Circular No. 20, by V. E. Iverson and H. C. Kelly, Montana Agricultural Experiment Station, Bozeman, Montana, April, 1940.

12. Observations on Field Currents from Tantalum. G. M. FLEMING AND D. M. HOLTONER, *Mount Holyoke College.*—An electron projector like that described by Müller[1] was used to study field emission from tantalum. A tantalum point was mounted at the center of a glass flask, the inner surface of which was coated with willemite. A positive potential applied to a ring anode produced a high radial field at the surface of the point. Emitted electrons were projected to the walls of the tube where they produced fluorescence. The fluorescent areas were of two types: One, sharply defined, brilliant, and easily measurable, was associated with large emission currents; the other, faint and rather diffuse and fragmentary, occurred with very low currents. Ordinarily the two types of emission did not occur simultaneously, although their voltage ranges overlapped. The slopes of the lines obtained by plotting $\log I/F^2$ against $1/V$ were compared with the values predicted by the Fowler-Nordheim theory[2] assuming various values for radius of curvature of the emitting point. To bring agreement these values were from two to ten times smaller than the measured radius. Current densities could be made to agree only for certain slopes.

[1] E. W. Müller, Zeits. f. Physik **108**, 668 (1938).
[2] R. H. Fowler and L. Nordheim, Proc. Roy. Soc. **119**, 173 (1928).

13. On the Ratio N of Scattering to Capture Cross Section for Thermal Neutrons in Paraffin. E. A. SCHUCHARD, *University of Washington.*—An exact solution of the Boltzmann equation previously presented[1] furnishes the relation: $N=R^2-2R$, where R is the ratio of the activity of a thin detector placed deep in the interior of a large paraffin block to that at the surface when a uniform interior production of thermal neutrons is present. Using a recent quotation of $R=14$, $N=168$ is obtained as compared to the value 196 predicted by the Fermi "albedo" formula $N=R^2$. The available experimental information on the thermal neutron emission from paraffin is not of sufficient precision to fix N's value by comparison with the theoretical predictions, though a lower limit of 150 is indicated if the interior thermal production is uniform. Some quite direct measurements for σ_s and σ_c may be combined in two ways to give for their ratio N the values: 169±8 percent, 195±8 percent. It is to be noted that these values of N make the numerical approximation ($N=\infty$) in the albedo relations

of Halpern, Lueneburg and Clark[2] quite serious. A slight dependence on N (2–4 percent change from $N=\infty$ to $N=150$) is to be found in the transmission ratio curve for pure absorbers placed on the standard paraffin cylinder.

[1] E. A. Uehling and E. A. Schuchard, Phys. Rev. **57**, 251A (1940).
[2] Halpern, Lueneburg and Clark, Phys. Rev. **53**, 182 (1938), Eq. (66a).

14. Spin-Orbit Coupling in He^5. S. M. DANCOFF, *University of California.*—The value of the splitting of the ground state of He^5 has been set by Staub at 0.25 ± 0.1 Mev. Attempts have been made to account for this on the basis of (a) Thomas relativistic spin-orbit coupling, and (b) the "tensor" spin-orbit interaction of mesotron theory. The Thomas doublet is in the right direction but is in magnitude only about 0.003 Mev. The tensor splitting is here calculated to second order and is found to be of the order of magnitude of 0.1 Mev but opposite in direction to the observed doublet. The possible effects of other types of force are discussed.

15. The Density Distribution in Steady-State Diffusion. E. A. UEHLING, *University of Washington.*—Steady-state conditions in many transport problems (radiative transmission in stellar atmospheres,[1] heat conduction in rarified gases,[2] diffusion with neglect of mutual interactions) are described by a Fredholm integral equation of the second kind

$$G(t)=I(t)+\tfrac{1}{2}\lambda\int_0^a K(|t-t'|)G(t')dt'$$

with

$$K(y)=\int_0^1 d\zeta\,\frac{e^{-y/\zeta}}{\zeta}.$$

Using the methods of Laplace transformation[3] and inversion, solutions in closed form for the case of $a=\infty$ may now be given. With particular reference to the diffusion problem, the coordinate t is measured in units of the total m.f.p., the parameter λ is the ratio of total and scattering mean free paths, and $I(t)$ is a function which may assume different forms depending upon the choice of boundary conditions (incident currents or interior source distributions). The corresponding problems are formally equivalent, a source distribution of the form e^{-bt} with b lying on a segment $(1, \infty)$ of the real axis corresponding to a delta-function distribution in angle of incident current. Values of b in the domain $R(b)\geq 0$, $b\neq(1, \infty)$ correspond only to source distributions. The two domains of b have, furthermore, distinct analytic properties. For $R(b)\geq 0$, $b\neq(1, \infty)$ including the limiting case of uniform source distributions the solution is

$$G(t)=B\left[\frac{1}{b}\frac{\ln\frac{1+b}{1-b}}{1-\frac{\lambda}{2b}\ln\frac{1+b}{1-b}}e^{-bt}-\frac{2(u_0^2-1)}{\lambda(1-bu_0)\{1-u_0^2(1-\lambda)\}}\frac{\beta(u_0)}{\beta(1/b)}e^{-t/u_0}-\frac{1}{\beta(1/b)}\int_0^1 e^{-t/u}\frac{\beta(u)}{\left(1+\frac{1}{2}\lambda u\ln\frac{1-u}{1+u}\right)^2+(\frac{1}{2}\pi\lambda u)^2}\frac{du}{1-bu}\right],$$

where $\beta(z)$ is a solving function analytic for $R(z)>0$, u_0 is given by

$$1+\tfrac{1}{2}\lambda u_0\ln\frac{u_0-1}{u_0+1}=0$$

and B is a constant proportional to the source strength.

[1] K. Schwarzchild, Berlin Sitz., pat. 2, 1191 (1914).
[2] V. A. Kostitzin, Mem. Sc. Math. 69 (1935).
[3] O. Halpern, R. Lueneburg and O. Clark, Phys. Rev. **53**, 173 (1938); E. A. Uehling and E. A. Schuchard, Phys. Rev. **57**, 251A (1940).

16. The Diamagnetism and the Quadrupole Moment of Hydrogen Molecules. N. F. RAMSEY,* *Department of Terrestrial Magnetism, Carnegie Institution of Washington.*—From the observed rotational radiofrequency spectra of H_2, D_2, and HD,[1] both the high frequency portion of the diamagnetic susceptibility and the dependence of the total diamagnetic susceptibility upon the orientation of the molecules may be evaluated. The former comes from the observed values of the rotational magnetic moments and from Wick's theory[2] of the moments. The value obtained is $\chi_{HF}=(1.53\pm0.12)\times10^{-31}$ per molecule. The latter is obtained by introducing into the Hamiltonian[3] used in the analysis of the radiofrequency spectra an additional term providing for the diamagnetism of the molecule. With this term included, the theoretical and experimental spectra agree completely if the difference in diamagnetic susceptibility perpendicular to and along the axis of the molecule is taken to be $(-12.5\pm5.0)\times10^{-31}$ per molecule. From these two results and from the previously observed[4] susceptibility of H_2 gas, the quadrupole moment of the electrons in H_2 may be evaluated. The value of $\overline{(3z^2-r^2)}$ for the electrons is thus found to be $(0.21\pm0.07)\times10^{-16}$ cm^2. The value calculated[5] from James-Coolidge wave functions is 0.15×10^{-16} cm^2. Observations of the radiofrequency spectrum in a stronger magnetic field should provide a more precise experimental determination.

* Now at the University of Illinois.
[1] N. F. Ramsey, Phys. Rev. **55**, 595A (1939).
[2] G. C. Wick, Zeits. f. Physik **85**, 25 (1933).
[3] J. M. B. Kellogg, I. I. Rabi, N. F. Ramsey and J. R. Zacharias, Phys. Rev. **56**, 728 (1939); **57**, 677 (1940).
[4] A. P. Wills and L. G. Hector, Phys. Rev. **23**, 209 (1924).
[5] H. M. James and A. S. Coolidge, Astrophys. J. **87**, 447 (1938).

17. Radiative K Capture. P. MORRISON AND L. I. SCHIFF, *University of California.*—Accompanying K capture, as in beta-activity, there is a weak high energy gamma-ray spectrum. We have calculated its intensity using the usual second-order perturbation theory employed by Bloch[1] and by Knipp and Uhlenbeck[2] for the radiative beta-activity. The major contribution to the effect is from magnetic radiative capture of a K electron. For an allowed transition using Fermi or Gamow-Teller coupling, the number of gamma-quanta per K electron captured is $(\alpha/12\pi)(W/mc^2)^2$, where W is the available energy. For other couplings and for forbidden transitions, the effect is of the same order of magnitude. We also show that an alternative calculation of Knipp and Uhlenbeck,[2] which regards the radiative beta-decay as a "first-order" transition from a singular spherical outgoing electron state to a plane wave, gives the correct answer only for couplings that are independent of the electron momentum, and thus *not* for forbidden transitions.

[1] F. Bloch, Phys. Rev. **50**, 472 (1936).
[2] J. K. Knipp and G. E. Uhlenbeck, Physica **3**, 425 (1936).

18. The Mean Lifetime of the Mesotron from Electroscope Data. H. V. NEHER AND H. G. STEVER, *California Institute of Technology.*—In order to detect the postulated decay of the mesotron and to secure data for the calculation for a mean rest lifetime, τ_0, an experiment which consisted of the measurement of cosmic-ray intensity at various depths in two lakes of widely differing altitude but of the same geomagnetic latitude was performed, using one of our self-recording electroscopes which has been used in other cosmic-ray work. In the higher lake, about 12,000 ft. above the lower, readings were taken at depths of 4.9, 5.9 and 6.9 meters and in the lower lake at 1.3, 2.3 and 3.3 meters, the difference in depth in the two lakes being about equal in mass to the air between the lakes. On the basis of the most recent theory, air and water were assumed to be gram for gram equivalent absorbers for the mesotrons involved. The ratio of intensities at equivalent points in the two lakes was theoretically calculated by finding the probability that a mesotron of mean lifetime, τ, and of energy E would reach the lower station, and integrating this probability over the energy distribution curves of Blackett from a minimum energy, E_0, just necessary to penetrate to the instrument in the lower lake. Matching observed and calculated ratios a mean rest lifetime, τ_0, of 2.5×10^{-6} sec. was found. For reasons outlined in a paper, to follow, this should be an upper limit on the correct mean lifetime.

19. The Electromagnetic Properties of Mesotrons. H. C. CORBEN AND JULIAN SCHWINGER, *University of California.*—A general theory of particles of unit spin and arbitrary magnetic moment is developed and applied to the motion of such particles in a Coulomb field. In the particular case of magnetic moment unity (Proca theory) the exact equations for the radial components of the wave functions possess regular solutions only for those states ($j=l\pm0$ and $j=0$, $l=1$) in which the orbital angular momentum l is a constant of the motion. For particles of magnetic moment two mesotron magnetrons the singularities disappear from the equations for all but the first state of each case $j=l+1$ and $j=l-1$. The cross section for the fractional energy transfer to electrons by energetic mesotrons is calculated for the various simple possibilities of mesotron spin σ (0, ½, 1) and magnetic moment μ (arbitrary except for zero spin) and it is shown that only for $\sigma=½$, $\mu\neq1$ (in particular $\mu=0$) and $\sigma=1$, $\mu=1$ is the cross section of the correct magnitude and form (i.e., essentially independent of the mesotron energy) to account for observed burst phenomena at energies greater than 2×10^{10} ev. Criteria for the validity of these formulae may be derived by requiring the smallness of the coupling energies involved.

20. Relativity Misconceptions Such as Relative Velocity. E. M. LITTLE, *Montana State University.*—There seems to be some confusion in the calculation of relative velocity in relativity. The usual expression is $(u+v)/(1+uv/c^2)$. This gives the velocity of A relative to B as measured by B if the velocities of A and B with respect to C are u and v, and is the usual idea of relative velocity. However, just as often a different concept of relative velocity is needed —the relative velocity of A and B as measured by C. This turns out to be merely $u+v$, not the above relativity expression. Reversal of cause and effect is another bad error. Order of events can be reversed but not to the extent of reversing cause and effect because the order of two events cannot be reversed unless they are far enough apart in space so that a light signal cannot get from one event to the other in the time interval. Another misconception is that a clock traveling away from the observer with a speed greater than that of light will have its hands move backward. At this speed, however, time, mass, and length are imaginary. Mercury's precession is mostly due to general relativity, not special. All things are not relative.

21. The Disintegration of Fluorine by Protons. J. F. STREIB, W. A. FOWLER AND C. C. LAURITSEN, *Kellogg Radiation Laboratory, California Institute of Technology.*—Excitation curves for the production of gamma-rays, pairs, and long range alpha-particles from $F^{19}+H^1$ have been obtained by bombarding a thin TaF_5 target with protons up to 1.5 Mev in energy. Resonance in both the pair and alpha-particle production occurs at 0.71, 0.84 and 1.35 Mev. The alpha-particle and pair resonances are, however, superimposed on a background which increases rapidly with voltage. This background becomes comparable to the resonances at about 0.9 Mev for the pairs and at much lower energies for the alphas. In the region between 0.9 and 1.3 Mev there is no apparent correlation between the pair and alpha-yields, the lack of correlation being very marked near 1.22 Mev where the pair yield shows strong resonance while the alpha-yield shows a flat minimum. The average pair and alpha-yields are comparable but each is only a few percent of the gamma-ray yields at 0.86, 0.93 and 1.36 Mev. No definite correlation in the gamma-ray and pair or alpha-resonances has been observed.

The existence of some simultaneous resonances in the pair and alpha-curves probably establishes the angular momentum and parity of the excited state of O^{16} which emits the pairs as O^+ and thus the transition to the ground state (O^+) can be due to electromagnetic interactions.[1]

[1] Oppenheimer and Schwinger, Phys. Rev. **56**, 1066 (1939).

22. Interaction of Mesotrons with γ-Rays. R. F. CHRISTY AND S. KUSAKA, *University of California.*—Differential cross sections for the production of a mesotron pair by a γ-ray and for the bremsstrahlung of mesotrons in the electromagnetic field of a nucleus have been calculated by Born approximation, using spin sum and spur techniques with Kemmer's[1] form of the Proca equations for mesotrons of unit spin and unit magnetic moment. The differential cross sections have been integrated in the limit where the energies of mesotrons and quantum are large compared to the rest energy of the mesotron. For a Coulomb field the total cross sections are $\sigma=A\alpha Z^2e^4E^2/(\mu c^2)^4$, where for pair production $A=19/72$ and E is the γ-ray energy, and for bremsstrahlung $A=11/72$ and E is the initial mesotron energy. These cross sections in an ideal Coulomb field do not correctly describe the electromagnetic effects in the neighborhood of an actual nucleus because the important

impacts are much closer than the nuclear radius. The cross sections in an electromagnetic field of the form $Ze(1-e^{-r/a})/r$, where a is the nuclear radius and is taken to be $\hbar Z^{\frac{1}{3}}/\mu c$, are $\sigma = B\alpha Z^{\frac{1}{3}}e^4E/(\mu c^2)^3$, where E is defined as before and $B=5\pi/36$ and $5\pi/108$, respectively, for pair production and bremsstrahlung. Here, since impacts near a are important, the constant B depends on the shape of the electromagnetic field near the nucleus; whereas even when the field is known, B cannot be uniquely determined by the approximate "method of virtual quanta."

[1] N. Kemmer, Proc. Roy. Soc. **A173**, 91 (1939).

23. Temperature Dependence of the Viscosity of Helium. E. J. HELLUND, *University of Washington.*—The idea has been frequently advanced that viscosity data may offer a good basis for the determination of intermolecular fields. A particular force law, which is assumed, leads to a definite temperature dependence which may then be compared with experiment.[1] Agreement between the two is taken accordingly as evidence for the correctness of the field on which the calculation has been performed.

The present paper is a preliminary work on a three parameter potential of a modified elastic sphere type. That is, the interaction consists of an impenetrable core surrounded by a finite repulsive barrier. The parameters which may then be varied are the two independent interaction diameters and the height of the barrier. The calculation of the transport cross section in this case reveals the presence of the three characteristics necessary for a correct temperature dependence. They are an increase of the cross section at intermediate temperatures, a sharp decrease at very low temperatures and an approach to the classical values at high temperatures. The results for a choice of field of 2A, hard core diameter, 2.5A, barrier diameter, and $(8\pi^2/h^2)mV_{\text{barrier}}=8\times10^{16}$ show a difference between theoretical and experimental values of approximately 4 percent from temperatures of 4.23°K to 290°K. The difference is, moreover, in the same direction, for all temperatures, indicating that closer agreement may be obtained by adjusting the inner diameter.

[1] Massey and Mohr, Proc. Roy. Soc. **A144**, 188 (1934); E. A. Uehling and E. J. Hellund, Phys. Rev. **54**, 479 (1938).

24. A High Yield Canal-Ray Ion Source for Nuclear Disintegration. W. H. GOSS AND J. E. HENDERSON, *University of Washington.*—A canal-ray ion source has been designed, built and tested which incorporates the following properties. It operates at low pressures and small exit canals, giving low gas consumption and low gas pressure in the disintegration tube. This permits acceleration to the target of the ions generated. Measurements at the target of the unresolved beam show a readily usable yield of 600 microamperes. The large yield has only been obtained when the "ion bundle" is experimentally centered on the exit canal. As the ion beam emerges with considerable energy the beam is a narrow pencil permitting easy focusing. The power consumption is small. Perhaps its greatest asset has been its long life. One source has been in use for more than 1000 hours without failure of any kind. For the immediate experiments for which it has been used resolution of the ions has not been important but neutron yields indicate the deuteron current to be at least 10 percent of the total current based on the reported yields of Amaldi, Hafstad and Tuve.

25. Low Energy β-Rays from Copper^{64}. JOHN BACKUS, *University of California.* (*Introduced by Luis W. Alvarez.*)—An electrostatic β-ray spectrograph has been constructed to explore the low energy distribution of positrons and electrons from Cu^{64}. The apparatus is equipped with a counter whose window is transparent to 3000-volt electrons. The source of radiocopper is electrolytically separated from zinc bombarded with 16-Mev deuterons, and is deposited on a film of the same type as the counter window, to minimize back-scattering. The β-ray distributions have been studied from 50–5 kev. The electron distribution is a straight line which extrapolates through the origin. The positron curve is concave upward and appears to pass through the origin with a high order of contact. While these curves may be distorted by some unsuspected source of error, the e^-/e^+ ratio appears to be free from suspicion. This ratio as a function of energy may be compared with theoretical prediction, as it is independent of Z, and almost independent of $E_{\max}$. The theoretical curve cannot be brought into agreement with the experimental. This is difficult to understand, as the phenomenon is essentially an extra-nuclear one involving the purely coulomb field of the nucleus.

26. Gamma-Radiation from $N^{15}+H^1$. W. A. FOWLER AND C. C. LAURITSEN, *Kellogg Radiation Laboratory, California Institute of Technology.*—The production of gamma-radiation by the bombardment of N^{15} by protons up to 1.4 Mev in energy has been studied using targets of ammonium chloride containing 14.8 percent N^{15} supplied to us by Professor H. C. Urey and Dr. Harry Thode of Columbia University. The excitation curves for thick targets indicate resonance (half-width$\leq$20 kv) in the gamma-ray production at proton energies of 0.88, 1.03 and 1.20 Mev. The yields above resonance were found to be 0.4, 0.3 and 1.2×10^{-7} quanta per proton, respectively. The yield from ordinary ammonium chloride targets was small compared to the yield from the enriched targets. Cloud-chamber investigations of the electron and pair secondaries produced in thin lead and carbon laminae by the gamma-radiation indicate that it consists mainly of a line at 4.4 ± 0.2 Mev. This line is to be attributed to the reaction N^{15} (p,α) C^{12*}, an excited state in C^{12} at this energy being well known.

27. High Energy Carbon Nuclei. LUIS W. ALVAREZ, *University of California.*—The 37-inch cyclotron chamber was filled with CH_4 and a beam of 50 Mev ${}_6C^{12+++++}$ ions was detected with a linear amplifier. To resolve these ions from alpha-particles, it was necessary to reduce the dee voltage and to adjust the magnetic field to the low side of the alpha-particle peak. Under these conditions, about 500 carbon nuclei entered the ionization chamber per minute. The pulses on the oscillograph were about nine times as high as those from Po alpha-particles, showing that their

charge was about $6e$. Their range was between 6 and 11 cm of air. The theoretical value is about 8 cm. e/m and v are known from the cyclotron constants. If the helium contamination in the cyclotron were not present, it would probably be possible to use these ions in disintegration experiments, for one could then set on the peak of the carbon resonance curve. Attempts to observe 100-Mev carbon ions in the 60-inch cyclotron gave no conclusive results, as the carbon beam was masked by a low energy deuteron beam with the same range and resonance magnetic field. These spurious ions emerge from the gap between dees, and do not pass through the deflector channel.

28. The Photonuclear Disintegration of Iron and Manganese. P. R. CARLSON AND J. E. HENDERSON, *University of Washington.*—Photonuclear reactions have been produced in a number of elements, the chief work having been done by Bothe and Gentner using the 17-Mv γ-rays from lithium bombarded with protons. By use of a positive ion source readily capable of producing 600 microamperes of unresolved ions together with an 800-kv transformer rectifier circuit capable of handling large currents, it has been possible to produce 17 Mv γ-rays of about three times the intensity used by Bothe and Gentner. A number of elements have been irradiated with these γ-rays in a search for photonuclear reactions too weak to be observed previously. The following elements, in addition to those previously reported by Bothe and Gentner, have been given a preliminary investigation: Na, Mg, Al, K, Ca, Mn, Fe, Co, Ni, Sn, Hg, Pb, Au, and Pt. Mn and Fe exhibit an activity which is definitely above the background. Although the activities are so weak that the half-lives are difficult to determine the periods appear to be 20 minutes for Mn, and 60–90 minutes for Fe. This would point to the reaction $Mn^{55}+\gamma \rightarrow Mn^{54}+n$, and $Fe^{56}+\gamma \rightarrow Fe^{55}+n$.

29. Ultra-High Frequency Power. DAVID H. SLOAN AND LAURISTON C. MARSHALL, *University of California.*—An oscillator, self-excited, delivers one kilowatt average power to a resistance load at 600 megacycles, using a.c. anode voltage, representing approximately 5 kilowatts on peaks. A more powerful tube is being constructed to operate at 1000 megacycles.

30. Propagation of Electromagnetic Waves Inside a Cylindrical Metal Tube and Along Other Types of Guides. HSÜ CHANG PEN, *California Institute of Technology.*—The prime purpose of this paper is to base the discussion of the properties of the propagation of electromagnetic waves inside a metal tube upon the theory of complex functions. The general expressions for the field components for different types of excitation systems are obtained in a rigorous manner starting from that of an electric and a magnetic dipole. The formal mathematical generalization is achieved by means of the transformation formulae of cylindrical functions and the results of the theory of integral equations. The integral equations thus obtained are expanded into series by aid of residual calculus for actual numerical calculation. The residues at the poles of singularities give rise to different "distinct modes" of propagation and thereby a comprehensive discussion of all the important physical properties is made. At the same time, problems arising in practical applications, say for long distance transmission for television purposes, are analyzed and some interesting conclusions obtained. The unique and rigorous analysis is only made possible by the free use of the results in the theory of complex functions. A comparison of the attenuations and the velocities of propagation inside a hollow cylindrical metal-tube-guide and that of a concentric system is made.

31. The Diurnal Variation of the Mobility Spectrum of the Atmospheric Ions and the Effect of Age of Ion. E. A. YUNKER,* *Stanford University.*—The determination of the mobility spectrum of the atmospheric ions using the classical air blast method was reported at the Stanford meeting of the Physical Society in June, 1939.[1] The same method is used to study diurnal variation of the mobility spectrum and the transitions from small atmospheric ions into the several types of intermediate and large ions. By placing polonium at various distances in a pipe leading to the apparatus, ions of predetermined age, up to 70 seconds, could be produced and studied. The shape of the mobility spectrum is found to be essentially the same throughout the day. All mobility groups including a group in the range 0.94 to 0.47 cm/sec./volt/cm, previously discussed in connection with the work of Chapman,[2] are found to grow at the expense of the small ion group (mobility 1.62 cm/sec./volt/cm for positive ions).

* Now at Oregon State College.
[1] To appear shortly in Terrestrial Magnetism and Atmospheric Electricity.
[2] Chapman, Phys. Rev. **52**, 184 (1937).

32. Gamma-Radiation from $C^{13}+H^1$. C. C. LAURITSEN AND W. A. FOWLER, *Kellogg Radiation Laboratory, California Institute of Technology.*—The gamma-radiation showing resonance at 560 kv in the bombardment of carbon by protons has been attributed[1] to the reaction $C^{13}(p,\gamma)N^{14}$ for which $Q=8.2$ Mev because the observed energy of the radiation (7.4 Mev) was greater than the available energy in the reaction $C^{12}(p,\gamma)N^{13}$ for which $Q=2.6$ Mev. We have confirmed this conclusion by bombarding a carbon target containing approximately 35 percent C^{13} prepared for us by Dr. C. H. Townes and Professor W. R. Smythe of the California Institute. The increase in intensity of the radiation at 560 kv was found to be in agreement with the isotope ratio found spectroscopically. Cloud-chamber investigations of the secondary electrons and pairs produced in thin lead and carbon laminae by the gamma-radiation indicate that it consists of three lines at 2.8 ± 0.4, 5.4 ± 0.3, and 8.1 ± 0.2 of approximately equal intensity. These results substantiate the analysis made by Rose[2] of the absorption curves measured by Dee and his collaborators. It is to be concluded that the excited state of N^{14} at 8.1 Mev radiates to the ground state directly or through an intermediate state at 2.8 or 5.4 Mev with equal probability.

[1] Dee, Curran and Petrzilka, Nature **141**, 642 (1938).
[2] Rose, Phys. Rev. **53**, 844 (1938).

33. Production and Properties of Carbon 14. MARTIN D. KAMEN, *Radiation Laboratory*, AND SAMUEL RUBEN, *Department of Chemistry, University of California.*—Various samples of graphite bombarded with 4-Mev deuterons have been found to possess the long-lived radioactivity isotopic with carbon reported recently.[1] Since the radiations emitted have been shown definitely to be electronic (absorption in aluminum and Cellophane identical), it is quite certain that the reaction is C^{13} (d,p) C^{14}. No positron emitters could have been formed with deuterons of the energy used in these investigations. The total yield at 4 Mev (apparently saturation energy for the thin target reaction) is approximately 0.03 μ-curie for 10,000 μ-ampere hours of bombardment. Using Pollard's estimate[2] for the cross section of this reaction, the half-life of C^{14} can be estimated to have a lower limit close to 1000 years. (Actually, the samples have shown no decay in six months.) This value coupled with the measured upper energy limit of 90 ± 15 kv for the beta-rays is in gross disagreement with that expected (*ca.* two or three days) from analogy with the case of He^6-Li^6. The difficulties involved in the preparation of strong samples of C^{14} will of necessity confine its use as a tracer in biochemical investigations to researches in which high dilution of tracer material is unavoidable.

[1] Phys. Rev. **57**, 549 (1940).
[2] Phys. Rev. **56**, 1168 (1939).

34. The Beta-Radiation from Si^{27} and P^{30}. W. H. BARKAS,* E. C. CREUTZ, L. A. DELSASSO, R. B. SUTTON AND M. G. WHITE, *Princeton University.*—Measurements have been made in the cloud chamber on the positrons emitted by Si^{27} and P^{30}. Spectra each containing about 2000 tracks give, respectively, 3.54 ± 0.1 Mev and 3.0 ± 0.1 Mev for the upper limits of Si^{27} and P^{30}. The radioactive isotopes were produced by the reactions Al^{27} (p,n) Si^{27} and Si^{30} (p,n) P^{30} by high energy protons from the Princeton cyclotron. The disintegration energy found for Si^{27} would indicate that the deviation, if any, from proportionality of nuclear volume to mass number is small.[1] While several measurements have previously been made on P^{30} the great dispersion in the published energies made another measurement important. P^{30} is one of the nuclei in the series of mass numbers $4k+2$ which are of interest in the study of the spin dependent forces. Our measurement is consistent with the hypothesis that the effect of this type of force in nuclear binding energies falls off inversely with the mass number.

* Member The Institute for Advanced Study.
[1] McCreary, Kuerti and Van Voorhis, Phys. Rev. **57**, 351 (1940).

35. The Latitude Effect of Cosmic Rays above 50°N Latitude. PAUL F. GAST AND D. H. LOUGHRIDGE, *University of Washington.*—Data have been collected continuously during 14 months over the range of geomagnetic latitude from 53°30'N (Seattle) to 61°36'N (Juneau). A Carnegie, Model C cosmic-ray meter, shielded with 12 cm of lead, was mounted in a specially constructed deck-house aboard the *M. S. Northland.* A complete trip was made every two weeks. The results were then averaged by seasons. It was found, in agreement with Compton and Turner[1] and Gill,[2] that the highest intensity occurred during winter and the lowest during summer. Furthermore, intensity increased slowly with increasing latitude, a rise of about 0.5 percent occurring in the range of latitude mentioned. A temperature coefficient was computed for each month using the half-trips with highest and lowest mean temperatures and these results were then averaged for the year giving -0.09 ± 0.03 percent per degree centigrade. A temperature coefficient was also computed by fitting a least-squares line to the daily mean intensities *vs.* daily mean temperatures plot for data at Seattle over the entire period of observation. The slope of this line gives for the temperature correction -0.11 percent per degree centigrade. The application of the temperature coefficient computed on the monthly basis makes the latitude curve flat within the limits of the probable error, which preliminary investigation indicates is about 0.1 percent.

[1] A. H. Compton and R. N. Turner, Phys. Rev. **52**, 799 (1937).
[2] Piara S. Gill, Phys. Rev. **55**, 1151 (1939).

36. The Sensitive Time of a Wilson Cloud Chamber. WAYNE E. HAZEN, *University of California.* (*Introduced by Robert B. Brode.*)—The sensitive time of a cloud chamber 30 cm in diameter and 30 cm deep was determined experimentally by means of a collimated source of high energy beta-rays (P^{32}) which was set in motion inside the chamber just before the expansion. A time scale was established by illuminating the moving source with a 60-cycle light in addition to the usual flash illumination for photographing the tracks. Photographs showed a series of images of the moving source and also beta-ray tracks issuing from the source for a certain portion of its path, corresponding to a certain time interval. The time interval for sharp tracks is the sensitive time. A theoretical expression for the sensitive time τ derived by E. J. Williams[1] is:

$$\tau=0.77\frac{\rho s}{\kappa(\gamma-1)^2}\left(\frac{V}{S}\right)^2\left(\frac{\delta r}{r}\right)^2,$$

where ρ, s, κ and γ are the density, specific heat, conductivity, and ratio of specific heats of the gas, V and S are the volume and surface area of the chamber, r is the expansion ratio, and δr is the increase of expansion ratio over that which will just give tracks. Experimentally it has been found that for nitrogen ($r=11$ percent) τ increases about linearly with δr up to $\delta r=1$ percent, reaches a maximum of $\frac{1}{4}$ sec. at $\delta r=1.5$ percent and then falls off. Experiments with He and H_2 gave qualitative agreement with Williams' expression as far as dependence of τ on the gas is concerned.

[1] E. J. Williams, Proc. Camb. Phil. Soc. **35**, 512 (1939).

37. Further Investigations of Air Mass Effect on Cosmic-Ray Intensity. D. H. LOUGHRIDGE AND PAUL F. GAST, *University of Washington.*—The authors have previously reported[1] the existence of a noticeable change in cosmic-ray intensity at the fronts separating different types of air masses. Using the same type of apparatus, a Carnegie, Model C cosmic-ray meter with a 12-cm lead shield, a survey has been made of the variation in cosmic-ray intensity in the vicinity of all the barometric lows observed

during a period of about 1 year, the passage of a front at the surface being associated with a low barometer. Data were then obtained from the Seattle airport office of the U. S. Weather Bureau as to the type of associated front with each low. It was found that of the 75 lows investigated 17 were cold fronts, 6 were warm, 34 were occlusions, 13 contained no fronts and 5 involved more than a single front passing the meter in a short time. These 5 were not included in the investigation. The cosmic-ray intensity in the vicinity of these lows was first corrected for the usual barometer effect. The mean of the 17 cold fronts showed an increase of about 1 percent. The 6 warm fronts gave a decrease of 0.7 percent. And the occluded fronts gave various types of fluctuation depending on whether warmer or colder air followed the occlusion.

[1] Donald H. Loughridge and Paul Gast, Phys. Rev. **56**, 1169 (1939).

38. The Occurrence of Trichell Pulses in Negative Point-to-Plane Corona in Air. L. B. LOEB, G. G. HUDSON AND A. F. KIP, *University of California.*—The appearance of the regular relaxation-oscillator-like pulses in negative point-to-plane corona in air at atmospheric pressure has appeared to be capricious and uncontrollable. This is due to several factors: (1) Dirty electrodes and air. (2) Electrodes with high field regions exceeding the 0.2 mm diameter size of an active spot will usually have multiple spots between which the discharge oscillates giving random irregularly spaced discharges. (3) Improperly polished or *conditioned* points will show irregular bursts of pulses until an active spot forms. (4) To form and maintain an active spot the air must have more than 30 percent relative humidity at 20°C. This gives enough H^+ ions in time to make and to maintain a clean unoxidized active spot of low work function. (5) Dry air yields positive ions which quickly oxidize and pit even Pt surfaces. (6) By conditioning small polished Pt points in H_2 at low negative corona currents they at once give Trichell pulses in moist air which continue indefinitely. (7) The various pre-onset potentials for negative points are not materially different from the analogous potentials for positive points. (8) Ultraviolet light aids onset by photoelectrons but produces chemical products which inhibit the currents. (9) No measurable differences were observed between brass, Cu, Al, Fe and Pt points, though in all cases the condition of the point was paramount.

39. Theoretical Calculations of Breakdown Potential for Sphere-Gaps. J. M. MEEK, *University of California.*—The potentials required for breakdown of symmetrical sphere-gaps for spacings up to a diameter are calculated on the basis of the streamer theory[1] of spark discharge giving agreement to within 3 percent of the measured values. Calculations including variation of air density are also found to agree with experiment. There are two types of mechanism for breakdown depending on gap-length: (1) The electron avalanche proceeds all the way across the gap from cathode to anode and there forms a positive streamer which leads to breakdown; this occurs for spacings in which the variation of field strength across the gap is small. (2) The electron avalanche which initiates the positive streamer has its origin in the gap near the anode; this occurs for larger spacings where the voltage gradient varies so much across the gap that the value of the Townsend primary ionization coefficient α is virtually zero over most of the mid-gap region. Since the sparking potentials calculated from processes (1) and (2) differ, a scattering of values may be expected in the transition region between the two mechanisms. This scattering is observed experimentally.[2] The transition region further accounts for the fact that at certain gap settings higher voltages are required for breakdown between spheres of small diameter than for larger spheres at the same gap setting.[3]

[1] J. M. Meek, Phys. Rev. **57**, 722 (1940); L. B. Loeb and J. M. Meek, J. App. Phys. **11**, 438 (1940); also July issue, in press.
[2] W. Dattan, Elektrotech. Zeits. **57**, 377 (1936).
[3] M. Toepler, Elektrotech. Zeits. **53**, 1219 (1932); J. Claussnitzer, *ibid.* **57**, 177 (1936).

40. A Four-Gram Radium Pack of Improved Design. A. H. WARNER, *University of California at Los Angeles and Los Angeles Tumor Institute,* AND R. H. NEIL, *Los Angeles Tumor Institute.*—Protection is obtained by the use of a mercury-filled steel sphere of fifteen centimeters radius. Radiation measurements show that while the radium is in safe position the dose at the surface is less than one-tenth roentgen per day. The radium is moved to treatment position by a remotely controlled oil pressure engine, and is returned to safe position by springs. The radium position is controlled by mounting it on a piston within a mercury-filled cylinder that slides in a hole through the center of the sphere. For treatment the radium is pushed to the end of the cylinder, which is adjusted to the desired treatment distance. By means of a stop this distance can be preset for any value from three to fifteen centimeters. The pack is supported on ball-bearing trunnions at a fixed distance from the ceiling. Vertical treatment angles are set by a worm gear and a handwheel. Horizontal angles are set by adjustment of the treatment table which has a motor-driven height adjustment. This design combines complete protection for the staff while adjusting the patient for treatment with remote control of the treatment period.

41. The Electrical Conductivity of Tartaric Acid Crystals. JAMES J. BRADY AND BRUCE ELLE, *Oregon State College.*—The electrical conductivity of tartaric acid crystals increases with time to reach a maximum value and then decreases to a small value as compared with the original conductivity. If an electrical field is not applied for a few days, the crystal recovers most of the original conductivity. Coating the crystal faces next to the electrodes with colloidal graphite produces three distinct changes: (1) The elimination of the maximum in the conductivity-time curve; (2) a lower final conductivity; and (3) the crystals do not recover their conductivity after standing with no field. The conductivity decreases rapidly as the temperature of the crystal is lowered. The temperature range studied was from 20°C to −74°C.

42. X-Ray Absorption Fine Structure Comparison for Two Elements in the Same Crystal. S. T. STEPHENSON, *State College of Washington.*—The fine structures on the

short wave-length side of the K-x-ray absorption edges of the elements Cu, Se, Br, Rb and Sr in the compounds $CuSeO_4$, Cu_2Se, CuBr, ZnSe, RbBr and $SrBr_2$ have been investigated with a focusing quartz crystal spectrograph. The structures of two elements in the same ionic crystal are not identical (in agreement with the results of some other workers for a few compounds containing elements of lower atomic number). The structures of Cu and Se in $CuSeO_4$ are different even at energy distances of 150 volts from the main edge contrary to the predictions of crystal energy zone theory. CuBr and ZnSe present interesting possibilities, because they are more homopolar than ionic and any ion charge effects should be minimized. Their structures are relatively weak, however, and comparison is difficult.

43. Some Anomalies in the Photographic Recording of Gamma-Radiation. R. A. MORRISON AND H. M. PARKER, *Tumor Institute of the Swedish Hospital, Seattle.*—Arrangements of radium sources to give uniform irradiation in radium therapy or radiobiological experiments can be precalculated.[1] Such arrangements should be confirmed by ionization methods or otherwise. An autophotograph of the radiation would be the quickest and simplest check, but it is shown that such photographs bear little relation, either qualitatively or quantitatively, to the gamma-ray distribution. The blackening obtained is approximately one-third due to gamma-rays and two-thirds due to beta-rays, although the ratio varies widely with the experimental arrangement. Under some conditions the secondary radiations produce peculiar patterns which are not readily explained in detail. Sometimes the beta-radiation can be removed by a magnetic field, but the field strength required is unreasonable in general. Electrostatic deflection is also inadequate. Even when the beta-radiation is removed the photographs cannot be visually interpreted, owing to subjective effects. These effects are shown in a striking manner in the radiation close to the end of a radium tube. The photographs show definite light rings, which are shown by microphotometry to be spurious. The use of powerful magnets and the necessity for photometry in all cases vitiates the apparent simplicity of a photographic technique.

[1] R. Paterson and H. M. Parker, Brit. J. Radiol. **7**, 592 (1934); **11**, 252 (1938); Patterson, Parker and F. W. Spiers, *ibid.* **9**, 487 (1936).

44. A General Purpose Dosimeter. H. M. PARKER, *Tumor Institute of the Swedish Hospital, Seattle.*—A utility instrument for most of the radium and roentgen-ray measurements required in the laboratory is described. The electrometer preferred is the Lindemann electrometer on account of its low capacity, stability, wide sensitivity range and first-order freedom from direct radiation effects. The electrometer can be connected in three ways: (1) Townsend null method for weak radiations or minute ionization chambers. Absolute measurements can be made by balance against a standard cell and standard condenser. The sensitivity is not better than one-tenth that obtained with a good electrometer tube system. (2) Direct reading of ionization current to 10^{-11} amp. by high resistance leak method. (3) Condenser chamber method in which the whole electrometer and shielding system is elevated to a potential of 240 volts, the electrometer needle and central chamber electrode being at 250 volts. This differential technique is approximately 100 times more sensitive than standard methods. The apparatus is suitable for the following measurements: (a) absolute absorption of radiation energy, (b) absolute intensity of roentgen-ray and gamma-ray beams, (c) rapid measurements of radioactive sources, (d) continuous observation of roentgen-ray intensity, (e) routine measurement of total dose (gamma- or roentgen rays) in radiotherapy, (f) testing of α-ray leakage from radium containers, (g) β-ray measurements, (h) stray radiation measurements.

45. The Variation of Sparking Potential with Dense Initial Photoelectric Currents. J. M. MEEK, *University of California.*—The minimum sparking potential of a discharge-gap is known to be lowered appreciably when the cathode of the gap is subjected to the intense ultraviolet radiations produced by an auxiliary spark-gap. This lowering is explained in terms of the streamer theory of spark discharge,[1] and is ascribed to the field distortion produced by the positive space-charge in the gap antecedent to breakdown as a result of the difference in mobilities of positive ions and electrons. The consequent variation of the Townsend primary ionization coefficient α across the gap is considered, and calculations of the breakdown potential are made for different values of initial photoelectric current. The calculated lowering is in fair agreement with that observed experimentally, when it is noted that in all experiments so far performed the source of illumination is a transient one, far shorter in duration than the time to establish the equilibrium space-charge calculated. The time-lag of sparking for large initial currents is shown to be related to the time of build-up of the space-charge field, and its variation with applied potential and initial current is indicated.

[1] J. M. Meek, Phys. Rev. **57**, 722 (1940); L. B. Loeb and J. M. Meek, J. App. Phys. **11**, 438 (1940); also July issue, in press.

46. Further Exact Solutions of the Boltzmann Equation Applicable to the Diffusion of Neutrons. E. A. SCHUCHARD AND E. A. UEHLING, *University of Washington.*—A solution previously given in the case of exponentially-distributed sources in a half-infinite medium[1] is extended by analytic continuation and superposition to cover any source distribution representable by a finite Fourier series. The analyticity of the solving function allows the decay factor in the exponential source term to assume pure-imaginary as well as positive-real values including zero. The superposition possibility follows from the linearity of the integral equation defining the solution function. Uniqueness is present for bounded solutions since the homogeneous integral equation has only the zero solution except in the limiting pure-scattering case when a one-signed solution exists which is not finite at the infinite point. Such a solution may be interpreted as due to an "infinitely-strong" incident current at the remote medium face in a manner completely analogous to that for the corresponding case in astrophysical radiation theory (law of star disk darkening[2]).

[1] E. A. Uehling and E. A. Schuchard, Phys. Rev. **57**, 251–2A (1940).
[2] E. Hopf, *Problems of Radiative Equilibrium* (Camb. Tract No. 31, 1934).

47. Radioactive Hydrogen—A Correction. LUIS W. ALVAREZ AND R. CORNOG, *University of California.*—The first sample of radioactive hydrogen was placed in the only chamber available at the time. To guard against the possibility that H^3 would diffuse through a rubber tube connected to the chamber, three specially designed chambers were constructed of brass and glass. Enough data have been accumulated from one of these to show that our previously reported decay was due to diffusion. No appreciable decay has been observed in five months with the improved chamber. If, as O'Neal and Goldhaber have suggested,[1] McMillan's Be+D activity[2] was really H^3, we can use his estimate of the life as greater than ten years. This agrees better with the extrapolated yield of the D−D reaction. The half-life will have to be computed from accurate data of that type, when they are available from laboratories equipped for such work. We observed some time ago that deuterium recovered from the cyclotron pumping system was more radioactive than could be explained by the D−D reaction. This is now explained in terms of the Be+D reaction. The enhanced specific activity of H^3 samples now made through the Be reaction increases the sensitivity of our electrostatic apparatus for measuring the upper limit, which is now in operation.

[1] O'Neal and Goldhaber, Phys. Rev. **57**, 1086A (1940).
[2] McMillan, Phys. Rev. **49**, 875 (1936).

AUTHOR INDEX TO ABSTRACTS OF SEATTLE MEETING

Alvarez, Luis W.—No. 27
—— **and R. Cornog**—No. 47

Backus, John—No. 25
Barkas, W. H., E. C. Creutz, L. A. Delsasso, R. B. Sutton and M. G. White—No. 34
Brady, James J. and Bruce Elle—No. 41

Carlson, P. R. and J. E. Henderson—No. 28
Christy, R. F. and S. Kusaka—No. 22
Cleveland, Forrest F.—No. 10
Cohn, Willi M.—No. 7
Corben, H. C. and Julian Schwinger—No. 19
Cornog, R.—see Alvarez, Luis W.
Creutz, E. C.—see Barkas, W. H.

Dancoff, S. M.—No. 14
Delsasso, L. A.—see Barkas, W. H.

Elle, Bruce—see Brady, James J.

Fitzsimmons, K. S., L. B. Loeb and J. M. Meek—No. 3
Fleming, G. M. and D. M. Holtoner—No. 12
Fowler, W. A. and C. C. Lauritsen—No. 26
——see Lauritsen, C. C.
——see Streib, J. F.

Gast, Paul F. and D. H. Loughridge—No. 35
——see Loughridge, D. H.
Goss, W. H. and J. E. Henderson—No. 24

Haseltine, William R.—No. 8
Hazen, Wayne E.—No. 36
Hellund, E. J.—No. 23
Henderson, J. E.—see Carlson, P. R.
——see Goss, W. H.
——see Wyckoff, H. O.
Holtoner, D. M.—see Fleming, G. M.
Hsu Chang Peu—No. 30
Hudson, G. G.—see Loeb, L. B.

Iverson, V. E.—see Kelly, Harry C.

Kamen, Martin D. and Samuel Ruben—No. 33
Kaplan, Joseph and Sidney M. Rubens—No. 5
——see Rubens, Sidney M.
Kelly, Harry C. and V. E. Iverson—No. 11
King, R. B. and D. C. Stockbarger—No. 2
Kip, A. F.—see Loeb, L. B.
Kusaka, S.—see Christy, R. F.

Laporte, Otto and J. E. Mack—No. 4
Lauritsen, C. C. and W. A. Fowler—No. 32
——see Fowler, W. A.
Little, E. M.—No. 20
Loeb, L. B., G. G. Hudson and A. F. Kipp—No. 38
——see Fitzsimmons, K. S.
Loughridge, D. H. and Paul F. Gast—No. 37
——see Gast, Paul F.

Mack, J. E.—see Laporte, Otto
Marshall, Lauriston C.—see Sloan, David H.
Meek, J. M.—Nos. 39, 45
——see Fitzsimmons, K. S.
Morrison, P. and L. I. Schiff—No. 17
Morrison, R. A. and H. M. Parker—No. 43
Mrozowski, S.—No. 9

Neher, H. V. and H. G. Stever—No. 18
Neil, R. H.—see Warner, A. H.

Parker, H. M.—No. 44
——see Morrison, R. A.

Ramsey, N. F.—No. 16
Ruben, Samuel—see Kamen, Martin D.
Rubens, Sidney M. and Joseph Kaplan—No. 6
——see Kaplan, Joseph

Schiff, L. I.—see Morrison, P.
Schuchard, E. A.—No. 13
—— **and E. A. Uehling**—No. 46
Schwinger, Julian—see Corben, H. C.
Sloan, David H. and Lauriston C. Marshall—No. 29
Stephenson, S. T.—42
Stever, H. G.—see Neher, H. V.
Stockbarger, D. C.—see King, R. B.
Streib, J. F., W. A. Fowler and C. C. Lauritsen—No. 21
Sutton, R. B.—see Barkas, W. H.

Uehling, E. A.—No. 15
——see Schuchard, E. A.

Warner, A. H. and R. H. Neil—No. 40
White, M. G.—see Barkas, W. H.
Wyckoff, H. O. and J. E. Henderson—No. 1

Yunker, E. A.—No. 31

Proceedings of the American Physical Society

MINUTES OF THE PITTSBURGH, PENNSYLVANIA, MEETING, JUNE 20–22, 1940

THE 236th regular meeting of the American Physical Society was held at Pittsburgh, Pennsylvania, on Thursday, Friday and Saturday, June 20, 21 and 22, 1940. The scientific sessions were held at the University of Pittsburgh, the Carnegie Institute of Technology and the Mellon Institute for Industrial Research. The presiding officers were Professor John Zeleny, President of the Society, Dean George B. Pegram, Vice President, and Professors O. H. Blackwood, Lee A. DuBridge and A. G. Worthing. The registered attendance at the meeting was about two hundred.

A symposium of invited papers sponsored by the Committee on Applied Physics of the American Physical Society was held on Saturday morning, June 22 at nine-thirty o'clock at the Mellon Institute for Industrial Research. Dr. Frederick Seitz of the University of Pennsylvania spoke on *The Theory of Internal Strains in Solids;* Dr. Paul D. Foote of the Gulf Research and Development Company on *Gasoline;* and Dr. R. H. Kent of the Aberdeen Proving Ground on *Physical and Chemical Characteristics of Explosives and Their Military Applications.*

On Thursday afternoon trips were made through the U. S. Bureau of Mines, the Mellon Institute and the Aluminum Company Works after which the Society was entertained at tea in the Commons Room of the Cathedral of Learning as the guests of the University of Pittsburgh. On Thursday evening the members of the Society were the guests of the Westinghouse Electric and Manufacturing Company at a broadcast program "Musical Americana," at the Syria Mosque. On Friday afternoon there were trips to the Westinghouse Research Laboratories and the Westinghouse East Pittsburgh Works. On Saturday afternoon, following an inspection of the Gulf Research Laboratories, a picnic was held on the grounds of the Laboratories.

An informal dinner was held on Friday evening, June 21, at the Webster Hall Hotel at seven o'clock. President Zeleny presided. This was followed by light entertainment. There were one hundred and forty-nine at the dinner.

Meeting of the Council. At its meeting held on Friday, June 21, 1940, the death of one fellow (Sinclair Smith) was reported. Eight candidates were transferred from membership to fellowship, one candidate was elected to fellowship, and sixteen candidates were elected to membership. *Transferred from membership to fellowship:* Otto Beeck, Newell S. Gingrich, Jerome M. B. Kellogg, John G. Kirkwood, P. Kusch, Sidney Millman, Chester M. Van Atta, and Clifford N. Wall. *Elected to fellowship:* Spiro Kyropoulos. *Elected to membership:* Mutsusuke Abe, B. N. Cacciapuoti, Ross W. Callon, Samuel R. Cook, Zaimoku Hai, Giiti Iwata, Charlotte L. Meaker, Teruo Momota, Keizo Muraoka, Frank Oppenheimer, Rene Planiol, Thomas M. Snyder, Martin Summerfield, Shozo Todani, Mary E. Warga, and Edwin A. Yunker.

The regular scientific program of the Society consisted of fifty-six papers, seven of which, numbers 6, 13, 39, 46, 51, 52 and 54, were read by title. The abstracts of these papers are given in the following pages. An author index will be found at the end.

HAROLD W. WEBB
Acting Secretary

ABSTRACTS

1. Application of a Cloud Chamber to the Detection of Charged Particle Groups. H. L. SCHULTZ, W. L. DAVIDSON, JR., AND L. H. OTT, *Yale University.*—The ranges of charged particles resulting from nuclear transmutations have been studied almost exclusively with the use of proportional counters and ionization chambers. Such methods suffer three definite limitations, particularly when a cyclotron is used to produce a high energy beam of bombarding particles. In the first place, the presence of a large neutron background interferes with the detection of weak groups. Secondly, absolute yields are difficult to obtain since a high counting level is necessary in order to discriminate against β-radiation. Finally, the finite depth of counting volume impairs the resolution of groups. All of these limitations may be overcome by allowing the particles to register in an expansion chamber. The funda-

mental technique has been described by Bower and Burcham. We have adapted a diaphragm type of expansion chamber for use in conjunction with the cyclotron in carrying out studies of this nature. Two argon flash tubes serve as an intense source of illumination over very short periods of time. Nonstereoscopic photographs are taken with the aid of an automatic camera. The particles are allowed to pass down an evacuated tube at right angles to the incident beam and enter the cloud chamber 40 cm from the target. Preliminary experiments have verified the presence of the strong 28-cm proton group from boron bombarded by 3.1 Mev deuterons as reported earlier by Pollard, Davidson, and Schultz. Evidence for an excited state in C^{13} has also been found. The reaction $Al^{27}(d,p)Al^{28}$ has been studied with an aluminum target of 0.15-cm air equivalent thickness. The groups found by McMillan and Lawrence also appear in the present work. In addition there is evidence for other groups. A detailed investigation of d-p reactions is now being carried out.

2. Longitudinal Extraction of Ions from Low Pressure Constricted Arc Discharge in H_2 and in BF_3. HOFF LU AND RALPH H. SCHUMAN, *University of Minnesota.*—We have attempted to extract ions efficiently from a low pressure arc confined in a cylindrical steel constriction. Ions are drawn out along the arc axis through a tungsten loop filament by a 1-mm hole probe at 2 kilovolts. A 3-mm shielding hole at arc potential in front of the probe produces a converging field which further concentrates the ions toward the center of the probe. By making the loop area of the filament smaller than the constrictional cross section, an arc of 2.5 cm length to the anode can be struck by the self-striking auxiliary arc to the constriction. A focusing cylinder accelerates the ions into a parallel beam which terminates at a collector biased to 50 volts to retain secondary electrons. The ion yield increases rapidly with decreasing pressure except near the threshold pressure where the arc goes off. Results are given below. A preliminary test with a second source improved in geometry and choice of materials indicates an increase in ion output by a factor of ten.

Arc in	H_2	BF_3
Lower pressure limit, mm of Hg	4×10^{-2}	2×10^{-2}
Satisfactory operating state:		
Pressure, mm of Hg	6×10^{-2}	3×10^{-2}
Arc current, milliamperes	125	150
Arc drop, volts	80	70
Steady ion beam current, microamperes	90	120

3. Some Experiments on the Irradiation of Deuterium, Beryllium, and Indium Nuclei by X-Rays. D. L. NORTHRUP, C. M. VAN ATTA, R. J. VAN DE GRAAFF AND L. C. VAN ATTA, *Massachusetts Institute of Technology.*—Yield curves will be shown for the disintegration of deuterium and beryllium[1] with continuous x-rays produced by the impact of a homogeneous beam of electrons on a gold target. The high voltage electrostatic generator and accelerating tube employed have been described.[2] The yield curves were observed as a function of the accelerating voltage applied to the electrons and extend from below threshold to a voltage of 2.65 Mev. The threshold voltages for both deuterium and beryllium, as measured on a generating voltmeter, were found to be in good agreement with values obtained in other laboratories. In both cases the neutrons from the disintegrations were detected by measurement of the radioactivity they produced in silver. Preliminary observations are in progress on the angular distribution of the neutrons from the deuterium disintegration. Excitation with x-rays of the 4.1-hour period in indium[3] was observed by surrounding a thin walled Geiger-Müller counter with the irradiated indium as well as by irradiation of counters constructed with indium cathodes. The latter counters showed, in addition to the 4.1-hour exponential decay, a more rapid exponential decay in counting rate consistently reproducible with a given counter, but shown by further experiments to be non-nuclear in origin.

[1] G. B. Collins, B. Waldman, and E. Guth, Phys. Rev. **56**, 876 (1939).
[2] Phys. Rev. **57**, 563A (1940).
[3] B. Pontecorvo and A. Lazard, Comptes rendus **208**, 99 (1939). G. B. Collins, B. Waldman, E. M. Stubblefield, and M. Goldhaber, Phys. Rev. **55**, 507L (1939).

4. Protons from Deuteron Bombardment of Separated Chlorine Isotopes. E. F. SHRADER AND E. POLLARD, *Yale University.*—Deuteron bombardment of chlorine yields three energy groups of protons. To determine the assignments of the groups a target of AgCl enriched in the heavy isotope has been bombarded. The isotope separation was accomplished by the use of a modified, multi-stage, Clusius and Dickel thermal diffusion column, employing hydrogen chloride gas at atmospheric pressure. The over-all length is 12 meters. After four days of continuous running a 40 cc sample was withdrawn at the bottom, dissolved in water, and activated simultaneously with a normal sample by bombardment with slow neutrons. The 37-minute beta-ray emission from Cl^{*38} of the two samples was compared simultaneously by means of two calibrated Geiger counters and the enriched sample was shown to contain 41.5 percent Cl^{37}. Targets of enriched and normal AgCl were bombarded with 3.3-Mev deuterons from a cyclotron and it was shown that the yield of the longest range group decreased relatively to the yield of the inside groups. This long range group is therefore due to $Cl^{35}(dp)Cl^{36}$ as expected. The group at $4.0Q$ value is therefore due to $Cl^{37}(dp)Cl^{38}$ and permits the calculation of the mass of Cl^{38}. The value obtained is 37.9803. This, using the known beta-ray upper limit of Cl^{38}, gives a mass of 37.9751 for A^{38} which agrees with the value from $Cl^{35}(\alpha p)A^{38}$.

5. Fast Neutron Threshold for Uranium Fission. R. O. HAXBY,* W. E. SHOUPP,* W. E. STEPHENS,* AND W. H. WELLS, *Westinghouse Research Laboratories.*—Using the neutrons from the Li (p,n) reaction, we have investigated the fast neutron excitation of fission in uranium. By increasing the proton energy, the maximum neutron energy is raised and the yield of fissions is measured by an ionization chamber and linear amplifier. The slow neutron fission background is minimized with cadmium and boron carbide shields, and with the use of sulfur insulation in the ionization chamber. The threshold is found to occur at a neutron energy of 0.35 ± 0.1 Mev.

* Westinghouse Research Fellow.

6. The Heat of Fission of Uranium. MALCOLM C. HENDERSON, *Princeton University.*—The heat produced during slow neutron bombardment in a 13.64g sample of metallic uranium was measured on a resistance thermometer.[1] Simultaneously the number of fissions produced in a 54-microgram layer of uranium was counted by an ionization chamber and pulse amplifier. The two uranium samples were within 1 cm of each other inside the same 1.27 cm lead shield and surrounded by 5.08 cm of paraffin. The source of neutrons was the Princeton cyclotron, using the beryllium-proton reaction at 6.5 Mev. The 54-microgram layer gave 40.1 ± 0.1 alpha-particles per minute into 2π solid angle and under slow neutron bombardment gave about 340 fissions per minute. At the same time the heat output was about 40 microwatts. Since thermal equilibrium is approached exponentially, the galvanometer deflection—the measure of the heat production—is the weighted and integrated effect of the heat produced in all preceding minutes. The heat produced in each minute is proportional to the number of fissions observed. A method of calculation based on these facts is necessitated by the continual fluctuation in the output of neutrons from the cyclotron, but has the advantage that every reading taken is significant. The weighted average of 13 runs, after various corrections which lower the result by 2½ percent, is 180 Mev per fission. The average deviation from this figure was 5 Mev and the maximum deviation was 12 Mev.

[1] M. C. Henderson, Phys. Rev. **56**, 703 (1939).

7. *P*-Wave Effects on Proton-Proton Scattering in the Meson Theory. HUBERT M. THAXTON, WILLIAM PRIVETTE AND DANIEL LEATHERBERRY, *Agricultural and Technical College of North Carolina.*—The potentials for the p-states derived[1] from the neutral meson theory are applied to the calculation of proton-proton scattering effects for the experimentally investigated energy region 670 to 1830 kev. The phase shifts K_1 are calculated by numerical integration and adjunction of Coulomb functions at $5e^2/mc^2$. The cut-off radius used was $0.46\hbar/\mu c = 1.006 \times 10^{13}$ cm with $\mu = 180$ m, corresponding to a potential which is constant inside the cut-off radius. The contribution to the ratio of scattering to Mott's due to the p-scattering is also calculated.[2] Series expansions in terms of energy are derived for the coefficients in the scattering formulas[2] and are used to calculate the coefficients necessary for the energies considered in these calculations for angles 15° to 45° at 5° intervals. For 670 kev the phase shifts are (−0.37°) for $V(^3P_0)$; (0.22°) for $V(^3P_1)$; (−0.09°) for $V(^3P_2)$ with an increase in value for the higher energies to (−1.72°) for $V(^3P_0)$; (1.11°) for $V(^3P_1)$; (−0.40°) for $V(^3P_2)$ at 1830 kev. A comparison of these phase shifts with those derived[3] for the attractive and repulsive p effects for the square and Gauss error well demonstrates that the p effects using the meson potentials are large and contribute appreciably to the ratio of scattering to Mott's value. The effect of change of mass $\mu = 180$ m to $\mu = 335$ m is being studied.

[1] H. A. Bethe, Phys. Rev. **57**, 260 (1940).
[2] G. Breit, C. Kittel and H. M. Thaxton, Phys. Rev. **57**, 255 (1940).
[3] H. M. Thaxton and A. M. Monroe, Phys. Rev. **56**, 616 (1939); A. M. Monroe and H. M. Thaxton, Phys. Rev. **56**, 616 (1939).

8. Pair Production by Electrons. J. R. FELDMEIER AND GEORGE B. COLLINS, *University of Notre Dame.*—The experimental values of the cross section for pair production by electrons, as determined by a number of investigators,[1] not only show large deviations from the theoretically predicted value, but also show discrepancies among themselves. The intense monochromatic source of electrons from the Van de Graaff generator at Notre Dame was employed for a study of the process of pair production by electrons in the energy range from 0.9 to 1.5 Mev, since this source offers a distinct experimental advantage over all the previous investigations, which employed β-rays. The trochoid method[2,3] of focusing was employed. The positron current was measured directly by collecting the positrons in a Faraday cage connected to an electrometer tube. This method was possible because of: (I) the high efficiency of the trochoid method of focusing; (II) the intense source of electrons available. A gold target 10^{-4} cm thick was irradiated with electron currents up to 10 μa. If the large experimental cross section ($\sim 10^{-22}$ cm²) as found by a number of workers[1] is correct, this should result in a positron current of 10^{-11} amp. per μa of incident current. Currents of this magnitude were not observed. There was, however, some indication of a positron current of 10^{-15} amp. per μa of incident current, which indicates a cross section for the process of pair production by 1.5 Mev electrons of the order of magnitude predicted by theory ($\sim 10^{-26}$ cm²).

[1] See review article by H. R. Crane and J. Halpern, Phys. Rev. **55**, 838 (1939).
[2] J. Thibaud, *Quelques Techniques Actuelles en Physique Nucleaire*, (Gauthier-Villars, Paris, 1938).
[3] M. Monadjemi, J. de Phys. **8**, 347 (1937).

9. A Theory of Cosmic-Ray Phenomena Based upon a Single Primary Component. W. F. G. SWANN, *Bartol Research Foundation of the Franklin Institute.*—The fundamental assumptions and conclusions are: (1) There is only one type of primary radiation, a charged particle radiation—probably protons—of heavy mass. (2) The primary radiation has an energy spectral distribution with a lower limit determined by entry through the magnetic field. (3) By processes at present unknown, each proton on entering the atmosphere experiences a certain probability of splitting into ten mesotrons, and to a first approximation these mesotrons are born at rest in the system of axes in which the protons are moving. (4) Under the conditions of (3) the mesotrons born from the entering protons of minimum energy will have too short a life to get out of the stratosphere. Moreover, on disintegrating into electrons and neutrinos they will, on account of the low energy of the mesotrons, show approximation to symmetry of emission and provide for the flat intensity-zenith angle curve characteristic of high altitudes in these latitudes. (5) The mesotrons born of higher energy protons have greater energy and longer lives, so that they descend to the lower regions of the atmosphere and the electrons resulting from their disintegration perpetuate more completely their original path directions. (6) A spectral distribution which would provide an exponential law for the case of mass absorption of mesotrons will, in view of mean life con-

siderations, give an absorption coefficient increasing with altitude and such as to simulate the participation of two components.

10. The Latitude Effect in Cosmic Rays at Far Southern Latitudes. E. T. CLARKE AND S. A. KORFF, *U. S. Antarctic Service and Bartol Research Foundation of the Franklin Institute.*—Cosmic-ray intensities have been measured at sea level using a single Geiger counter inside a lead shield 7.5 cm thick. The counts were scaled down 4 : 1 by a conventional thyratron circuit and then recorded on a dial recorder. Roughly 190,000 counts per day were recorded. The instrument was operated on board the *U.S.S. North Star* on its two voyages to Antarctica, reaching on the first a maximum geomagnetic latitude of 77°S. and on the second 57°S. It was found that the cosmic-ray intensity showed the well-known "knee" at approximately 39°S., and that between this latitude and 77° the intensity continued to rise slightly. The rate of rise in this portion of the curve, observed in February and March, was found to be the same as that reported by Compton[1] between 35° and 55°N. during the northern summer months. The total rise between the knee and 77°S. was found to be about 3 percent, while the "magnetic" latitude effect between the knee and the equator (at 78°W. longitude) was 8 ± 0.4 percent. It was found that if an external air temperature coefficient[2] of -0.15 percent per degree centigrade was applied to the counting rates obtained between the knee and 77°S., the curve of intensity against latitude in this region would be flat. The agreement obtained between the measurements with this counter and with electroscopes over this same course indicates that the specific ionization of the cosmic-ray particles does not, to within the accuracy of this determination, vary with latitude at sea level.

[1] A. H. Compton and R. N. Turner, Phys. Rev. **52**, 799 (1937).
[2] V. F. Hess, Phys. Rev. **57**, 781 (1940).

11. Single Scattering of Electrons. R. B. RANDELS, K. T. CHAO AND H. R. CRANE, *University of Michigan.*—The single scattering of electrons has been measured by means of a cloud chamber, for the following gases and energies:

GAS	ENERGY RANGE, MEV	LENGTH OF TRACK, METERS
Air	1.0– 4.5	800
A	1.0– 9.5	508
Kr	1.9– 9.5	112
Xe	1.5–11.5	804

Stereoscopic pairs of photographs were taken, although up to the present the angles have been measured in the projection only. The energy of each electron was measured, and in plotting the results the energies were separated into narrower ranges than those given in the table. The distributions obtained were compared with those calculated by projecting the Mott[1] distribution onto a plane. The plots for all the energy and atomic number groups were very similar to each other, in respect to their deviations from the Mott curve. The amount of scattering was in all cases greater than that predicted by Mott, by a factor of roughly 1.5, at those angles measured, namely greater than 15 degrees. It is to be noticed that the wild diversity of results (factors 0.1 to 30) for various atomic numbers and energies which one finds in the literature is absent. The credence given to our factor 1.5 will depend upon a careful investigation of possible systematic errors, rather than upon obtaining more tracks.

[1] N. F. Mott, Proc. Roy. Soc. **A124**, 440 (1929).

12. The Effect of Crystalline Structure on the Multiple Scattering of Electrons. N. L. OLESON, K. T. CHAO AND H. R. CRANE, *University of Michigan.*—Experiments[1] on the multiple scattering of electrons of 10^6 to 10^7 ev in lead have given significantly lower values than those calculated.[2] An important part of the multiple scattering is made up of numerous small deflections, of the same order as the angular separation between maxima in the crystal diffraction pattern. Therefore we must inquire whether diffraction phenomena such as extinction play an important part, since most scatterers used to date have been polycrystalline in structure. Wheeler[3] has probed into the question theoretically, and found reason to believe that the effect may be important in accounting for the apparent deficiency in the scattering by metallic lead. To test this, we have compared the multiple scattering in polycrystalline lead with that in a solution of lead chlorate in water. A cell having 0.2-mm glass walls contained a layer of solution 2 mm thick. This contained 0.35 g of lead per cc. The scattering power of all the atoms of the cell other than lead was taken into account, but was small compared to that of the lead. At the dilution used, there could be little "order" among the lead atoms. Since the scattering power of the other constituents was comparatively small, the cell was very nearly equivalent to a lead gas. Three hundred and thirteen particles of average energy 6 Mev gave the same result as was obtained with an equivalent amount of polycrystalline lead. While it is still important to know theoretically the extent of this effect we believe we have shown that it is too small to account for the major part of the discrepancy in lead.

[1] C. W. Sheppard and W. A. Fowler, Phys. Rev. **57**, 273 (1940); N. L. Oleson, K. T. Chao and H. R. Crane, Phys. Rev. **57**, 1063A (1940).
[2] E. J. Williams, Proc. Roy. Soc. **A169**, 569 (1939); S. A. Goudsmit and J. L. Saunderson, Phys. Rev. **57**, 24 (1940).
[3] J. A. Wheeler, Phys. Rev. **57**, 352 (1940).

13. The Radioactive Isotopes of Gold. J. M. CORK AND J. HALPERN, *University of Michigan.*—In studying the radioactivity induced in gold two new emitters of half-life 54 hours and 164 days have been found. In addition the half-lives of three previously announced activities have been more precisely determined. The beta- and gamma-energies associated with each radioactivity have been measured by absorption methods and by the cloud chamber. Gold has a single stable isotope of mass 197 and while each of the five radioactivities can be reasonably assigned to a particular isotope, the placement is not as yet uniquely determined. The half-lives, energies and probable responsible isotopes appear to be as follows: 67.8 hr., β^- (0.74), γ (0.24, 0.50) [198]; 54 hr., β^- (0.57), γ (0.53) [195 or 196]; 5.6 days, β^- (0.36), γ (0.41) [196]; 164 days, β^- (0.45), γ (0.11) [199] and 37 m, β^+ [195].

14. Abnormal Diamagnetism of Ge at Low Temperatures; the Specific Heat of Zr. CHARLES F. SQUIRE, *University of Pennsylvania.*—The diamagnetic susceptibility per gram of pure germanium changes from -1.0×10^{-7} to -1.0×10^{-6} in cooling through a transition of the cooperative type according to our measurements. The specific heat has a large hump at the transition (75°K) according to measurements of F. Simon and S. Critescu.[1] According to H. Nitka,[2] the x-ray evidence shows no change of crystal structure (diamond type) but about 1 percent contraction of volume on cooling through the transition. The large diamagnetism has an analogy in the case of Bi; it seems unlikely that it can be identified with the enormous diamagnetism of a superconductor. However, the transition may be caused by a cooperation between electrons so that a lower energy state is formed and so that electrons may move through large areas in the crystal under the influence of a magnetic field. We believe that a Debye $\theta=177$°K on the low temperature side and a $\theta=290$°K on the high temperature side of the transition explains the true abnormality of the specific heat curve. There is also a hump in the specific heat of Hf at 85°K;[1] we have therefore measured the specific heat of Zr down to 80°K but without finding the expected hump. A Debye $\theta=190$°K fits our curve very well.

[1] F. Simon and S. Critescu, Zeits. f. physik. Chemie **25**, 273 (1934).
[2] H. Nitka, Physik. Zeits. **38**, 895 (1937).

15. The Theoretical Magnetic Susceptibility of Molecular Deuterium as Compared with That of Molecular Hydrogen. ENOS E. WITMER, *University of Pennsylvania.*—The molar magnetic susceptibility χ_M of molecular hydrogen or molecular deuterium is given by

$$\chi_M=-\frac{Le^2}{6mc^2}(\overline{r_1^2}+\overline{r_2^2})+\frac{Le^2}{6m^2c^2}\sum_{n'\neq n}\frac{|P(n,n')|^2}{h\nu(n,n')}.$$

The first term has been evaluated exactly and the second approximately, using the wave functions of James and Coolidge for the normal electronic state of molecular hydrogen. Furthermore, a Morse wave function was used as the vibrational function in evaluating the first term. This function for D_2 differs from that for H_2, leading to slightly different values for the first term. Thus for H_2 the first term is -4.115×10^{-6} and for D_2 it is -4.080×10^{-6}. The second term in the formula above may also yield slightly different results for H_2 and D_2, but since the value of this term is less than 8 percent of the value of the first term, this difference is not important. The best value of χ_M for H_2 is probably -3.965×10^{-6}. Hence the value for D_2 should be about -3.93×10^{-6}.

16. The Fock Equations and Diamagnetic Susceptibility for Magnesium III. W. JACQUE YOST, *Brown University.*—The calculation of a self-consistent field including the exchange terms has been completed for Mg III in the normal state. The methods used are similar to those reported in the case of Mg III without exchange.[1] None of the final $Z(nl|r)$ diverge from self-consistency by more than ±0.003. Three approximations were necessary in both s groups and four for the $2p$ group. The inclusion of the exchange terms produces a shift in the charge distribution in such a manner as to make the ion more compact. The $2s$ functions show a greater change than the $2p$ functions, which is contrary to results for similar configurations. The greater difficulty encountered in the numerical solution of the Fock equations is shown to arise from the inhomogeneity of the equations. An interpolation method is suggested for obtaining a good approximation to the solutions with exchange, whenever the solutions without exchange are known for the same configuration. The diamagnetic susceptibility for Mg III, as calculated from the solutions with exchange, is -3.74×10^{-6}. This is in good agreement with the value -3.3×10^{-6}, which Pauling[2] quotes as the best average value from several experiments. This calculation indicates that the earlier value of -8.6×10^{-6}, given by Joos,[3] is too high.

[1] W. J. Yost, Phys. Rev. **57**, 557 (1940).
[2] L. Pauling, Proc. Roy. Soc. **114A**, 204 (1927).
[3] G. Joos, Zeits. f. Physik **19**, 347 (1923).

17. Theory of the Approach to Magnetic Saturation. WILLIAM FULLER BROWN, JR., *Princeton University.*—Ferromagnetic saturation is not attained in finite fields because of internal forces that turn the spontaneous magnetization J_s out of the direction of the field H. These deviating forces are due to crystal anisotropy and to internal stresses. When they are uniform or vary slowly from point to point, a standard theoretical treatment[1] leads to a formula $J_s-J=b/H^2$. But if they change rapidly over short distances, this treatment is no longer valid; for then the interatomic coupling forces responsible for the spontaneous magnetization prevent it from changing its direction fast enough to follow the deviating forces exactly.[2] A calculation has been made for the case of deviating forces concentrated in points, lines, or planes. These lead to terms in J_s-J of the form $a/H^{n/2}$, with $n=1$, 2, 3, respectively, provided $H\ll$ or $\gg4\pi J_s$; at intermediate fields the formulas are more complicated because of magnetic interactions. Experimentally[3] an a/H term is found as well as the b/H^2 term, and the coefficient a is increased by plastic flow. This suggests that the a/H term may be due to stress concentrations associated with dislocation lines.[4]

[1] F. Bitter, *Introduction to Ferromagnetism* (McGraw-Hill, 1937), p. 222.
[2] Cf. J. App. Phys. **11**, 160 (1940), especially Figs. 2 and 6.
[3] A. R. Kaufmann, Phys. Rev. **57**, 1089A (1940).
[4] J. M. Burgers, Proc. Phys. Soc. **52**, 23 (1940).

18. Electron Band Treatment of Susceptibilities of Nickel and Nickel Alloys. KENNETH E. KEYES, *Carnegie Institute of Technology.*—The temperature dependence of the susceptibilities of nickel and its alloys (nickel-copper and nickel-zinc) has been measured by various experimenters.[1] It has been found possible to explain this dependence formally by a straightforward application of the Fermi-Dirac statistics to the electron bands taking, of course, proper account of exchange forces. For nickel and its alloys the bands that need be considered are those arising from the ($3d$) and ($4s$) energy states. The theory of metals indicates that the proper distribution of the ($3d$) band near the top is given by $N(\epsilon)=a(\epsilon_m-\epsilon)^{\frac{1}{2}}$, while for the $4s$-bands the distribution is given sufficiently accurately for our purpose by $N(\epsilon)=$constant$=b$. By properly choosing the parameters a and b it is possible to obtain good

agreement with experiment. The results are discussed in relation to the measurements of Keesom and Kurrelmeyer[2] on the specific heat of nickel-copper alloys at low temperatures. The present treatment differs from that of Stoner[3] in that it takes account of the presence of the (4*s*) band which overlaps the (3*d*) band.

[1] Mary A. Wheeler, Phys. Rev. **56**, 1137 (1939).
[2] W. H. Keesom and B. Kurrelmeyer, Phys. Rev. **57**, 1068A (1940).
[3] E. C. Stoner, Proc. Roy. Soc. **A165**, 372 (1938).

19. High Frequency Resistance and Permeability of Iron in a Magnetic Field. J. Barton Hoag and C. R. Cox, *University of Chicago.*—The effect of a superimposed steady magnetic field on the high frequency resistance and permeability of iron has been investigated in the wave-length region from 11 to 160 meters. The substitution method of determining resistance was used in conjunction with a resonant circuit coupled to an oscillator. Permeabilities were computed from resistance measurements by the use of Kelvin's skin effect equation. It was found that the effect of an applied field is to reduce the permeability and the resistance of iron, the reduction amounting to 60 or 70 percent for fields of 850 oersteds. The percentage decrease in radiofrequency resistance due to the application of a field was found to be approximately constant over the range from 30 to 160 meters and to rise to a greater value at wavelengths less than 30 meters. The permeability with zero applied field was found to be approximately constant over the range from 30 to 160 meters and to decrease appreciably from 30 to 11 meters. A comparison will be made of the present permeability values (for $H=0$) with those of other workers in this range.

20. Magnetic Properties of Iron-Aluminum Alloys. R. M. Bozorth, H. J. Williams and R. J. Morris, Jr., *Bell Telephone Laboratories.*—The alloy containing about four percent aluminum has been found to have a valuable combination of magnetic, electrical and mechanical properties. After melting in hydrogen or in air, rolling hot and then cold, and annealing at 1000°C, maximum permeabilities (μ_m) of over 25,000 have been attained. The cold rolling produces marked directional properties and in the direction of rolling and at right angles the permeability (μ) after annealing is as high as 8000 at a flux-density (B) of 14,000. In swaged rod, $\mu=12{,}000$ at $B=14{,}000$, and 7000 at 15,000, and the coercive force (H_c) is 0.20. After cold rolling and annealing for one hour, torque curves show that the directional character is marked when the annealing temperature lies between 700° and 1200°C. Special annealing in hydrogen at a high temperature reduces the coercive force to 0.08. The material is less brittle than iron-silicon alloys containing the same amount of silicon, the permeabilities at high flux-densities are higher than the commercial iron-silicon alloy and the resistivity is about the same. Ingots of 250 pounds have been satisfactorily cast and worked. Although μ_m is about the same as that previously obtained,[1] H_c is much lower and μ is much higher at $B=14{,}000$ and 15,000. The hysteresis loss at $B=15{,}000$ is about one-fourth of that formerly reported.

[1] T. D. Yensen and W. A. Gatward, University of Illinois Bull. No. 95, 1–50 (1917).

21. Vicalloy, a New Permanent Magnet Material. E. A. Nesbitt and G. A. Kelsall, *Bell Telephone Laboratories.*—A new permanent magnet material with unusual mechanical as well as magnetic properties has been developed. In the best specimens, the coercive force (H_c) is 400 oersteds, the residual induction (B_R) 9600 gauss, and the energy product (BH) as high as 2.8×10^6. Before it is given its final heat treatment, it can be rolled and machined almost as readily as mild steel. The composition is 36 to 62 percent cobalt, 6 to 16 percent vanadium and 30 to 52 percent iron. The heat treatment and mechanical treatment used to attain the best magnetic properties were as follows: cast, hot swaged, cold drawn with a reduction in area as high as 95 percent, then heat treated for an hour at 600°C. Good mechanical properties and energy products as high as 1.0×10^6 are obtained without cold working. The alloy differs from most age-hardening alloys in that the γ phase stable at high temperatures is dispersed in the α phase stable at low temperatures, instead of vice versa. The cold work transforms γ to α and the anneal at 600°C transforms a part of the alloy to γ. This material is not commercially available at present.

22. Change of Length and Young's Modulus with Magnetization and Heat Treatment. H. J. Williams, R. M. Bozorth and H. Christensen, *Bell Telephone Laboratories.*—The purpose of this investigation has been to study the changes in certain physical properties that result from different treatments given to an alloy in a temperature range reaching to 1000°C. The magnetostriction at saturation varied from 2.5×10^{-6} to 21×10^{-6} and the variation in Young's modulus with magnetization varied from 0.09 percent to over 8 percent. The alloy studied, permalloy containing 68 percent nickel, was chosen because it is especially sensitive to such heat treatments. The treatments were (1) the usual anneal followed by slow cooling, (2) the permalloy treatment (air quenched from 600°C), heat treatment (3) in a longitudinal and (4) in a transverse magnetic field. Measurements were also made on cold-rolled material before annealing. The results are interpreted in terms of the domain theory as far as possible. Young's modulus was determined by measuring the natural frequency of vibration of a hollow rectangle magnetized parallel to its sides so that the magnetic circuit was complete without air-gaps or end effects.

23. Wave Reflections at Oblique Incidence. C. D. Thomas and R. C. Colwell, *West Virginia University.*—In the troposphere, the temperature of the air does not always decrease with increased height above the earth's surface. Very frequently inversion layers are encountered at heights of from one to ten kilometers, in which there is an abrupt transition from cold dry air to warm moist air. The difference in dielectric constant between these two regions is sufficient to cause a reflection of radio waves. At perpendicular incidence the reflected wave is weak compared to the direct wave; but at oblique incidence, the reflected wave may be fairly strong. An application of Maxwell's equations to these boundary layers gives a

quantitative relation which is in fair agreement with the experimental results. Short radio waves are bent around the curving surface of the earth by reflection from the inversion layers as well as by diffraction.

24. The Variation in Intensity of Radio Signals. R. C. COLWELL, *West Virginia University.*—For several years, the strength of radio signals from nearby broadcasting stations has been taken at midday. When the results are plotted, it is found in every case that the signals in winter are much stronger than in summer. There is also a day to day variation caused by the changing weather cycle.

25. The Influence of "Cold Ends" on Performance of Vacuum-Tube Air Coolers. I. E. MOUROMTSEFF, *Westinghouse Lamp Division, Bloomfield, New Jersey.*—Mathematical expressions are derived for longitudinal temperature distribution in a hollow cylinder under the assumption of uniform heating of the middle portion of the cylinder on the inside and uniform cooling on the outside of the entire cylinder. The results obtained are applied to a practical case of an air cooler designed for a vacuum tube with an external copper anode. Temperature distribution along the core of the cooler is calculated and represented graphically. The effect of variable air velocity on temperature distribution is discussed; curves for the "normal" and 50 percent and 200 percent of the normal velocity are calculated. Permissible anode dissipation is plotted as function of air velocity. It is shown that without taking the actual temperature distribution into consideration an error of approximately +25 percent to −50 percent in maximum ratings can be made.

26. Arc Cathodes of Low Current Density at High Amperage. JOSEPH SLEPIAN AND W. E. BERKEY, *Westinghouse Electric & Manufacturing Company.*—From photographs, and from the marking on the electrodes, Slepian and Haverstick[1] found that short duration arcs of 25 amperes in gases at a pressure of a few centimeters had apparent current densities at the cathode of less than 100 amp. per cm². This is in sharp contradiction to the density of several thousand amperes per cm² which seems to be required by generally accepted theories of the cold cathode arc.[1] Similar results have been found up to currents of 5000 amperes, burning for 1/120 sec. with electrodes of various metals in air at less than 10 cm pressure. Apparent cathode current densities calculated from the observed marking on the electrodes were less than 1000 amp. per cm². The markings on the electrodes were apparently produced by oxidation only, the energy density developed at the electrodes being insufficient to bring the electrode surface to the melting point in the 1/120 second duration of the arc. The circuit interrupting capacity of these short low current density arcs was found to be not less than that of short arcs at atmospheric pressure.

[1] Phys. Rev. **33**, 52–55 (1929).

27. Short Time Photographs of a Low Pressure Copper Arc. R. C. MASON, *Westinghouse Research Laboratories.*—By the use of a narrow slit in a synchronously rotating disk as a shutter, photographs with an exposure time as short as 2×10^{-5} sec. have been made of a 200-amp. (peak) a.c. arc between copper electrodes in air at about 10 mm pressure. The light from the cathode region in general was diffuse, as if the cathode spot covered a comparatively large area. In a few photographs, the diffuse area appeared absolutely uniform in brightness, while in many cases there were in addition extremely small concentrated points of light on the cathode. The cathode current density, as judged from the diffuse area, would be from 200 to 1000 amp. per sq. cm. Two successive photographs, separated in time by 2×10^{-4} sec., as well as comparison of the marking left on the electrode by the arc with the photographs, revealed that the arc was usually in motion over the cathode. Typical photographs will be shown.

28. Simple Calculation of Klystron* Efficiency. E. U. CONDON, *Westinghouse Research Laboratories.*—The behavior of the energy modulated electron beam in an oscillation generator of the Klystron* type can be understood in a simple way by considering the trajectories of the individual electrons and averaging over the phase of the oscillation at which the various electrons enter the oscillating field. This point of view permits a simple calculation of Webster's approximate formula[1] for the efficiency of power conversion in the Klystron.*

* Sperry Gyroscope Company trademark.
[1] D. L. Webster, J. App. Phys. **10**, 501 (1939).

29. A Thermistor Voltage Regulator. C. B. GREEN AND G. L. PEARSON, *Bell Telephone Laboratories.*—Thermistor is a contraction of the words "thermal resistor" and designates an electrical resistance whose value is markedly dependent upon its temperature.[1] Thermistors with a large negative temperature coefficient of resistance can be made of metallic oxides. One such thermistor which is commercially available is described and its thermal and electrical characteristics given. A considerable portion of its voltage-current characteristic has a negative slope, i.e., the voltage decreases as the current increases. This suggests a number of interesting applications for thermistors, among which is their use as automatic voltage regulators. If a properly chosen ohmic resistance is placed in series with the thermistor, the voltage drop existing across the terminals of the thermistor-resistance combination will remain constant despite a large variation of current through it. The electrical characteristics of a typical thermistor voltage regulator are presented and the effect of ambient temperature upon its operation discussed. A model regulator has been constructed which over a limited ambient temperature range will maintain a voltage of 13 volts to ±1 percent across a high impedance load when operating from a nominally 120 volt a.c. supply varying ±30 percent, or from a 35-volt supply varying ±20 percent.

[1] Phys. Rev. **57**, 1065A (1940).

30. A Magnetic Ultra-Micrometer for Measurement of Thin Films or Nonmagnetic Material Superimposed Upon a Base of Magnetic Material.—W. B. ELLWOOD, *Bell Telephone Laboratories.*—A magnetic bridge is described

which measures without destruction the average thickness over a given area of a nonmagnetic film of any kind upon one side of a magnetic base material. The thickness is in terms of an equivalent resistance or galvanometer deflection and is empirically calibrated and is only slightly affected by large variations in the permeability of the base material. The sensitivity of the bridge can be made to detect 10^{-6} inches of film. The bridge consists of two short collinear magnetic probes provided with primary windings excited with a.c. The test specimen is clamped between the ends of the probes perpendicular to them and the differential voltage between two secondary coils on the probes is a measure of the thickness of the film. This a.c. e.m.f. is measured by a d.c. galvanometer which is connected to the coils through a vibrating reed rectifier enclosed in glass which is driven synchronously by the a.c. power supply to the bridge. This device provides ample sensitivity without amplification.

31. The Effect of Pressure Variation of Viscosity on the Lubrication of Plane Sliders. M. MUSKAT AND H. H. EVINGER, *Gulf Research & Development Company.*—The Reynolds theory has been applied to the calculation of the lubrication properties of plane sliders—thrust bearings—of infinite width provided with lubricants whose viscosities increase with the pressure. The variation of viscosity with pressure was assumed to be exponential. The important variable characterizing the lubricant and the effect of the pressure variation of its viscosity was found to be the product of the viscosity pressure exponent and the bearing load per unit area. Curves for the friction coefficient, minimum film thickness, and lubricant flow were calculated for fixed values of this product, both for fixed wedge angle and pivoted sliders. It was found that for each choice of this product there will be a limiting position of the pivot line of the slider or of the equivalent Sommerfeld variable at which the film pressures and friction forces would become infinite, and beyond which it will be impossible to operate the slider. Moreover the absolute maximum value for this product under any conditions was found to be the value 2. This means that the absolute maximum load per unit area which can be carried by such bearings is equal to twice the reciprocal of the viscosity pressure exponent.

32. Experiments on Boundary Lubrication. F. MORGAN, M. MUSKAT, AND D. W. REED, *Gulf Research & Development Company.*—Apparatus has been constructed somewhat similar to that of Bowden to study the stick-slip behavior of the friction and temperature at the contact between metallic sliders under various conditions of speed and load, with different types of surfaces, and with sliders having given periods of free vibration. Simultaneous records were obtained of the instantaneous values of the friction and temperature. The friction determinations were made by reflecting light directly from the vibrating element onto a photographic film. The temperature fluctuations were recorded in terms of the thermoelectric voltages, generated between the sliding surfaces, which, after amplification, were sent to a high frequency galvanometer recorder. To check that these voltages were not due to spurious effects records were obtained for the sliding of steel on steel. In these no thermoelectric voltage was observed even though the friction traces showed large fluctuations. For constantan on steel the characteristics of the traces were found to depend on the relative speed and load, as well as on the natural frequency of the vibrating element. Preliminary results indicate that under certain conditions of lubrication some stick-slip may still take place while in other cases it disappears entirely and no temperature jumps occur.

33. Precipitation of Dirt. R. A. NIELSEN, *Westinghouse Research Laboratories.*—The unwanted deposition of dirt and smoke on room walls is a nuisance in industrial cities; this is especially true in a community where soft coal is used as a fuel. The deposits that occur are of two kinds: a uniform deposit resulting in a fairly inconspicuous darkening of the walls; and patterned deposits silhouetting laths, studdings, nails, etc., that often become very conspicuous before the end of a heating season. The action of convection, diffusion, and thermal gradients in producing the deposits that are observed on the walls will be discussed. Data on the magnitude of thermal gradients near wall surfaces of homes will be presented together with suggestions for minimizing the deposition of dirt on walls.

34. On the Heat Emission Associated with the Processes in Oversaturated Solid Solutions ("Aging"). H. CALUS AND R. SMOLUCHOWSKI, *Warsaw Institute of Technology and Princeton University.*—"Aging" a process little understood, especially at its early stages, occurs in oversaturated solid solutions which lead to precipitation. Its study is interesting in view of the problem of mechanism of diffusion in crystal lattice and equilibrium conditions. The process is accompanied by changes of mechanical, electric and magnetic properties and is important for the applications of duraluminum alloys. As a further step in its study, in particular of the rate of reaction, accurate measurements were made of the heat effects associated with the beginning of aging. The Swietoslawski microcalorimetric technique used before for similar research was applied. The method of measurements consisted in following the change of temperature difference between a quenched metal block and a thermostat (± 0.002°C) by means of a differential thermocouple. One obtained the rate of heat emission from the formula: $H = c[m - k(t_0 - t)]$ where m is the slope of the time-temperature curve, $t_0 - t$ the thermocouple indications, k a constant, and c the specific heat. The results were checked by an adiabatic method in which the thermostat and the block have the same temperature. One was able to make measurements soon enough after the quenching to observe the increase of the heat emission before it reaches a maximum and decreases asymptotically. It was thus possible to measure the total heat and the value 1.75 ± 0.05 cal. per gram was obtained for Duralumin. Studies were made on the influence of temperature of aging on the heat emission, and also of the composition for pure Al-Cu alloys (up to 5 percent Cu by weight). The heat emission increases with the amount of copper, being zero for pure aluminum.

* W. Swietoslawski and J. Czochralski, Wiad. Inst. Met. 3, 59 (1936).

35. Field Emission X-Ray Tube. C. M. SLACK, *Lamp Division, Westinghouse Electric & Manufacturing Company, Bloomfield, New Jersey.*—It has been found possible to draw currents of the order of several thousand amperes from cold metals by field emission in vacuum. This principle has been put to use in the design of a condenser discharge x-ray machine for high speed radiography. For a practical tube it seems necessary to use an auxiliary electrode spaced close to the cathode and connected to the anode through a high resistance. This electrode serves to initiate the discharge which is then transferred to the anode. It can also be made to serve as a focusing electrode. Radiographs of bullets and other high speed objects will be shown.

36. An Attempt to Measure Young's Modulus and Poisson's Ratio by X-Ray Methods. L. L. DAVENPORT, *University of Pittsburgh. (Introduced by S. S. Sidhu.)*—Measurements of longitudinal extension and transverse contraction of polycrystalline tungsten wires under stress have been made by back reflection photograms using Ni $K\alpha$ radiation. The effect of strain in 321 direction has been determined. The preliminary results appear satisfactory and indicate an additional possibility of a determination of the yield point. A method of measuring radii of diffraction rings has been developed. The values for a single crystalline direction may be computed by this technique.

37. Atomic Distribution in Aluminum-Silver Alloys During Aging. CHARLES S. BARRETT AND ALFRED H. GEISLER,* *Carnegie Institute of Technology.*—Laue photographs of aluminum-rich aluminum-silver crystals during aging at 20° and 150°C show more or less clearly defined streaks along certain zonal ellipses, in addition to the streaks caused by thermal agitation. These have been analyzed by stereographic and reciprocal lattice projections and are found to result from cross-gratings parallel to planes of the form {111}. The streaks with 20° aging are more diffuse than with 150° aging; no streaks were found with 200° aging. When full precipitation occurs, sharp spots appear along the streaks at places predicted from earlier studies of the Widmanstatten structure[1] formed by the visible precipitated crystals. Two theories can account for the cross-grating diffraction: (a) silver atoms collect in plate-like clusters on irregularly spaced {111} planes in a way analogous to that proposed in aged aluminum-copper alloys,[2,3] and (b) certain {111} planes shift parallel to themselves as required for the transformation from face-centered cubic to hexagonal close-packed lattices, the shift occurring on random planes in such a way as to destroy the periodicity normal to the planes.

* Aluminum Company of America Graduate Fellow.
[1] R. F. Mehl and C. S. Barrett, Trans. Am. Inst. Min. Met. Eng., Met. Div. 78, 1931.
[2] A. Guinier, Comptes rendus **204**, 1115 (1937); **206**, 1641 (1938); Nature **142**, 569 (1938).
[3] G. D. Preston, Nature **142**, 570 (1938); Phil. Mag. **26**, 855 (1938); Proc. Roy. Soc. **A167**, 526 (1938).

38. X-Ray Diffraction Studies of Anhydrous Chromic Oxides Prepared by Different Methods. S. S. SIDHU, *University of Pittsburgh,* AND MARC DARRIN, *Mellon Institute.*—Anhydrous chromic oxides prepared by different methods and analyzing from 99 to 100 percent in purity show marked differences in their physical properties. They vary in appearance from a very bulky powder to a very dense, visibly crystalline material. Their crystalline structure, however, remains the same, rhombohedral (hexagonal system). The size of the unit cell in each case has the normal x-ray value. Powder diffraction photograms prepared with standard-size specimens and a camera of the same effective diameter are identical with respect to the number and positions of the diffraction lines, but the intensities of the corresponding lines originating from the same crystal planes vary considerably, depending upon the method of preparation. For example, in some samples the 102 and 110 intensities are exactly the same, but in others the former increases and the latter decreases. Whether the intensity anomalies result from (1) the orientation of scattering centers owing to the movement of the molecules, (2) the formation of unstable small crystallites in which the molecules from certain crystal planes diffuse to other planes as the size of the crystallite grows, or (3) a temporary substitution of oxygen atoms for chromium atoms, as in the passivity of chromium, will be discussed.

39. An Electron and X-Ray Diffraction Study of the Grain Boundary Substance in Cadmium. BERNARD L. MILLER, *University of Pennsylvania. (Introduced by Raymond Morgan.)*—All metals in their usual state consist of a conglomeration of microscopic grains. Insoluble impurities collect at the boundaries of these grains and form films between the crystals. As such they may exercise considerable influence on the mechanical, diffusion, corrosion, recrystallization, electrical and magnetic properties of the metal. The grain boundary material in commercial cadmiums was isolated by dissolving laminae of cadmium in ammonium nitrate solution, the boundary substance remaining as insoluble films. Electron diffraction patterns were made of such films using 40 to 50 kilovolt electrons and x-ray diffraction patterns were obtained of powders of these films employing copper $K\alpha$-radiation. Guided by a knowledge of the elements present as indicated by a spectrographic analysis, the diffraction patterns were identified as belonging to the compounds cadmium carbonate and basic lead carbonate. Since it is known that normal lead carbonate converts to basic lead carbonate in ammonium nitrate solution it is concluded that cadmium carbonate and normal lead carbonate were present at the grain boundaries in the cadmium metals.

40. X-Ray Diffraction Studies of Silver-Rich, Silver-Magnesium Alloys. HAROLD R. LETNER, HENRY H. GEORGE AND S. S. SIDHU, *University of Pittsburgh.*—A preliminary survey of the α and β solid solutions of magnesium in silver has been made using a Debye-Scherrer camera and Cu $K\alpha$-radiation. The lattice parameters of both the face-centered cubic α-phase and the body-centered cubic β-phase are found to increase with increasing mag-

nesium content. Line intensities of alloys in the β-phase, allowed to cool in the furnace, indicate a highly ordered structure in the region of 50 percent magnesium. Quenched alloys having compositions in the two-phase region between the α- and β-phases and also some of the alloys in the β-phase annealed for 113 hours at 775°C, exhibit substantially less order. Further experimental work to study the magnesium-rich, silver-magnesium alloys is in progress.

41. X-Ray Absorption Edges in Gaseous, Liquid and Solid States. T. DRYNSKI AND R. SMOLUCHOWSKI, *Warsaw University, Warsaw, and Princeton University.*—The fine structure of the x-ray absorption edges depends mainly upon the structure of the energy spectrum above the occupied levels and on the transition probabilities. Although a quantitative interpretation is not always possible it is of interest to compare the fine structure of the x-ray absorption edges in gaseous, liquid and solid states. As absorbing substances were chosen: (i) $GeCl_4$, which in gaseous state has a Ge K-edge which structure is experimentally and theoretically known; (ii) $AsCl_3$, which has a similar molecular structure. Special experimental arrangements have been developed in order to obtain a thin layer of absorbing substance in liquid (room temperature) and in the solid (melting point for $GeCl_4$ −52°C, for $AsCl_3$ −18°C) state. The absorbing substance was kept in both cases in a thin glass capillary tube of proper inside diameter and thin walls. The structure of the Ge K-edge of solid $GeCl_4$ differs considerably from that obtained with both liquid and gaseous $GeCl_4$, the structure in the two latter states being practically identical. For $AsCl_3$ the edges in the case of gaseous and liquid state were obtained and show in general the same effects as for $GeCl_4$. The results are in accord with general qualitative expectations which one can formulate in considering the characteristic features of the gaseous, liquid and solid states.

42. An X-Ray Study of Liquid Benzene, Cyclohexane, and Their Mixtures. WHEELER P. DAVEY AND PAUL H. BELL, *The Pennsylvania State College.*—X-ray (Mo K alpha) studies were made of pure benzene, pure cyclohexane, and their mixtures, by using a Geiger-Mueller counter with balanced filters. The benzene showed at 25°C a rather sharp intense peak at the customary 8°40′ and a new broader peak of about one-eighth intensity at 4°20′. The cyclohexane showed a similar pair of peaks at 8°0′ and 4°0′. The mixtures all showed a broad peak of low intensity reaching from 4° to 8° and three sharp peaks at 8°0′, 8°20′, and 8°40′ superimposed on a broad peak which reached from about 8°0′ to about 8°40′. The positions of the three sharp peaks were not affected by the proportions of the two components, and their relative intensities are independent of amount of stirring. The customary shift with temperature was observed on all peaks. The results are consistent with a cybotatic type of picture. Benzene is pictured as having short-lived highly organized groups of *–B–B–B–B–* floating in a chaotic sea of disorganized benzene molecules. The peak at 8°40′ is thought to be due to resonating groups of *–B—B–B—B–B—B–* and *—B–B–B–B—B–B—*. Cyclohexane would contain similar groups of *–C–C–C–C–*, etc. The mixtures are assumed to contain *–B–B–B–B–*, *–C–C–C–C–*, and *–B–C–B–C–*. The presence of any considerable amount of more complicated groupings is obviously highly improbable.

43. The Structure of Liquid Argon. E. P. MILLER AND K. LARK-HOROVITZ, *Purdue University.*—A special high vacuum camera has been constructed which allows the investigation of liquids at low temperatures in a plane parallel cell with mica windows 0.01 mm thick and about 4 mm in diameter. Liquid argon in a layer 1.3 mm thick has been investigated at a pressure of 910 mm Hg with monochromatic Ag $K\alpha$-radiation. The diffraction pattern shows three distinct rings at $\sin\vartheta/\lambda$: 0.152, 0.284, 0.410 and a faint ring at $\sin\vartheta/\lambda \sim 0.59$. From a Fourier analysis the atomic distribution curve has been determined: there are about 10 nearest neighbors in a distance of 3.80A (as compared to 12 neighbors at 3.82A in the solid). This number is comparable to the 9.8 Cl atoms found around any Cl atom in LiCl as reported some time ago. A concentration of next nearest neighbors is indicated at 5.4A and further concentrations at 6.7A and 7.9A. From these results we conclude that the transition solid-liquid in argon produces a disorder without however changing the essential pattern of coordination as observed in the solid.

44. The Diffraction and Reflection of Molecular Beams. WILLIAM H. BESSEY, *Carnegie Institute of Technology.**—The diffraction and reflection of helium atoms and hydrogen molecules by lithium fluoride cleavage surfaces were studied by the method of molecular beams. A search was made for diffraction maxima very close to the specularly reflected beam; their presence would be direct evidence for the secondary structure of crystals postulated by Zwicky. The results were negative. Anomalous reflection curves were found, however, which were similar to those obtained by Renninger[1] for the reflection of x-rays by certain rock salt crystals. Both results can apparently be explained by assuming that crystals are made up of small pieces, crystallites, which are slightly tipped with respect to each other.

* Now at the South Dakota State School of Mines.
[1] M. Renninger, Zeits. f. Krist. **89**, 344 (1934).

45. On the Color of Solutions of Alkali Metals in Ammonia. HANS VON R. JAFFE, *Allegheny College.*—The concentrated solutions of alkali metals in liquid ammonia show metallic reflection with a remarkable dependence of the color of the reflected light on the angle of incidence. For the extreme case of the saturated solution of lithium the author has reported[1] a change of color from deep red to yellow, green, and finally white as the angle of incidence was increased from 0 to 90°. Measurements of the Hall effect of the solid compound $Li(NH_3)_4$ carried out at the same time led to the conclusion that the solid compound as well as the saturated solution contains one free electron for each atom of Li present. It is now shown that, using this electron density, the classical theory of dispersion of free electrons satisfactorily accounts for the observed color phenomena. To explain the absorption spectra of the dilute solutions the potential energy of the electron in the

field of surrounding NH_3 molecules must be taken into account. An energy of 1 ev would be in agreement with the data on absorption so far available.

[1] Hans Jaffe, Zeits. f. Physik **93**, 741 (1935).

46. Halation on Kinescope Screens. RICHARD F. BAKER, *Columbia University.*—Halation in the conventional kinescope is caused by light which has returned to the phosphor by way of total internal reflection and has then been scattered. Halation is objectionable in television reception because of the resultant loss of contrast and is especially annoying in any quantitative oscillograph work. The use of an absorbing medium between the phosphor and the glass envelope or in the glass itself for reducing halation has been proposed, and in conjunction with a small degree of optical contact between the phosphor and the glass is quite effective. Another method for minimizing halation is to combine with the advantages of an attenuating film a high index of refraction n_m which is greater than the index of either the glass n_g or the phosphor n_p. An analysis taking account only of the two total reflections at the film-glass and glass-air interfaces and assuming the validity of Lambert's law shows that the fraction of the total flux leaving an elementary area of the phosphor which reaches the air is

$$\log (1-1/n_m^2)^{\frac{1}{2}}/\log (1-n_g^2/n_m^2)^{\frac{1}{2}}.$$

For the conventional phosphor-glass combination the fraction is

$$\log (1-1/n_p^2)^{\frac{1}{2}}/\log (1-n_g^2/n_p^2)^{\frac{1}{2}}.$$

In all cases where $n_m > n_p > n_g$ the film offers an advantage insofar as the percentage of flux returning to the phosphor is concerned. This advantage of the film is increased when the absorption of the halo-forming flux in the film is taken into account. The advantages of this method in practice may be realized by depositing a film of high refractive index, low absorption index and low reflection coefficient between the phosphor and the glass envelope. The increase in contrast achieved in this manner is of course attained at the expense of spot intensity due to attenuation in passing through the film.

47. Rotational Structure of Some Fundamental Infra-Red Bands of Deuterated Formic Acid. LINCOLN G. SMITH AND V. WILLIAMS, *Princeton University.*—The rotational structures of the following infra-red bands have been obtained: ν(C−H) in HCOOD, ν(C−D) and ν(O−D) in DCOOD, and ν(C−D) in DCOOH. The approximate band centers are, respectively, 2944, 2232, 2632, and 2219 cm^{-1}. The ν(C−H) band of HCOOD is similar to that of HCOOH previously reported[1] in that no qQ branch is present, whereas each of the other three shows a definite qQ branch. This indicates that the axis of least moment of inertia is perpendicular to the C−H bond in HCOOH and HCOOD, but is appreciably shifted from this position when deuterium is substituted for the carbon hydrogen. The similarity of the ν(O−D) and ν(C−D) bands in DCOOD shows that these bonds make approximately equal angles with the axis of least moment of inertia. These results are in qualitative agreement with the structure of formic acid presented by Badger and Bauer. The structure of the molecule will be further discussed in the light of these new data.

[1] Paper No. 117, Washington meeting, April 26, 1940.

48. Transmission Line Method of Measuring the Dielectric Constant of Gases and Water Vapor at Ultra-High Frequencies. JOHN P. HAGEN, M. DISTAD AND F. C. ISELEY, *Naval Research Laboratory.*—A concentric transmission line, with the inner conductor a quarter wavelength long and grounded to the outer sheath at one end, was loosely coupled to an external ultra-high frequency oscillator. A detector was also loosely coupled to the quarter-wave line and the frequency of the oscillator adjusted to produce resonance in the line. Measurements were made of the resonant frequency first with dry air surrounding the inner conductor and then with moist air at various humidities and temperatures. Since the dielectric constant of the surrounding gas is inversely proportional to the square of the resonant frequency, the dielectric constant of the gas can be readily calculated. The experimental results for water vapor at 50°C with a frequency of 150 megacycles agree very well with those of other workers using frequencies below one megacycle. This shows that the dielectric constant of water vapor is practically independent of frequency up to at least 150 megacycles. This method is also suitable for measuring the dielectric constant of other gases at ultra-high frequencies.

49. Ultrasonic Absorption in Liquids. E. C. GREGG, JR., *Case School of Applied Science.*—The absorption coefficient in liquids was determined by measuring the voltage which must be applied to the vibrating crystal in order to bring the points of convergence[1] of parallel light into focus in a microscope set at various distances down the sound beam.[2] As was expected by theory, a linear relationship was found between the square root of the voltage and the reciprocal of the convergence distance and also between the logarithm of the voltage and the distance of the light beam from the radiator along the sound beam. In the latter case, the absorption coefficient was measured as a function of the slope of the line. Values of α (Biquard's notation) at 1901.5 kc are as follows: benzene, 0.032; toluene, 0.0099; and chloroform, 0.051. Due to unequal amplitudes of vibration present over the surface of the crystal[3] and the corresponding effect on the depth of focus, a quantitative estimate could not be made of the errors involved. Investigation of the values of the absorption coefficient, presented both above and in the literature, shows that for most liquids the absorption over the frequency squared becomes a constant only above a frequency of about one megacycle. Only an approximate correlation appears between viscosity and absorption.

[1] Lucas and Biquard, J. de Phys. et le Rad. **3**, 464 (1932).
[2] Gregg, Abstract 6, Kenyon Meeting of Am. Phys. Soc., April 6, 1940.
[3] Dye, Proc. Roy. Soc. London **A138**, 1 (1932).

50. Absorption of Supersonic Waves in Gases. I. F. ZARTMAN AND FRED H. SMITH, *Muhlenberg College.*—The absorption of supersonic waves in CO_2-free dry air, H_2

and CO_2 was measured at a frequency of 606 kc at room temperature and atmospheric pressure. The variable path acoustic interferometer developed by Hubbard was used, precautions being taken to insure the maintenance of plane parallelism between reflector and source for all positions of the reflector, proper support for the crystal and prevention of acoustic radiation from the unused face of the crystal. Contamination of the purified gases was avoided by using only metal, glass and quartz in the construction of the apparatus. The following energy absorption coefficients were obtained: CO_2-free dry air, 0.244; H_2, 0.350; CO_2, 1.26.

51. The Theory of Gaseous Isotope Separation in a Force Field with Application to the Ultracentrifuge. G. HAROLD WILSON, *University of Delaware.* (*Introduced by Enos E. Witmer.*)—This investigation deals with the problem of the rate of change of concentration of each component kind of molecule in a mixture of isotopic molecules when in a field of force. A kinetic theory derivation of the equation for the transport of molecules in a field of force is given for each component in the mixture. From this are derived the differential equations governing diffusion in a force field. The diffusion equations were solved subject to the conditions obtaining in an ultracentrifuge of special form by means of a differential analyzer. These solutions are used to make a calculation for a typical case. Approximate analytic expressions for the solutions of the fundamental differential equations are obtained which are valid if the speed of the centrifuge is not too high. Other expressions which hold if the force field is constant are also derived.

52. Elasticity of Solids at Different Temperatures, Especially Near Phase Transitions. H. F. LUDLOFF, *Cornell University.*—As indicated,[1] the thermoelastic properties can be computed from the solid state theory. One needs an equation of state relating the internal pressure of a solid to its volume and temperature. In general it is sufficient to consider one term referring to the pressure of the electrostatic forces and another term containing the pressure of the thermal waves. However, near phase transition regions a third term has to be added which takes into account the configurational change in the lattice during the transition. This term, according to Bethe and Kirkwood,[2] yields the expression:

$$p_3=\int_0^T C_p^{an}dT\times\frac{1}{v}\frac{\partial V}{\partial v}$$

(C_p^{an} anomaly in the specific heat curve, V interaction energy between neighboring atoms). It is shown that $V(v)$ can be computed if C_p has been measured. An equation of state containing these three terms enables one to compute the variation of the elastic parameters for all temperature ranges. At low temperatures one gets a T^4-law, at high temperatures a T-law; the elastic behavior near phase transitions can be derived if measurements of one of the thermal parameters are available.

[1] Phys. Rev. **57**, 558 (1940).
[2] Bethe and Kirkwood, J. Chem. Phys. **7**, 578 (1939).

53. A Self-Consistent Solution to the Vacancy Problem in Metals. H. B. HUNTINGTON, *University of Pennsylvania.*—Previous calculations have indicated a preference for the hole mechanism for substitutional diffusion, but the nonorthogonality of the wave functions then employed made quantitative estimates of the involved energies somewhat unreliable. A more thoroughgoing procedure was here followed—namely to find a Hartree-Foch self-consistent solution for the electrons in the neighborhood of the vacancy. A free electron model was used with parameters fitting the copper lattice. Initially analytic functions, determined from a square barrier approximation, were used to calculate the exchange potentials for S and P functions. An electrostatic potential was also determined. With these fields the wave functions were integrated, and a repetition of the process brought a reasonable degree of self-consistency. Preliminary calculations give a value of about 2 to 3 ev for the energy needed for the formation of a hole.

54. Pressure-Temperature Dependence of the Compressibility Factor and Density of Hydrocarbons.* BRUCE L. HICKS, *University of Wyoming.*—Several successful empirical equations which describe the P-d-T relations of liquids and gases have been of the form $P=P(T, d)$, which is indicated by theoretical treatments. However, for many purposes it is desirable to know some inverse function such as density or volume as a function of temperature and pressure. Especially useful in applications is the function $Z(T, P)=PV/RT$, the compressibility factor, and, particularly at low pressures, the function $\underset{\sim}{V}(T, P)=(RT/P)-V$, the residual volume. The inverse functions, Z and $\underset{\sim}{V}$, and likewise the density d may be calculated from the function $P=P(T, d)$ by means of Lagrange's formula for the reversion of series. The expressions are

$$\frac{P(T,d)}{d}=\frac{P}{d(T,P)}=ZRT=RT+\frac{P}{RT}\left[\frac{\partial}{\partial d}\left(\frac{P(T,d)}{d}\right)\right]_{d=0}-\sum_{n=1}^{\infty}\frac{P^{n+1}}{(n+1)!n}\left[\frac{\partial^{n+1}}{\partial d^{n+1}}\left\{\frac{d}{P(T,d)}\right\}^n\right]_{d=0},$$

from which $\underset{\sim}{V}$ may be obtained since $\underset{\sim}{V}=(1-Z)RT/P$, and

$$\frac{d}{P(T,d)}=\frac{d(T,P)}{P}=\frac{1}{RT}+\sum_{n=1}^{\infty}\frac{P^n}{(n+1)!}\left[\frac{\partial^n}{\partial d^n}\left\{\frac{d}{P(T,d)}\right\}^{n+1}\right]_{d=0}.$$

With the help of Faa' di Bruno's formula[1] for the derivatives of a function of a function, the necessary partial derivatives of the functions $\{d/P(T, d)\}^m$ taken for $d=0$ may be computed directly without forming the intermediate derivatives. Explicit calculation of the coefficients of some of the lower powers, P^n, using a recently developed equation of state, $P=P(T, d)$ for the saturated hydrocarbons,[2] will be reported in the near future. These coefficients will be polynomials in T and $1/T$ as are the coefficients of d^n in the original function, $P(T, d)$.

* To be read by title.
[1] F. Faa' di Bruno, Annali di Scienze Matematiche e Fisiche di Tortolini **6**, 479 (1855).
[2] Benedict, Webb and Rubin, J. Chem. Phys. **8**, 334 (1940).

55. Explanation of Anomalous Magnetic Torque Curves. R. M. BOZORTH AND H. J. WILLIAMS, *Bell Telephone Laboratories.*—When a disk cut from a cubic crystal of a ferromagnetic material is placed in a magnetic field parallel to its plane, the torque exerted on the disk by the field generally increases continually with the strength of the field, approaching a finite limit (saturation) in very high fields. An exception to this course for one orientation of a crystal of iron-silicon alloy has recently been observed by Tarasov.[1] We have confirmed his findings and observed a similar effect for a series of orientations of disks cut parallel to the (110) and (100) planes. As the field strength is increased, the torque passes through a well-defined maximum before beginning the final approach to saturation. This "anomalous" peak is explained in terms of the well-known energy equation:

$$E=E_K+E_H=K_1(\alpha_1^2\alpha_2^2+\alpha_2^2\alpha_3^2+\alpha_3^2\alpha_1^2)-HI_s\cos\theta,$$

in which the α's are the direction cosines with respect to the crystal axes of the magnetization vector (I_s) of one domain and θ is the angle between I_s and H. As H increases, the path traced on a sphere by the end of the vector I_s is determined by minimizing the energy for specific values of H. The graphical method developed is simple and can be used for calculating torque and magnetization curves for any direction of the applied field. A necessary condition for the occurrence of the peak is that $dE_K/d\theta$ have a maximum between the direction of H and the nearest direction of easy magnetization. In (100) disks the demagnetizing factor must be small.

[1] L. P. Tarasov, Phys. Rev. **56**, 1224 (1939).

56. Spark Gaps with Short Time Lag. JOSEPH SLEPIAN AND W. E. BERKEY, *Westinghouse Electric & Manufacturing Company.*—Short spark gaps (order of one mm) in air at atmospheric pressure, unless specially radiated, show large spark lag when tested at little above the sparking potential. In engineering literature this property is measured by the impulse ratio, i.e., the ratio of the voltage at which breakdown occurs under a voltage surge rising at a specified rate (about 50 kilovolts per microsecond) to the voltage at which breakdown occurs with slowly increasing impressed 60-cycle voltage. The spark lag shows statistical variations, and its mean has been shown to be nearly equal to the mean time for emission of an electron from the cathode, prior to the spark.[1] The electron current from the cathode prior to the spark is greatly increased by the presence of a pointed projection on the cathode, so that the mean spark lag at a given voltage is greatly reduced. However, if a single pointed projection is used, of sufficient size to reduce the spark lag at a given voltage, it also reduces the 60-cycle sparking potential, so that the impulse ratio, which is the quantity important in engineering applications, is not reduced. By using a very large number of extremely small pointed projections on the cathode, the spark lag can be reduced without appreciable lowering of the 60-cycle sparking potentials. Thus impulse ratios little greater than unity can be obtained. Small particles of carborundum, rutile, Alundum and porcelain of various sizes were attached to the cathodes of spark gaps, and the impulse ratios tested. Minimum impulse ratios were obtained when the particle linear dimensions were between 2×10^{-3} and 15×10^{-3} cm.

[1] R. Strigel, Wiss. Veröff a.d. Siemens-Konzern 11-2, 52-74 (1932).

AUTHOR INDEX OF ABSTRACTS OF PITTSBURGH MEETING

Baker, Richard F.—No. 46
Barrett, Charles S. and Alfred H. Geisler—No. 37
Bell, Paul H.—see Davey, Wheeler P.
Berkey, W. E.—see Slepian, Joseph
Bessey, William H.—No. 44
Bozorth, R. M.—see Williams, H. J.
—— **and H. J. Williams**—No. 55
—— **H. J. Williams and R. J. Morris, Jr.**—No. 20
Brown, William Fuller, Jr.—No. 17

Calus, H. and R. Smoluchowski—No. 34
Chao, K. T.—see Oleson, N. L.
——see Randels, R. B.
Christensen, H.—see Williams, H. J.
Clarke, E. T. and S. A. Korff—No. 10
Collins, George B.—see Feldmeier, J. R.
Colwell, R. C.—No. 24
——see Thomas, C. D.
Condon, E. U.—No. 28
Cork, J. M. and J. Halpern—No. 13
Cox, C. R.—see Hoag, J. Barton
Crane, H. R.—see Oleson, N. L.
——see Randels, R. B.

Darrin, Marc—see Sidhu, S. S.
Davenport, L. L.—No. 36
Davey, Wheeler P. and Paul H. Bell—No. 42
Davidson, W. L., Jr.—see Schultz, H. L.
Distad, M.—see Hagen, J. P.
Drynski, T. and R. Smoluchowski—No. 41

Ellwood, W. B.—No. 30
Evinger, H. H.—see Muskat, M.

Feldmeier, J. R. and George B. Collins—No. 8

Geisler, Alfred H.—see Barrett, Charles S.
George, H. H.—see Letner, H. R.
Green, C. B. and G. L. Pearson—No. 29
Gregg, E. C., Jr.—No. 49

Hagen, J. P., M. Distad and F. C. Iseley—No. 48
Halpern, J.—see Cork, J. M.
Haxby, R. O., W. E. Shoupp, W. E. Stephens and W. H. Wells—No. 5
Henderson, Malcolm C.—No. 6
Hicks, Bruce L.—No. 54
Hoag, J. Barton and C. R. Cox—No. 19
Huntington, H. B.—No. 53

Iseley, F. C.—see Hagen, J. P.

Jaffe, Hans von R.—No. 45

Kelsall, G. A.—see Nesbitt, E. A.
Keyes, Kenneth E.—No. 18
Korff, S. A.—see Clarke, E. T.

Lark-Horovitz, K.—see Miller, E. P.
Leatherberry, D.—see Thaxton, H. M.
Letner, H. R., H. H. George and S. S. Sidhu—No. 40
Lu, Hoff and Ralph H. Schuman—No. 2
Ludloff, H. F.—No. 52

Mason, R. C.—No. 27
Morgan, F., M. Muskat and D. W. Reed—No. 32
Miller, Bernard L.—No. 39
Miller, E. P. and K. Lark-Horovitz—No. 43
Morris, R. J., Jr.—see Bozorth, R. M.
Mouromtseff, I. E.—No. 25
Muskat, M.—see Morgan, F.
—— **and H. H. Evinger**—No. 31

Nesbitt, E. A. and G. A. Kelsall—No. 21
Nielsen, R. A.—No. 33
Northrup, D. L., C. M. Van Atta, R. J. Van de Graaff and L. C. Van Atta—No. 3

Oleson, N. L., K. T. Chao and H. R. Crane—No. 12
Ott, L. H.—see Schultz, H. L.

Pearson, G. L.—see Green, C. B.
Pollard, E.—see Shrader, E. F.
Privette, W.—see Thaxton, H. M.

Randels, R. B., K. T. Chao and H. R. Crane—No. 11
Reed, D. W.—see Morgan, F.

Schuman, Ralph H.—see Lu, Hoff
Schultz, H. L., W. L. Davidson, Jr. and L. H. Ott—No. 1
Shoupp, W. E.—see Haxby, R. O.
Shrader, E. F. and E. Pollard—No. 4
Sidhu, S. S.—see Letner, H. R.
—— **and Marc Darrin**—No. 38
Slack, C. M.—No. 35
Slepian, Joseph and W. E. Berkey—Nos. 26, 56
Smith, Fred H.—see Zartman, I. F.
Smith, Lincoln G. and V. Williams—No. 47
Smoluchowski, R.—see Calus, H.
——see Drynski, T.
Squire, Charles F.—No. 14
Stephens, W. E.—see Haxby, R. O.
Swann, W. F. G.—No. 9

Thaxton, H. M., W. Privette and D. Leatherberry—No. 7
Thomas, C. D. and R. C. Colwell—No. 23

Van Atta, C. M.—see Northrup, D. L.
Van Atta, L. C.—see Northrup, D. L.
Van de Graaff, R. J.—see Northrup, D. L.

Wells, W. H.—see Haxby, R. O.
Williams, H. J.—see Bozorth, R. M.
—— **R. M. Bozorth and H. Christensen**—No. 22
Williams, V.—see Smith, Lincoln G.
Wilson, G. Harold—No. 51
Witmer, Enos E.—No. 15

Yost, W. Jacque—No. 16

Zartman, I. F. and Fred H. Smith—No. 50